EXPERIMENTAL STUDY ON REHABILITATED RC BEAM-COLUMN CONNECTIONS UNDER CYCLIC LOADING

Thesis submitted

in partial fulfillment of the requirements

for the Degree of

DOCTOR OF PHILOSOPHY

By

Comingstarful Marthong

CIVIL ENGINEERING DEPARTMENT
INDIAN INSTITUTE OF TECHNOLOGY GUWAHATI
GUWAHATI-781039, INDIA
NOVEMBER, 2011

CERTIFICATE

This is to certify that the thesis entitled **"*Experimental study on rehabilitated RC beam-column connections under cyclic loading*"** submitted by ***Mr. Comingstarful Marthong*,** Roll No. 07610401 to the Indian Institute of Technology Guwahati, for the award of the degree of Doctor of Philosophy in Civil Engineering is a record of bonafide research work carried out by him under our supervision and guidance. The thesis work, in our opinion, has reached the requisite standard fulfilling the requirement for the degree of Doctor of Philosophy.

The results contained in this thesis have not been submitted in part or full to any other University or Institute for award of any degree or diploma.

(Dr. Anjan Dutta)
Professor
Department of Civil Engineering
Indian Institute of Technology Guwahati
Guwahati-781039, INDIA
Date:
Place: Guwahati

(Dr. Sajal Kanti Deb)
Professor
Department of Civil Engineering
Indian Institute of Technology Guwahati
Guwahati-781039, INDIA.
Date:
Place: Guwahati

STATEMENT

I do hereby declare that the matter embodied in this thesis is the result of investigations carried out by me in the Department of Civil Engineering, Indian Institute of Technology Guwahati, Assam, India.

In keeping with the general practice of reporting scientific observations, due acknowledgements have been made wherever the work described is based on the findings of others investigators.

Guwahati- 781039

Date: (Comingstarful Marthong)

ACKNOWLEDGEMENT

The writing of this doctoral thesis would not have been possible without the help and support of the kind people around me. The satisfaction with which during my sojourn at the institute and the friendship developed and associated with, need to express my sincere gratitude to those that made it possible and to only some of whom it is possible to give particular mention here.

First of all I would like to express my deepest sense of gratitude from my heart to Prof. Sajal Kanti Deb and Prof. Anjan Dutta, my dearest supervisors for initiating an interesting and innovative research topic to carry out and for their personal commitment in discussion and valuable advice during my entire research days. They have been continuously encouraging me during times when my confidence is low which boost me to work harder for my goal.

Since substantial part of my research work is based on experimental investigation, it would not have been possible for me to carry out the work without the support of technical staff of the Structural Engineering Laboratory, IIT Guwahati and I therefore, express my deep sense of gratitude to Mr. Arun Chandra Borsaikia, Scientific Officer, for his earnest effort in operating the Servo Hydraulic Dynamic Actuators during testing. I would also like to express my thanks to Mr. Suresh Boro, Mr. Bhuiya and Mr. Nripen Kalita, for their continuous help and ideas for fixing and removing the specimens during the course of casting and testing.

I'm most grateful to Dr. A.M. Choudhury for helping me in understanding the analysis on the test results and in allowing me to use some of his data collected during his PhD research work. Once again, I thank him for allowing me to carry out tests on his specimens.

My gratitude of thankfulness is also for Prof. Sudip Talukdar, Prof D. Chakravorty and Dr. H. Kaushik who were the members of my doctoral committee and who contributed with valuable remarks, suggestions and ideas to obtain the final results of this research work.

I am grateful to Prof. G. Karayannis, Democritus University of Thrace, Greece, Prof. S.P Shah, Northwestern University, USA, Dr. Bing Li, Nanyang Technological University, Singapore and Dr. Siddhartha Ghosh, IIT-Bombay, India, who has taken lot of pain for collecting and sending photocopy of some of the journal, which were not available in IIT Guwahati.

My best wish is to my friend Mr. K. Vizo, who helped me during the experimental work and I am grateful to him.

I would like to thank the Director, Higher and technical Education, Govt. of Meghalaya, India for allowing me pursue PhD and financially supporting me during my PhD tenure.

Finally, I express my thanks to my wife Damela-Aibianghun, who has been looking with enormous patience after my family during the days of my research duration. My heartfelt thanks are for my parents, by whose blessings I could complete this work successfully.

Above all, I bow down to the Almighty for keeping me in good health and made me able to come to this stage and to finally submit my PhD thesis.

Comingstarful Marthong

IIT, Guwahati (India)

November , 2011

CONTENTS

ABSTRACT

Post-earthquake investigations into damaged structures generally showed that in many cases, damages of RC frame structure were localized in beam-column connections which might have led to partial or total collapse of the building. It was observed that the exterior beam-column connections had suffered more in comparison to the interior ones. The failure of these connections during past earthquakes opened a new research direction in the field of repair of damaged structures. Research in this area is essential as engineers in seismic-prone regions often face the task of analyzing and designing repair or strengthening works for damaged buildings. Thus, it is difficult to decide always whether to discard the damaged structure or to rehabilitate the same for retrieving the lost capacity without any quantitative guidance. After an earthquake, a building may suffer damages and depending on the overall level of structural integrity, it can be rehabilitated by repairing or strengthening the damaged areas. Several methods of rehabilitation on RC beam-column connections damaged during earthquake have been reported. Each of these methods possesses its own practical limitation. The effectiveness of any rehabilitation / strengthening techniques however depends on the treatment provided to the fragmented concrete in the damaged region. Hence, in this study an effort has been focused on rehabilitating the affected damage zone of RC beam-column connections by employing different rehabilitation strategies depending on extent of damages.

Several experimental studies have been carried out to evaluate the behavior of rehabilitated RC beam-column connections under cyclic loading. However, no record could be found where the comparative studies covering various deficiencies were addressed together. Further, the nature and extent of damage in a structure during an

earthquake depends on the characteristic of loading. Thus, a holistic approach was initiated to cover different deficient cases of RC beam-column connections with different loading characteristic so as to gather a comprehensive knowledge about the behaviour of these connections. Generally, severely damaged structures are thought to be irreparable and are abandoned in spite of huge economic loss. To ensure further usability of the distressed or damaged structure, effective and reasonable techniques are needed to be investigated for rehabilitations of the damaged structures for post-earthquake usage.

Some of the researchers conducted tests on beam-column connections without considering the effect of size of the tested specimens. Moreover, most of the investigators conducted tests on scaled down models. The results of scaled down models cannot be used directly for prototype implementation in actual field as the size of specimen plays an important role. Available theories of material behavior that predict size effects are receiving increasing attention in the technical literature. Concrete is a heterogeneous material, which is generally full of micro cracks. Upon loading, these micro cracks propagate and the accumulation of such micro cracks leads to failure of specimens. It is well established that the mathematical modeling of such behavior should be based on the theories of fracture mechanics. Material models based on fracture mechanics can predict a size effect, if geometrically similar specimens of different sizes are considered.

Literature survey shows that the experimental study of size effect was primarily done for RC columns and beams. A beam-column connection which is vital structural elements and plays a very crucial role during earthquake needs attentions. Experimental studies on rehabilitation of such connections were also carried out without any due consideration to the size of specimens. Thus, it was felt necessary to explore the possibility of existence of size effect in RC beam-column connections before and after rehabilitations.

Various damage indicators that can quantify damaged structures are available in the technical literature. The index has the potential to play a vital role in rehabilitation / retrofit decision making. Making use of these indicators the damage level of a distressed specimen can be quantified and used by researchers for ascertaining the effectiveness of adopted rehabilitation technique for damaged seismic structural members. Further, in order to scientifically carry out repairing of distressed or damaged structures, guidelines are required so that an effective and reasonable rehabilitation technique can be employed for post-earthquake usage. These guidelines will be highly useful to the field engineers while taking decision to adopt an appropriate rehabilitation strategy during post disaster period.

Fragility functions are useful tools for post-earthquake damage assessment. There are many ways to obtain fragility functions. Developing fragility functions from experimental studies are considered to be the most reliable one among the different methods. However, development of fragility functions from experimental studies is not well reported, since such experiments involve time, infrastructures and sufficient investment. Thus, data generated from the experimental investigation of beam-column connections carried out in the laboratory, an attempt to develop specific repair-fragility functions were also undertaken in the present study.

Three common types of deficiencies in RC beam-column connections were considered and these specimens were tested under three loading types. Depending on the extent of damages, the damaged control specimens were rehabilitated with two rehabilitation strategies. These were (a) partial replacement of loose concrete on the damaged area by a high strength concrete (micro concrete) followed by epoxy injection into crack zone and (b) complete replacement of crushed concrete on the damaged area by a high strength concrete (micro concrete) followed by epoxy injection into crack zone. Forty two

specimens were tested (eighteen specimens each under loading type-1 and type-2 and six specimens under loading type-3) consisting of control and rehabilitated types of three different sizes. All the three dimensions of two third and one third scaled specimens were arrived at by geometrically scaling down the dimensions of full size specimens. The diameter of the reinforcing bars, development length, length of special confinement zone, cover of reinforcement etc. were also scaled down appropriately. All the constituent materials used for casting and rehabilitating the specimens were tested for various properties as per relevant codes.

A constant axial load on the column was maintained by hydraulic jack during testing to simulate gravity loading. An "*A* frame" was fabricated to facilitate the application of the axial load. Roller supports and fixtures were fabricated for maintaining symmetrical boundary conditions at the ends of the columns. The cyclic load was applied using a servo hydraulic dynamic actuators (MTS make). In order to explore the effect of loading characteristic on the performance of the connections, three different loading types were considered in this study. The loading types considered in the test program were characterized by a number of cycles for a particular displacement (type-1 and type-2) and frequency of excitations (type-3). The frequency of cyclic displacement under loading type-3 was kept as 1.0 Hz, which is forty times higher than those of loading type-1 and type-2. Displacement controlled loading was applied to all the specimens using a servo hydraulic dynamic actuators. Amplitude of the displacement histories were scaled down for two-third and one-third models. The data recorded from these tests were used for post processing to evaluate many important parameters related to seismic capacity of these connections such as load carrying capacity, stiffness degradation, energy dissipation, displacement ductility etc. Comparisons were made between the tests results of control and rehabilitated specimens in term of all the above mentioned parameters and

conclusions were drawn regarding the effectiveness of the adopted rehabilitation techniques.

The analysis of results revealed that the rehabilitated RC beam-column connections under different loading types exhibited equal or even marginally better performance than the corresponding control specimens and hence the adopted rehabilitation strategy could be considered as satisfactory.

The results obtained by testing the specimens were used to draw bi-logarithmic plots to explore the possible existence of size effect. It was observed that the bi-logarithmic plots for both control and rehabilitated specimens followed closely the size effect law as proposed by Bażant [1984] in all the cases studied. Parameter considered in the study such as cumulative energy dissipation and stresses also showed existence of size effect. Further, it was observed that the size effect became more pronounced with increase in brittleness of specimens.

The Park and Ang [1985] damage index model were employed in this study for evaluating the damage level of the connections in both control as well as rehabilitated specimens. It was observed that most of the rehabilitated specimens showed lower damage indices. Thus, it indicated that the adopted rehabilitation strategy was effective. Based on the above study, guidelines for rehabilitation of beam-column connections were prepared. These guidelines would be highly useful to the field engineers while taking decision on identification of an appropriate rehabilitation strategy during post disaster period. The prepared guidelines correlated the physical damage of specimens and the repair methods for restoring the damaged specimens to original state. Ultrasonic Pulse Velocity (UPV) was also used for assessing the quality of repair in the damaged zone.

Further, fragility functions for exterior RC beam-column connections were developed based on the results of current experimental studies. The results of this effort were families of fragility functions that would identify the required repair method for a damaged connection. Further, it was observed that the developed fragility functions for control specimens and corresponding rehabilitated specimens were of similar shape. Therefore, the probability of suitability a repair method would also be nearly same.

LIST OF TABLES

CHAPTER 7

CHAPTER 8

APPENDIX B

APPENDIX C

LIST OF FIGURES

LIST OF SYMBOLS AND ABBREVIATIONS

SYMBOLS

V_{col}	Shear force in Column
V_{jh}	Shear force in the beam-column joint
Z_b	Lever arm of beam in a beam-column joint
h_c	Depth of column in a beam-column connection
l_c	Distance between consecutive points of contraflexure in a column
C_b	Compressive force developed by compressive steel in beam
T_b	Tensile force developed by tensile steel in beam
V_b	Vertical beam shear on the face of the joint
M_R	The ratio of column-to-beam flexural capacity
M_c	Flexural capacities of the columns meeting at the joint
M_b	Flexural capacities of the beam meeting at the joint
μ	Displacement ductility factor
Δ	Displacement at any instant
Δ_y	Displacement at yield
Δ_{20}	Displacement at 20 % drop of peak load
Δ_u	Ultimate displacement
θ_u	Ultimate rotation
θ_y	Rotation at yield
μ_θ	Rotational ductility
ϕ_u	Ultimate curvature
ϕ_y	Yield curvature

μ_ϕ	Curvature ductility
βe	Energy parameter
σ_{N_U}	Ultimate stress at failure used in bi-logarithmic plot
B	Dimensionless constant used in Bažant's size effect law
f_t'	Tensile strength of concrete material
D	Depth of specimen
D_0	A constant with the dimension of length used in Baźant's size effect law
Φ	Standard normal (Gaussian) cumulative distribution function
θ	Median
β	Standard deviation
k_0	Initial tangent stiffness
k_m	Maximum stiffness
k_f	Element stiffness at failure.
$\Delta\delta^+$	Value of the positive change in plastic deformation
$\Delta\delta^-$	Ratio of the negative change in plastic deformation
$\Delta\delta_f$	Positive change in plastic deformation in a one cycle to failure.
$E_{p,i}^{\pm}$	Energy absorbed in a primary half cycle (PHC)
$E_i^{\pm}$	Energy of follower half cycle (FHC)
$E_f^{\pm}$	Energy absorbed in a monotonic test to failure
δ_m	Maximum deflection attained during seismic loading
δu	Ultimate deflection capacity under monotonic load
$\int dE$	Dissipated hysteretic energy
e_N	Energy dissipation per unit volume of D-region
E_S	Modulus of elasticity of steel
E_T	Tangent modulus of elasticity of steel

ϕ	Diameter of reinforcing bar
D_n	K-S test parameter
H_0	Null hypothesis
α	significance level
χ^2	Chi- Square

ABBREVIATIONS

ACI	American concrete institute
BWFLC	Beam weak in flexure large control
BWFMC	Beam weak in flexure medium control
BWFSC	Beam weak in flexure small control
BWFLRe	Beam weak in flexure large rehabilitated
BWFMRe	Beam weak in flexure medium rehabilitated
BWFSRe	Beam weak in flexure small rehabilitated
BWSLC	Beam weak in shear large control
BWSMC	Beam weak in shear medium control
BWSSC	Beam weak in shear small control
BWSLRe	Beam weak in shear large rehabilitated
BWSMRe	Beam weak in shear medium rehabilitated
BWSSRe	Beam weak in shear small rehabilitated
CWSLC	Column weak in shear large control
CWSMC	Column weak in shear medium control
CWSSC	Column weak in shear small control
CWSLRe	Column weak in shear large rehabilitated
CWSMRe	Column weak in shear medium rehabilitated
CWSSRe	Column weak in shear small rehabilitated
CDF	Cumulative distribution functions

DI	Damage index
DM	Damage measure
DS	Damage states
EDP	Engineering demand parameter
HYSD	High yield steel deformed
IS	Indian standard
K-S	Kolmogorov-Smirnov
LVDT	Linear-variable differential transformer
MPa	Mega Pascal
MS	Mild steel
PDF	Probability distribution function
RC	Reinforced concrete
UPV	Ultrasonic pulse velocity

CHAPTER 1

INTRODUCTION AND LITERATURE REVIEW

1.1 INTRODUCTION

1.1.1 Preamble

In the past, numerous reinforced concrete frame structures collapsed due to severe earthquake. Post-earthquake investigations into damaged structures generally showed that in many cases, damages of RC frame structure were localized in beam-column connections which might have led to partial or total collapse of the building. Further, it was observed that the exterior beam-column connections had suffered more in comparison to the interior ones. A typical case of distressed beam-column connections are shown in Fig. 1.1. The failure of these connections during past earthquakes opened a new research direction in the field of repair of damaged structures. Research in this area is essential as engineers in seismic-prone regions often face the task of analyzing and designing repair or strengthening works for damaged buildings. Thus, it is difficult to decide always whether to discard the damaged structure or to rehabilitate the same for retrieving the lost capacity without any quantitative guidance. After any major earthquake, there is a general concern on the issue of deciding the strategy of effective and reasonable rehabilitation of damaged structures for post-earthquake usage. Depending on the level of damage, location and usage of the structure, methodology of rehabilitation can be ascertained. However, in most cases, after a strong earthquake if the level of damage is severe then the structures are thought to be irreparable and are abandoned in spite of huge economic loss. In view of this, to ensure further usability, it is required to

quantify the damage in a structure after an earthquake. Various damage indicators that can correlate damage in concrete structure sustained during earthquake and the rehabilitation techniques are available in technical literature. These data are also used as guidelines for arriving at rehabilitation strategies.

(a) (b)

Fig.1.1 Distressed RC beam-column connections (a) during the 1999 Kocaeli, Turkey earthquake [Sezen *et al.,* 2000], (b) during 2009 L'Aquila Earthquake [Dr Anna Brignola, University of Genoa]

During the last few decades, several method of rehabilitation / strengthening of seismic deficient RC external beam-column joints and connections damaged by earthquakes have been reported. Of the various techniques, the most commonly used were jacketing with concrete and steel. These techniques possess its own practical limitations like labour intensive, artful detailing, increased dimension of structural element, susceptibility to corrosion etc. To overcome the difficulties associated with these techniques recent research efforts have focused on the use of epoxy-bonded fiber-reinforced polymer (FRP). This technique eliminates many of the previously mentioned limitations that concrete and steel jacketing possess. FRP jacketing has also been used as a strengthening technique for damaged RC beam-column joints region. Although the use of FRP jackets enhanced the joints seismic performance, anchoring of FRP materials has evolved as a difficult problem

for the effectiveness of this technique (Ghobarah *et al.,* 2002). Effectiveness of the above rehabilitation / strengthening technique however depends on the treatment provided to the fragmented concrete in the damaged region.

Depending on the level of damages, FEMA-308 [1998] provides a guideline regarding the various types of repairing techniques. In case of moderately damaged, the epoxy pressure injection technique was recommended. This technique includes injecting of a high strength epoxy under high pressure into the cracked zone of a structural element for the purpose of filling the cracks and adhering to the substrate materials. This ensures the restoration of the bonding of reinforcing bars and the surrounding concrete. In the case of highly damaged specimens, concrete with partial or complete removal and replacement of damaged portion is required. However, the repair material used must be compatible with the existing substrate. There are various products commercially available for repair of damaged concrete. Polymer-modified concrete (micro concrete) is the most cost effective one for improving the early compressive, tensile and flexural strength as well as in reducing the brittle nature of specimen. Repair of damaged RC element like beam, column, beam-column connections etc., where access is restricted and compaction is not possible, are carried out using micro concrete.

Further, many researchers conducted tests on beam-column connections without varying the sizes of tested specimens. Some tests results are available for scaled models for a particular deficiency. These results cannot be used directly for prototype implementation in actual field because the size of specimen plays an important role for various properties. Available theories of material behaviour that predict size effects are receiving increasing attention in the technical literature nowadays. It has been demonstrated that the size of the specimen plays an important role. However, in classical theories of solid mechanics, it is assumed that material properties such as the tensile or compressive strengths are not scale

dependent. In engineering practice, such properties are generally measured on standard samples of the material, and it is usually assumed applicable to structural elements whose size may differ from those of the test samples. Thus, the use of test results from standard specimen should be judiciously used in practice giving due consideration to the existence of size effect.

Fragility functions are useful tools for post-earthquake damage assessment. In most cases, results of previous experimental studies were used to developed empirical relationships between damage states and traditional engineering response measures, which are influence by many parameters such as loading sequence, geometry and specimens sizes, nature of test program etc. The correct identification of damage states which is associated with specific repair methods however depends on the correctness of information available from literatures, written documents or published photographs etc. Developing fragility functions from experimental studies were considered to be the most reliable one as it directly correlates the actual observed damage. However, development of fragility functions from experimental studies is not well reported, since such experiments involve time, infrastructures and sufficient investment.

1.1.2 Beams-column joint and connection

A beam-column joint is defined as that portion of the column within the depth of the deepest beam that frames into the column and while a beam-column connection is the joint plus the columns, beams, and slab adjacent to the joint [ACI 352R-02, 2002]. The role of the joints is to maintain the equilibrium and compatibility by transferring member-end-forces between the beam(s) and column(s). Connections exist in different types and forms in frame structures. The connection type is determined by the number and the configuration of the frame structures. Fig. 1.2 (a) shows the two dimensional

configuration of connections (corner, interior and exterior) in a moment resisting frame. The categorization is more complex for three dimensional space frames as shown in Fig. 1.2 (b) where the out-of-plane framing conditions must be considered. The severity of forces and demands during earthquake on the performance of these connections necessitate a comprehensive understanding of their seismic behavior. These forces develop complex mechanisms involving bond and shear within the joint.

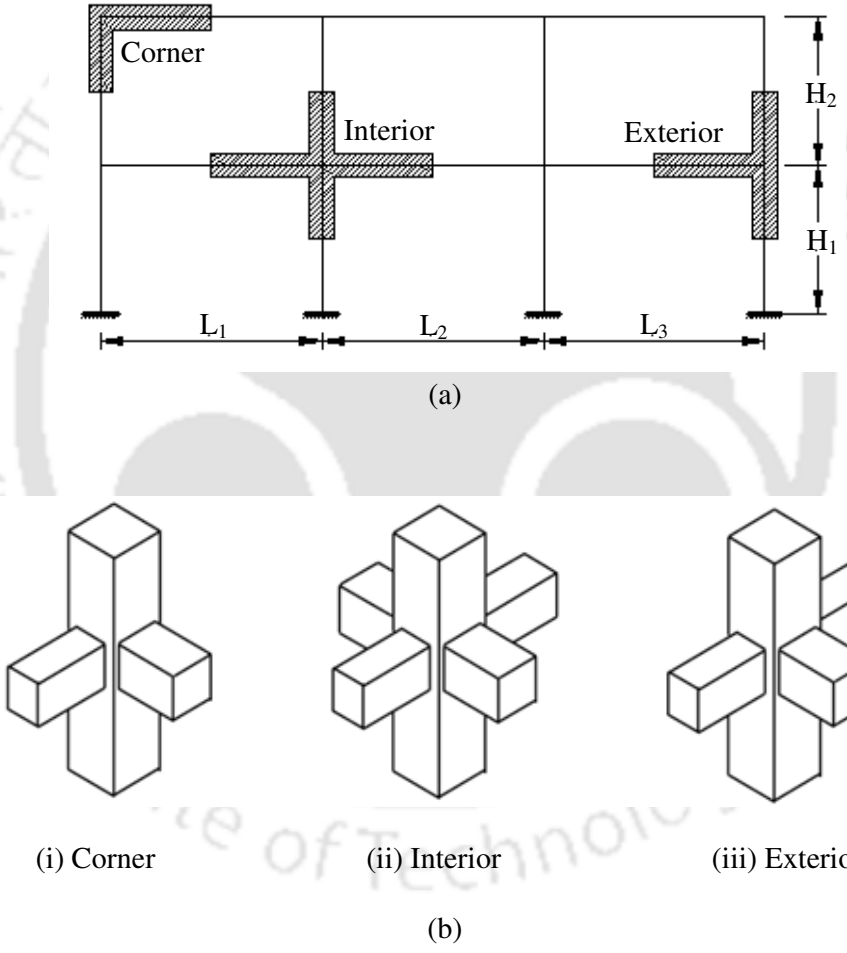

Fig. 1.2 Typical RC beam-column connections in (a) 2D and (b) 3D RC frame model

1.1.2.1 Forces on exterior beam-column connections

Post earthquake investigation on damaged structures showed that in many cases exterior connection suffered more in comparison to the interior. Hence a discussion on force system acting on exterior connections is furnished here. Fig. 1.3 shows the features of exterior beam-column connection, where one beam frames into the column. Based on the equilibrium principles, the shear force acting on the joint can be computed. From Fig.1.3 (b), it can be clearly observed that the nature of the bending moment above and below the joint changes and shows a steep gradient within the joint region. This causes large shear forces in the joint region as compared to that in the column. Fig. 1.3(c) indicates that the intensity of horizontal shear in the joint V_{jh} is typically four to six times as large as across the column V_{col} [Paulay, 1989]. The horizontal shear force across the joint can be obtained based on equilibrium criteria. Assuming the beams to be symmetrically reinforced, tensile force T_b and a compressive force C_b is developed in the beam reinforcement. The vertical beam shear on the face of the joint is V_b. Assuming $C_b = T_b$, the column shear (V_{col}) and the horizontal shear force (V_{jh}) in the joint can be calculated as follows:

The column shear force is

$$V_{col} = \frac{T_b Z_b + V_b h_c / 2}{l_c} \tag{1.1}$$

and the horizontal shear across the joint can be expressed as:

$$V_{jh} = V_{col}\left(\frac{l_c}{Z_b} - 1\right) - V_b\left(\frac{h_c}{2Z_b}\right) \tag{1.2}$$

In the above equations, h_c is column depth, l_c the center-to-center height of the column and Z_b is the lever arm.

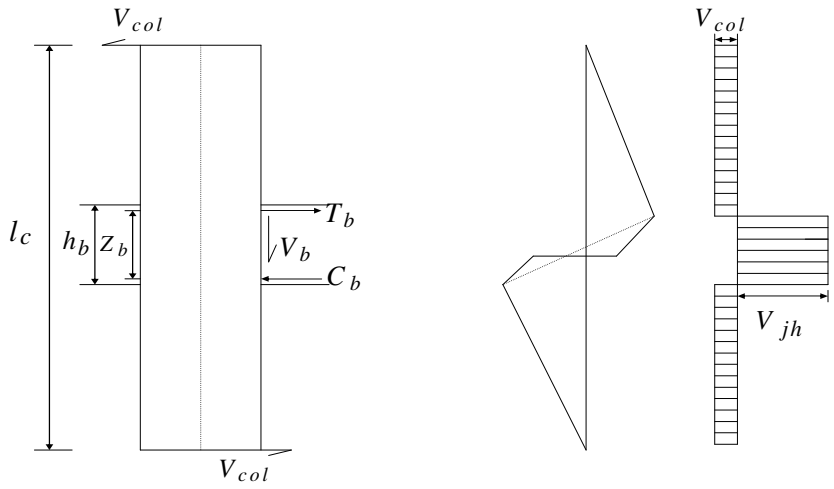

(a) Forces on column (b) Bending moment diagram. (c) Shear force diagram

Fig. 1.3 Free body diagram of exterior beam-column connections [Paulay, 1989]

1.1.2.2 Strong column-weak beam principle

According to this design principle, connections are to be designed in such a way that the joint region and the column remain essentially elastic under the action of high lateral loads such as earthquake and high pressure winds while the main energy dissipation occurs within the plastic hinges formed in the beams. One of the factors to ensure a strong column-weak beam in a ductile moment resisting framed structure is restricting the value of M_R (ratio of column-to-beam flexural capacity) and it is given by the equation.

$$M_R = \frac{\sum M_C}{\sum M_B} \tag{1.3}$$

where $\sum M_C$ is the sum of flexural capacities of the columns meeting at the joint under consideration and $\sum M_B$ is the sum of flexural capacities of beams at the same joint. The strong column-weak beam criteria is satisfied if M_R in Eq.1.3 is greater than 1.1 [Jain and Murty, 2006] or 1.2 as per American standard ACI 318 [2005] respectively.

1.1.2.3 Ductility of RC structures

Ductility is basically the ability of a structure to accommodate deformations well beyond the elastic limit. It is the capacity to dissipate energy in hysteretic loops and to sustain large deformations. For this reason, it is the most important characteristic required to be sought in the design of buildings that are located in earthquake prone regions. Therefore, a designer must carefully select the design parameters to ensure adequate ductility in the joints. Any rehabilitation/strengthening techniques should ensure that it does not reduce the ductility from the original level. Rather, it should enhance the ductility of original structure, if possible. Ductility demand on a structure subjected to a severe lateral force can be estimated analytically by nonlinear time-history analysis. It can also be estimated experimentally by shaking table or pseudo dynamic tests. Ductility factors have been commonly expressed in terms of various response parameters such as displacements, rotations and curvatures. The displacement ductility factor μ is defined by the ratio of the total imposed displacement Δ at any instant to that at the onset of yield Δ_y. Using the idealized behaviour as shown in Fig. 1.4, the displacement ductility may be written as:

$$\mu = \Delta / \Delta_y \tag{1.4}$$

The ductility developed, when failure is imminent is written as:

$$\mu_u = \Delta_u / \Delta_y \tag{1.5}$$

Another common ductility term is the rotational ductility defined as:

$$\mu_\theta = \theta_u / \theta_y \tag{1.6}$$

where θ_u is the maximum rotation at the plastic hinge and θ_y is the corresponding rotation at the onset of yield.

Structural designers however, sometimes desire to evaluate curvature ductility defined as:

$$\mu_\phi = \phi_u / \phi_y \tag{1.7}$$

where ϕ_u is the maximum curvature expected to be attained and ϕ_y is the yield curvature.

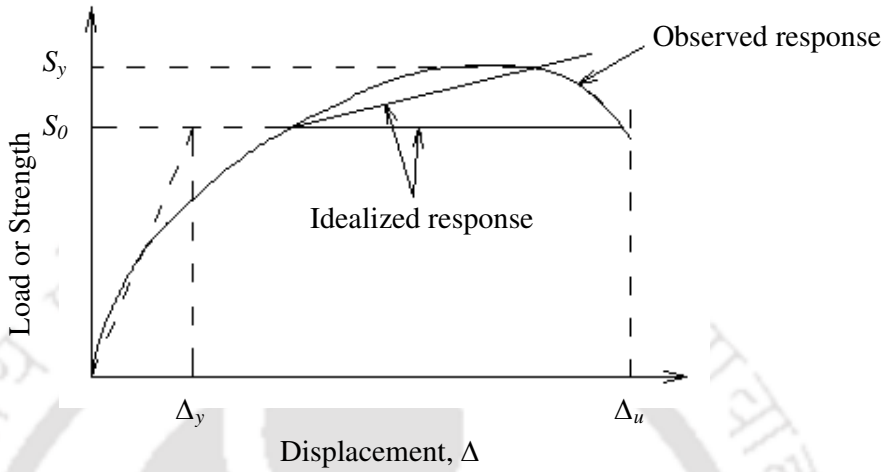

Fig. 1.4 Typical load-displacement relationship for RC ductile element [Paulay and Priestley, 1992]

For estimation of ductility factors, the yield deformation of structures (displacement, rotation or curvature) is required. This is however difficult to estimate since the load deformation curve may not present a well-defined yield point. Fig. 1.5 illustrates various alternatives definitions which have been used by researchers to compute the yield displacement.

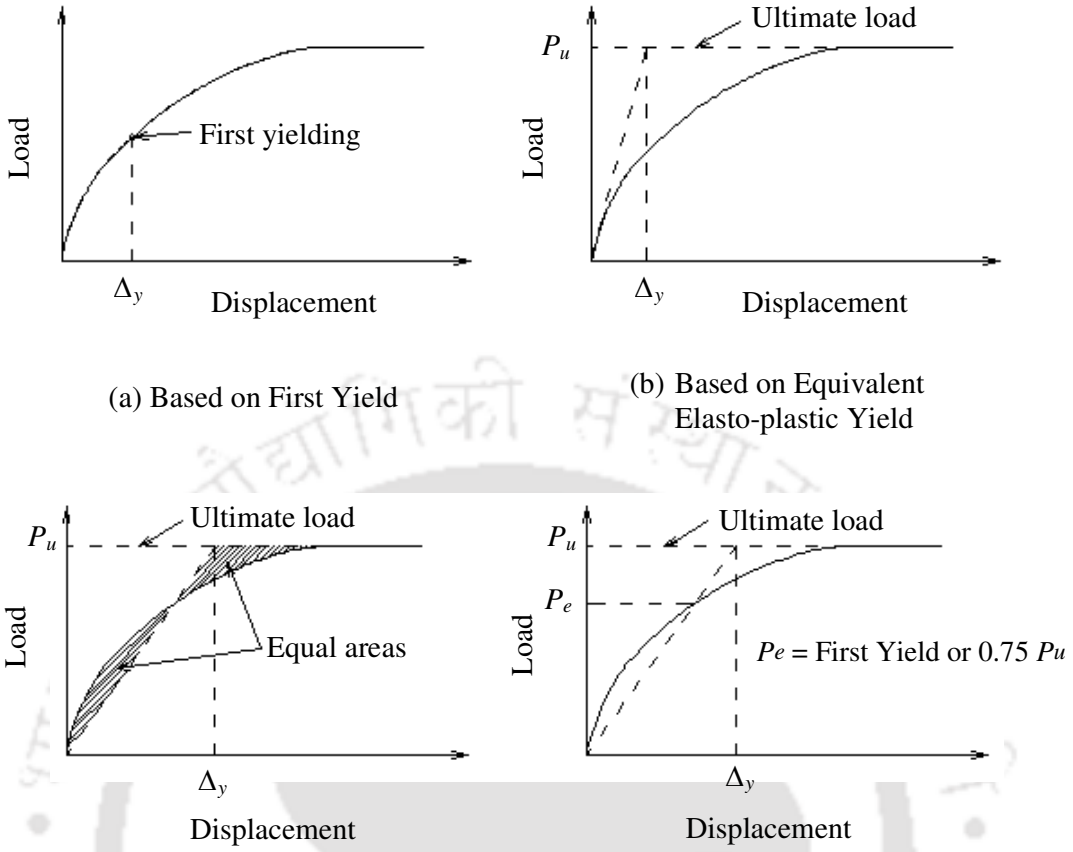

Fig. 1.5 Alternative definitions for yield displacement [Park, 1986]

1.1.3 Rehabilitation technologies

Rehabilitation is aimed at repairing of distressed or damaged structural components. The scope of repairs for individual structural element depends on the objectives of the repair program. This section presents a series of repairing techniques which can be used to restore damaged reinforced concrete structural components to its original seismic and ductility capacity.

A number of studies have addressed the repair of reinforced-concrete components damaged as a result of earthquake events. Testing of repaired / rehabilitated connections

was performed by Tsai [1992], Filiatrault *et al.* [1996] and Karayannis *et al.* [1998]. Application of repair techniques after damaging the connection provided information regarding the effectiveness of the repair. Tsai [1992] and Filiatrault *et al.* [1996] described the improvement of the behavior of the connection after injection of epoxy resin at cracked region. Karayannis *et al.* [1998] prescribed properties of the cementitious material for patching of spalled and crushed concrete. Pagni and Lowes [2006] reviewed the results of previous experimental research, reviewed manuals of standard practice and interviewed practicing engineers to identify following information:

(a) the repair method that could be used to restore the strength and stiffness of damaged RC components due to seismic events.

(b) damage level that would help in deciding the use of a particular repair method.

Specifically, FEMA 308 [1998] and ACI 546-96 [1996] were used by many researchers as a basis for defining and validating repair method.

The repair techniques were organized into five repair methods progressing from the minimal to the most substantial. These are:

(a) Cosmetic Repairs

When earthquake damage is limited to minor cracking, the strength and stiffness degradation of the component will be insignificant and repair will not be required to restore the component to pre-earthquake conditions. Cosmetic repair is required when damage is sustained by the finish. Removal and replacement of the damaged finish materials define this method of repair. These repairs have no structural impact and do not contribute to strength or stiffness of the component. Pagni and Lowes [2006]

recommended employing cosmetic repair method for hairline cracking up to a maximum crack width of 0.02 in (0.5mm).

(b) Epoxy injection into cracked zone

Injection with epoxy at cracked zone consists of applying a structural binding agent into cracked part for the purpose of filling the crack and adhering to the substrate materials. Various types of materials and methods can be used for injection depending on the required performance. Crack width as small as 0.002 in can be injected with epoxy. However, crack width upto 0.012 in can be permitted in RC in humid or moist air conditions (ACI-224r, 1994a). Epoxy injection is typically accomplished either by drilling holes along the cracked zone and using pressure injection to push epoxy through these holes or by injecting into one area of cracking in the specimen and applying a vacuum to another area of cracking to pull the epoxy through. Studies conducted by French *et al.,* [1990] confirmed that epoxy injection can effectively restore the bond with reinforcing bars. However, there need to be sufficient amount of cracked surface around the debonded reinforcing bars for the epoxy to penetrate along the surface of the reinforcing bars to restore the bond. For the current study, specimens with maximum crack width in excess of 0.02 in (0.5mm) have been considered for epoxy injection.

(c) Patching of spalled concrete

Experimental investigation of joint response showed that the concrete covering column longitudinal reinforcement in the joint region will spall under moderate earthquake loading. Spalled concrete needed to be brushed away prior to repair exposing the undamaged aggregate and the rebar underneath. Previous research showed that patching spalled concrete with a cementitious material could restore strength and stiffness to the

original components. Cementitious materials possessing properties such as low shrinkage, high compressive and tensile strength, rapid hardening were used by Karayannis *et al.* [1998] for repairing an exterior connections that exhibited spalling of concrete cover. The test results showed that the performance of repaired joints were comparable to that of the original.

(d) Removal and replacement of damaged concrete

The removal and replacement of the damaged concrete in a component may be required if earthquake loading on the joint is severe. Spalling of cover concrete is extensive or concrete damage extends to crushing in the joint core resulting in exposure of the column and/or beam longitudinal reinforcement. The concrete may separate from the component due to severe cracking that completely disintegrate joint core concrete. To ensure that full bond capacity is recovered, all of the damaged and potentially damaged concrete must be removed and equal amount of new material must be added.

(e) Removal and replacement of damaged Rebar

Longitudinal reinforcement in a column may buckle or fracture under earthquake loading. Action in this repair method includes removing concrete using chipping or jack-hammering, removing the damage sections of reinforcing bars, replacing the reinforcing bars and fresh concreting is done. Mechanical connections such as a sleeve, splice, or threaded coupler are generally used to connect new and existing reinforcing bars (FEMA 308, 1998).

1.1.4 Size effect law

Classical theories assume that the strength of geometrically similar structural elements is not size dependent. This assumption is based on plasticity analysis. Concrete structures, which are quasi-brittle in nature, however do not follow this trend. Therefore, the size effect implies the dependence of strength of structural elements on its size. The strength is usually defined as nominal stress at peak load. The size effect involves the variation of nominal strength σ_{N_U} with the characteristic dimension of the structure, *D*. There are various possible correlations of the size effect, but bi-logarithmic representation is the most accepted one. In bi-logarithmic plot, log σ_{N_U} is plotted against log *D*. The size dependency of concrete structural elements may be described by the size effect law proposed by Bažant [1984] covering various practical cases. The mathematical expression of this law is given as:

$$\sigma_{N_U} = \frac{Bf_t'}{\sqrt{1+\frac{D}{D_0}}} \tag{1.8}$$

where, f_t' is the tensile strength of concrete, *B* and D_0 are two empirical constants depending on the shape of structures and obtained by linear regression analysis of the test results. D/D_0 is the relative structural size ratio. Fig. 1.6 show a typical plot where strength theory based on yield or strength criteria predicts no size effect, represented by horizontal line. The size effect is stronger with the response lying closer to the linear elastic fracture mechanics (LEFM). With the help of LEFM it is established that the slope of the bi-logarithmic plot for brittle material is -1/2.

Further, it can be noted that for small specimen, $D << D_0$ and hence Eq. 1.8 gets modified as

$$\sigma_{N_U} \simeq Bf_t' \tag{1.9}$$

where as, for large specimen, $D >> D_0$ and hence Eq. 1.8 yields

$$\sigma_{N_U} \propto D^{-1/2} \tag{1.10}$$

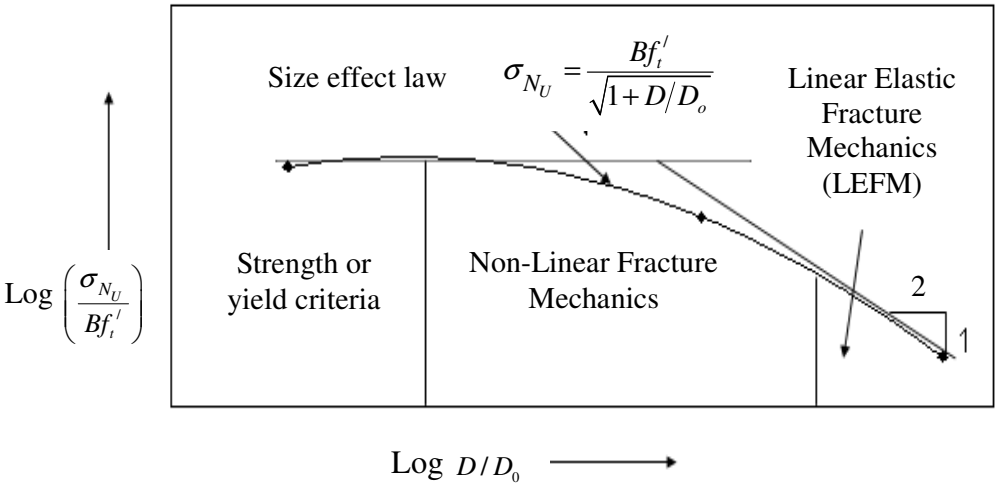

Fig. 1.6 Plot of size effect law [Bažant, 1984]

To facilitate the evaluation of the constants in the size effect law, Eq. 1.8 can be rearranged as follows:

$$\left(\frac{f_t'}{\sigma_{N_U}}\right)^2 = \frac{1}{D_0 B^2} D + \frac{1}{B^2} \tag{1.11}$$

The above equation is of the form of $Y = AX + C$ where $Y = \left(f_t'/\sigma_{N_U}\right)^2$, $X = D$ and the constants C and A are given by $C = 1/B^2$ and $A = C/D_0$. Since σ_{N_U} and f_t' are known for various values of D, a plot of $\left(f_t'/\sigma_{N_U}\right)^2$ against D allows C and A to be determine from a regression analysis of the test result as shown in Fig. 1.7.

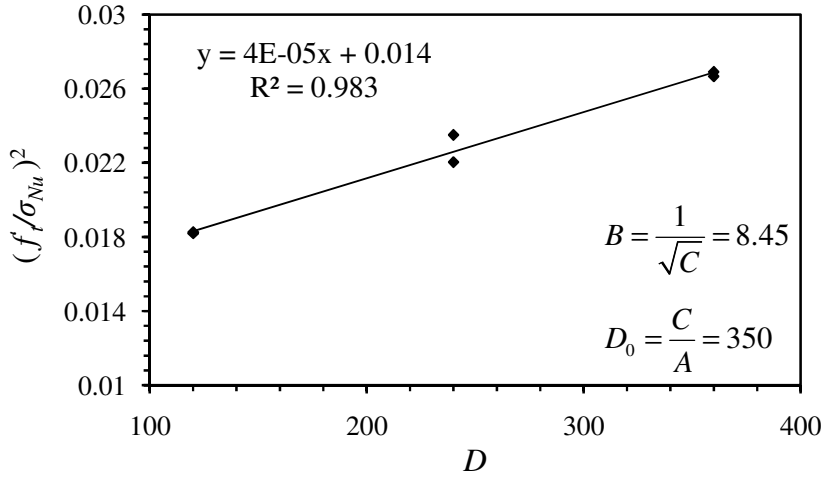

Fig. 1.7 Typical regression plot

Further, the existence of size effect may be attributed to various factors (Bažant and Planas, 1998):

1. Boundary layer effect (also known as wall effect).
2. Diffusion Phenomena (such as heat conduction or pore water transfer).
3. Hydration Heat (or other phenomena associated with chemical reaction).
4. Statistical size effect.
5. Fracture mechanics size effect.
6. Fractal nature of crack surfaces.

The size effect can be observed if models of different scale are considered by maintaining geometric similarity i.e. when similitude criterions are strictly followed.

1.1.5 Damage indices

Damage in reinforced concrete structures during an earthquake may be due to excessive deformations or it may be accumulated damage sustained under repeated loading. Cyclic loading may accumulate damage in the member in terms of strength deterioration, stiffness degradation and low-cycle accumulation. However, small amplitude cycles

within the elastic limit cause insignificant and negligible damage in terms of minor cracking. The accumulated damage is expressed in terms of plastic deformations or in terms of hysteretic energy absorbed during the loading. Low-cycle accumulated damage can however be an important issue depending on the amplitude and number of inelastic cycles since earthquake loading induces large inelastic reversals. Therefore, a damage index is aimed to provide a means of quantifying damage in concrete structures with particular reference to their use in rehabilitation, strengthening or retrofit decision making. In most cases damage indices are dimensionless parameters intended to range between 0.0 for an undamaged element and 1.0 for a completely failed element, with the intermediate values giving some measures of the levels of damage.

1.1.6 Fragility functions

The demand parameters commonly referred to as the engineering demand parameter (*EDP*) is the measure of earthquake demand on a structural component. The *EDP* should reflect the deformation and the fatigue sustained by the joint. A damage measure (*DM*) is a measure of damage sustained by a structural component. *DM* is quantified as damage states (*DS*). The *DS* describe the progression of damage sustained by a joint under seismic loading. Different categories of repair method are used to repair these *DS*. Probability models links the *EDP* to the *DM* and ultimately to the method of repair. The probability of exceeding the damage requiring a specific repair method is modeled in the form of fragility curves. In brief, a fragility functions defines the probability that damaged structure will require the use of a specific repair method to restore a joint to its original conditions for a specific level of earthquake demand. The data used to generate the fragility curves is the damage data derived from the experimental studies. Therefore,

experimental data, demand parameters, damage state and the repair methods are the basic parameters for developing specific-repair fragility functions.

Previous studies (Shome and Cornell 1999, Shinozuka *et al.* 2000, Aslani 2005) showed that lognormal distributions are the commonly used distribution for development of fragility functions. The lognormal distributions can be expressed in the form of two-parameter (median, θ and logarithmic standard deviations, β). Estimation of these parameters performed with the aid of the maximum likelihood method.

Fig.1.8 (a) shows the form of a typical fragility functions when plotted in the form of a cumulative distribution function and Fig.1.8 (b) shows the calculation of the probability that a component will be in damage state *i* at a particular level of demand, *d*. Each level of demand in Fig.1.8 (b) corresponds to a specific repair effort (repair methods to restore damaged concrete elements to an undamaged state).

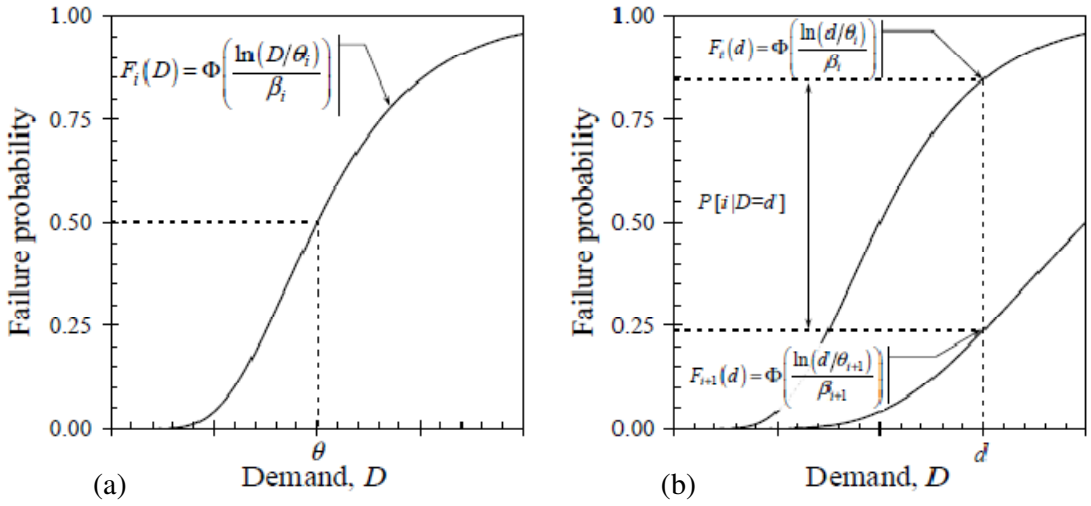

Fig. 1.8 (a) Typical fragility functions (b) Evaluating individual damage-state probabilities [Porter *et al.,* 2007a]

1.2 LITERATURE REVIEW

Wealth of literatures related to experimental investigation on RC beam-column joints and connections are available. A detailed survey has been carried out to identify the research objective. In this section, works carried out by the past researchers have been discussed and their important features have been highlighted with critical comments. Review presented in this section has been grouped into the following five different categories:

i) Experimental studies on RC beam-column joints and connections

ii) Rehabilitation / strengthening of damaged RC beam-column joints and connections with concrete jacketing, steel jacketing, epoxy repairing and FRP wrapping

iii) Size effect of concrete structural elements

iv) Seismic damage indices for RC structures

v) Development of fragility functions

1.2.1 Experimental studies on RC beam-column joints and connections

The first experimental study on RC beam-column joint was conducted in the United States by Hanson and Connor [1967]. In their study seven exterior beam-column joints were tested under simulated cyclic earthquake loading. Performance of these specimens including moment capacities at first yield of reinforcements, ultimate moment and ductility of the assemblies, maximum beam deflection and anchorage bond stresses of beam reinforcements were reported. The authors concluded that properly designed cast-in-situ RC frames could resist severe earthquakes without loss of strength and moderate earthquakes without damage. These tests became the standard reference for subsequent investigations.

Megget and Park [1971] reported experimental investigation on the behaviour of exterior RC beam-column joints subjected to seismic loading with a low column axial load. Three specimens were designed using different methods, which were tested under the same cyclic loading in their investigation. The authors found that the joints of the specimens were not adequately reinforced against large shear stresses at inelastic loading conditions.

Scribner and Wight [1980] investigated the strength decay in RC beam-column joints under load reversals. Eight half-scale and six full-scale RC exterior beam-column connections were tested in order to study the effect of intermediate longitudinal reinforcement on shear deterioration of flexural members subjected to repeated type of loading. Some specimen contained only vertical web reinforcement while some contained intermediate vertical reinforcement along with vertical web reinforcement. Specimens were tested under displacement-controlled cyclic loading. The authors concluded that severe loss of strength and energy dissipation was observed for the members which were subjected to high shear stress. It was also concluded that the increase in size of vertical ties increased the energy dissipation capacity along with damage at a concentrated location, while longitudinal intermediate bars was capable of spreading the damage throughout the beam plastic hinge region.

Durrani and Wight [1985] reported results of an experimental investigation on the performance of an interior beam-column joint under earthquake-type loading, which had less joint reinforcement than recommended by ACI-ASCE Committee 352. They concluded that the joint shear stress had a pronounced effect on the behavior at large ductility levels and the joint hoop reinforcement. Some guidelines were suggested to simplify the design of joints.

Shah *et al.* [1987] reported the effects of loading rates on the performance of RC beam-column joints. Small scale joints designed as per ACI codal provisions were tested under

two cyclic loading rates of 0.025 Hz and 1.0Hz. The author concluded that at the faster rate the maximum load carrying capacity of the specimens was higher. Further, the faster rate of loading caused greater damage and produced more localized cracks than that at slower rate. Thus, it was indicated that the rate effect is related to the transfer of forces between reinforcing bars and concrete.

Abdel-Fattah and Wight [1987] studied the relocating of plastic hinging zones for earthquake-resistant design of RC buildings. In their investigation, twelve full-size interior beam-column connections were tested under cyclic loads. In addition to the main reinforcement in beam, intermediate longitudinal reinforcing bars were passed through the joint and were extended up to a specific length away from the column face in beam. The aim of the research was to relocate the potential beam plastic hinges away from the column face by the addition of these intermediate longitudinal bars. Three basic modes of failure including joint shear failure, localized beam hinging zone and distributed beam hinging were observed in their tests. The authors concluded that the performance of extra reinforcement in the joint could help in successfully relocating the plastic hinge away from the column face.

Ehsani and Alameddine [1991] investigated the behaviour of corner joints constructed with high-strength concrete. Twelve specimens were tested in their study in order to examine the recommendations of ACI-ASCE Committee 352 on the design of high-strength ductile moment resisting beam-column joints. The authors showed that the recommendations which were developed for normal strength concrete could not be applied to high-strength concrete frame. They presented new requirements such as allowable joint shear stress and joint confinement for ductile design of RC beam-column joints.

Tsonos *et al.* [1994] tested fourteen exterior joints to study the effect of variable axial loading in comparison to constant axial loading. The main variables for the study were the axial load, ratio of column flexural capacity to that of the beam, the joint shear stress level and the amount of transverse reinforcement in the joint. The authors concluded that the increased axial load lead to major deterioration of the joints.

Chutarat and Aboutaha [2003] investigated a solution for relocating potential beam plastic hinge zones by the use of headed bars in the exterior RC joints. Four large-scale beam-column connections, with and without headed bars, were tested under quasi-static cyclic lateral loads. The results showed that straight-headed bars could relocate beam potential plastic hinge regions very effectively.

Murty *et al.* [2003] tested twelve half-scale exterior beam-column joints under displacement-controlled cyclic loading to study the effectiveness of anchorages of longitudinal beam bars and the transverse reinforcement in the joint core. Four different reinforcement details for anchorage into the column for beam longitudinal bars were followed. The authors concluded that out of all the different joint reinforcement detailing investigated, the performance of the joint constructed following ACI standard hook was the best and it was easy to construct as well.

Joshi *et al.* [2005] tested four full scale exterior precast beam-column joint under cyclic loading in order to identify a suitable technique for connecting precast beam and column components. Following two different types connection techniques, precast and monolithic specimens were cast. Out of two types of detailing, one was done by the provisions of Indian standard code while the other was cast by using single U bar as top and bottom reinforcement of beam. The column was placed horizontally and beam was placed vertically in the test set up. The axial movement of the column was restrained by providing stiff supports fixed to the strong floor by steel studs. The ends of the column

were supported on rollers equidistant from the beam centre. The authors concluded that the performance of the monolithic specimen with U bar detailing was better than all other types of joints used in their study.

Nie *et al.* [2008] tested six beam-column joints comprising of three interior and three corner joints for proposing a new connection system for concrete filled steel tube composite column and RC beams. According to the new system, the column was encased by a steel tube. The tube was cut at the beam-column joint and the steel reinforcing bar in the RC beam was kept continuous at the floor level in which concrete was confined by multiple lateral hoops in the joint region. The specimens were tested under cyclic loading. The authors concluded that the new connection was capable of dissipating enough energy in addition to showing a good performance from ductility aspect.

Li and Kulkarni [2010] carried out an experimental and numerical investigation on RC wide beam-column joints subjected to seismic loads. It was concluded that wide beam-column joints when designed with suitable parameters would perform quite well in carrying the horizontal lateral loads. Moreover, due to the larger section of the wide beam, the shear stresses in the beam transverse reinforcement were very low and therefore, the requirement of beam shear reinforcement might be relaxed.

Choudhury [2010] tested beam-column connections with three typical deficiencies and three geometrically similar specimens of full scale, two-third scale and one-third scale sizes. All specimens were subjected to slow cyclic loading test. The performances of the connections in each category were evaluated in terms of displacement ductility, cumulative energy per unit volume, cumulative energy dissipation, variation of stress with deflection etc. The study was aimed at to explore the existence of size effect and it was observed that the size effect in RC beam-column connection followed closely the law proposed by Bažant [1984].

The literature survey revealed that the test on beam-column joints and connections were initiated as early as 1967. Since then, other research studies were carried out to improve the performance for beam-column joints and connections. Experimental studies were conducted on both exterior and interior joints/connections on full scaled as well as scaled down specimens. Quasi static loading were used by many researchers to simulate the seismic actions. These frequencies are however substantially lower than those corresponding to the frequencies of actual seismic excitations. Characteristic of loading such as number of repeated loading cycle of displacement, frequency of excitation and the level of excitation plays a vital role in the behavior of the joints and connections. However, very little informations were reported on the performance of beam-column connections considering different deficiencies of these connections having different sizes and subjected to different loading characteristics.

1.2.2 Rehabilitation / strengthening of damaged RC beam-column joints and connections

Research on the rehabilitation/strengthening of beam-column joints and connections included jacketing with concrete or steel, epoxy repairing and FRP sheet wrapping. The available literatures are discussed in the following sub-sections.

1.2.2.1 Concrete Jacketing

The earliest conventional method for rehabilitations of concrete frames was to provide an RC jacket on the damaged zone. These jackets are usually constructed with high-strength concrete, additional longitudinal and transverse reinforcement also may be added. Brief review on some of the past researches where concrete jacket were employed is given below.

Corazao and Durrani [1989] tested three single (two exterior and one interior) and two multiple connections, some including a floor slab by jacketing the column, the joint region and some portion of the beam damaged by earthquake. Due to the difficulties experienced with in-place bending of the crossties hooks in the joint region, the additional joint reinforcement was modified to a set of dowel bars with a hook. The repaired specimens including the enlargement of section and addition of rolled steel elements. The repaired techniques were successful in restoring strength, stiffness and energy dissipation capacity of all three single joints. In some of the specimens, the damage was successfully moved away from the column face due to the added beam bottom bars hooked both in the joint. However for a multiple joint the technique was unsuccessful in improving the behavior. The authors concluded that load transfer mechanism between beams and column should be well addressed for a multiple joints; simply jacketing the column alone will not improved the performance of the joints.

Alcocer and Jirsa [1993] performed experiments to study the suitability of jacketing of non-ductile frame elements as a rehabilitation technique. The need to drill holes through the beams for placing joint confinement reinforcement was eliminated. This was achieved by welding a steel cage around the joint. The cage was made by steel angles and flat bars. It was reported that the steel cage and the cornet ties confined the beam-column joint satisfactorily up to 4% drift. Important findings indicated that the shear strength of jacketed joints could be estimated using current recommendations for the design of beam-column joints in new construction. It was suggested that the current criteria on bar development should be met by longitudinal reinforcement in the jackets.

Stoppenhagen *et al*. [1995] repaired a two-third scale model of two bays and two stories of an exterior moment-resisting frame with heavily damaged columns. The damage was characterized by heavy shear cracking and spalling of concrete in the window space

between the spandrel beams. In addition to repairing the damaged, the new columns were designed to increase the lateral capacity of the frame and to shift the mode of failure from shear in the columns to flexural hinging in the beams. The test results under applied cyclic loading indicated that the columns were successfully repaired and that the governing failure mechanisms of the frame were successfully achieved. The results also indicated that the encased columns behaved monolithically and that the lateral strength of the frame was substantially increased.

Hakuto *et al.* [2000] tested three one-way interior beam-column joints with no joint reinforcement. The damaged specimens were rehabilitated by RC jacketing provided at the beams, columns and joints. The core of the joint strengthened by plain circular hoops, which was made up of two circular U-shaped ties placed through holes drilled in the beams and welded in place. The undamaged specimens were strengthened by providing column jacket only. The strengthening scheme changed the behaviour of the joint in ductile mode with formation of plastic hinges in beam, except for the specimen in which only column jacket was provided. The major drawback of this technique was the addition of joint core hoops was very labor-intensive.

Tsonos [2002] studied the effectiveness of RC jackets applied in areas which were inaccessible due to presence of adjacent structures in one or more sides of the columns and beam-column connections. A two sided-concrete jacket with strength of 60 MPa was used for repairing. Additional joint ties were placed by coring the beam and short bars were placed in a transverse direction inside the hooks of the beam. The author reported that the mode of failure before jacketing which involved severe loss of joint core was significantly improved. A formation of a beam hinge and buckling of beam bars after jacketing were also observed.

Bligh *et al.* [2005] used concrete jackets as a rehabilitation scheme to enhance the confinement that would be provided by framing members on all four sides of the connections. Due to concrete jacketing, the clear span of beams and columns were reduced which led to increase in shear demand in beam and column. Their study suggested that re-checking of the shear strength must be done for structural components after repaired with a concrete jacket.

Karayannis *et al.* [2008a] rehabilitated ten exterior beam-column connections where a thin RC jacket with light and dense reinforcement of small diameter has been provided locally at the damaged joint region and partly at beam / column. The jackets were made of a high strength, nonshrink and flowable cement mortar. The authors observed that apart from exhibited higher values of load carrying capacity and hysteretic energy dissipation, locally applied jacketing improves the damage behaviour of the joint by changing the brittle failure mode to a ductile one. Furthermore, the authors indicated that the structural geometry and building mass were not modified as the damaged regions were encased with a thin jacket. Therefore, the dynamic characteristic of the structures remain practically unaffected. They also suggested that RC jacket enhances the beam flexural strength due to beam rehabilitating and shear strength capacity accordingly increase. Thus, in real structures an after-repair shear capacity check has to be performed in order to re-establish the capacity design concept for the whole building.

1.2.2.2 Steel Jacketing

Jacketing by steel plates fabricated in different configurations has been used for damaged and undamaged deficient beam-column joints and connections to increase the strength and ductility. The space between the jacket and RC members is grouted with non-shrink

or epoxy materials. Attaching steel plates are also mechanically anchored to the concrete to improve confinement.

Moshe *et.al* [1993] tested and evaluated the repair technique on four scaled (1/7.5) heavily damaged T-beam section by attaching thin plates of different configuration for the repair of joints. The peripheries of the plates were sealed by quick setting epoxy and high strength epoxy resin was injected through the inlet holes. Prior to the injection, the concrete from deteriorated joint region were removed and patched with a commercial, ready-to-use powder (mortar is rheoplastic, flowable and nonshrink with high bond to steel and concrete). Authors concluded that the test results were satisfactory as the repaired joints were capable of resisting harder cyclic loadings. They recommended that the technique could be used for mass repairing or upgrading of structures not suitably designed to withstand earthquakes. Even though the technique is found to be simple and efficient yet doubt remains on the injected epoxy to fill all the internal cracks. Otherwise, bonding between reinforcement and deteriorated concrete will not be achieved.

Hadi [2010] rehabilitated an RC T- connection using a galvanized steel strap attached to the concrete surface. Prior to the attachment of steel plate with high strength epoxy, all visible cracks (0.01-0.2mm) were gravity filled with thin epoxy resin. A steel jacket of galvanized sheets (0.55mm thick) was used to externally reinforce the connection by fitting and strapping it with steel strap. The purpose of the steel strap was to provide confining pressure. The rehabilitated specimens were retested in the same way as were done for the original specimens. An increase in the ultimate load carrying capacity of about 88 % was achieved. Although the reinforcing steel yielded during the initial test, the rehabilitated specimen was still capable of carrying considerable loads before failure. Thus it is observed that repaired specimens using the epoxy performed satisfactorily.

However, it is difficult to judge the contribution of the external steel reinforcement on the performance of the structures.

Sasmal *et al.* [2010] proposed a technique for repairing and strengthening of non ductile beam-column connections. The specimens designed as per Indian codal provision with consideration of seismic loads but without adopting ductile detailing. The technique was a combination of epoxy mortar injection, steel plates strengthening and FRP wrapping. The damaged specimens were repaired using an epoxy mortar for filling the cavities, internal cracks were grouted with low viscous polymer and then beams and columns were wrapped with FRP. The joints were confined with the provision of steel plates tightened with bolts. The experimental results showed that the repair and strengthened specimens not only regained its original strength and stiffness but also overcame the deficiencies of non ductile specimen. Further, the authors indicated that hybrid strengthening techniques consisting of FRP wrapping and steel plates jacketing could overcome the well known constraint of both the materials.

1.2.2.3 Epoxy Repairing

Epoxy pressure injection technique has been normally used for repairing moderately damaged RC structures. However, for highly damaged case, partial or total removal and replacement of damaged concrete is required. Usually a high-strength, low or non shrink concrete is used as a replacement materials. Some of the past researches where these techniques were employed are summarizes here.

Popov and Berbeto [1975] presented a comparison of performance of reinforced concrete interior beam-column connections tested under cyclic loading with that of a repaired specimen using epoxy resin. The results showed that the repairing technique could restore the destroyed bond between the concrete and the reinforcing steel.

Lee *et al.* [1980] investigated the effectiveness of repairing of RC exterior beam-column connections. The epoxy injection technique and the removal and replacement technique using with high early strength materials were used to repair the beams of the connections. They observed that there is possibility of damage moving from the beam to the unrepaired joints and column because of the increase in beam strength due to the use of high strength repair materials. However, the over all performance was acceptable.

Corazao *et al.* [1988] investigated the effectiveness of different repairing and strengthening techniques in restoring or improving the seismic parameters of RC beam-column connections damaged by earthquake loading. The author concluded that the performance of specimens repaired with epoxy injection rely on the quality of the injection works. Further, the data obtained from testing of a repaired specimen that involved the removal and replacement of the damaged concrete in the joint region demonstrated that the stiffness and strength of the specimen had been completely restored.

French *et al.* [1990] conducted two test series in order to determine the effectiveness of epoxy techniques for repairing damaged joints. They pre-loaded two interior RC joints and then repaired one with pressure injection and the other by vacuum impregnation. Their repaired specimens were then subjected to the same load history as that was imposed on the original test specimens. The authors concluded that both techniques worked well in restoring the strength, stiffness, energy-dissipation capacity and the bond. Authors recommended the vacuum impregnation technique due to its advantage in repairing of larger areas. The epoxy and resin injection techniques are usually employed when the damage level is low.

Beres *et al.* [1992] tested deficiently detailed, lightly reinforced interior beam-column joints. Methyl-methacrylate resin was used for repairing by vacuum injection. The failure

of the specimens occurred by formation of extensive diagonal crack in the joint along with pullout of the embedded beam bottom bars. The repairing process was capable of restoring 75% of initial stiffness, 72% column shear capacity for the specimen tested by them. There was no change observed in the energy dissipation which was due to reduced rate of strength deterioration.

Filiatrault and Lebrun [1996] tested two one-way exterior beam-column joint, which were damaged by earthquake. One with non-seismic detailing conforming to the construction of fifties and sixties and other following seismic codal details were considered. The specimens were tested by the load history which was imposed on the original structure. The damaged specimens were repaired by epoxy pressure injection. The authors concluded that the repair procedure was effective in improving the strength, stiffness and energy dissipation.

Karayannis *et al.* [1998] tested eleven beam-column connections after repairing only with epoxy injection. Their study was focused on the effect of joint reinforcement arrangement on the efficiency of epoxy repair by pressure injection. Though the failure took place by beam hinging, yet the cracks were observed even in the first cycle itself. The authors reported the increase in load carrying capacity and energy dissipation was 8 to 40% and 53 to 139% respectively due to repairing. The change in stiffness varied between a 27% decrease and a 10% increase. The variations in performance were partially attributed to the variation in being able to inject epoxy successfully into the joint cracks.

Tsonos [2001] repaired two identical half-scale exterior connections by removing the concrete in the entire joint and part of the column end. The removed concrete was replaced with high-strength (70 MPa), non-shrink mortar. Two additional horizontal ties were provided in each specimen. The author observed that the same failure mode exhibited which involved the formation of a beam hinge and the damage concentrated at

the joint region. The repaired specimens resulted in significant increase in the strength, stiffness and energy dissipation capacity. Finally, author concluded that joint transverse reinforcement might be relaxed with the use of high-strength mortar as a replacement material for the repair of heavily damaged joints.

Shash [2005] reported a case study where the cracks in reinforced beams of a single storey building were repaired by epoxy injection and the effectiveness of repairing was assessed by load test. The cracks were filled by injecting liquid epoxy resin. By performing the load test on the repaired beam the deflection noted was only 2.0 mm, which was less than the allowable deflection of 6.4 mm (as per ACI 318). The author finally concluded that the repaired beam could safely carry the expected loads.

Issa and Debs [2007] tested fifteen concrete cubes for investigating the effectiveness of repairing cracks by using epoxy (Sikadur-52). Out of fifteen cubes cast, twelve cubes were cracked artificially. Six cracked cubes were tested without repairing and rest six were tested after repairing the cracks with epoxy by the method of gravity filling. Three virgin control cubes were also tested (without any crack). The comparison of compressive strength of the tested specimens revealed that the crack resulted the reduction in strength by 40.93% in comparison to control specimen. The repaired specimens also failed to regain the original strength and showed a reduction in strength by 8.23% in comparison to the control specimen.

Karayannis *et.al* [2008b] experimentally investigated the behaviour of critical external beam-column joints repaired with epoxy pressure injection and further strengthened with carbon-fibre reinforced plastic sheets (C-FRP). The composite sheets were used with the aim to provide a confining system to the damaged concrete. The control specimens were subjected to a single cyclic displacement history so as to induce damage on the specimen similar to that caused by an earthquake. From the observed response of the examined

specimens, they concluded that epoxy resin injection technique was appropriate for rehabilitations of damaged joints, since no damages were observed at the joint area of the specimen after testing of the repaired joint. Further, a combination of epoxy injection with C-FRP sheets led to significant improvement of the load carrying capacity, energy absorption capacity and ductility. Finally it led to improvement on the type of damaged compared with the damage modes of the original specimens.

1.2.2.4 Fiber reinforced polymer (FRP)

To overcome the difficulties associated with various techniques such as concrete and steel jacketing, recent efforts are focused on the use of epoxy-bonded fiber reinforced polymer (FRP) sheets or strips. Apart from strength and corrosion resistance, the materials are most attractive for their tailorability.

Mosallam [2000] investigated the performance of glass epoxy and carbon-epoxy quasi-isotropic systems for retrofitting and repairing of beam-column connection. Six half-scale specimens, simulating interior beam-column connection were tested. Two were treated as control specimens and two as retrofitted specimens. The control specimens after failure were repaired by epoxy injection along with carbon-epoxy and E-glass-epoxy quasi-isotropic laminates. The specimens were tested by applying reversal loads to the top of column at the loading frequency of 0.25 Hz. It was found that the repaired specimen could be upgraded for attaining the ultimate load carrying capacity and displacement to a considerable extent. The retrofitted specimen showed an improvement in strength ranging from 10-44%. A slight increase in ductility and stiffness was also observed. The author concluded that the use of quasi-isotropic polymer laminates increased both the stiffness and the ultimate strength of the reinforced concrete moment-resistant frame. The author

gave eight recommendations for future research. Out of these, one was to see the effect by changing the specimen size and varying the beam and column cross sections.

Four beam-column joints without transverse reinforcement in the joints and in accordance with the strong-beam weak-column concept were tested by Ghobarah and said [2002]. The specimens were rehabilitated and strengthened using four different rehabilitation schemes, some specimens with and without mechanical anchorage, including steel plates and threaded rods core-drilled through the joints. The applied composites was extended above and below the joint and wrapped around the column. The flexural strength of the column increased as a result. The beams with no anchorage ruptured by joint shear failure whereas those with anchorage failed by flexural hinging of the beam. This result clearly indicated the importance of anchoring for the FRP joints strengthening technique.

Mukherjee and Joshi [2005] conducted tests on two sets of scaled down RC beam-column joints to study the performance of FRP used for up gradation. One set of joints were cast with ductile adequate steel reinforcement following ductile joint reinforcement, while the other set were cast non-ductile joint reinforcement. Both sets of specimens were strengthened with different strategies. Some specimens were retrofitted with GFRP/CFRP sheets, some with GFRP/CFRP wraps, while some with CFRP plates and wraps. CFRP plates were used to improve bending stiffness. The control specimens were rehabilitated after testing, and their performance were also checked. A constant axial load was maintained during the application of displacement-controlled cyclic loading. There was considerable increase in initial stiffness, yield load, deflection at yield, ultimate deflection and energy dissipation for all the strengthened cases. The authors concluded that both GFRP and CFRP could be used for seismic retrofitting and rehabilitation of damaged specimens.

Al-Salloum and Almusallam [2007] examined the performance of interior beam-column joints retrofitted and rehabilitated using two different schemes. The scheme comprised of using externally bonded CFRP with and without mechanical anchorage. Three numbers of cycles in each displacement amplitude were gradually applied to the specimens till failure. The test results showed that using any of the two schemes, shear failure of the joints was delayed substantially. The specimens with no anchorage experienced a joint shear failure proceed by debonding of FRP. By contrast, the specimens with anchorage failed by flexural hinging of the beam.

Karayannis *et al.* [2008b] experimentally investigated the behaviour of 12 critical external beam-column joints repaired or/and strengthened with a combination of epoxy resin injections and carbon-fibre reinforced polymers sheets. It was observed that combination of the two techniques leads to a significant improvement of the loading carrying capacity, energy absorption capacity and ductility. Finally it leads to improved type of damages compared with the damage modes of the specimens during the initial loading.

More recently, Saleh *et al.* [2010] employed two different schemes to upgrade and rehabilitate the exterior beam-column joints. The scheme comprised of using externally bonded CFRP with and without mechanical anchorage. The authors observed that the shear failure of the joints was delayed substantially. Further, the specimens with mechanical anchorage failed with flexural hinging of the beam. While specimens with no anchorage experienced a joint shear failure, proceed by debonding of FRP.

Thus, from the detailed review of literature on various rehabilitation / strengthening techniques, the following observation may be made:

- Epoxy repair techniques have been used extensively for the repair of damaged concrete structures, although a few research works have been published on the

effectiveness of this technique. Systematic studies to evaluate the performance of rehabilitated RC beam-column connection having different deficiencies under cyclic loading at different stages of damage level are still limited and are not well established.

- A combination of epoxy injection with FRP jacketing could overcome the limitation encountered by other techniques in rehabilitating damaged structures. FRP jacket further acts as a confining layer on the damaged area. This led to the change in failure mode and improved the ductile behaviour of the potential plastic hinge area. However, anchoring of FRP were observed to be a difficult for ensuring the effectiveness of this technique. Using FRP as confining materials will be more difficult with common constructional limitation (spandrel beams, existence of slabs and transverse beam) which needs reliable mechanical anchorage.
- Partial or total removal and replacement of concrete was done prior to injection and FRP wrapping of heavily damaged joints region with crushed concrete, buckled longitudinal bars. Generally, high strength, low-or non shrink concrete is used for the replacement. Transverse reinforcement of a repaired specimens might be relaxed with the used of high strength concrete.
- Concrete jacketing is labour-intensive involving drilling through the beams, floor slabs and even in-place bending of the added joint transverse reinforcement.
- Steel jacketing is vulnerable to corrosion, difficult to handle due to heavy weight and has objectionable aesthetics.
- The investigation related to the evaluation of seismic behavior of repaired and strengthened specimens were limited to testing of scale models which may not truly represent the actual behavior of a prototype structure.

1.2.3 Size effect of concrete structural element

The experimental research on size effect of concrete structural elements may be traced long back in 1925. Sabnis and Mirza [1979] reported that Gonnerman [1925] conducted the earliest study on size effect in concrete cylinder. He varied the diameter of cylinder from 100 to 250 mm and examined the influence of age, cement aggregate ratio, relative consistency and aggregate fineness on compressive strength. One of the sample results is shown in Fig. 1.9**.** The figure shows that the compressive strength decreases with increase in diameter of the test-specimen, supporting the size effect.

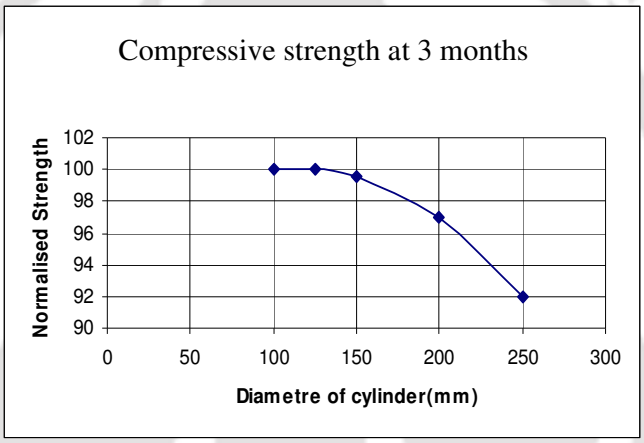

Fig. 1.9 Typical sample result of Gonnerman's test [1925]

Mirza *et al.* [1972] tested more than 500 cylinders ranging from 25×50 mm to 150×300 mm at ages of 3, 7 and 14 days. It was shown that for various concrete mixes, 75 and 100 mm diameter cylinders exhibited strength increase of approximately 5 to 15% and for 50 mm diameter cylinders, strength increased up to 40% over the strength of 150 mm diameter cylinders.

In the last couple of decades, there have been numerous researches on size effect of specimens made of concrete. Bažant [1984] proposed the size effect law in line with the idea as proposed by Walsh [1972]. Walsh was apparently the first person to plot the test

result as "$\log\sigma_{N_U}$ versus log D". However, he did not try to describe this plot mathematically or generalize it. Walsh's classical test was of limited range and included only one type of fracture specimen, which were not conclusive.

A stronger experimental verification was reported by Bažant and Pfeiffer [1986, 1987], which covers a broader size range and four different types of specimens. This research included test on mortar and test on concrete specimens. The results were plotted and found to satisfy the size effect law proposed by Bažant.

The result of the test performed by Jeng and Shah [1985] also support the size effect law proposed by Bažant, although a good fitting of the test data was not possible as the size range was very limited compared to the scatter obtained.

Sener *et al.* [1999] tested two groups of RC beams with splices located either in the mid span region with a uniform bending moment, or in one of the end regions with a uniform shear force. Beams of three different depths were considered, which were geometrically similar in all the three dimensions. The reinforcing bar diameters and cover thicknesses were also scaled in the same proportion. The results revealed the existence of a significant size effect, which was approximately described by the size effect law proposed by Bažant.

Sener *et al.* [2002] tested notched beams with and without steel fibres. Three different depths of beam were chosen and four point bending test were conducted. Failure bending stresses in all the cases were plotted in a bi-logarithmic plot and the results of failure of beams clearly confirm the existence of a significant size effect on the nominal strength with steel fibers, accompanied by an increase in failure brittleness followed Bažant's size effect law.

Krauthammer *et al.* [2003] investigated numerically and experimentally the size effect phenomenon of high strength concrete (HSC) in the form of cylindrical specimens

subjected to axial impact load. Results from their tests and simulations showed the existence of size effect in HSC cylinders under impact loading.

Sener *et al.* [2004] tested a large number of geometrically similar columns with three different slenderness ratios. The failure strength was calculated from the failure load *P* found experimentally. Linear regression analysis was carried out to find characteristic depth D_0 and dimensionless parameter *B*. Finally, bi-logarithmic plotting of $\log(D/D_0)$ versus $\log(\sigma_{N_U}/Bf_t')$ was done and was found in agreement with Bažant's size effect law. Further, the size effects become stronger as the slenderness ratio increases.

Elfahal *et al.* [2005] investigated numerically and experimentally the size effect phenomenon of normal strength concrete (NSC) for a cylindrical specimens that subject to axial load impact. Results from their tests and simulations showed the existence of a size effect in NSC cylinders under impact loading.

Bindiganavile and Banthia [2006] studied size effect of plain concrete beam under impact loading. Plain concrete of three different sizes were tested under three point impact load. The result of the impact test from their study as well as those from some of the previous studies was fitted to Bažant's size effect law. Similarly, same data were plotted according to Multifractal scaling law. The plot of compressive strength followed both Bažant's size effect law and Multifractal scaling law.

Leung *et al.* [2007] conducted test on CFRP retrofitted beam (strengthened in shear) of three different sizes. A number of specimens with different retrofitting strategies were tested. It was observed that the retrofitted specimens with complete FRP wrapping did not show any size effect, whereas FRP-U stripped retrofitted specimen showed size effect in term of gain in strength. The result showed that the failure in the strengthened specimen with U configuration was due to debonding of FRP strips, while in the other strengthened

case it was due to rupture of strips. The authors concluded that for the debonding failure, the bond capacity was directly proportional to the square root of the thickness and hence, with increase in thickness of FRP strips, the shear capacity was at a slower rate. In the second case of failure by debonding, the failure strength was directly proportional to thickness and hence with increase in size, there was increase in strength in same proportion leading to no size effect.

Belgin and Sener [2008] reported the failure of full-scale singly over reinforced concrete beam under four-point loading. The specimens were made of concrete with a maximum aggregate size of 10 mm. The beams were geometrically similar in all the dimensions. The bar diameter and cover thicknesses were similarly scaled in proportion. The results of a bi-logarithmic plot ($\log(D/D_0)$ versus $\log(\sigma_{N_U}/Bf_t')$) revealed the existence of a significant size effect, which can approximately be described by the size effect law previously proposed by Bažant. Finally, they concluded that the size effect is stronger in two-dimensional similarities than for one and three-dimensional similarities.

Koc and Sener [2009] tested geometrically similar columns of different sizes with different types of notches for both normal and high strength concrete to study the size effect. Three different slenderness ratios were covered in their study. Some specimens were having very shallow wide notch, some with deep and some with narrow notches. Axial loads were applied to the specimens till failure. Maximum ultimate stress was calculated and bi-logarithmic plot was drawn. The bi-logarithmic plots in all the cases followed Bažant's size effect law. It was observed that, with increasing strength, the size effect becomes more pronounced as the brittleness is increased. The authors concluded that out of all three different types of notches, the specimens made with surface-notch showed more pronounced size effect than all other types of notches. Also, they observed

that, with increasing strength, the size effect becomes more pronounced as the brittleness is increased.

Choudhury [2010] tested eighteen specimens with nine control and nine retrofitted specimens of three different sizes (full, two third and one third) for exploring the existence of size effect. All the three dimensions of the specimens and the amplitude of the displacement histories were scaled down from the full scaled specimen for two third and one third size specimens. Diameter of the reinforcing bars, development length, length of special confinement zone, cover of reinforcing bars etc. were also scaled down appropriately. Three different typical deficient beam-column connections (beam weak in flexure, beam weak in shear and column weak in shear) were considered. The deficient connections were retrofitted using Carbon Fiber Reinforced Polymer (CFRP) and Glass Fiber Reinforced Polymer (GFRP) wrapping. All the specimens were tested under cyclic loading until failure. Correlation on various parameters like gain in ultimate strength, ductility, energy dissipation of specimens per unit volume of joint, cumulative energy dissipation and variation of stresses with respect to relative deflection for all specimens due to retrofitting indicated the existence of size effect. Moreover, maximum ultimate stresses were calculated and bi-logarithmic plots were drawn. The investigator observed that the bi-logarithmic plots for both control as well as retrofitted specimens followed closely the size effect law proposed by Bažant. However, the size effect became more pronounced with the increase in brittleness of specimens.

Literature survey showed experimental studies on size effect were mainly done for RC beams and column with limited studies on beam-column connections related to size effects were reported. Further, size effect study on beam and beam-column connections strengthened with FRP were also carried out and reported. The survey of existing

literature could not however present any findings on size effect of rehabilitated beam-column connections.

1.2.4 Seismic damage indices for RC structures

Selecting the right damage model for RC component is a delicate task which requires knowledge of the available damage model as well as the behaviour of RC components under monotonic and cyclic loading. Large numbers of damage indices have been reported in literature and were reviewed by Williams and Sexsmith [1995]. A damage index aims to give a consistent numerical indication of the damage level. Traditional measures such as ductility and interstorey drift can be useful damage indicators, but most recently proposed indices even include the accumulation of energy. Indices may be defined as local or global level. Different approaches that have been adopted for the formulation of damage indices are briefly summarized here.

1.2.4.1 Local damage indices

Local indices characterize the damage due to seismic loading in an individual members or joints. Typically it is based on the ductility measurement, energy adsorption or a combination of both. Some damage indices model also considered the accumulation of degradation induced by the cyclic loading. Generally, local index values range between zero, for an undamaged structures and one for a collapsed structures. Commonly used local damage indices are described below.

(a) Non-cumulative indices

Non-cumulative damage indices use the envelope of maximum response such as component ductility or loading as the basic variable to calculate the damage. Ductility is

usually expressed in terms of curvature, rotation or deformation; while the loading envelope is defined for moments, stresses or forces.

The rotation ductility (μ_θ) is defined as the ratio of the maximum rotation (θ_u) at the end of member and the yield value (θ_y)

$$\mu_\theta = \frac{\theta_u}{\theta_y} = 1 + \frac{\theta_u - \theta_y}{\theta_y} \tag{1.12}$$

The curvature ductility (μ_ϕ) is defined as the ratio of the maximum curvature (ϕ_u) expected to be attained and the yield value (ϕ_y)

$$\mu_\phi = \frac{\phi_u}{\phi_y} = 1 + \frac{\phi_u - \phi_y}{\phi_y} \tag{1.13}$$

The displacement ductility (μ) represents the most elementary index to quantify structural damage. It is defined as the ratio of the maximum displacement (Δ_u) sustained by the structures and its yield displacement (Δ_y)

$$\mu = \frac{\Delta_u}{\Delta_y} = 1 + \frac{\Delta_u - \Delta_y}{\Delta_y} \tag{1.14}$$

The above indices (Eq. 1.12-1.14) are based exclusively on the peak values and it neglects the fatigue contribution due to cyclic loading. Nevertheless, these are used as damage indicators because of its simplicity in evaluation and for their physical interpretation (Sordo *et al.,* 1989).

To overcome some of the deficiencies of the traditional damage measures, Banon *et al.* [1981] proposed a measure of local stiffness degradation and called it as the flexural damage ratio (*FDR*). In terms of stiffness, it is expressed as the ratio of initial tangent stiffness (k_0) of the structural element considered to the maximum element stiffness (k_m) of the same member during a complete cycle as shown in Fig. 1.10 (where M_y, M_m and

M_f are yield moment, the max. moment reached in the loading and the moment at failure respectively). The *FDR* index expressed as:

$$FDR = \frac{k_0}{k_m} \tag{1.15}$$

This index is an improvement on the ductility ratio as it takes some account of the stiffness and strength degradation that occur under cyclic loading. However, after comparing to the test data, Banon *et al.* conclude that the neither ductility ratios nor the *FDR* gave a consistent indication of failure.

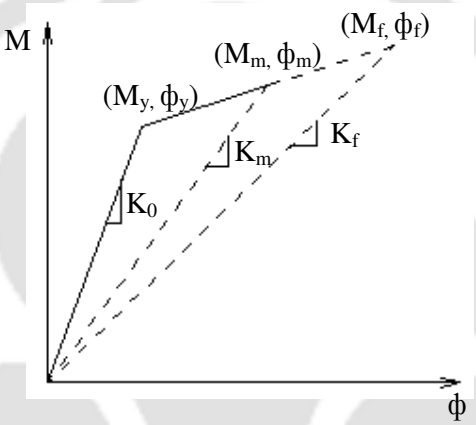

Fig. 1.10 Definition of stiffness degradation

Roufaiel and Meyer [1987a] suggested a modified version of the *FDR* considering the increase in flexibility between the initial condition and the instant of maximum deformation divided by the increase in flexibility at failure. This can be expressed in terms of stiffness as:

$$FDR = \frac{k_f}{k_m} . \frac{(k_m - k_0)}{(k_f - k_0)} \tag{1.16}$$

where k_f represents the element stiffness at failure. The maximum value achieved during the positive and negative loading cycles is taken as the *FDR*. This parameter showed a

good correlation with residual strength and stiffness from experimental investigation under flexural loading.

(b) Cumulative indices

Cumulative damage models are employed to represent the damage under cyclic loading. Accumulative plastic deformations or hysteretic energy are commonly used for calculating cumulative damage indices. The deformation based cumulative damage models are mostly developed based on the low-cycle fatigue formulation.

The index proposed by Banon *et al.*[1981] is a measure of ductility and captures the effect of repeated cyclic loading on the structures. It used a normalized cumulative rotation (*NCR*) similar to the rotational ductility. Considering *N* loading cycles, the index expressed as

$$NCR = \frac{\sum \left| \theta_u - \theta_y \right|}{\theta_y} \tag{1.17}$$

Test carried out on reinforced concrete frame showed that the index was closely associated with the hysteretic behavior of the structures.

Stephens and Yao [1987] developed a cumulative damage index based on the plastic displacement ductility with positive and negative displacement increment as shown in Fig. 1.11. Considering *N* cycles, the damage index was expressed as

$$DI = \sum_{i}^{N} \left(\frac{\Delta \delta^{+}}{\Delta \delta_f} \right)^{1-br} \tag{1.18}$$

in which $\Delta \delta^{+}$ was defined as the value of the positive change in plastic deformation and $\Delta \delta_f$, the positive change in plastic deformation in a one cycle test to failure conducted at the relative deformation ratio of cycle *i*. Coefficient *r* represents the relative deformation ratio, defined as the ratio of the negative change in plastic deformation ($\Delta \delta^{-}$) in i^{th} cycle

to the positive change in plastic deformation ($\Delta\delta^+$) in cycle *i*. Parameter *b* is a calibrated constant based on different type of structure and damage levels and it has a recommended value of 0.77. Stephens and Yao used this index for assessment of two test structures. The index provided useful measures of damage sustained by the structures. However, it showed a moderate correlation with the observed damage and the degree of scatter increased with the damage level. Further, calibration of parameter *b* represented a potential limitation of this method.

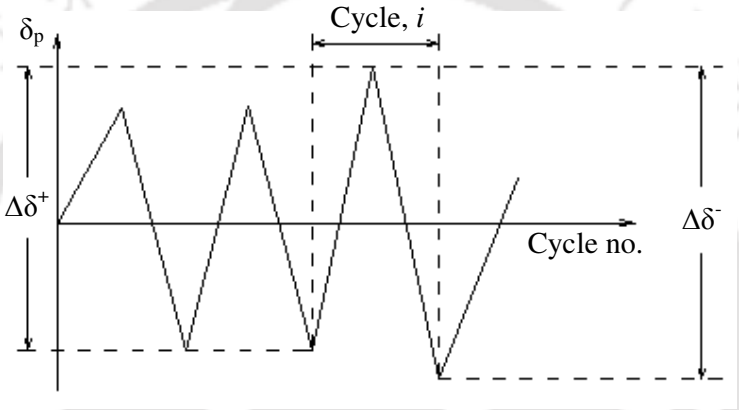

Fig. 1.11 Plastic displacement increments [Stephens and Yao, 1987]

Wang and Shah [1987] proposed a cumulative damage model which assumed that the development of damages dependent on the maximum deformation occurring in a cycle and that the rate of accumulation of damage is proportional to the damage already affecting the structures. They proposed the following exponential equation to characterize the damage. Corresponding N cycles, the index was expressed as

$$DI = \frac{\exp(s\alpha) - 1}{\exp(s) - 1} \tag{1.19}$$

where

$$\alpha = c\sum_{i}^{N} \frac{\delta_{m,i}}{\delta_f} \tag{1.20}$$

Parameter $\delta_{m,i}$ and δ_f were the maximum displacement of cycles *i,* and the final displacement after the complete loading pattern of *N* cycles respectively. Parameters *c* and *s* were constant with recommended values of 0.1and 1.0 for well-reinforced concrete members. The index could be observed as a measure of strength degradation. The yield load in a deformation cycle was given by the maximum load in the previous cycle multiplied by (1-DI) as shown in Fig.1.12. Wang [1994] stated that the model was of limited use due to the need for calibration against observed damage.

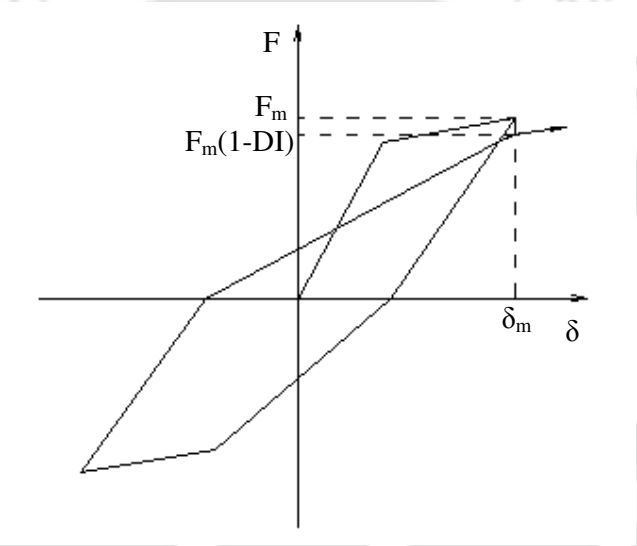

Fig. 1.12 Physical meaning of Wang and Shah [1987] damage index

Jeong and Iwan [1988] quantified damage under cyclic loading using an expression combining the effect of cycles at varying amplitudes. It measured the influence of both duration and ductility of response. Considering *N* loading cycles of varying amplitude, the index was expressed as:

$$DI = \sum_{i}^{N} \frac{n_i}{n_{f,i}} \tag{1.21}$$

where n_i the number of cycles at amplitude *i* and $n_{f,i}$ was the number of cycles to failure at that same amplitude and evaluated as:

$$n_{f,i}\mu_i^s = c \tag{1.22}$$

Constant c and s were recommended values of 6.0 and 416 respectively for reinforced concrete structures. The index provides an adequate qualitative estimation of structural damage. However, calibration of parameters c and s, affected by the design details of the structure is a limitation of the index.

Gosain *et al.* [1977] were the first to adopt energy adsorption. They proposed a simple cumulative energy ratio as

$$DI = \sum_i \frac{F_i \delta_i}{F_y \delta_y} \tag{1.23}$$

where F_i and F_y were the forces at cycle i and the yield force respectively, and δ_i and δ_y are the displacement corresponding to cycle i and the yield displacement respectively. Only cycles with $F_i / F_y \geq 0.75$ are considered in the calculation, because they assumed that the remaining capacity becomes negligible when it is 25% less than the initial capacity. The author also introduced modification terms to account for the effect of shear and axial load. It was observed that this index correlated very closely with normalized cumulative rotation (Eq.1.17).

The index proposed by Kratzig *et al.* [1989] is based on the hysteretic energy. The index applies the concept of primary half cycle (*PHC*) and follower half cycle (*FHC*) to account for both the excursion with the maximum amplitude and the cumulative damage of smaller excursions. Fig.1.13 illustrates the terminology used in this model. The primary half cycle refers to the half cycle of loading at a given displacement level. Any other half cycle are treated as follower unless they induced higher displacement than the previous primary half cycle. The positive and negative are treated separately, cumulative damage parameters for each loading cycle i defined as:

$$DI^{\pm} = \frac{\sum_{i}^{N} E_{p,i}^{\pm} + \sum_{i}^{N} E_{i}^{\pm}}{E_{f}^{\pm} + \sum_{i}^{N} E_{i}^{\pm}} \tag{1.24}$$

where $E_{p,i}^{\pm}$, was the energy absorbed in a *PHC*, $E_i^{\pm}$ was the energy of *FHC* and $E_f^{\pm}$ was the energy absorbed in a monotonic test to failure. The overall damage index is finally expressed as:

$$DI = DI^{+} + DI^{-} - DI^{+}DI^{-} \tag{1.25}$$

From various database obtained from laboratory experiments or on literature, Kratiz *et al.* [1989] successfully verified the ability of the index to quantify damage in a structure. Calibration of the index against observed damage in flexure-dominated test showed that the index reliably converged to a value of unity at failure. This index however involves considerable calculation effort compared to the other local indices.

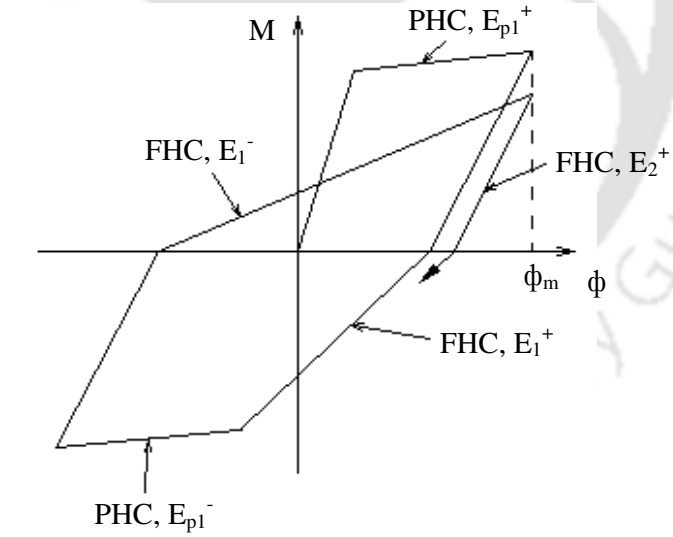

Fig. 1.13 Parameters used used in Kratzig *et al.* [1989]

(c) Combined damage models

The damage models consider a combination of damage due to excessive deformation and energy absorption. The index proposed by Park and Ang [1985] is a combined damage model. The damage index model is defined as

$$DI = \frac{\delta m}{\delta u} + \frac{\beta_e}{\delta u Q y} \int dE \tag{1.26}$$

where δ_m is the maximum deflection attained during seismic loading, δu is the ultimate deflection capacity under monotonic load, β_e is strength degradation parameter, Q_y is the yield force and dE is the incremental dissipated hysteretic energy.

The first terms (Eq. 1.26) is a pseudo static displacement measure; the second term is an energy term accounting for accumulated damage. Most researcher prefer this model for quantifying damages because of its simplicity and the fact that it has been calibrated against significant amount of observed seismic damage. Park *et al.* [1987] suggested the following damage classifications (Table. 1.1)

Table 1.1 Park and Ang [1987] damage classification levels

Damage level	Damage index	Damage measure
I	DI < 0.1	No damage; localized minor cracking
II	0.1 ≤ DI < 0.25	Minor damage; light cracking throughout
III	0.25≤ DI < 0.4	Moderate damage; severe cracking localized spalling
IV	0.4 ≤ DI < 1.0	Severe damage; crushing or cracking reinforcement exposed
V	DI ≥1.0	Collapse

DI = 0.4 was suggested by the same authors as a threshold values between repairable and irreparable damage. Ang *et al.* [1993] suggested a value of *DI* = 0.8 to represent complete collapse.

Kunnath *et al.* [1992] slightly modified the original damage index proposed by Park and Ang. In their proposed index, the yield deformation was removed from the first term. Moment and curvature were used instead of force and displacement. The damage index model is defined as

$$DI = \frac{\phi_m - \phi_y}{\phi_u - \phi y} + \frac{\beta_e \int \delta E}{M_y \phi_u} \tag{1.27}$$

The index was formulated for use in IDARC (Inelastic Damage Analysis of Reinforced Concrete). Kunnath *et al.* stated that the intent of introducing the β_e parameter was to provide a correlation between strength loss and damage. The strength degrading parameter (β_e) can have varying values as shown in Table 1.2

Table 1.2 Typical ranges of values for β_e

Description for β_e	β_e
Well Detailed Section- No Deterioration	0.05
Nominal Deterioration	0.1
Poorly Detailed Section- Severe Deterioration	0.4

Stone and Taylor [1993] calibrated the damage index proposed by Kunnath *et al.* [1992] based on the damage conditions of 82 CALTRANS circular bridge columns. On the basis of these related tests, they proposed the damage classification as shown in Table 1.3.

Table 1.3 Damage condition and corresponding limiting damage indices

Damage Condition	Damage Index
No Damage or localised cracking	DI < 0.11
Repairable- extensive spalling but inherent stiffness remains	0.11≤ DI < 0.4
Irreparable-still standing but failure imminent	0.4≤ DI < 0.77
Collapsed	DI ≥0.77

1.2.4.2 Global damage indices

Global indices quantify damage for the complete structure or for part of the structure when several of its structural elements were considered. The indices evaluated by weighing local damage indices of different members composing the structure.

Most common global index uses the amount of energy absorbed at different locations as a weighting function (Park *et al.*, 1985, 1987; Chung *et al.*, 1990; Kunnath *et al.*, 1990, 1992). The index evaluated for a complete structure of *N* elements or part of a structure composed of *N* members. The global damage index for a single storey is defined as

$$DI_{storey} = \frac{\sum_{i}^{N} D_i E_i}{\sum_{i}^{N} E_i} \tag{1.28}$$

where DI_i is the local damage index at location *i* and E_i is the energy adsorbed at the same location *i*.

Severely damaged members limit the overall stability of the structures. The above Eq. 1.28 however does not reflect while averaging the index. Hence, Bracci *et al.,* [1989] developed a global index that emphasizes the severity of damage in a structural elements. The index expressed as

$$DI_{storey} = \frac{\sum_{i}^{N} w_i D_i^{(b+1)}}{\sum_{i}^{N} w_i D_i^{b}} \tag{1.29}$$

High values of parameters *b* are used when more emphasis on the most severely damaged elements are required. This formulation defines the weights w_i as the ratio of the gravity load supported by element *i* to the total gravity load of the structure. These weighting functions reflect the greater dependence of the overall structural stability in which damage occurring at the base is weighted higher than that of the upper structure. Test performed on reinforced concrete frame (Bracci *et al.,*1989) verified the ability of the indicator to quantify damage. Corresponding index value showed a good correlation with the observed and measured damage.

Damaged structures usually exhibit reductions in their natural frequencies due to stiffness degradations. Roufaiel and Meyer [1987] came out with a correlation for a simple global damage index who proposed a correlation between a simple global damage parameter expressed in terms of deflections at roof and the corresponding change in fundamental frequency.

$$DI_{global} = \frac{\delta_m - \Delta_y}{\delta_u - \Delta_y} = \frac{14.2\delta_y \left(\sqrt{\frac{f_{und}}{f_{dam}}} - 1 \right)}{\delta_u - \Delta_y} \tag{1.30}$$

where f_{und} and f_{dam} were the fundamental frequencies of the structure before and after it is damaged. δ_u and Δ_y were the ultimate and yielding deformation capacity under monotonic loading. A range of different softening indices which are functions of the change in fundamental period of the structure during an earthquake are the maximum softening (DI_{ms}), the plastic softening (DI_{ps}) and the final softening (DI_{fs}) . The indices are presented

in Eq.1.31. The indices formulated in terms of three fundamental periods are shown in Fig. 1.14 is expressed as

$$DI_{ms} = 1 - \frac{T_{und}}{T_m}; DI_{ps} = 1 - \frac{T_{dam}^2}{T_m^2}; DI_{fs} = 1 - \frac{T_{und}^2}{T_{dam}^2} \tag{1.31}$$

where T_{und} and T_{dam} were the fundamental period of the structure before and after the earthquake and T_m was the maximum period obtained during the earthquake.

Mork [1992] extended the maximum softening index to include the second mode. He defined two damage parameters

$$DI_1 = 1 - \sqrt{\frac{k_{1,m}}{k_{1,und}}}; DI_2 = 1 - \sqrt{\frac{k_{2,m}}{k_{2,und}}} \tag{1.32}$$

where k_1 and k_2 values were the spring constants for a two degree of freedom system having two equal masses and giving the same first and second periods as the actual structure. Thus k_1 and DI_1 may be assumed to represent the lower part of the structure and k_2 and DI_2 the upper part.

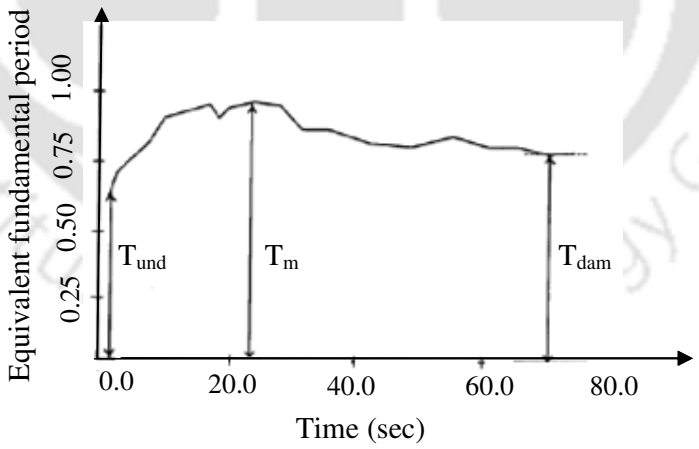

Fig. 1.14 Evolution of equivalent fundamental period for Millikan Library [Williams and Sexmith, 1995]

The review on the damage indices with local indices in particular shows that all indices have its own limitations. Nevertheless, with the aid of some further development and validation studies, damage indices have the potential to become valuable tools in rehabilitation, strengthening or retrofit decision-making and structural assessment. William *et al.* [1997] make used of eight damage indices for comparative studies to quantify the damaged of structures. They found that all indices are prone to quite a high degree of scatter. Based on these results they suggested that a relatively simple, predominantly deformation-based model such as the Park and Ang model [1985] provide more reliable indication of the various damage levels than many of the apparently more sophisticated models. Moreover, the Park and Ang model has been calibrated using experimental data from various structures damaged during past earthquakes.

1.2.5 Development of fragility functions

There are various ways from simple to complex to obtain fragility functions. Certainly, using simple method gives approximate fragility functions whereas complex method result in realistic and more accurate fragility functions.

One of the simplest methods of obtaining fragility functions is to use expert opinion. The most systematic study using this method is conducted by Applied Technology Council-13 [1985]. Fragility functions of 40 different structural types were obtained with the opinion of 58 experts. Basically, the damage states of the structures at different seismic demand levels estimated by various experts are obtained and the results are submitted as probability matrices. Apparently, the disadvantage of this method is the subjective data based on personal opinion of experts. The subjectivity of expert opinion is included besides the randomness of the ground motion and the uncertainty in the structural response.

Another way of obtaining fragility functions is to observe the actual post–earthquake structural damage. Hence the information concerning the observed damage can be collected and statistically converted to fragility functions. This approach is suitable for structures with little engineering intervention like masonry structures. One of the early studies that were based on this method investigated the structural damage of 5–story buildings after the San Fernando earthquake, 1971 in California. This study obtained fragility functions based on the actual statistical structural damage database (Whitman *et al.,* 1974). In a recent fragility research, damage of RC structures after 19 different earthquakes has been observed and used (Rossetto and Elnashai, 2003). However, researchers stated the difficulties about systematic grouping of the structural responses observed by different expert groups after each earthquake, although they have a comprehensive database.

Using experimental data is an alternative way of obtaining fragility functions. Recently, the increasing of testing large scale and realistic experimental models has caused research interest to shift toward experimental data. However, large scale realistic experiments have time and economic constraint and other difficulties.

In the absence of experimental or observational data and expert opinion, the only way of investigating structural vulnerability is to use analytical methods. The advantage of employing analytical methods is the possibility of executing numerous structural analyses. In the case of analytical methods, structural simulations and corresponding algorithms are important. The simplest structural model is single–degree–of–freedom (SDOF) system. Simple SDOF model with only few parameters enables the computation in a short period of time. Hence SDOF models have been used by many researchers (Jeong and Elnashai, 2004).

In addition to the above general information about fragility functions development, some of the past researches where components fragility functions have been developed are summarized here.

Shinozuka *et al.* [2002] developed fragility functions for two bridges retrofitted by column jacketing. Fragility functions were constructed as a function of PGA utilizing nonlinear dynamic analysis to investigate the effect of column retrofit. Two–parameter lognormal distribution functions were used to represent the fragility functions utilizing the maximum likelihood method. Median values before and after retrofit were compared to quantify the improvement in fragility with retrofitting. The authors conclude that the simulated fragility curves after retrofit showed excellent improvement. Median PGA values are up to three times less fragile.

Aslani [2005] in his thesis include the development of fragility functions for beam-column joints to estimate the probability of experiencing different damage states at component level which were used for probabilistic damage assessment in a building. Interstory drift-based fragility functions were developed for different damage states. Damage states were defined based on tested specimens from previous experimental studies and linked with the repair method suggested by *FEMA* 308[1998]. The probabilistic models used were assumed to be lognormally distributed. It was found that the results from using deformation-based fragility functions provide improved estimates of the probability of experiencing damage at component-level and therefore leads to improved estimates at the building level.

Pagni *et al.* [2006] developed fragility functions for predicting the method of repair that required to restore a pre-1967 beam-column joints subjected to earthquake loading. Empirical relations between damage states and engineering response measures or engineering demand parameters (*EDPs*) were developed from the previous studies. The

proposed damage states were characterized by parameters such as concrete crack width, extent of concrete spalling and yielding and buckling of reinforcement. Based on the previous research data, 12 damage states were indentified ranging from the hair line cracking in beam-column interface to the failure due to pull-out of discontinuous beam longitudinal reinforcement. Probabilistic model such as lognormal, Weibull and beta distribution were used for functions development. Standard goodness-of-fit test were also employed. The authors concluded that defining engineering demand using nonlinear function such as interstorey drift and number of load cycles resulted in the best model evaluated by *K-S* test.

Porter *et al.* [2007b] introduced a comprehensive set of procedures for creating fragility functions from various kinds of data. They addressed the damage analysis whose input was the engineering demand parameters (*EDP*) calculated using the structural analysis, and whose output was the damage measures (*DM*) of each damageable structural and nonstructural component. The analysis uses fragility functions, which in turn give the probability a damage state as a function of *EDP*. The probability that the component reached or exceeds a damage state given a particular *EDP* was idealized by a lognormal distribution.

Gulec *et al.* [2010] developed fragility functions for low aspect ratio reinforced concrete walls such as rectangular, barbell and flanged for future assessment of building. Story drift was considered as the efficient response demand parameter. The information for defining damage states (e.g. cracking and crushing of concrete etc.) and corresponding repair method (e.g. cosmetic repair, epoxy injection, partial wall replacement etc.) were gathered from the past experimental data and expert opinion. Different probabilistic models (lognormal, Weibull and beta distribution) were employed in generating the fragility functions. Among all probabilistic models considered, lognormal distribution

was the best fitted for all repair methods for all class of wall geometry. The authors conclude that future performance assessment of building incorporating these walls will make use of fragility functions that relate the probability of exceeding one or more damage threshold to an efficient response parameter. It may be noted that, the damage states and the scope of each repair methods were established from the previous data with the analysis of sketches and photographs of damaged specimens.

Lignos *et al.* [2010] developed fragility functions to estimate the probability of reaching or exceeding different damage state in reduced beam in beam-column moment connections steel frame as a function of peak interstory drift ratio (*IRD*). Seventy one experimental tests that have been conducted over a past 14 years were used to develop the functions. Lognormal, beta, Weibull and gamma are the four probability distributions considered. Out of the four, the lognormal distribution was the best fitted for all the damage states followed by the gamma distribution. Further, epistemic uncertainty of fragility functions also have been studied by incorporating three source of uncertainty such as specimen-to-specimen uncertainty, statistical uncertainty and demand parameter uncertainty. It was observed that, for all damage states the first source of uncertainty was significantly larger than the other two.

Literature survey shows that components fragility functions have been created in the past. There are many ways to create fragility functions. Creating fragility functions from experimental studies considered to be the most reliable one, since data considered for functions development are influenced by many factors. However, in spite of minimizing the various uncertainties, development of fragility functions from experimental studies is not well reported because realistic experiments have time and economic constraints along with others difficulties. Further, various probabilistic distribution models were used by

many researchers in developing fragility functions. The lognormal distribution considered to be the best fit distribution among all types of distribution.

1.3 SCOPE AND OBJECTIVE OF THE PRESENT STUDY

Literature survey showed that several experimental studies have been carried out to evaluate the behavior of rehabilitated RC connections under cyclic loading. However, no record could be found where the comparative studies covering various deficiencies like beam-column connections with beam weak in flexure, beam weak in shear and column weak in shear were addressed together. The nature and extent of damage in a structure during an earthquake depends on the characteristic of loading such as number of loading cycle in a displacement time history, frequency of excitation and the level of displacement amplitude. Although loading characteristic play a vital role in the behavior of the connections, there was not much research focused specifically on this issue. Thus, a holistic approach was initiated to cover different deficient cases of RC beam-column connections subjected to loading with different characteristics so as to gather a comprehensive knowledge about the behaviour of these connections. Loadings were applied in the forms of repeated displacement cycles of gradually increasing amplitude and with two different frequencies. Generally, severely damaged structures are thought to be irreparable and are abandoned in spite of huge economic loss. To ensure further usability of the distressed or damaged structural elements an effective and reasonable technique are needed to be investigated for rehabilitations of the damaged structures for post-earthquake usage. Hence, the specimens which were damaged by different loading characteristics were rehabilitated with two different strategies. Comparative studies on various parameters related to seismic capacity such as ultimate strength, stiffness

degradation, displacement ductility, energy dissipation etc. were carried out to understand the effectiveness of applied rehabilitation strategies.

Experimental study on size effect was primarily done for RC columns and beams. Beam-column connections which are vital structural elements and play a very crucial role during earthquake needs attention. Size effect study of RC beam-column connections with and without retrofitting has been carried out and reported. It was shown that the size of the specimen plays a role for various properties like ultimate strength, ultimate strain, energy dissipation etc. Thus, it was felt necessary to explore the possibility of existence of size effect on RC beam-column connections both before and after rehabilitations.

Various damage indicators that can quantify damaged structures are available in the technical literature. The index has the potential to play a vital role in rehabilitation/retrofit decision making. Among all the available cumulative damage index, the Park and Ang [1985] damage index model is the most used in recent years because of its simplicity and the fact that it has been calibrated using experimental data from various structures damaged during the past earthquake. Making use of this indicator the damage level of a distressed specimen can be quantified and used by researchers for ascertaining the effectiveness of adopted rehabilitation technique for damaged seismic structural members. Further, in order to scientifically carry out repairing of distressed or damaged structural elements, guidelines are required so that an effective and reasonable rehabilitation technique can be employed for post-earthquake usage. These guidelines will be highly useful to the field engineers while taking decision to adopt an appropriate rehabilitation strategy during post disaster period.

Further, fragility functions are useful tools for post-earthquake damage assessment. There are many ways to obtained fragility functions. Developing fragility functions from experimental studies were considered to be the most reliable one as it directly correlates

the actual observed damage to the repair method. In most cases, results of previous experimental studies were used to developed empirical relationships between damage states and traditional engineering response measures, which are influence by many parameters such as loading sequence, geometry and specimens sizes, nature of test program etc. It may be noted that, damage states describe the progression of damage sustained by a beam-column connections under seismic loading. The correct identification of damage states which is associated with specific repair methods however depends on the correct information available from literatures, written documents or published photographs etc. In view of these uncertainties, an attempt to develop specific repair-fragility functions from the current experimental studies was also undertaken in the present study.

Thus, based on the issues discussed above, the objectives of this research work are framed as:

1. To carry out experimental studies on various types of deficient RC external beam-column connections under cyclic loading.
2. To rehabilitate the damaged RC beam-column connections by employing different rehabilitation strategies depending on the extent of damages.
3. To carry out experimental studies on both control and rehabilitated specimens of different sizes for exploring the existence of size effect.
4. To interpret the experimental findings for exploring the existence of size effect in term of various parameters like stress, energy dissipation, relative deflection etc. for both control as well as rehabilitated RC beam-column connections.
5. To study the performances of deficient RC beam-column connections subjected to cyclic displacement of higher frequency before and after rehabilitations.

6. To evaluate damage indices of RC beam-column connections by employing Park and Ang [1985] damage index model and then to utilize the same for ascertaining the effectiveness of the adopted rehabilitation techniques.
7. To prepare guidelines regarding rehabilitation of damaged structural elements for direct field application.
8. To develop fragility functions for both control and rehabilitated RC exterior beam-column connections employing different probabilistic distribution model.

1.4 ORGANIZATION OF THE THESIS

The thesis has been divided into nine chapters. Chapter 1 presents introduction, literature review, scope and objective of the present study**.** Chapter 2 covers the characterization of various materials used for casting of the test specimens. Detailed description of experimental program including selection of specimens, design and constructions of specimens, material and rehabilitations procedure are also discussed in this chapter. In Chapter 3, 4 and 5 experimental studies of RC exterior beam-column connections with beam weak in flexure (BWF), beam weak in shear (BWS), column weak in shear (CWS) and their corresponding rehabilitated specimens under different loading types have been covered. All the observations during testing and interpretation of results in terms of various parameters related to seismic capacity such as ultimate strength, stiffness degradation, energy dissipation, ductility etc. have been detailed. Correlations of various parameters for the existence of size effects for both control as well as rehabilitated specimens have been presented. Chapter 6 describes the finding of experimental investigation and interpretation of experimental results of different RC deficient exterior beam-column connections subjected to cyclic displacement of higher frequency for both control and rehabilitated specimens. Comparisons on the performance of the connections

under two different loading frequencies in terms of various parameters related to seismic capacity have also been presented. Chapter 7 presents the evaluation of damage indices of RC beam-column connections. A guideline on identification of an appropriate rehabilitation strategy during post disaster period has also been presented in this chapter. Chapter 8 presents the development of fragility functions for exterior RC beam-column connections considering the current experimental results. Identifying damage states, demand parameters and their corresponding repair action are also presented. Further, comparison on the developed fragility functions are also made in order to quantify the vulnerability of rehabilitated RC beam-column connections. Finally, Chapter 9 summarizes the conclusions derived from the entire study. Further, few identified issues are also recommended as the scopes for future research on the present topic.

1.5 CONCLUDING REMARKS

Post earthquake investigations show exterior beam-column connections is more vulnerable to seismic attack. Several experimental studies have been carried out to evaluate the behaviour of connections under cyclic loading. Though various techniques have been used by many researchers to rehabilitate and strengthen the damaged connections. However, systematic studies to evaluate the performance of rehabilitated RC beam-column connection having different deficiencies under cyclic loading at different damage levels are still limited and are not well established. Further, research efforts on size effect in civil engineering have been started in recent past year and hence very limited research findings have been observed on size effect of RC structures. Testing numerous models for creating of fragility functions is not practically feasible because of economic limitations and difficulties. Hence, developing components fragility functions are limited to obtaining data from previous experimental studies. An extensive literature

review has been presented in this chapter covering entire domain of studies on RC beam-column joints and connections. For convenience, literatures have been grouped into five different classes, namely, (i) Experimental studies on RC beam-column joint and connections (ii) Rehabilitation / strengthening of damaged RC beam-column joint and connections with concrete jacketing, steel jacketing, epoxy repairing and FRP wrapping (iii) Size effect of concrete structural elements (iv) Damage indices on RC structures (v) Development of fragility functions. Based on detailed studies of literatures and identifying various shortfall and inadequacies of earlier studies, finally the scope and objectives of the present study have been enumerated.

CHAPTER 2

MATERIAL CHARACTERIZATION, TEST ARRANGEMENT AND LOADING CHARACTERISTICS

2.1 INTRODUCTION

This chapter presents the characterization / descriptions of materials used for construction of the undamaged (control) specimens and that for rehabilitations of the damaged specimens. Selection of test specimens, detailed descriptions of each deficiency types, testing arrangement and loading program are also presented. Further, rehabilitation strategy along with step-by-step procedures has also been described. Procedure for assessment of damaged control specimen both before and after repair using an ultrasonic pulse velocity test has also been discussed. The control specimens used in this study was the same as that used in the study carried out by Choudhury [2010]. Hence, the same results of materials properties and detailing of specimens were adopted. However, the same has been reproduced for completeness of all necessary information related to this study.

2.2 MATERIAL CHARACTERIZATIONS

The precision of the experimental works depend on to a large extent on proper characterization of the materials used for design of concrete mix. Successful repair of damaged specimens also depend on the quality, strength of the repair materials as well as quality of repairing the specimens. However, it also depends on the condition of the parent materials of the original specimen. Therefore, materials characterization has been carried out as per relevant standard codes. Result of materials properties of original specimens reported by Choudhury [2010] has been adopted.

2.2.1 Materials for casting of control specimens

All constituent materials used in the concrete mix design have been tested as per relevant codal provisions. The details results are presented in Table 2.1-2.4. Target cube strength of 30 N/mm^2 was used for beam-column connections with beam weak in flexure and beam weak in shear while a lower grade with target strength of 25 N/mm^2 was used for column weak in shear. The largest size of coarse aggregates used for the full size specimens was 24 mm down. For two third and one third scaled specimens the largest aggregates sizes used were 16 mm and 8mm down respectively. Six different mixes were designed for two different target strengths and for three different sizes. The details of concrete mixed designed are furnished in Table 2.5. The average compressive strength of collected cubes was 32.2 N/mm^2 for beam weak in flexure and beam weak in shear specimens while the same was 26.7 N/mm^2 for column weak in shear specimens.

Table 2.1 Results of tests on cement (Ordinary Portland Cement of 53 grades)

Sl. No.	Name of test	Details of relevant code	Test result
1	Standard Consistency	IS: 4031(4)-1988.	28%
2	Initial Setting Time	IS: 4031 (5)-1988	1 hr 20 minutes
3	Final setting time	IS 4031: (5)-1988	5 hr 25 minutes
4	Specific gravity (ρ)	IS: 4031(11)-1988	3.12

Table 2.2 Compressive strength of cement

No of days	Compressive strength (MPa)	
	According to IS 12269:1987	Test results
3	27	27.31
7	37	37.36
28	53	54.3

Table 2.3 Result of sieve analysis for sand

Sl.No	Sieve size	Weight retained (gm)	% Weight. retained	Cumulative % weight retained	% fine	Remark
1	4.75 mm	0	0	0	100	
2	2.36 mm	31	3.1	3.1	96.9	Falls in **Zone II** [as per to IS: 2386 (1)-1963]
3	1.18 mm	52	5.2	8.3	91.7	
4	600 μ	388	38.8	47.1	52.1	
5	300 μ	348	34.8	81.9	18.1	
6	150 μ	137	13.7	95.6	4.4	
7	75 μ	34	3.4	99	1	
8	Pan	10	1.0	100	0	
Specific gravity = 2.51 as per IS: 2386 (III)-1963.						

Table 2.4 Result of sieve analysis for coarse aggregates

Sl.No	Sieve size	Wt. retained (gm)	% Weight. retained	Cumulative % retained	% Fine
1	20 mm	1401	23..35	23.35	76.65
2	10 mm	3785	63.08	86.43	13.57
3	4.75mm	730	12.17	98.6	1.4
4	2.36 mm	56	0.93	99.53	0.47
5	1.18 mm	10	0.16	99.69	0.31
6	600 μ	2	0.03	99.72	0.28
7	300 μ	2	0.03	99.75	0.25
8	150 μ	3	0.05	99.8	0.2
9	<150 μ	10	0.16	99.96	0
Specific gravity=2.62 as per IS: 2386 (III)-1963 Fineness Modulus = 8.06 as per IS: 2386 (I)-1963					

Table 2.5 Details and results of concrete mixes

Sl. No.	Target strength (N/mm^2)	Nominal size of coarse aggregates	Mix ratio	w/c	Average compressive strength (N/mm^2)
1.	30	24 mm down	1:1.85:3.82	0.59	32.0
2.	30	16 mm down	1:1.84:3.18	0.59	32.2
3.	30	8 mm down	1:1.82:2.77	0.59	31.6
4.	25	24 mm down	1:2.3:4.75	0.65	26.4
5.	25	16 mm down	1:2.26:4.0	0.65	26.7
6.	25	8 mm down	1:2.25:3.41	0.65	26.0

Fe 500 steel was used predominantly as longitudinal and transverse reinforcements. However, Fe 250 steel was also used in limited number of cases. The results of materials properties of tested rebar as per provisions of IS: 432(I)-1982 and IS: 1608-1995 are presented in Table 2.6. Further, a typical stress-strain plot for a sample rebar is given in Fig. 2.1.

Table 2.6 Material properties of steel rebars

Sl.No	Diameter of the rebar (mm)	Yield stress (MPa)	Ultimate stress (MPa)	Young's modulus (MPa)	Elongation (%)
1	20	560	640	$2x10^5$	19.78
2	12	530	620	$2x10^5$	16.44
3	8	510	632	$2x10^5$	16.89
4	6	295	483	$2x10^5$	28.67
5	4	285	450	$2x10^5$	26.67
6	2	295	471	$2x10^5$	26.7

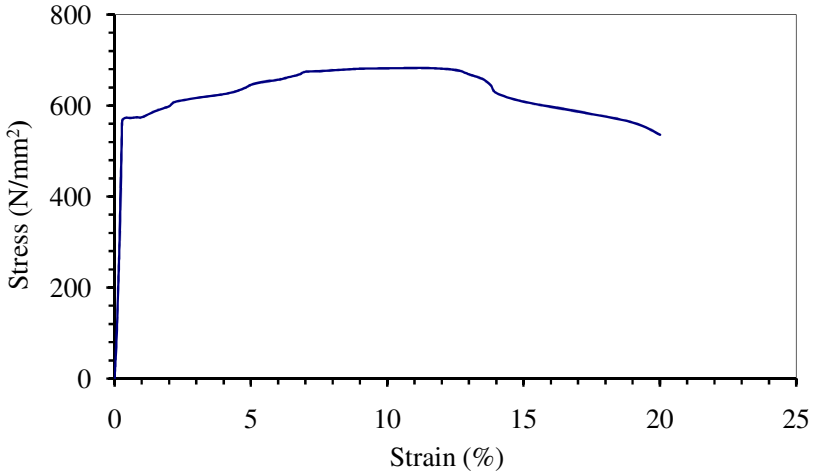

Fig. 2.1 Sample stress-strain curve of 20 mm diameter Fe 500 grade rebar

2.2.2 Materials / equipment for rehabilitation of damaged specimens

The materials used for repairing the damaged control specimens are low viscous epoxy resin (Conbextra EP10), micro concrete (Renderoc RG), concrete bonding agent (Nitobond EP) and Sealant material (Nitocote VF). All these materials were procured from Fosroc Chemicals (India) Pvt. Ltd.. Further, an injection pump (hand operated) and injection packer manufactured by WEBAC Chemie GmbH (Germany) were used for injecting epoxy resin into the cracked zone. The properties of the materials, their applications and specification of equipment are furnished here.

(a) High strength epoxy resin (Conbextra EP10)

High strength epoxy resin is a solvent free resin grout designed for grouting of crack width ranges from of 0.25 to 10 mm. Epoxy resin is an all liquid system consisting of base and hardener. The resin has various advantages such as excellent durability, versatile, excellent service performance, cost effective etc. The properties of resins obtained from the data sheet supplied by the manufacturer are presented in Table 2.7.

Table 2.7 Properties of epoxy resin

Pot life	90 min. @ 20ºC and 40 min. @ 35ºC
Density	approx. 1050 kg/m^3
Tensile strength	26 N/mm^2 @7days
Flexural strength	63 N/mm^2 @7days
Compressive strength	93 N/mm^2 @7days

(b) Micro concrete (Renderoc RG)

Micro concrete is a polymer modified concrete which is supplied as a ready to use dry powders that requires only addition of clean water at site to produce a free-flowing non-shrink repair micro concrete. The materials is based on Portland cements, graded aggregates, fillers and additives which impart controlled expansion characteristic in plastic state. For larger repair the mixed micro concrete may be modified by the addition of 5 mm to 12 mm clean, graded, saturated surface dry aggregates at site. The properties of normal and modified micro concrete obtained from the data sheet supplied by the manufacturer are presented in Table 2.8. Further, concrete cubes of different ranges of aggregate size were collected during the repairing works. The average compressive strength obtained are presented in Table 2.9.

Table 2.8 Properties of normal and modified micro concrete at water: powder ratio of 0.16@30°C and micro concrete: Coarse aggregate of 1:0.75

	Normal	Modified
Compressive strength (Tested on 70.7mm cube as per BS 4551-80)	40 N/mm^2 @ 7 days 50 N/mm^2 @ 28 days	45 N/mm^2 @ 7 days 55 N/mm^2 @ 28 days
Tensile strength (BS 4551-80)	2.0 N/mm^2 @ 28 days	-
Flexural strength (BS 4551-80)	5.0 N/mm^2 @ 28 days	-
Fresh wet density	2100-2200 Kg/m^2	-

Table 2.9 Strength of modified concrete at water: powder ratio of 0.16@30°C and micro concrete: Coarse aggregate of 1:0.75

Aggregate size	Average compressive strength (Tested on 70.7mm cube)
0	53 N/mm^2 @ 28 days
4.75 - 6.3mm	66 N/mm^2 @ 28 days
4.75 - 12mm	58 N/mm^2 @ 28 days

(c) Concrete bonding agent (Nitobond EP)

The bonding agent is based on solvent free epoxy resins containing pigments and fine fillers. The bonding agent is use for bonding newly added cementitious materials to existing concrete surfaces. Nitobond EP has been designed with an overlay time of 10 hrs at 20 ºC and 6 hrs at 30 ºC making it more suitable for use where additional reinforcing bars and formwork has to be fitted. The compressive and tensile strength at 7 days are 50 N/mm^2 and 26 N/mm^2 respectively.

(d) Epoxy resin based putty (Nitocote VF)

Epoxy resin based putty is a thixotropic, solvent free, three component compound based on epoxy resins, graded fillers and thixotropic agents. Nitocote VF can apply directly on the concrete surface to seal the cracks, blow holes etc. Table 2.10 shows the properties obtained from the data sheet supplied by the manufacturer.

Table 2.10 Properties of epoxy resin putty

Pot life	40 min. @ 27ºC
Density	1.6 g/cc
Compressive strength	50 N/mm^2 @ 7days
Drying time	8 hrs @ 27ºC
Fully cure	7 days @ 27ºC

(e) Injection Pump

The pump used in the repairing work was a hand operated suitable for the injection of low viscous resins up to an injection pressure of 100 bar. The pump is equipped with various components (Fig. 2.2). The injection pressure is monitor through the pressure gauge. The pump has a delivery rate capacity of 0.07 L/stroke.

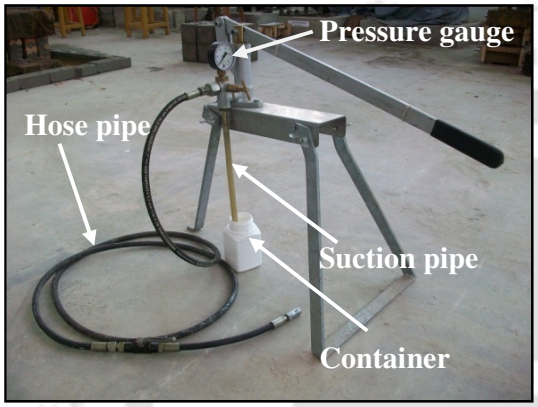

Fig. 2.2 Epoxy injection pump

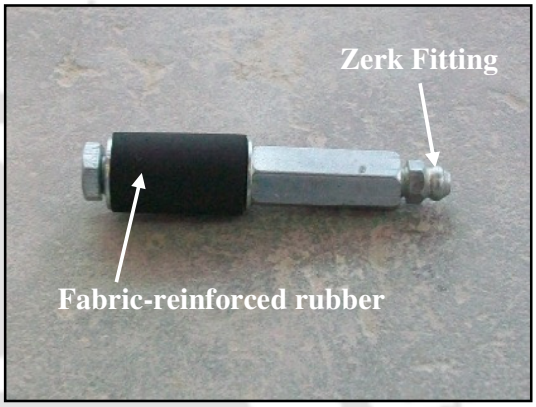

Fig. 2.3 Injection packer

(f) Injection packers

Injection packers are filler necks used as connection pieces between the injection device and the building component when repairing cracks. Zerk head fittings located on the top of the injection packer form the connection to the injection device. Mechanical packers (type S, length of 70 mm and dia. of 13 mm) are used in the repairing works (Fig. 2.3). The packers are drill-hole packers which are screwed into the drill-holes. When tightening the packers a fabric-reinforced rubber sleeve and firmly pressed against the drill-hole sides so that the packers can withstand even highest injection pressures in the drill-hole.

2.3 SELECTION OF FULL SCALE SPECIMEN

The deflected shape of a frame under the action of lateral loading is shown in Fig. 2.4 (a), where the points of contraflexure lie at the mid-span and mid-height of beams and

columns respectively. A free body diagram of an isolated beam-column connection in its deformed position is shown in Fig. 2.4 (b). It comprises of half height of a column at top and bottom as well as half of a beam length. In this figure, h_c is the story height, l_b is half beam span corresponding to the length of the beam connected to the selected joint, N is the internal axial force of the column, P is the beam-tip load, V_{col} *is* the column shear force and Δ is the vertical beam-tip displacement. It may be noted that the symmetric boundary condition should be maintained at both the ends of column for isolation of a single unit of beam-column connection. In this study, a typical full scale residential building with floor to floor height of 3.3 meters and the beam effective span of 3.0 meters were considered. The present study was concentrated on a sub-structure consisting of an external beam-column connection as shown in Fig. 2.4(b).

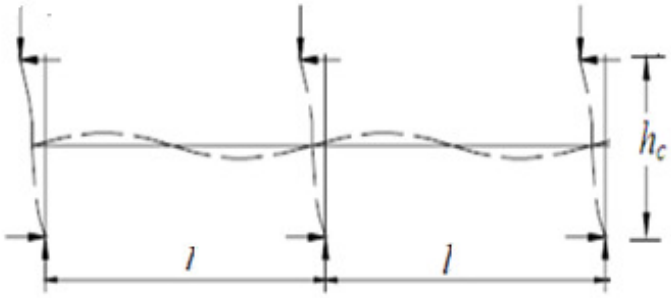

Fig. 2.4(a) Deflected shape of a frame under lateral loading

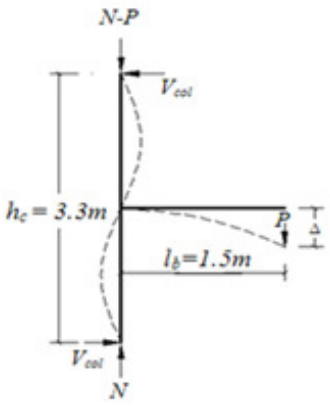

Fig. 2.4 (b) Isolated exterior beam-column connections

2.4 DESCRIPTION OF SPECIMENS

The present study considered three typical deficiency namely, (a) beam-column connections with beam weak in flexure (BWF), (b) beam-column connections with beam

weak in shear (BWS) and (c) beam-column connections with column weak in shear (CWS). In each type, three geometrically similar specimens: full scaled, two-third scaled and one-third scaled sizes were considered. These specimens are treated as control (undamaged). The damaged control specimens were rehabilitated by two rehabilitation strategies.

The naming of the specimens was done with five alphabets; the first three alphabets cover the deficiency type. The fourth for the size, the fifth without the subscript alphabet for the types of specimen which was assigned to the control or undamaged specimens and with the subscript alphabet it was for the rehabilitated specimens. For example, 'BWFLC' stands for beam weak in flexure large control specimen, similarly 'BWSMRe' stands for beam weak in shear medium rehabilitated specimen and 'CWSSC' stands for column weak in shear small control specimens. The detailed descriptions of all the specimens are given in Table 2.11.

2.4.1 Beam Weak in Flexure: Control Specimen

Fig. 2.5 shows the detailing of all beam-column connections with beams weak in flexure: control specimens. For full scaled model, the cross section of the column was 300 mm x 300 mm and that of the beam was 300 mm x 360 mm. Four numbers of high strength deformed bars (Yield strength 500 MPa) of 20 mm diameter was used as reinforcement in column and beam. A lateral tie of 12 mm diameter (HYSD) bar at 75 mm c/c spacing was used in the special confinement zone of the column. In the remaining part of the column, a lateral tie of 6 mm diameter mild steel bars was used with a spacing of 150 mm c/c. In the beam, shear reinforcement of 8 mm diameter (HYSD) bar with a spacing of 75 mm c/c was used near the beam-column joint for a length of 675 mm and 6 mm diameter with a spacing of 120 mm c/c was provided for the remaining part of the beam. The beam has

been designed as under reinforced beam following the provisions of IS: 456 [2000], IS: 1893 [2002] and IITK-GSDMA guidelines for design and detailing of buildings [2006]. The supporting calculations have been furnished in Appendix-A. Strong column-weak beam principle has been adopted for the design of the beam-column connections. For arriving at the tip failure load, the beam was idealized as a cantilever beam. Adequate shear reinforcement was provided to avoid shear failure. Two third and one third scaled specimens were proportionately scaled down in all the three dimensions. The diameter of the reinforcing bars, development length, length of special confinement zone, cover of reinforcement etc. were also scaled down appropriately. The specimens of this category have been cast with concrete of target cube strength of 30 N/mm^2.

2.4.2 Beam Weak in Shear: Control Specimen

Under this category, the specimens were exactly similar in all respect to that of beam weak in flexure: control specimens, except the shear reinforcement provided in beams. The amounts of shear reinforcements were reduced to make the beam weak in shear. For full scaled specimen, 2-legged 6 mm diameter mild steel bars with a spacing of 600 mm c/c were provided as shear reinforcement. In order to maintain a pre-defined failure location, only the first two stirrups near the joint was placed with spacing of 600 mm c/c and for the remaining part of the beam the spacing was reduced to 240 mm c/c. Shear reinforcement was proportionately reduced for scaled down models maintaining geometric similarity. The dimensions and reinforcement details of all the three specimens are shown in Fig. 2.6. The specimens of this category have been cast with concrete of target cube strength of 30 N/mm^2.

2.4.3 Column Weak in Shear: Control Specimen

In this category, for making the column weak in shear, specimens with comparatively weaker grade of concrete than those used in earlier cases were cast. Concrete of target strength of 25 N/mm^2 was used. The cross section of the column was reduced than earlier cases while the cross section of beam was increased to make the beam-column connections as a strong beam-weak column. The design details are furnished in Appendix-A. The main reinforcements in column were maintained similar to those of earlier cases, while same was increased in beam. To ensure the shear weakness of these specimens, spacing for lateral ties in the column was increased. 2-legged 6 mm diameter mild steel bars with a spacing of 900 mm c/c were provided as lateral ties for full scaled specimen. Geometrically similar shear reinforcement was proportionately reduced for scaled down models. The detailing of these specimens is shown in Fig.2.7.

Table 2.11 Descriptions of beam-column connections for control specimens

Specimen	Beam			Column			% Reinforcement
	Span (mm)	Section (mm×mm)	Longitudinal Reinforcement	Length (mm)	Section (mm×mm)	Longitudinal Reinforcement	
BWFLC & *BWSLC	1500	300×360	2-20 ϕ-top 2-20 ϕ-bottom	3300	300×300	4-20 ϕ-total	Beam: 0.58 Col.: 1.396
BWFMC & *BWSMC	1000	200×240	2-12 ϕ+1-8 ϕ-top 2-12 ϕ+1-8 ϕ-bottom	2200	200×200	4-12 ϕ+2-8 ϕ-total	Beam: 0.578 Col.: 1.382
BWFSC & *BWSSC	500	100×120	1-8 ϕ+2-6 ϕ-top 1-8 ϕ+2-6 ϕ-bottom	1100	100×100	2-8 ϕ+4-6 ϕ-total	Beam: 0.65 (equivalent) Col.:1.57 (equivalent)
CWSLC	1500	240×450	3-20 ϕ-top 3-20 ϕ-bottom	3300	240×300	4-20 ϕ-total	Beam: 0.873 Col.: 1.745
CWSMC	1000	160×300	3-12 ϕ+1-8 ϕ-top 3-12 ϕ+1-8 ϕ-bottom	2200	160×200	4-12 ϕ+2-8 ϕ-total	Beam: 0.812 Col.: 1.723
CWSSC	500	80×150	2-8 ϕ-top 2-8 ϕ-bottom	1100	80×100	2-8 ϕ+4-6 ϕ-total	Beam: 0.837 (equivalent) Col.: 1.963 (equivalent)

*Beam weak in shear specimens have same dimensions and longitudinal reinforcement as that of beam weak in flexure specimens except the shear reinforcement provided in beam. Refer Sec.2.4.2 and Fig. 2.6.

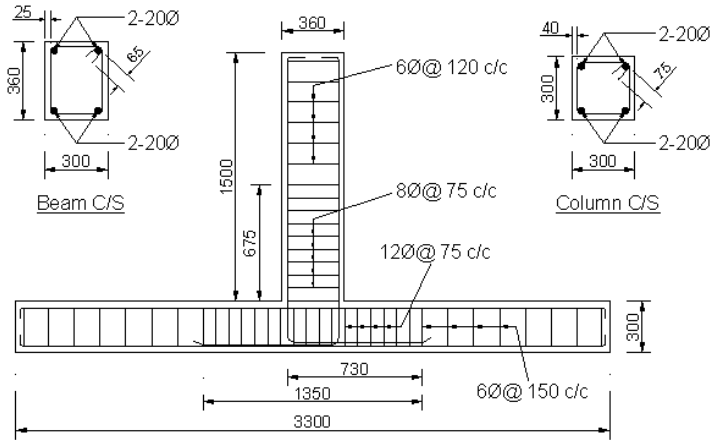

(a)

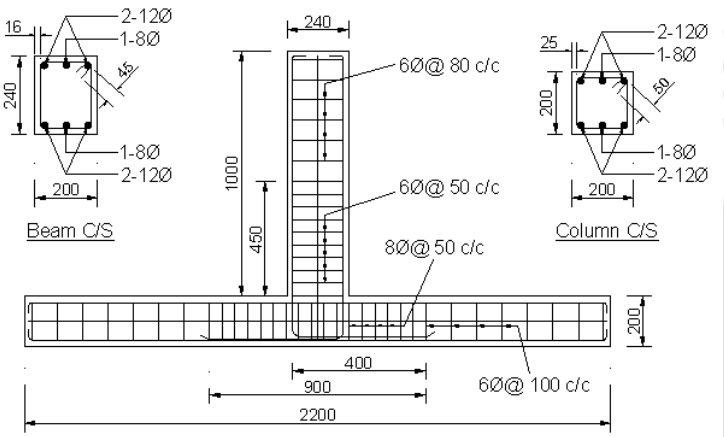

(b)

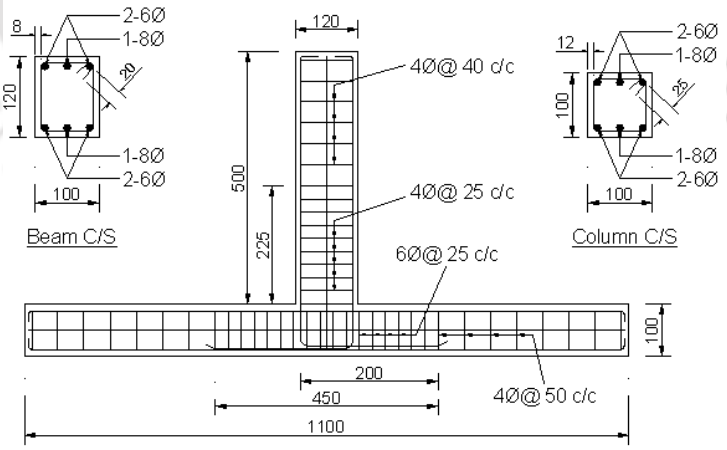

(c)

Fig. 2.5 Reinforcement details of beam weak in flexure: control specimens (a) Full scaled (BWFLC) (b) Two-third scaled (BWFMC) and (c) One- third scaled (BWFSC)

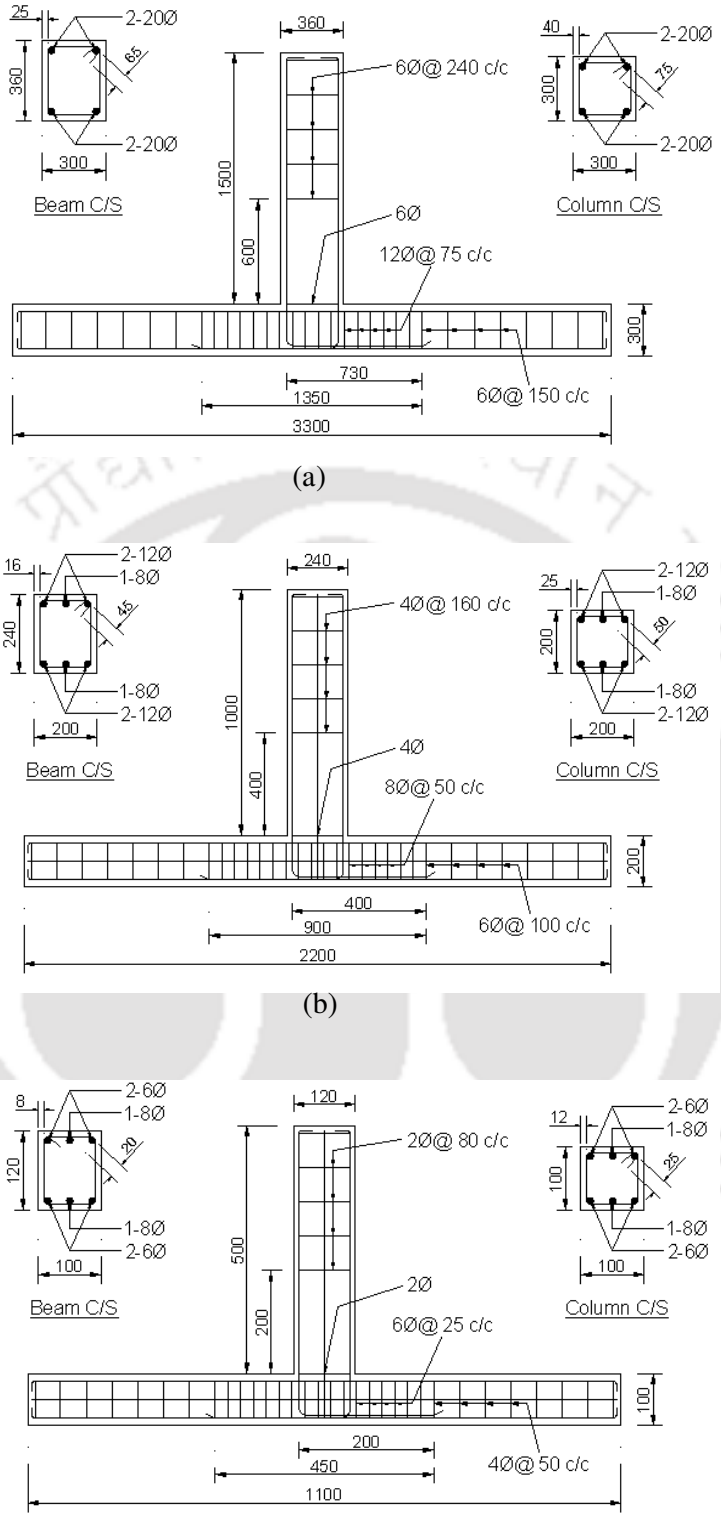

Fig. 2.6 Reinforcement details of beam weak in shear: control specimens (a) Full scaled (BWSLC) (b) Two-third scaled (BWSMC) and (c) One- third scaled (BWSSC)

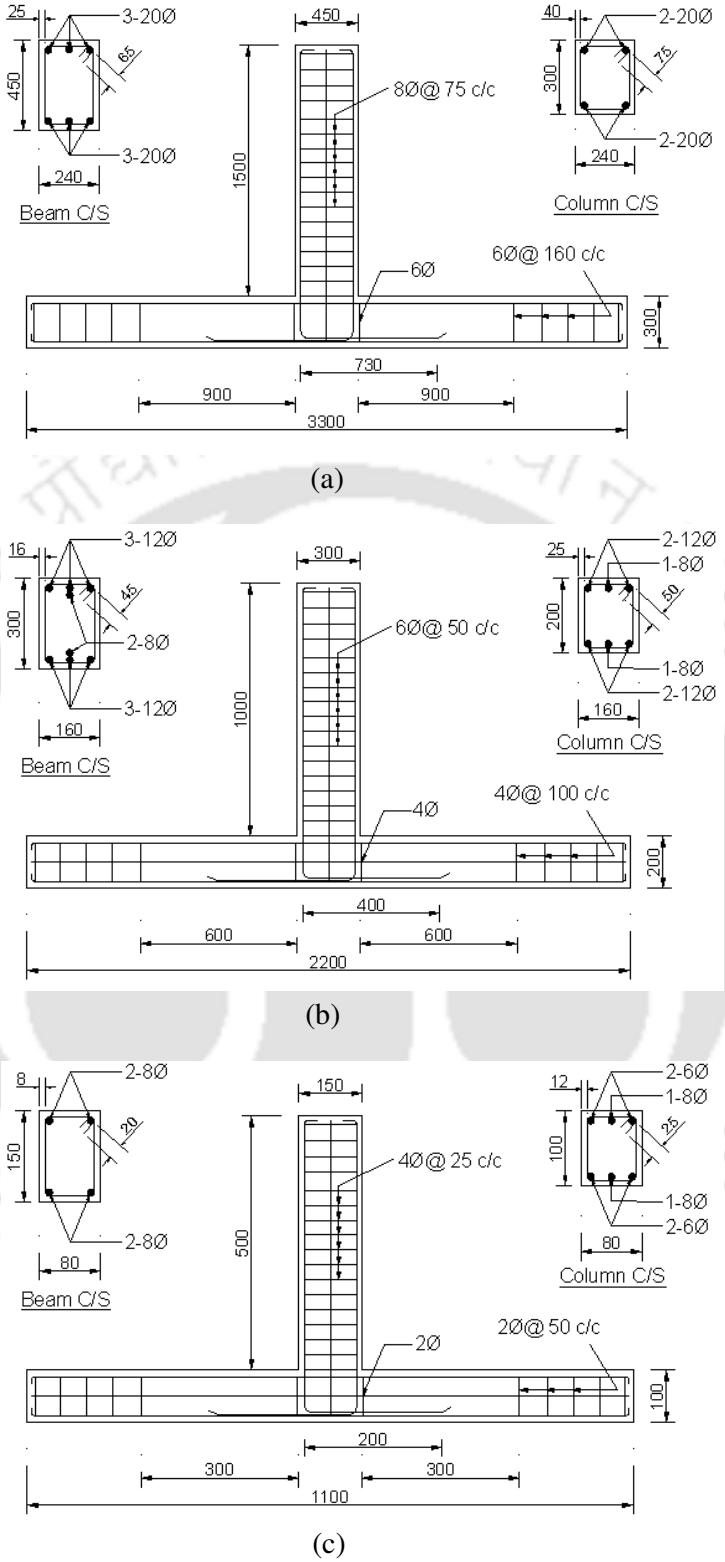

Fig. 2.7 Reinforcement details of column weak in shear: control specimens (a) Full scaled (CWSLC) (b) Two-third scaled (CWSMC) and (c) One- third scaled (CWSSC)

2.5 TEST SET-UP AND LOADING CHARACTERISTICS

2.5.1 Test set-up and instrumentations

Typical schematic diagram of the set-up as shown in Fig. 2.8 was used for experimental investigation. An MTS actuator of 250 kN capacity with an *A* frame was used for testing of large and medium specimens. An MTS actuator of 100 kN capacity was used with two *A* frames for testing of small specimens.

The column of the connection was placed in horizontal position while the beam was placed in vertical position in the set-up. An axial load of 10% of gross capacity of column was applied to the column to represent gravity load. The load on column was applied by a 500 kN capacity jack, which was properly calibrated. The jack was abutting against an *A* frame, which was fabricated for the specified load carrying capacity (Fig. 2.9). To simulate the support condition at both ends of the column, roller supports were fabricated by making grooves inside mild steel plates (Fig. 2.10). The actual testing arrangement for large and medium specimens is shown in Fig. 2.11, while the same for small specimens is shown in Fig. 2.12.

The MTS actuator is equipped with internal load cell and linear-variable differential transformer (LVDT) for measuring applied force and displacement respectively. The LVDT is coaxially mounted within the actuator piston rod. The controller can generate prescribed dynamic displacement or force for the actuator. The actuator is of double ended and double stroke nature. Two actuators of different capacities were used in the testing. The actuator of capacity ±250 kN (Model 244.31) was used for large and medium specimens, while the actuator of capacity ±100 kN (Model 244.22) was used for small specimens. Displacement amplitude is ±125 mm for both the actuators.

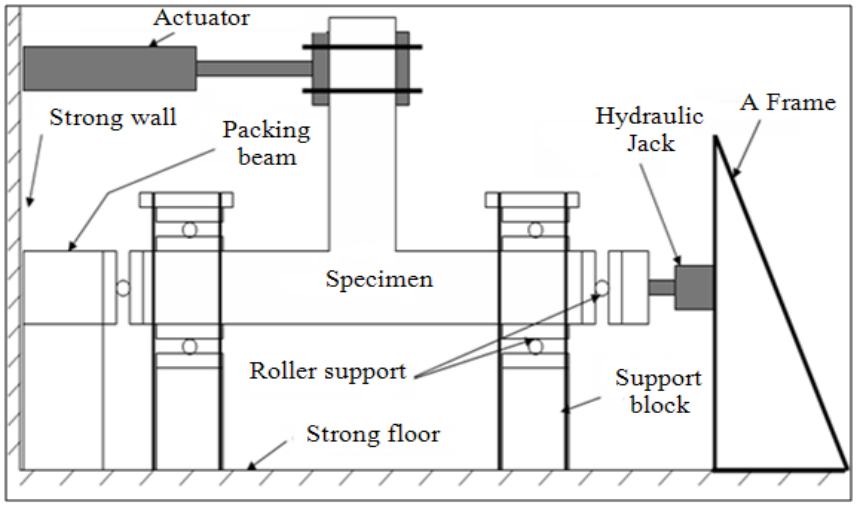

Fig. 2.8 Test set-up for large and medium specimens

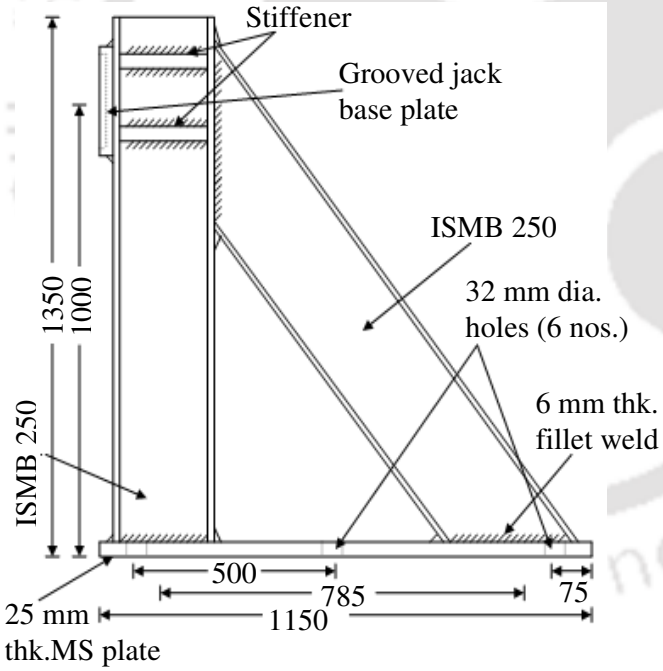

Fig. 2.9 Schematic diagram of '*A*' frame

Fig. 2.10 Roller support at column end

Fig. 2.11 Test arrangement for large and medium specimens

Fig. 2.12 Test arrangement for small specimens

2.5.2 Loading characteristics

The nature and extent of damage in a structure during earthquake depends on the characteristic of loading. Number of cycle in the displacement time history, frequency of excitation and the level of displacement amplitude are some of the parameters which contributes to the extent of damage in a specimen. It was stated in FIB Bulletin 24 [2003] that from several alternative load histories the most severe strength degradation could be observed in specimens subjected to three repeated number of loading cycles at every

amplitude of displacement history.

To accomplish the objectives of this study, test programs were divided based on three loading types.

(a) **Loading type-1**

Displacement controlled mode with a loading frequency of 0.025 Hz was applied to the specimens. The displacement amplitudes were increased after completion of three cycles in each of the amplitude.

(b) **Loading type-2**

Same as loading type-1 with one loading cycle at every displacement amplitude.

(c) **Loading type-3:**

Same as loading type-2 with increased loading frequency of 1.0 Hz.

In type-1 loading, numbers of cycles are three times that of the type-2 loading. Therefore, effects of numbers of cycles on different parameters influencing performance of beam-column connection will be investigated on the basis of these two types of loading. Most of the test conducted for RC beam-column connections are of quasi-static nature. The frequencies are substantially lower than those corresponding to the actual seismic excitation. Therefore, to explore the effect of cyclic loading frequency on the behaviour of RC beam-column connection, loading frequency in type-3 is 40 times higher than that of type-1 and type-2. Different loading types were adopted in order to have different extent of damages on the specimens. Therefore, different rehabilitation strategies may be adopted depending on these damages.

The typical displacement histories of all loading types are shown in Fig. 2.13-2.15 respectively. The details descriptions of test specimens corresponding to the loading characteristics are shown in Table 2.12.

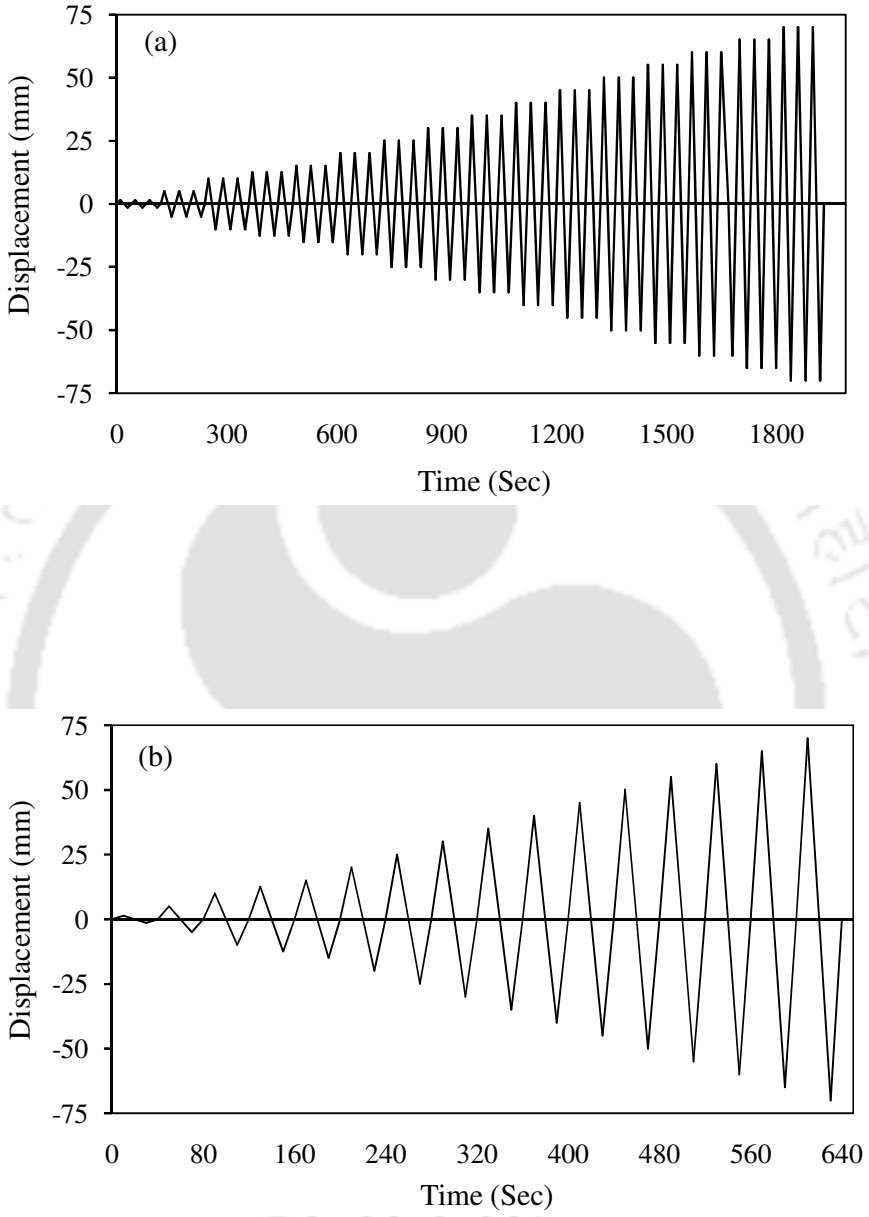

Fig. 2.13 Typical displacement history for full scaled specimens
(a) Loading type-1 and (b) Loading type-2

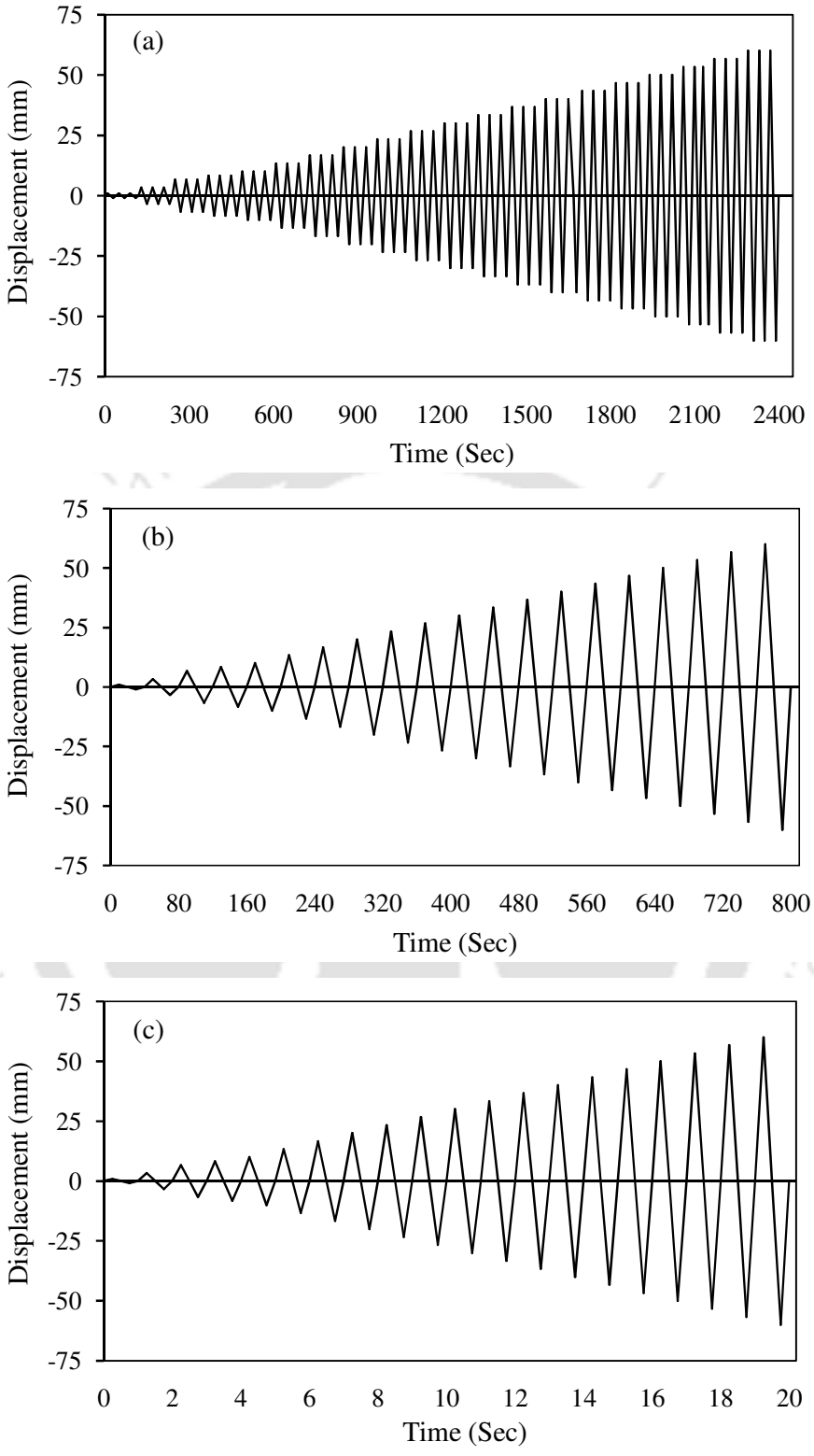

Fig. 2.14 Typical displacement history for two-third scaled specimens
(a) Loading type-1 (b) Loading type-2 and (c) Loading type-3

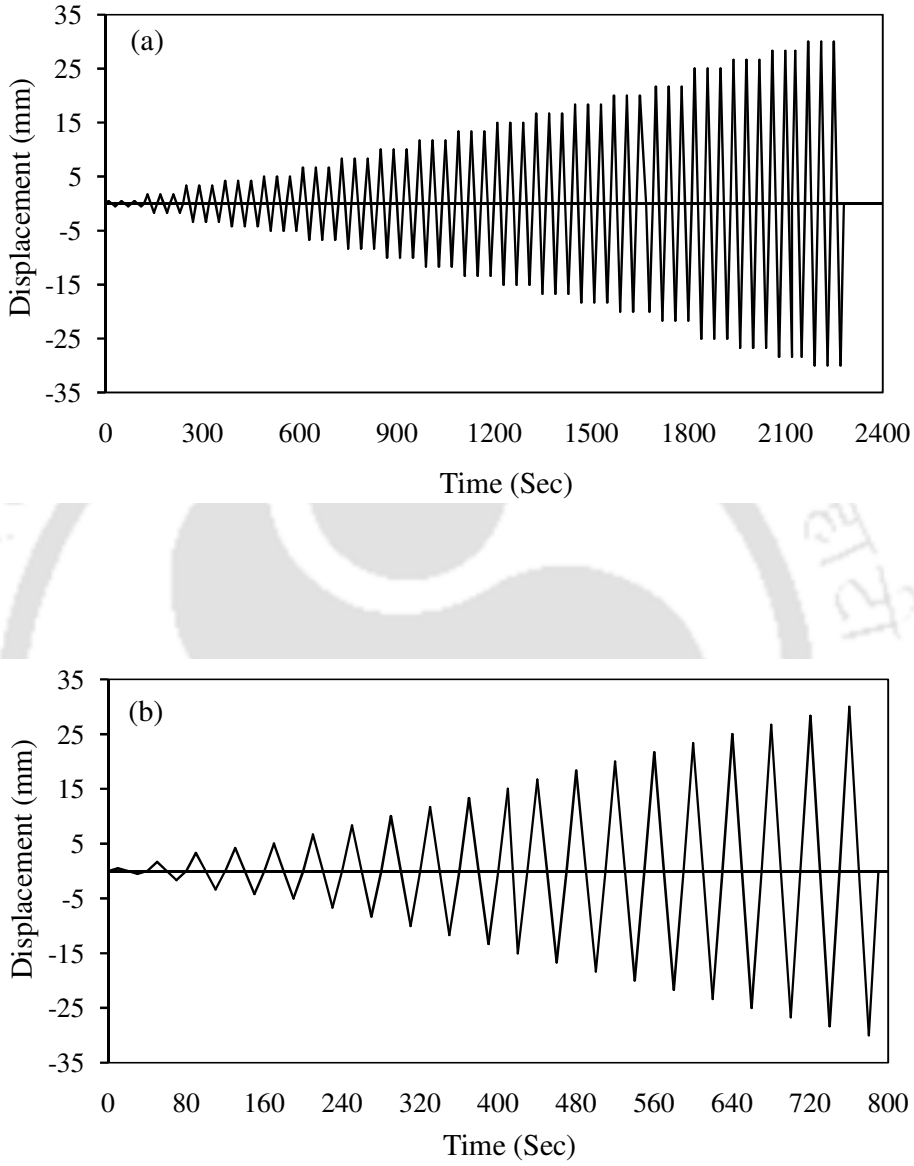

Fig. 2.15 Typical displacement history for one-third scaled specimens (a) Loading type-1 and (b) Loading type-2

Table 2.12 Description of the test specimens and loading characteristics

Deficiency type	Sl.No.	Loading Type-1	Loading Type-2	Loading Type-3
Beam Weak in Flexure (BWF)	1	BWFLC	BWFLC	BWFMC
	2	BWFMC	BWFMC	BWFMRe
	3	BWFSC	BWFSC	
	4	BWFLRe	BWFLRe	
	5	BWFMRe	BWFMRe	
	6	BWFSRe	BWFSRe	
Beam Weak in Shear (BWS)	7	BWSLC	BWSLC	BWSMC
	8	BWSMC	BWSMC	BWSMRe
	9	BWSSC	BWSSC	
	10	BWSLRe	BWSLRe	
	11	BWSMRe	BWSMRe	
	12	BWSSRe	BWSSRe	
Column Weak in Shear (CWS)	13	CWSLC	CWSLC	CWSMC
	14	CWSMC	CWSMC	CWSMRe
	15	CWSSC	CWSSC	
	16	CWSLRe	CWSLRe	
	17	CWSMRe	CWSMRe	
	18	CWSSRe	CWSSRe	

Note, *C* = Control specimens, *Re* = Rehabilitated specimens

The amplitudes of the displacement histories reported by Choudhury [2010] have been adopted in this study. It may be noted that Choudhury [2010] carried out nonlinear static analysis for facilitating appropriately planning of the experimental investigation, where the information about loading at first crack, crack pattern, load and deflection at yielding, ultimate load etc. were obtained. The first amplitude applied in full scaled models was ± 1.4 mm. This displacement level corresponds to appearance of first crack as per result of numerical analysis. This was followed by displacement amplitude of ±5.0 mm, ±10.0

mm, ±12.5 mm ±15.0 mm and there after displacement amplitude increment of 5.0 mm was applied. Displacement amplitude of ±12.5mm was chosen because at this displacement level yielding of steel was expected as per prediction from numerical analysis. Amplitude of the displacement histories were scaled down for two-third and one-third models respectively. The experiment for control specimens was stopped at a stage when the load came down in the range of 60-70 % of the ultimate load carrying capacity. All rehabilitated specimens were retested with the same loading sequence as that imposed on the control specimens. However, control specimens were subjected to slightly lower final displacement level as the failure occurred earlier compared to those of the rehabilitated.

2.6 REHABILITATIONS METHODOLOGY

The repairing strategy was aimed to retrieve back the lost capacity of the damaged connections to the original seismic capacity in term of strength, energy dissipation, ductility etc. Two rehabilitation strategies were employed depending on the degree of damages. These were (1) partial replacement of loose concrete on the damaged area by micro concrete followed by epoxy injection into crack zone and (2) complete replacement of crushed concrete on the damaged area by micro concrete followed by epoxy injection into crack zone.

The voids created after removal of loose materials were patched or filled with micro concrete after a suitable bonding agent was applied on the clean surface for attaining adequate bond between old and fresh concrete. Holes were drilled along cracks and packers were inserted through these holes, which served as filler neck for epoxy injection. Visible cracks were sealed and a low viscous epoxy resin was injected under high pressure into the cracked zone. The repaired specimens were kept undisturbed for 7 days.

After an injected epoxy resin attained sufficient strength, the installed packers were removed by striking its head and thereafter a grinding machine was used to remove the sealing materials. Fig. 2.16 illustrates various steps of repair operation under repair method-1 for a typical damaged beam-column connection. The repair method was adopted to rehabilitate all damaged specimens under loading type-2, BWFM and CWSM specimens under loading type-3. Similarly, the step by step repairing strategies for method-2 has been demonstrated in Fig. 2.17. All specimens under loading type-1 and BWSM specimen under loading type-3 were rehabilitated by this repair method.

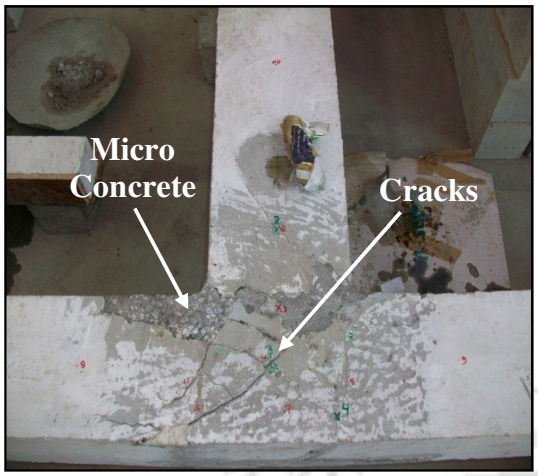

(a) Patching of spalled concrete

(b) Drilling holes along cracks

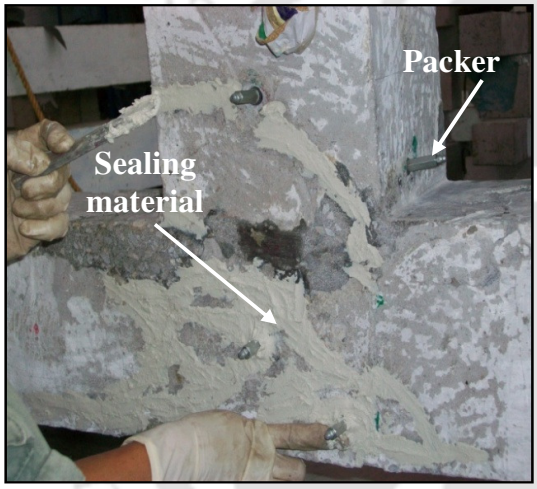

(c) Installed packers and sealing cracks

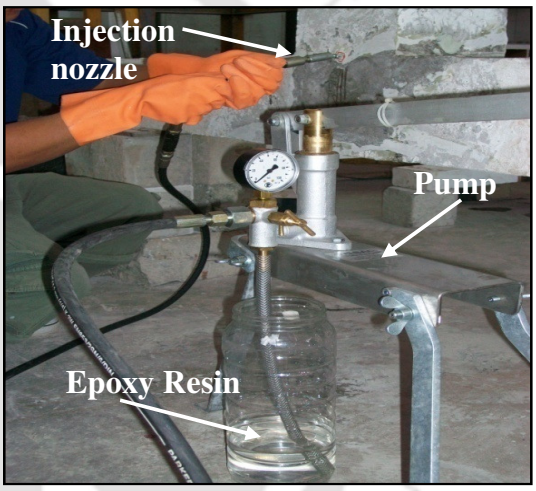

(d) High pressure epoxy injection

(e) Removing of installed packers

(f) Removing of sealing materials

Fig. 2.16 Step by step repairing strategy (Method-1)

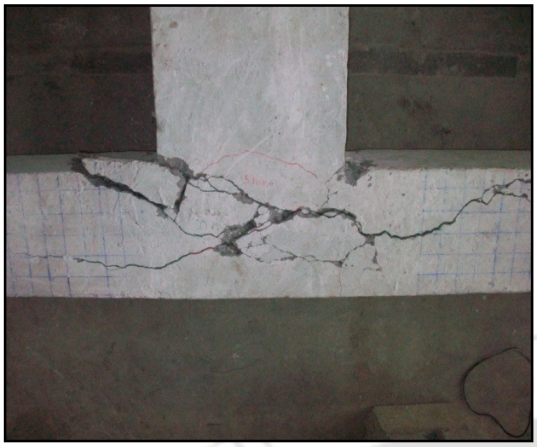

(a) Damaged specimen

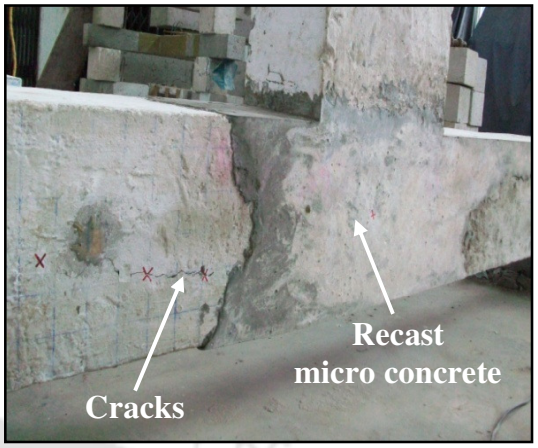

(b) Replacement of loose concrete

(c) Drilling holes along cracks

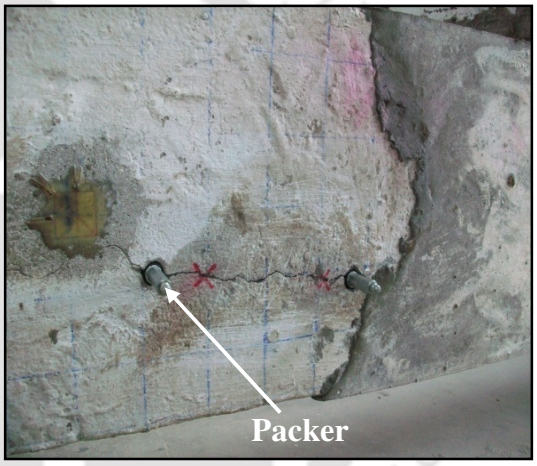

(d) Packers installation

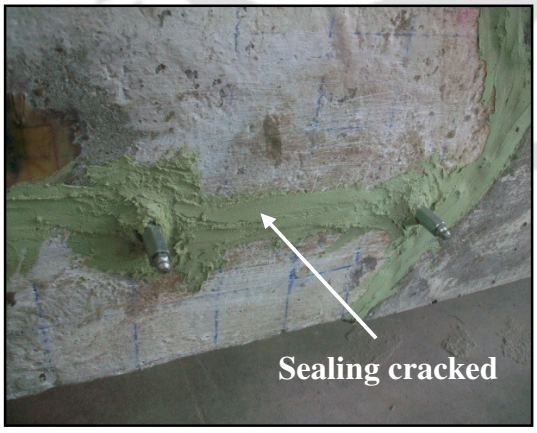

(e) Sealing of crack

(f) Epoxy resin injection

Fig. 2.17 Step by step repairing strategy (Method-2)

2.7 CRACKS MEASUREMENT AND ASSESSMENT OF SPECIMENS USING ULTRASONIC PULSE VELOCITY TESTING

Specimens subjected to cyclic loading cause various cracks. The specimens suffer more and more wide cracks as the displacement amplitude increases. In this study, specimens were monitor during testing to gather information about the nature and pattern of cracks, crack width at every stage of loading till the experiment was stopped. An approximate amount of epoxy resin to be injected into the cracked zone may be estimated if information about the crack width, depth of crack and length of crack are known. Measurement of cracks was done with vernier or steel ruler. A typical cracks measurement is shown in Fig. 2.18.

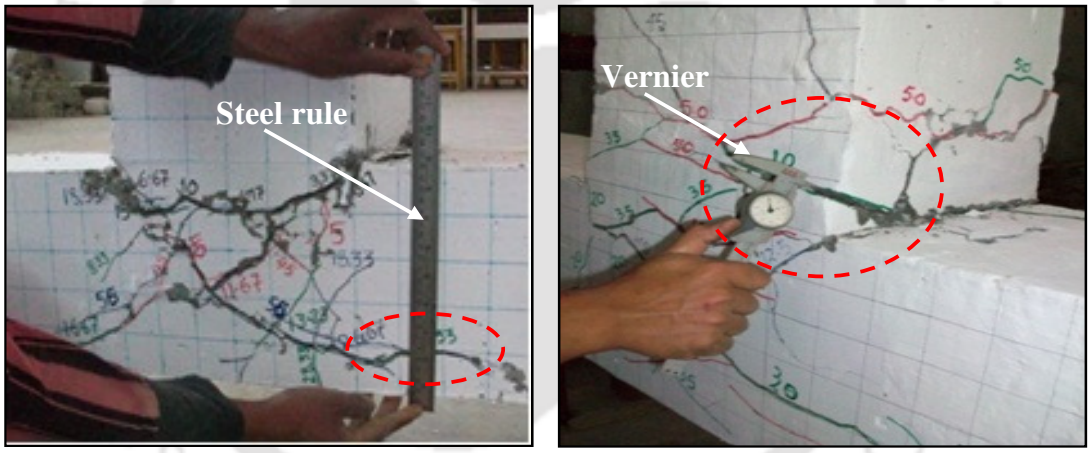

Fig. 2.18 Typical cracks measurement

Ultrasonic scanning is a recognized non-destructive test method to assess the homogeneity and integrity of concrete. Typical UPV test of specimens before and after rehabilitation are shown in Fig.2.19. Similar locations of transducers (receiving and transmitting) during the UPV test were maintained in both specimens before and after rehabilitations. This was done for facilitating comparative understanding of the UPV

values. Guidelines regarding qualitative assessment of concrete quality based on the UPV test was adopted as per IS: 13311 (Part I)-1992.

Before rehabilitation After rehabilitation

Fig. 2.19 Typical UPV test on specimens

2.8 CONCLUDING REMARKS

In this chapter, characterization of all materials needed for casting and rehabilitating the beam-column connections have been presented. Detailed descriptions of beam-column connections, rehabilitation strategies and the testing arrangement have been discussed. Test program to achieve the objectives have been identify. An '*A*' frame of appropriate capacity was used to facilitate the application of gravity loads and keeping the specimens in proper position during testing. A roller support was used by drilling groves inside MS plate for maintaining appropriate boundary conditions at all contact point of the columns during testing. Finally, measurement of cracks and assessment of specimens using UPV testing has also been discussed.

CHAPTER 3

STUDY ON REHABILITATED RC BEAM-COLUMN CONNECTIONS WITH BEAM WEAK IN FLEXURE

3.1 INTRODUCTION

This chapter describes the findings of experimental investigation and interpretation of those experimental results of beam-column connections with beam weak in flexure. Connections with different sizes namely large, medium and small sizes were tested. The control specimens were subjected to either loading type-1 or type-2. Depending on the degree of damage, the specimens were rehabilitated with either repair method-1or method-2. All specimens were monitored during testing in order to gather information about the crack location, pattern and width at every stage of loading till the experiment was stopped. Data recorded during testing were used for post processing to evaluate many important parameters related to seismic capacity of the connections. Effectiveness of the applied repair technique was assessed based on the comparison of the seismic performance of rehabilitated specimens with those of the respective control specimens. Further, Bi-logarithmic plots were drawn to explore the possibility of existence of size effect in term of strength. Correlations of specimen sizes with cumulative energy dissipation per unit volume of D-region and stresses were also made.

3.2 TESTING OF LARGE SIZE CONNECTIONS

The nature and extent of damage in a structure during earthquake depends on the characteristic of loading. Number of cycle in the displacement time history, frequency of excitation and the level of displacement amplitude are some of the parameters which

contributes to the extent of damage in a specimen. The displacement histories as shown in Fig. 2.13 (a,b) of Sec. 2.5.2 were applied to these specimens using a servo hydraulic dynamic actuator of loading capacity ± 250 kN and having a maximum displacement range of ± 125 mm. The experiment was stopped for control specimens at a stage when the load came down in the range of 60-70 % of the ultimate load carrying capacity. Similarly, the experiment on rehabilitated specimens was also stopped at about the same magnitude of load at which experiment was stopped for control specimens.

3.2.1 Behaviour of connections under loading type-1

In this category of loading, the displacement amplitudes were gradually increased with three repeated number of loading cycles at every amplitude of displacement history. The actual testing arrangement for large specimens has been shown in Fig. 2.11. A close view of the damaged area of a specimen at the end of the experiment is shown in Fig. 3.1. Some of the important observations made during testing along with those made during analysis of the hysteresis loops have been discussed in details in this section.

The nature of failure in both control as well as rehabilitated specimens were generally similar. The first flexural crack appeared in the beam very close to the beam-column joint at a displacement of ± 5.0 mm. More cracks started to develop in the joint region as the displacement amplitude of the displacement history was increased.

The hysteretic response obtained by plotting the test data is presented in Fig. 3.2. It is observed from these loops that both control as well as rehabilitated specimens attained their maximum loads at 22^{nd} cycles at a displacement amplitude of ± 30 mm. Control specimen attained its maximum values of 72.02 kN in the push and 74.55 kN in the pull direction. However, a slightly higher load of 83.78 kN and 84.39 kN in push and pull directions respectively were attained by the rehabilitated specimen.

The cracks at the beam-column joint interface in both control as well as rehabilitated specimens got further widened on reaching a displacement of ± 35 mm. At a displacement of ± 40 mm, few cracks formed in the joint region started propagating toward the column region for both the specimens. At a displacement amplitude of ± 50 mm, spalling of concrete started from the joint region of the control specimen with further widening of existing cracks. The beam could be observed to rotate at the beam-column joint region and development of plastic hinge at the joint interface was evident. The rehabilitated specimen exhibited similar behaviour at a slightly higher displacement of ± 55 mm. The experiment for the control specimen was stopped at a displacement amplitude of ± 65 mm at which the load came down about 67 % of the ultimate load carrying capacity. The maximum load obtained by averaging the peak load in the push and pull directions was considered as the ultimate load carrying capacity of the specimen. The load carrying capacity for BWFLC specimen was thus found to be 73.285 kN. However, the rehabilitated specimen was observed to be still capable of carrying further load at the displacement level where the test for control specimen was stopped. The experiment for rehabilitated specimen was finally stopped at ± 70 mm for ensuring safety of testing equipment. The maximum load for BWFLRe specimen was found out to be 84.085 kN.

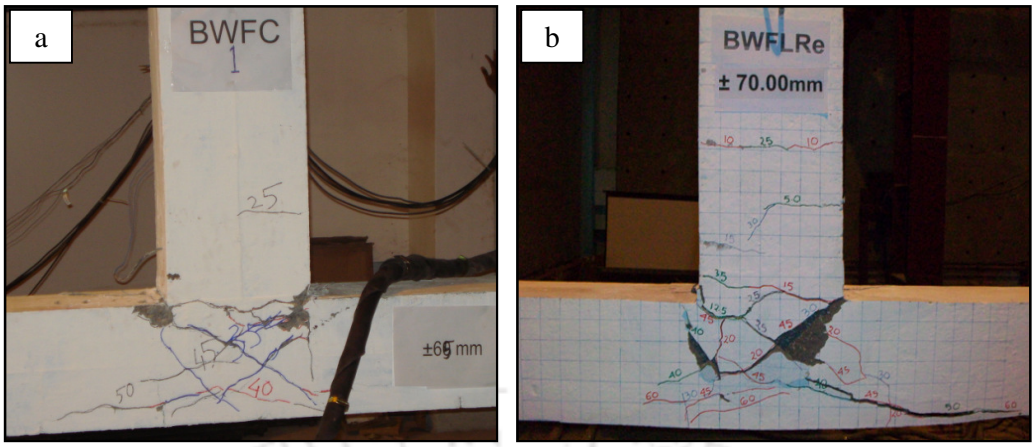

Fig. 3.1 BWFL specimens at the end of test under loading type-1:
(a) Control and (b) Rehabilitated

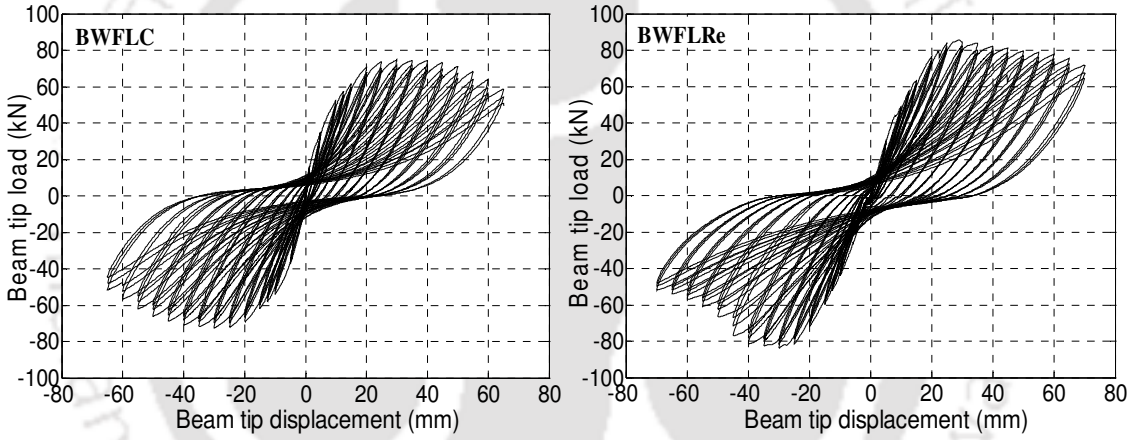

Fig. 3.2 Hysteretic response of BWFL specimens subjected to loading type-1

3.2.2 Behaviour of connections under loading type -2

In this category of loading, the displacement amplitudes were gradually increased with one loading cycle at every amplitude of displacement history. Appearances of cracks during the initial loading and the damaged specimen at the end of test are shown in Fig. 3.3 and Fig. 3.4 respectively for both control and rehabilitated specimens. From these figures, it is clear that the crack pattern on both the specimens were generally similar. However, on comparing the extent of damage with the specimens under loading type-1, it

was observed that the crack width of the control specimen was a little wider in this category of loading type; but no major crushing of concrete had taken place at the joint region. Minor crushing at the joint interface and joint edges could only be observed. Some of the important observations made during testing along with those made during analysis of the hysteresis loops have been discussed in details in this section.

The first flexural crack appeared in the beam-column joint interface at a displacement of ± 5.0 mm for both the specimens. More cracks started to develop in the junction and joint region on further increase in displacement (Fig. 3.3). It is observed from the hysteresis loop as shown in Fig. 3.5 that the control specimen attained its maximum loads of 74.98 kN and 72.23 kN at 9^{th} and 10^{th} cycle in the push and pull direction respectively. At the same loading cycle, a slightly higher load of 83.35 kN and 72.78 kN corresponding to push and pull directions were attained by the rehabilitated specimen.

Crack of comparable magnitude at the joint interface of both control and rehabilitated specimens got further widened at a displacement of ± 40 mm. At ± 50 mm displacement, these cracks at the joint region started propagating towards the column part. There was however no spalling of concrete at the joint region even at a displacement of ± 55 mm for the control specimen. Instead, an X shaped crack that propagated from the joint region toward the column part got further widened. However, at a displacement of ± 55 mm, minor crushing of concrete was observed at the joint region for the rehabilitated specimen. The joints started to behave like a hinge and closing/opening of cracks became distinct at a displacement of ± 60 mm for both the specimens. The experiment on control specimen was stopped at the same displacement level of ± 65 mm as in the case of loading type-1 for the control specimen. This was for facilitating comparative understanding of their behaviour. At this displacement amplitude, crack width of about 5 mm was observed at the joint region for the control specimen. The ultimate load carrying

capacity for control specimen was found to be 73.605 kN. Rehabilitated specimen also suffered similar magnitude of damaged at the same displacement level as that of control specimen. However, the rehabilitated specimen was observed to be still capable of carrying further load at the displacement level of ± 65 mm where the test for control specimen was stopped. The experiment for rehabilitated specimen was finally stopped at ± 70 mm for ensuring safety of testing equipment. The maximum load for BWFLRe specimen was found out to be 78.065 kN.

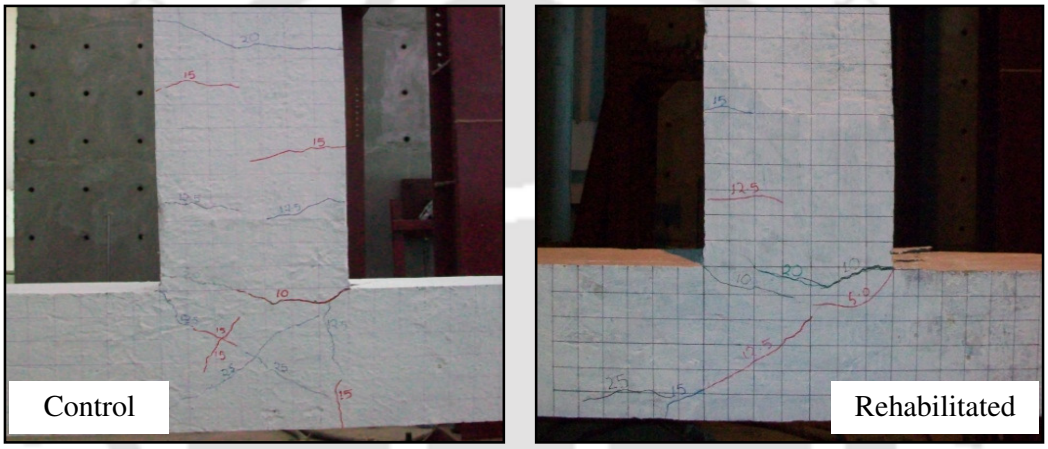

Fig. 3.3 Cracks appearance at initial loading cycles for BWFL specimens under loading type-2

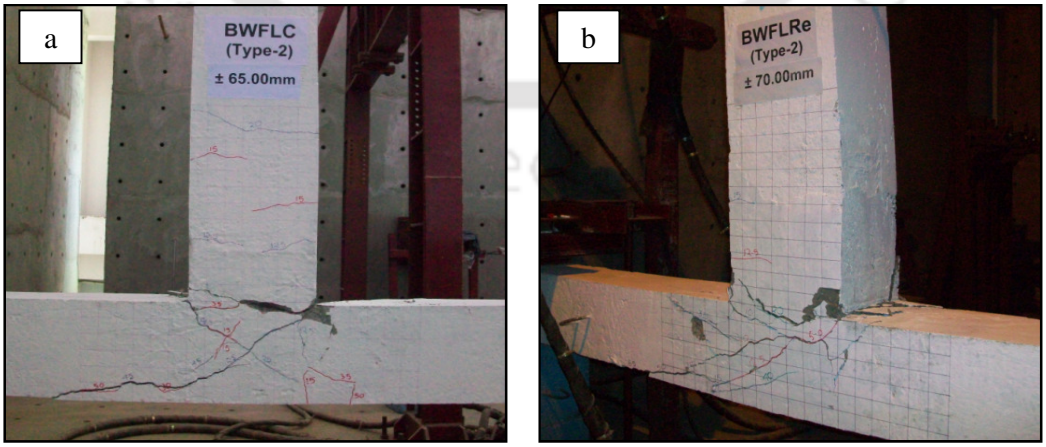

Fig. 3.4 BWFL specimens at the end of test under loading type-2: (a) Control and (b) Rehabilitated

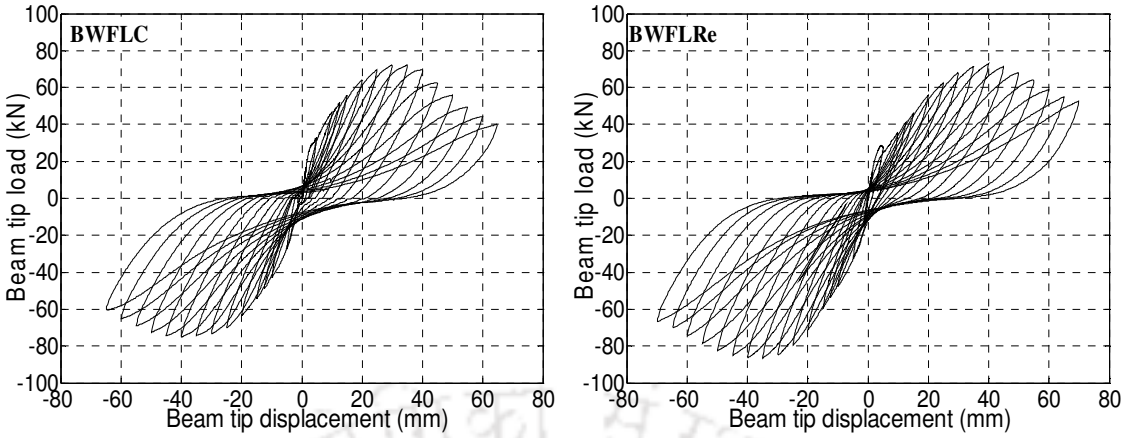

Fig. 3.5 Hysteretic response of BWFL specimens subjected to loading type-2

3.3 TESTING OF MEDIUM SIZE CONNECTIONS

The displacement histories as shown in Fig. 2.14 (a,b) of Sec. 2.5.2 were applied to these specimens using a servo hydraulic dynamic actuator of capacity ±250 kN. The experiment was stopped when the percentage reduction in load carrying capacity was of similar order as that in the case of largest specimens.

3.3.1 Behaviour of connections under loading type-1

Loading characteristics (number of cycle in the displacement time history and loading frequency) was same as that of large size specimens under loading type-1. Appearance of first visible crack is shown in Fig. 3.6. The condition of the specimen at end of testing is shown in Fig. 3.7. The hysteretic response obtained by plotting the test data is shown in Fig. 3.8. Some of the important observations made during testing along with those made during analysis of the hysteresis loops have been discussed in details in this section.

No crack was observed up to the applied displacement amplitude of ±3.33 mm. As soon as the next amplitude of ±6.67 mm was applied, the first flexural crack appeared in the beam part for both the specimens. Just after the appearance of the first crack, 2nd and 3rd

cracks also appeared at the joint interface and joint area in the consecutive cycles of the same amplitude. All these developed cracks are seen in Fig. 3.6. For control specimen, the load reached the maximum of 32.74 kN in push direction at 25th cycle at a displacement of 26.67 mm and 36.95 kN in pull direction at 16th cycle at 16.67 mm displacement. Rehabilitated specimen attained its maximum load of 39.86 kN and 42.13 kN at same cycles of 34th in both push and pull directions at displacement of 33.33 mm. At a displacement of $\pm$26.67 mm opening of cracks for the control specimen started and gradually continued from both ends of the joint and few cracks also started propagating toward the column part. Initial cracks for rehabilitated specimens started to get widened at displacement amplitude of $\pm$33.33 mm. Cracks started propagating towards the joint region as the displacement amplitude was increased. Spalling of concrete was also observed at the beam-column joint edges. In both the specimens the opening and closing of cracks became apparent and many cracks started to become wider at displacement amplitude of $\pm$36.67 mm. No new crack was observed when the displacement reached to $\pm$ 40 mm. On further increase in displacement, crushing of concrete at the joint region and joint edges were observed to be quite severe for both the specimens. Finally, the experiment was stopped at $\pm$60 mm for control specimen while for rehabilitated specimen; $\pm$63.33 mm was the ultimate displacement. The ultimate load carrying capacity of control and the rehabilitated specimens were found to be 34.845 kN and 40.995 kN respectively.

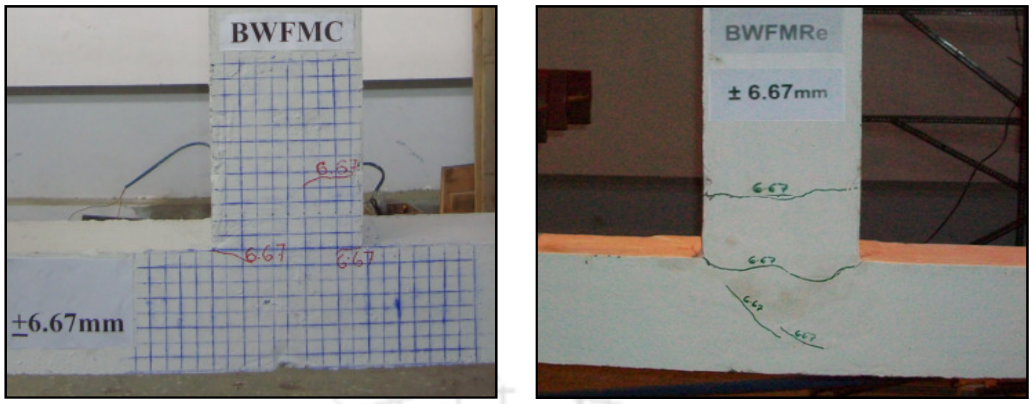

Fig. 3.6 Appearance of first cracks for BWFMC and BWFMRe specimens under loading type-1

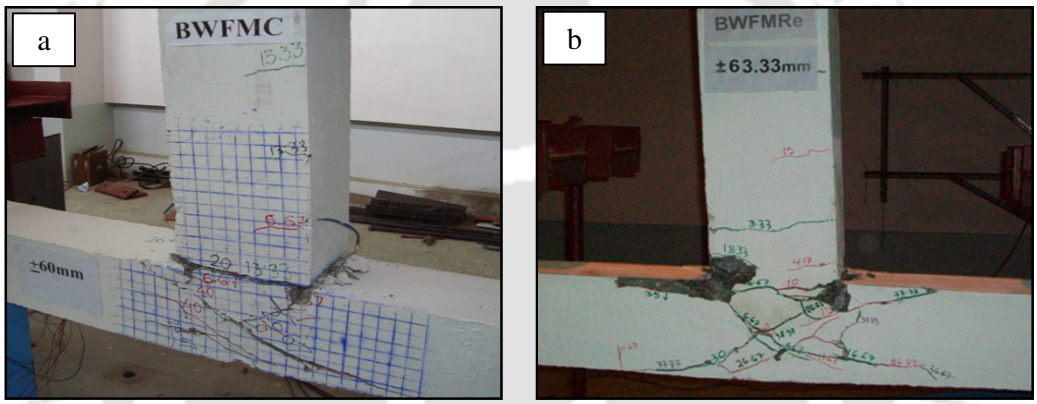

Fig. 3.7 BWFM specimens at the end of test under loading type-1: (a) Control (b) Rehabilitated

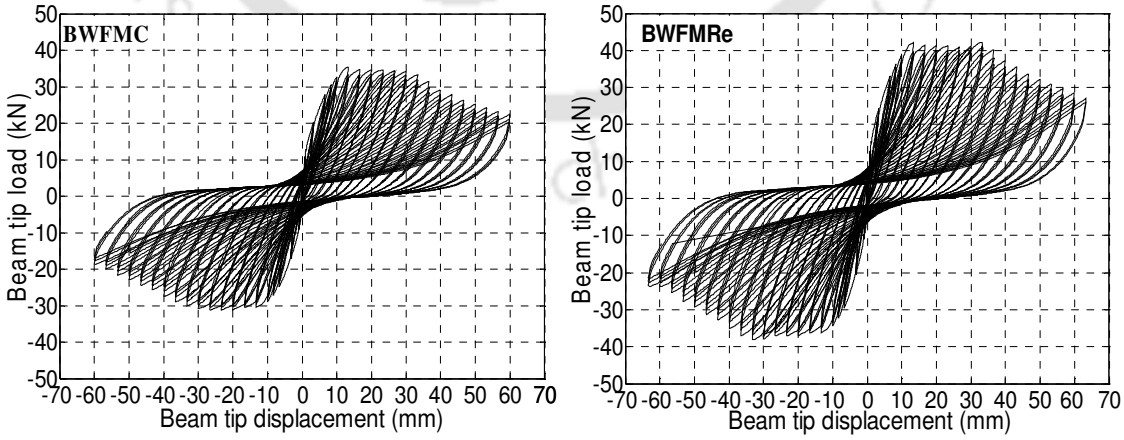

Fig. 3.8 Hysteretic response of BWFM specimens subjected to loading type-1

3.3.2 Behaviour of connections under loading type -2

Loading characteristics (number of cycle in the displacement time history and loading frequency) was same as that of large size specimens under loading type-2. Initiation and propagation of cracks at the early loading stage and the damaged specimen at the end of test are shown in Fig. 3.9 and Fig. 3.10 respectively for both control and the rehabilitated specimens. The crack patterns at the joint region in both the specimens at the end of the experiment were generally similar. It was also observed that while most of the cracks were concentrated at the joint areas for the control specimen, the cracks were wide spread at the beam part for the rehabilitated specimen.

Further, the first flexural crack was observed at a displacement of $\pm$ 6.67 mm, which appeared at the beam-column joint interface for the control specimen, while the same for the rehabilitated specimen got shifted toward the beam part. This showed that the injected epoxy prevented the early opening of cracks at the repaired zone. It is observed from the hysteresis loop in Fig. 3.11 that the control specimen attained its maximum load of 35.99 kN and 36.00 kN at 8^{th} cycle in the push and pull directions respectively. At the same loading cycles a slightly higher values were attained by the rehabilitated specimen with maximum of 39.00 kN and 39.50 kN at the same displacement of $\pm$ 20 mm in the push and pull direction respectively.

At a displacement of $\pm$ 30 mm, a wide crack at the joint area and joint interface of the control specimen was observed and some crack from the joint area started propagating toward the column part. At $\pm$ 46.67 mm, though no new cracks were formed, existing cracks at the joint area and column part got further widened. However, for the rehabilitated specimen, the cracks were mostly concentrated at the beam-column joint interface and on the beam part. At $\pm$ 50 mm, the joint started to behave like a hinge and closing and opening of crack became distinct with crushing of concrete at the beam-

column joint interface and joint edges. The experiment was stopped at the same displacement level of ± 60 mm for BWFMC and ± 63.33 mm for BWFMRe. The displacement limits were kept same as those for testing under loading type-1. This was for facilitating comparative understanding of their behaviour. The ultimate load carrying capacity for BWFMC and BWFMRe specimens were found out to be 35.995 kN and 39.250 kN respectively.

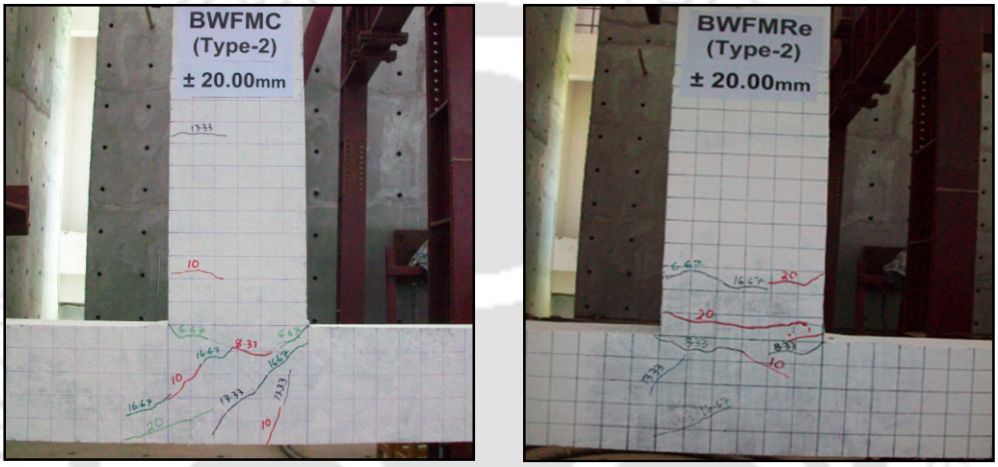

Fig. 3.9 Initial appearance of cracks for BWFM specimens under loading type-2

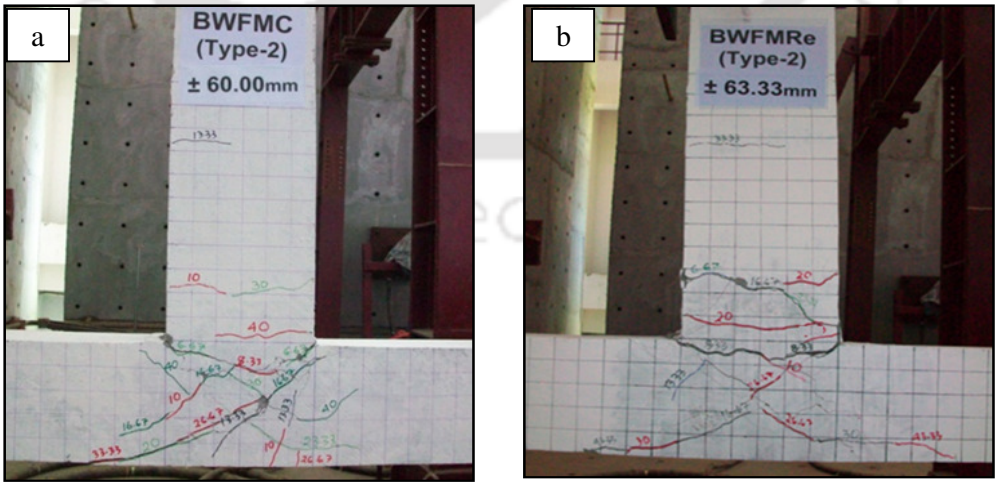

Fig. 3.10 BWFM specimens at the end of test under loading type-2: (a) Control and (b) Rehabilitated

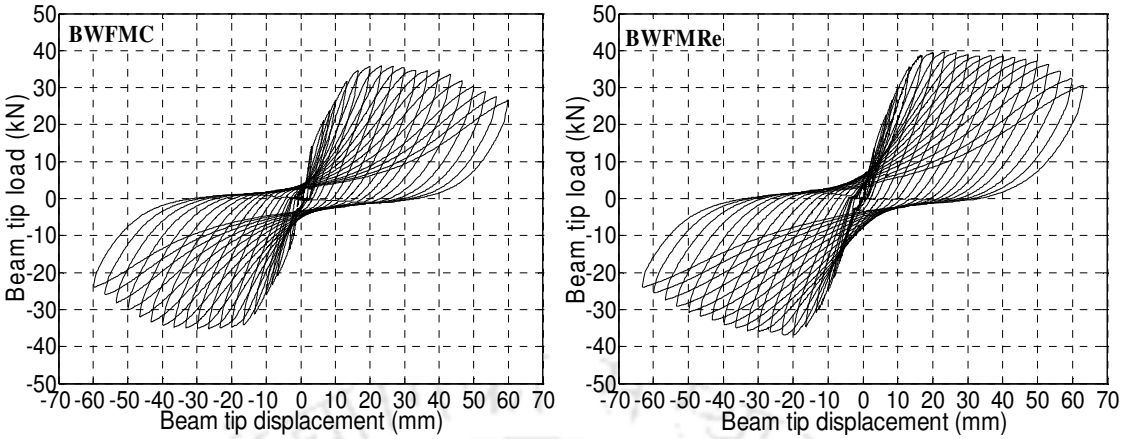

Fig. 3.11 Hysteretic response of BWFM specimens subjected to loading type-2

3.4 TESTING OF SMALL SIZE CONNECTIONS

The displacement histories as shown in Fig. 2.15 (a,b) of Sec. 2.5.2 were applied to these specimens using a servo hydraulic dynamic actuator of capacity ± 100 kN and having a maximum displacement range of ± 125 mm. The experiment was stopped when the percentage reduction in load carrying capacity was of similar order as that in the case of large and medium size specimens.

3.4.1 Behaviour of connections under loading type-1

Loading characteristic (number of cycle in the displacement time history and loading frequency) was same as that of large and medium size specimens under loading type-1. The testing arrangement of this specimen and crack pattern is shown in Fig. 3.12. The condition of specimens at the end of testing is shown in Fig. 3.13. The hysteretic responses obtained by plotting the test data are shown in Fig. 3.14. Some of the important observations made during testing along with those made during analysis of the hysteresis loops have been discussed in details in this section.

The first flexural crack in both control as well as the rehabilitated specimens was observed in the beam near the joint interface at a displacement amplitude of ±3.33 mm. The second crack appeared in the beam-column joint interface at amplitude of ±5.0 mm. The control specimen attained its maximum load of 9.79 kN and 9.98 kN in the push and pull directions at a displacement of 10.0 mm and 13.33 mm respectively. However, for rehabilitated specimen, a maximum loads of 9.45 kN and 14.33 kN were attained at a displacement of 13.33 mm and 23.33 mm in push and pull directions respectively. Both the specimens experienced fine cracks at the joint region upto a displacement of ±11.67 mm. The beam could be observed to rotate at the beam-column joint region due to the development of plastic hinge at an amplitude of ±21.67 mm. On further increase in displacement upto ±26.67 mm, spalling of concrete at the joint region of the control specimen followed by major crack development near that portion. However, at the same displacement of ±26.67 mm, no separation of concrete at the joint interface and edges could be observed for the rehabilitated specimen. The experiment for control specimen was stopped at the displacement amplitude of ±31.67 mm. At the same displacement of ±31.67 mm, the rehabilitated specimen was observed to be still capable of carrying further load and hence the experiment was further continued. The experiment for rehabilitated specimen was finally stopped at ±36.67 mm for ensuring safety of testing equipment. A crack width of 3 mm was observed at the joint region for both the control and rehabilitated specimens at the end of the experiment. The ultimate load carrying capacity of the BWFSC and BWFSRe were found out to be 9.885 kN and 11.89 kN respectively.

Fig. 3.12 Test set up for BWFS specimens and cracking pattern under loading type-1

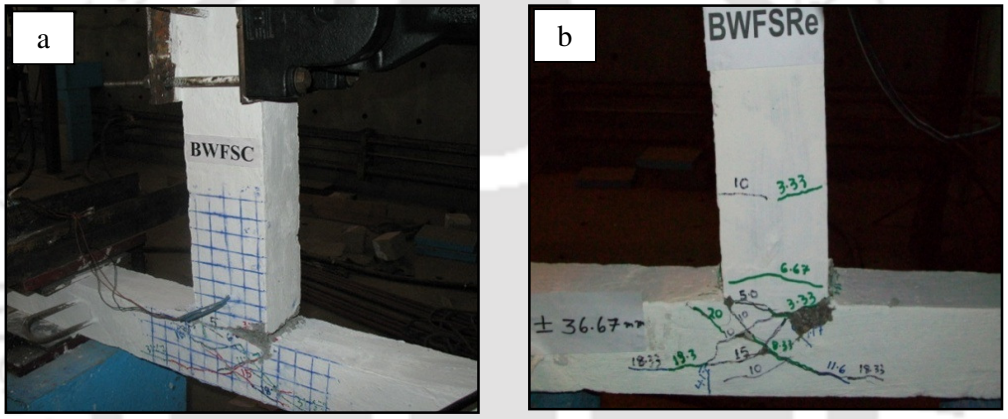

Fig. 3.13 BWFS specimens at the end of test under loading type-1: (a) Control and (b) Rehabilitated

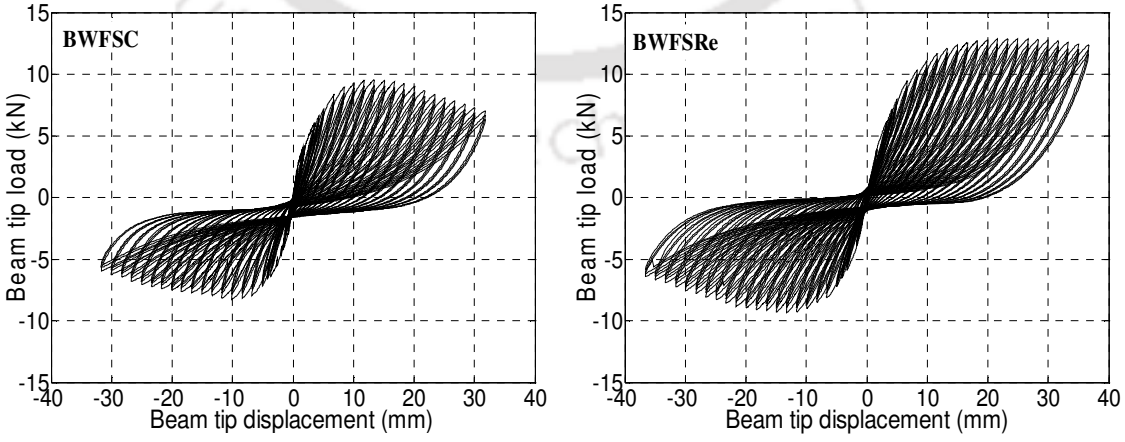

Fig. 3.14 Hysteretic response of BWFS specimens subjected to loading type-1

3.4.2 Behaviour of connections under loading type-2

Loading characteristics (number of cycle in the displacement time history and loading frequency) was same as that of large and medium specimens under loading type-2. Views of the damaged area of the specimens at the end of the experiment are shown in Fig. 3.15. The figure clearly shows that the extent and pattern of damage for both control and the rehabilitated specimens were generally similar. However, on comparing the extent of damage with the specimens under loading type-1, it was observed that the crack width of the control specimen was a little wider in this category of loading type; but no crushing of concrete had taken place either at the joint region or joint interface. Some of the important observations made during testing along with those made during analysis of the hysteresis loops have been discussed in details in this section.

Fig. 3.15 shows that the first crack appeared in the beam when the beam tip displacement was ±3.33 mm and the plastic hinge was observed to develop in the beam close to the joint region towards the end of the experiment. The force-displacement hysteresis loops are shown in Fig. 3.16. It demonstrates that the hysteretic behavior of the joint was stable and ductile. For control specimen, the peak push load carrying capacity was 10.05 kN corresponding to a displacement of 16.67 mm, while peak pull load carrying capacity was 10.35 kN, corresponding to a displacement of 25 mm. The maximum displacement capacity, corresponding to the near complete failure state was observed as ±31.67mm. Similarly, load-carrying capacity of rehabilitated specimen was observed to be 11.00 kN and 11.72 kN in push and pull directions corresponding to a displacement amplitude of 21.67 mm and 26.67 mm respectively. X shaped crack at the joint region started propagating towards the column part on reaching a displacement of ±11.67 mm for control specimen and ±13.33 mm for the rehabilitated specimen. At a displacement of ± 30 mm, no crushing of concrete was observed at the joint region and joint interface,

instead existing X shaped crack at the joint region got further widened (about 3 mm width) in both the specimens. Corresponding to the ultimate displacement of control specimen, the rehabilitated specimen was observed to be still capable of carrying further load and hence the experiment was further continued. The experiment was stopped at a displacement of ±36.67 mm. At the end of the test, crack of comparable magnitude and pattern was observed in both control and rehabilitated specimens.

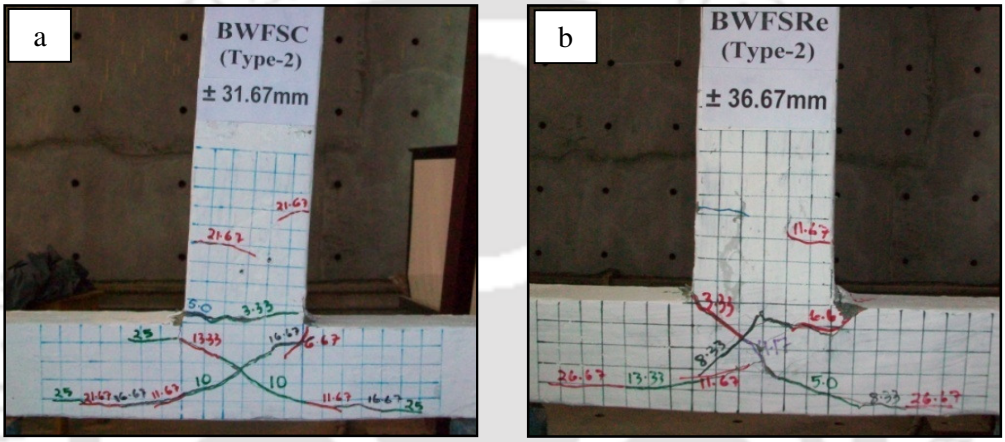

Fig. 3.15 BWFS specimens at the end of test under loading type-2:
(a) Control and (b) Rehabilitated

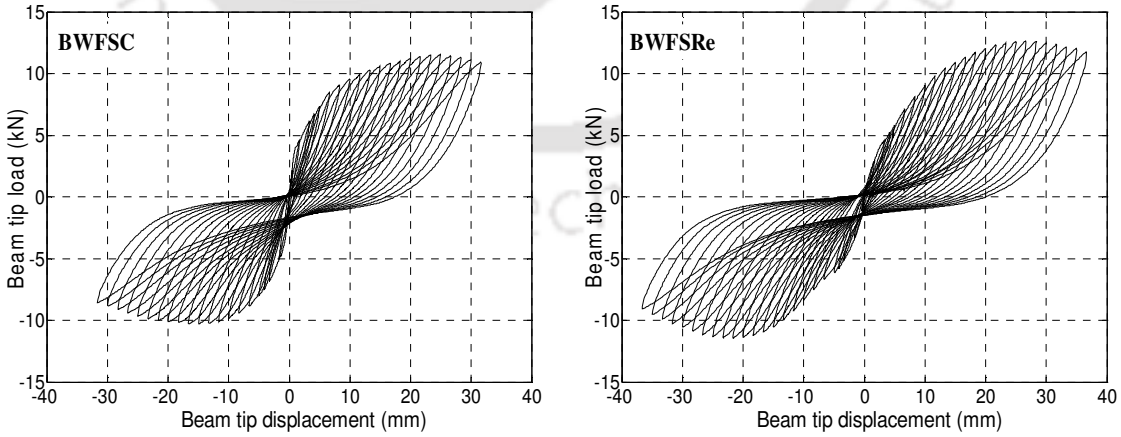

Fig. 3.16 Hysteretic response of BWFS specimens subjected to loading type-2

3.5 COMPARISON OF TEST RESULTS OF CONTROL AND REHABILITATED SPECIMENS

Effectiveness of the adopted repair techniques were evaluated by comparing seismic performance of the rehabilitated specimens with the corresponding control specimens. The hysteretic responses of all the connections have been shown in the previous section. The parameters related to seismic capacity such as ultimate strength, stiffness degradations, energy dissipation and ductility of the specimens were evaluated from these hysteretic responses.

(a) Response cycles and peak loads

The hysteresis loops with loading type-1 show that the load carrying capacity is the highest in its first cycle out of three cycles for a particular displacement amplitude. Therefore, peak values of the capacity corresponding to first cycle for each of the displacement amplitude were considered to plot envelope of hysteresis loops. The envelope of hysteresis loops for control as well as rehabilitated specimens for all loading types are as shown in Fig. 3.17-3.19. Comparing these curves (control and rehabilitated) at each displacement, it can be observed that all the rehabilitated specimens show a similar trend of load recovery with the rate of recovery being relatively low. The envelope of hysteresis loops of the rehabilitated specimens show slightly higher load carrying capacity in both push and pull directions. It is also observed that comparable load carrying capacities were attained by the control specimens under both loading type-1 and type-2. Though, slightly different in peak push and pull load were observed. Thus, it indicates that the characteristic of applied loading did not significantly influence the ultimate load carrying capacity of the specimens. On the other hand, comparison on the ultimate load carrying capacity attained by the rehabilitated specimens under loading

type-1 and type-2 can not be made because of different applied rehabilitation strategies. Depending on the extent of damage, different rehabilitation strategies were considered. The appropriately chosen repair strategy could retrieve back the lost capacity even for a severely damaged connections. Table 3.1 summarized load carrying capacities of all the specimens. It is seen from table 3.1 that specimens damaged under loading type-1 and type-2 could restored their load carrying capacity after rehabilitation. Thus, it may be inferred that the applied repair techniques are effective in restoring the load carrying capacity.

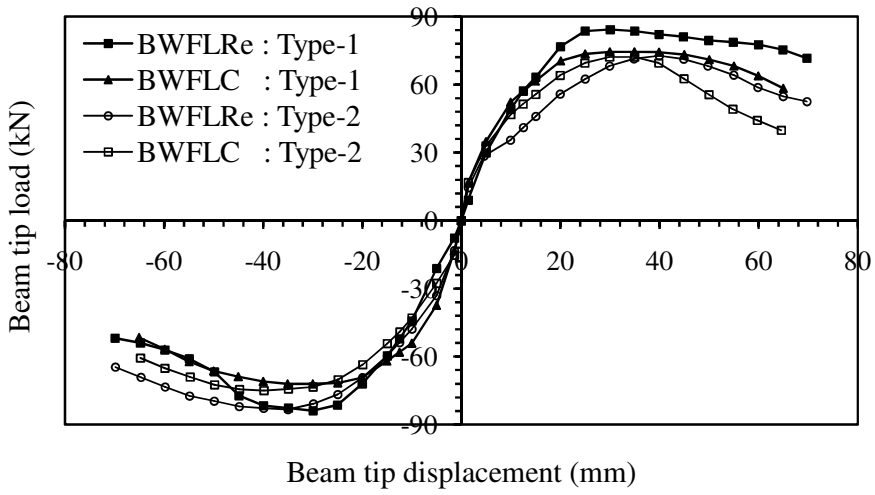

Fig. 3.17 Envelope curves for BWFL specimens

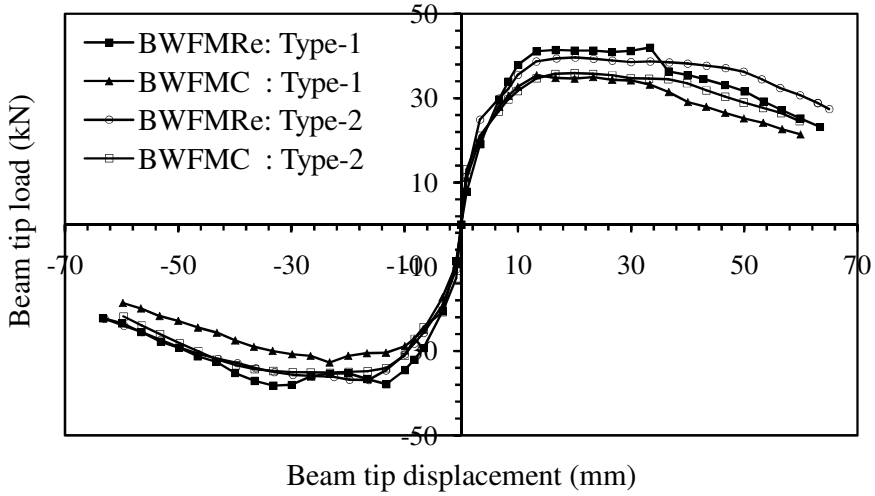

Fig. 3.18 Envelope curves for BWFM specimens

Table 3.1 Ultimate load carrying capacity for beam weak in flexure (BWF) specimens

Specimen size	Control specimens			Rehabilitated specimens		
	+ve load (kN)	- ve load (kN)	Avg.load (kN)	+ve load (kN)	- ve load (kN)	Avg. load (kN)
	Specimens subjected to loading type-1					
Full	74.55 *30, #22	72.02 *30, #22	73.285	84.39 *30, #22	83.78 *30, #22	84.085
Medium	36.95 *16.67, #16	32.74 *26.67, #25	34.845	42.13 *33.33, #34	39.86 *33.33, #34	40.995
Small	9.98 *13.33, #28	9.79 *10, #25	9.885	14.33 *23.33, #49	9.45 *13.33, #28	11.89
	Specimens subjected to loading type-2					
Full	72.23 *40, #10	74.98 *35, #9	73.605	72.78 *40, #10	83.35 *35, #9	78.065
Medium	36.00 *20, #8	35.99 *20, #8	35.995	39.50 *20, #8	39.00 *20, #8	39.250
Small	10.35 *25, #17	10.05 *16.67, #12	10.200	11.72 *26.67, #18	11.00 *21.67, #15	11.360

Note: * and #: displacement and cycle number corresponding to its maximum load
-ve: Push direction and +ve: Pull direction

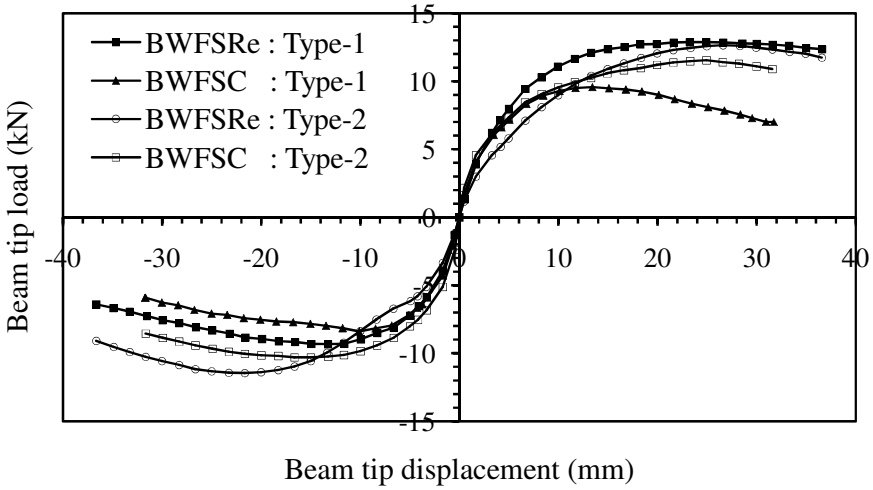

Fig. 3.19 Envelope curves for BWFS specimens

(b) Stiffness degradation

Secant stiffness is evaluated as the peak-to-peak stiffness of the beam tip load-displacement relationship. The secant stiffness is an index of the response of the specimen during a cycle and its strength degradation from a cycle to the following cycle. It is calculated as the slope of the line joining the peak of positive and negative capacity at a given cycle. The procedure for calculation is shown in Fig. 3.20. Two points A and A$^{/}$ in positive and negative direction of the envelope curve for a particular amplitude are joined by a straight line. The slope of this straight line is the stiffness (K) of the joint assemblage corresponding to that particular amplitude and is calculated by the following expression as recommended by Naeim and Kelly [1999].

$$K = \frac{F_D^+ - F_D^-}{D_D^+ - D_D^-} \tag{3.1}$$

where D_D^+ and D_D^- in Eq. 3.1 are the X co-ordinates of A and A$^{/}$ respectively, F_D^+ and F_D^- are the corresponding Y co-ordinates in the envelope curve (Fig. 3.20).

Drift angle is defined as the ratio of beam tip displacement to the length of the beam. Drift obtained by horizontally displacing the beam ends are equivalent to the inter storey drift angle of a frame structure subjected to lateral loads.

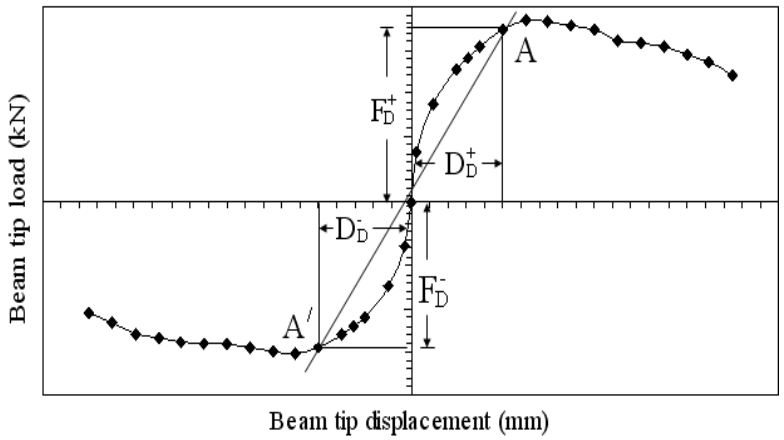

Fig. 3.20 Determination of secant stiffness from envelope curve

The effectiveness of a rehabilitation techniques in restoring the stiffness of damaged connections may be evaluated by comparing stiffness versus drift angle plots for different cases. These plots for all the specimens under loading type-1 and type-2 are shown in Fig. 3.21-3.26. Comparing these curves (control and rehabilitated), the stiffness attained by the rehabilitated specimen at the beginning of the test was observed to be significantly lower. However, at the end of the test, the stiffness attained in both control and rehabilitated specimens are comparable.

Fig. 3.21 shows the variation of stiffness with drift angle for both control and the rehabilitated large size specimens under loading type-1. The stiffness attained by the control specimen corresponding to the first displacement amplitude of ± 1.4 mm (drift angle of 0.103 %) is 11.56 kN/mm, while that for rehabilitated is 8.02 kN/mm. Thus, after repairing there was a reduction in stiffness of about 30.62 %. At the second amplitude of ± 5.0 mm (drift angle of 0.37 %), the stiffness of control specimen got reduced by 32.45 %. At the same drift angle of 0.37 %, the reduction in stiffness for the rehabilitated specimen was found to be 20.60 %.

Similarly, variation of stiffness with drift angle for both control and the rehabilitated large size specimens under loading type-2 is shown in Fig. 3.22. The stiffness of the rehabilitated specimen is 9.00 kN/mm, while that for control specimen is 11.54 kN/mm. A reduction in stiffness of 22.01 % after repairing was observed. The reduction in stiffness corresponding to a displacement amplitude of ± 5.0 mm were calculated in both control and rehabilitated specimens. The degradation of stiffness is little slow for the repaired specimen at the same displacement level.

The variation of stiffness with drift angle for BWFMC and BWFMRe specimens under loading type-1 is shown in Fig. 3.23. It can be observed that the stiffness attained by the rehabilitated specimen is more than that of control except at the initial stage. The stiffness

for rehabilitated specimen is 8.65 kN/mm, while the same for control specimen is 11.00 kN/mm. Thus, repaired specimen exhibited a reduction in stiffness by 21.36 %.

Fig. 3.24 shows the plot of stiffness against drift angles for both control and the rehabilitated medium size specimens subjected to loading type-2. The stiffness of the rehabilitated specimen is 8.95 kN/mm, while that for control specimen is 11.30 kN/mm. A reduction of stiffness about 20.80 % after repairing was observed. The stiffness of control specimen got reduced by 54.34 % at drift angle of 0.37 % while the reduction in stiffness for rehabilitated specimen was found to be 44.29 % at the same drift angle.

The stiffness degradation for both control and the rehabilitated small size specimens with loading type-1 and type-2 are shown in Fig. 3.25 and Fig. 3.26 respectively. The plot also showed similar trend of degradation in stiffness as that of full and medium size specimens.

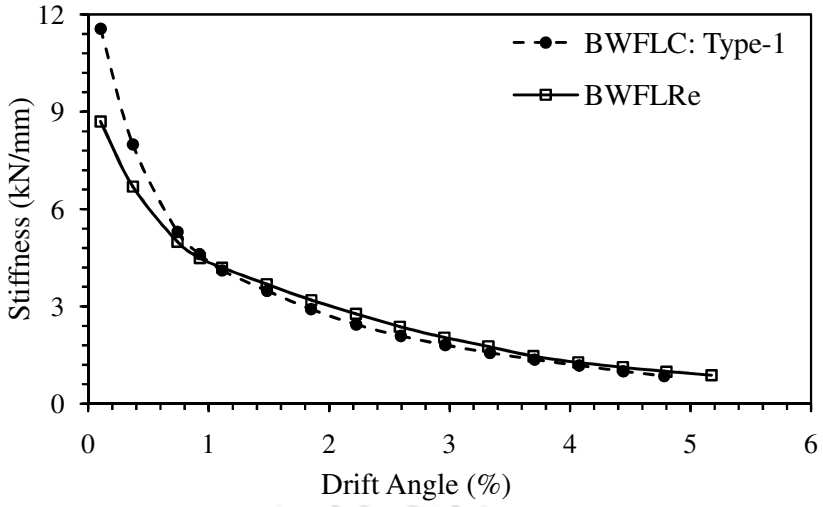

Fig. 3.21 Stiffness versus drift angle for BWFL specimens under loading type-1

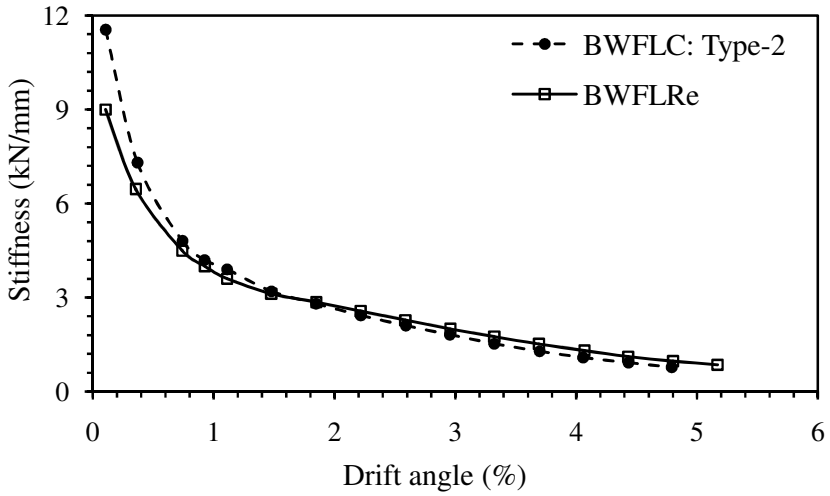

Fig. 3.22 Stiffness versus drift angle for BWFL specimens under loading type-2

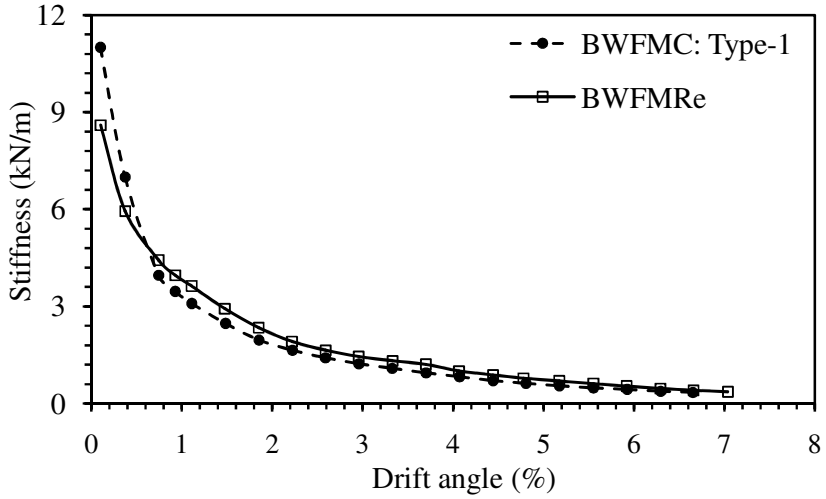

Fig. 3.23 Stiffness versus drift angle for BWFM specimens under loading type-1

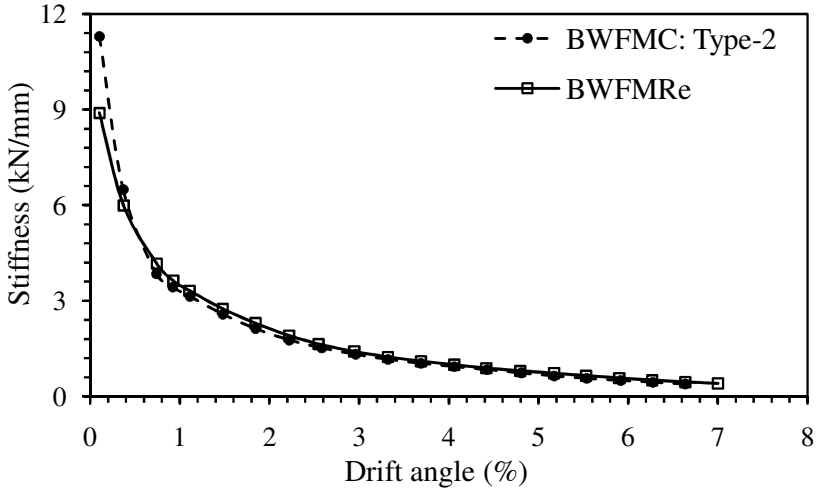

Fig. 3.24 Stiffness versus drift angle for BWFM specimens under loading type-2

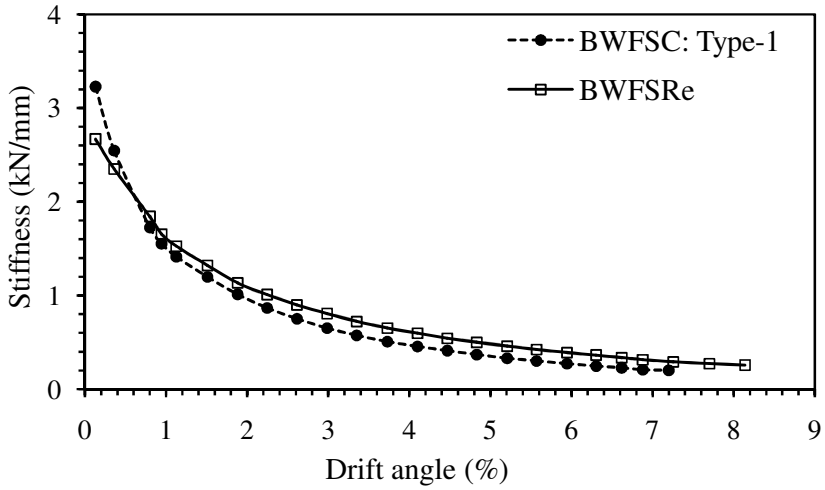

Fig. 3.25 Stiffness versus drift angle for BWFS specimens under loading type-1

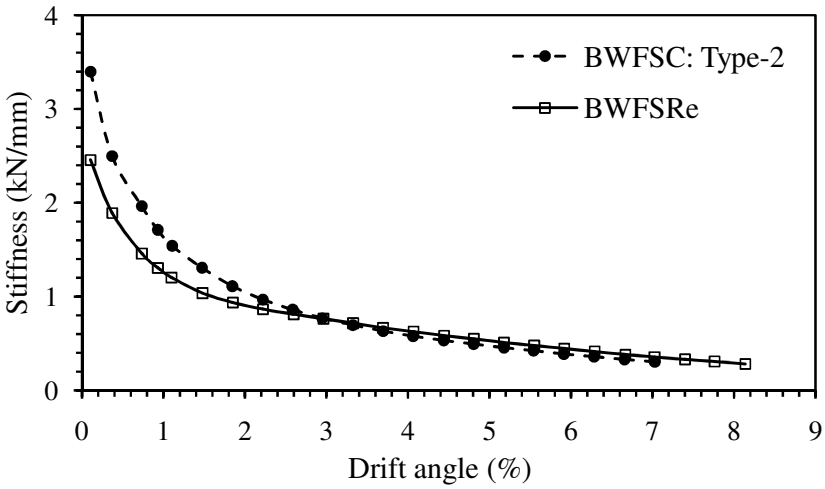

Fig. 3.26 Stiffness versus drift angle for BWFS specimens under loading type-2

Thus, comparing all these curves irrespective of loading types, a similar degradations trend was observed. Further, it is also observed that the degradation in stiffness for damaged specimens after rehabilitation is little slow with increase in lateral movement as compared to the control specimens. This behaviour may be attributed to the ductile properties introduced by the repairing materials. The lower degradation is a desirable property in earthquake like situations. It was observed during the past earthquake that most of the RC structures failed due to sudden loss of stiffness with increasing lateral

movement. Therefore, from these comparisons it can be concluded that all rehabilitated specimens satisfactorily achieved stiffness level which is well comparable to the control specimens.

(c) Energy dissipation

The ability of a structural element to resist an earthquake load depends to a large extent on its capacity to dissipate its energy. The area of hysteresis loop is a measure of the energy dissipated. The cumulative energy dissipated at a particular amplitude was calculated by summing up the energy dissipated in all the preceding cycles including that amplitude. The plots of cumulative energy dissipation versus drift angle for control as well as rehabilitated specimens are shown in Fig. 3.27-3.29. It may be noted that though the energy dissipation for loading type-1 and type-2 have been presented in the same figure, comparison between these two can not be made due to different loading characteristic.

On examination of these plots, it may be seen that the cumulative energy dissipated by the rehabilitated specimens are relatively lower during the initial stages of loading. On the contrary, in subsequent loading cycles, the energy dissipated by the damage specimen after rehabilitation are observed to be at par with those of the corresponding control specimens. The increase in stiffness at end of imposed displacement history attracted more load corresponding to any drift angle for the rehabilitated specimens in comparison to that of the control specimen. Thus, the total area enclosed by the plot of beam tip load versus beam tip displacement was more for rehabilitated specimens than those of the control specimen. This was perhaps the reason for improvement in cumulative energy dissipation in the subsequent loading cycles. Corresponding to the drift level upto which the control specimens were tested, the energy dissipated by the rehabilitated specimens

are slightly higher than the respective control specimens (Table 3.2). Thus, it may be observed that by adopting an appropriate rehabilitation methodology, even a severely damaged structure can successfully restore the energy dissipation capacity which is comparable to those of control specimens.

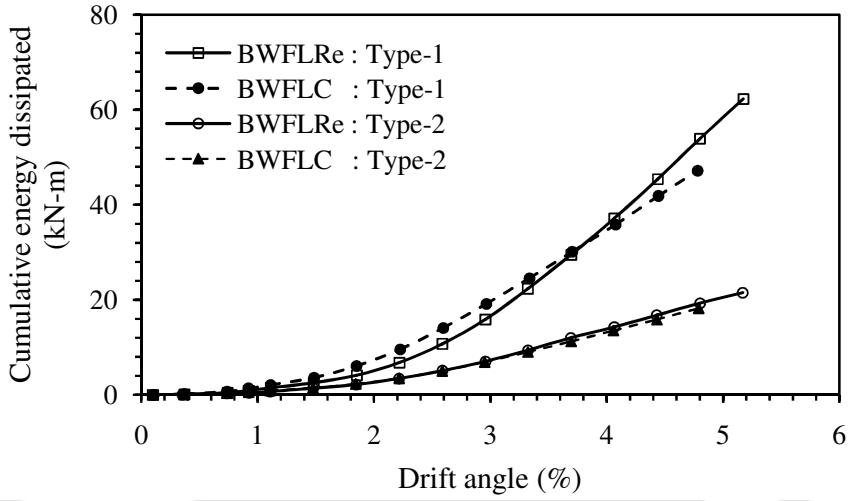

Fig. 3.27 Cumulative energy dissipation for BWFL specimens

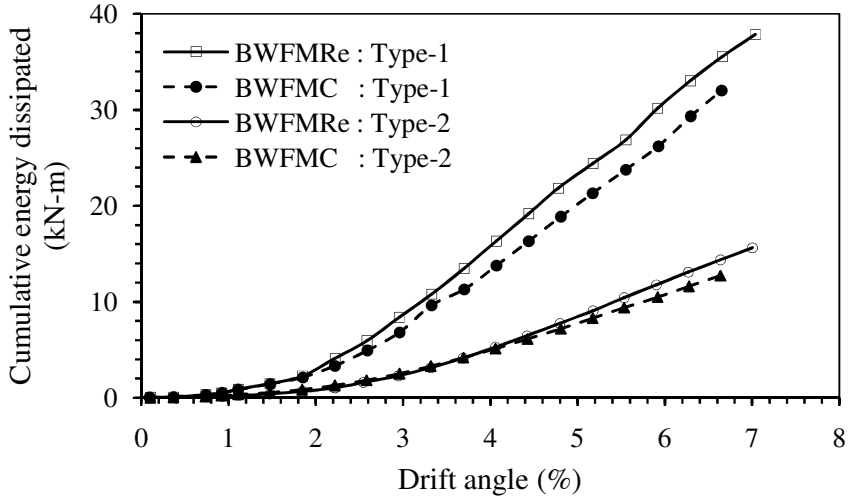

Fig. 3.28 Cumulative energy dissipation for BWFM specimens

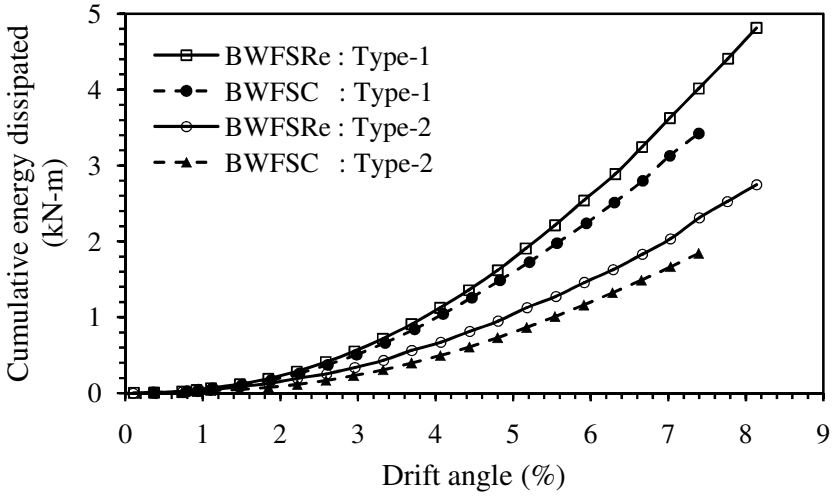

Fig. 3.29 Cumulative energy dissipation for BWFS specimens

Table 3.2 Energy dissipation (kN-m) for beam weak in flexure (BWF) specimens

Specimens sizes	Loading type-1		Loading type-2	
	Control	Rehabilitated	Control	Rehabilitated
Large	47.18	53.91	18.18	19.29
Medium	32.02	35.53	12.72	14.38
Small	3.32	3.62	2.02	2.31

(d) Displacement ductility

Displacement ductility for all specimens were calculated from the respective envelope curves as per the procedure proposed by Shannag *et al.* [2005] which has been explained in Fig. 3.30. As shown in the figure, the yield displacement is calculated as the point of intersection between two straight lines drawn in the envelope curve. The first line was obtained by extending the line joining the origin and 50 % of ultimate load capacity point on positive and negative sides of the envelope curve, while the second line was obtained by drawing a horizontal line through the 80 % of ultimate load capacity point on either side. In the figure, dy_1 and dy_2 represent the yield displacement in positive and negative

direction on the envelope curve respectively. The average value of yield displacement obtained from both positive and negative direction was calculated. Horizontal lines drawn through the 80% of ultimate load capacity point on positive and negative side intersect the envelope curve at far end at points x_1 and x_2. The average of abscissa of these two points (denoted by du_1 and du_2 in figure) was taken as maximum displacement. The displacement ductility was calculated as the ratio of maximum displacement to the yield displacement. The calculated values are listed in Table 3.3. It may be noted that the yield displacement for rehabilitated specimens was taken same as respective values of control specimens (Alsayed *et al*., 2010). The displacement ductility attained by the damaged control specimens after rehabilitation are found to be marginally higher than those of the control specimens. Further, the ductility attained by the specimens (control and rehabilitated) are found to be least for largest specimens and highest for small specimen in both loading type-1 and type-2.

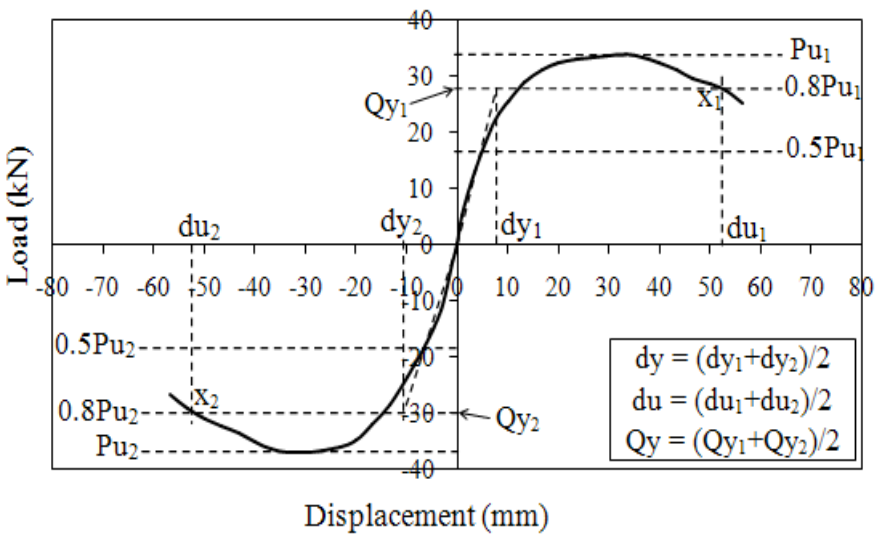

Fig. 3.30 Procedures for ductility calculation

Table 3.3 Displacement ductility of beam weak in flexure (BWF) specimens

Loading type	Specimens	Control			Rehabilitated		
		Δ_y	Δ_{20}	Δ_{20}/Δ_y	Δ_y	Δ_{20}	Δ_{20}/Δ_y
Type-1	Large	8.25	58	7.03	8.25	60	7.27
	Medium	5.5	40.5	7.36	5.5	42.5	7.73
	Small	3.25	26	8	3.25	32	9.85
Type-2	Large	8	58.5	7.31	8	62.5	7.81
	Medium	5	47	9.4	5	52	10.4
	Small	3	31	10.33	3	36	12

Δ_y and Δ_{20} : Displacement at first yield and at 20 % drop of peak load (mm)

3.6 INVESTIGATION FOR THE EXISTENCE OF SIZE EFFECT

To explore the existence of size effect, the results obtained from testing of the specimens were analyzed and bi-logarithmic plot were drawn. Various parameters, which are of practical relevance were also considered and the possible existence of size effects were investigated.

3.6.1 Bi-logarithmic plot

The failure mode of both control and the rehabilitated specimens under consideration was in flexure. Hence, ultimate bending stress (σ_{N_U}) was calculated for all the specimens. The calculation of bending stress is presented in Appendix-B. Using σ_{N_U} and characteristic dimension (D), bi-logarithmic plots were drawn for control and rehabilitated specimens. The size effect law as proposed by Bažant [1984] was used for the statistical regression of the data. The mathematical expression of this law is given as:

$$\sigma_{N_U} = \frac{Bf_t'}{\sqrt{1 + D/D_0}} \tag{3.2}$$

B and D_0 are the two unknown constants which can be determined by statistical regression analysis. The value of tensile strength of concrete (f_t') was calculated as per IS: 456 [2000] and was taken as 2.504 N/mm^2. To facilitate the evaluation of the constants in the size effect law, Eq. 3.2 can be rearranged as follows:

$$\left(\frac{f_t'}{\sigma_{N_U}}\right)^2 = \frac{1}{D_0 B^2} D + \frac{1}{B^2} \tag{3.3}$$

The above equation is of the form of $Y = AX+C$ where $Y = \left(f_t' / \sigma_{N_U} \right)^2$, $X = D$ and the constants C and A are given by $C = \frac{1}{B^2}$ and $A = \frac{1}{D_0 B^2}$, Hence value of B and D_0 are:

$$B = \frac{1}{\sqrt{C}} \quad \text{and} \quad D_0 = \frac{C}{A} \tag{3.4}$$

The calculated value of bending stress and other parameters necessary to carry out regression analysis and to draw bi-logarithmic plot for control as well as rehabilitated specimens are presented in the Table 3.4. The typical regression analysis for control specimens is shown in Fig. 3.31. From this figure (using Eq. 3.4), the value of B and D_0 were found to be 8.45 and 350 respectively. Using these values, the bi-logarithmic plot were drawn with log (D/D_0) in the X axis and log (σ_{N_U} / Bf_t') in the Y axis as shown in Fig. 3.32. The bi-logarithmic plots were drawn considering all six data irrespective of the loading types. This was to facilitate the best fitting curve. Similarly, values of B and D_0 for rehabilitated specimens were calculated as 11.18 and 200 respectively and the bi-logarithmic plot is shown in Fig. 3.33.

Table 3.4 Parameters of BWF specimens for bi-logarithmic plotting

Type of specimen	Name of specimen	Bending stress, σ_{N_U} (N/mm^2)	Depth of specimen , D (mm)	$\left(\frac{f_t'}{\sigma_{N_U}}\right)^2$	Log *(D/Do)*	$Log\left(\frac{\sigma_{N_U}}{Bf_t'}\right)$
Control	Large	15.2677	360	0.02689	0.01223	-0.14172
		15.3344	360	0.02666	0.01223	-0.13982
	Medium	16.3336	240	0.02350	-0.16386	-0.09041
		16.8726	240	0.02202	-0.16386	-0.09831
	Small	18.5344	120	0.01825	-0.46489	-0.05751
		19.1250	120	0.01819	-0.46489	-0.05685
Rehabilitated	Large	17.5177	360	0.02043	0.25527	-0.20359
		16.2635	360	0.02370	0.25527	-0.23586
	Medium	19.2168	240	0.01697	0.07918	-0.15309
		18.3984	240	0.01852	0.07918	-0.17009
	Small	22.2937	120	0.01261	-0.22185	-0.12891
		21.3000	120	0.01382	-0.22185	-0.11869

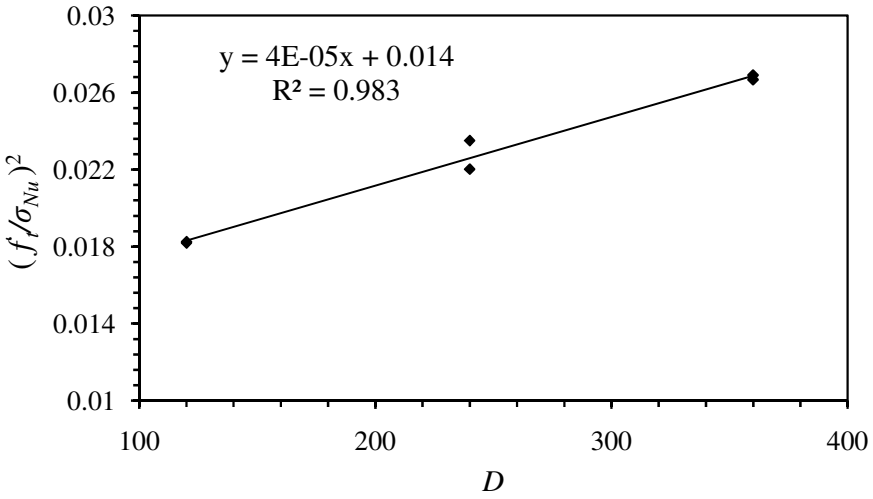

Fig. 3.31 Typical regression plot for Control BWF specimens

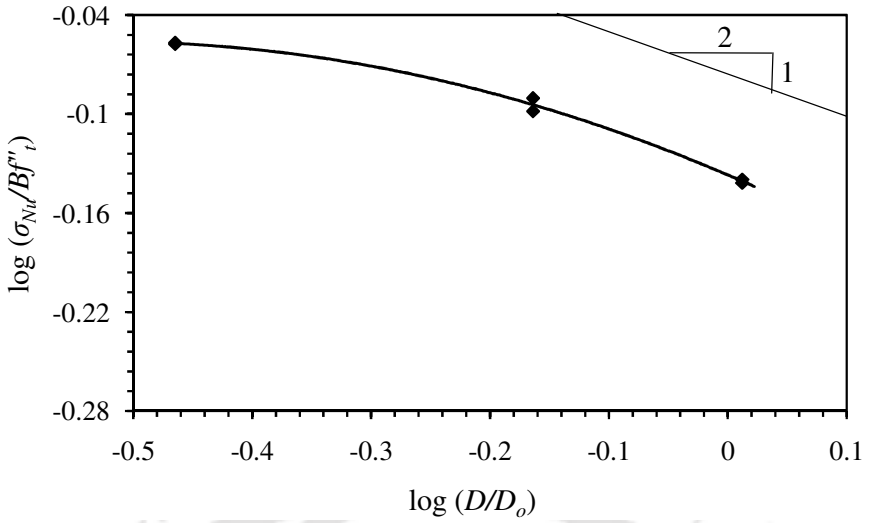

Fig. 3.32 Bi-logarithmic plot for control BWF specimens

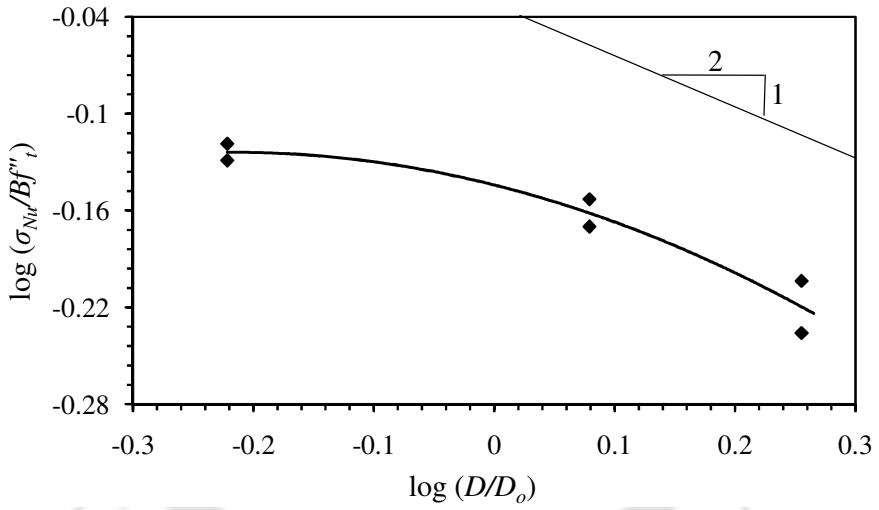

Fig. 3.33 Bi-logarithmic plot for rehabilitated BWF specimens

It is observed from these plots that it follows a horizontal line at the initial part, indicating no size effect. The curve approaches a straight line with slope of about -1/2 towards the end (LEFM zone). In the intermediate zone there is a smooth curved transitional part. Thus, it can be concluded that the plot shows presence of size effect in accordance with Bažant's size effect law.

3.6.2 Size effect on energy dissipated per unit volume of D-region

The D-region (ACI 318-08, 2008) was considered to calculate the representative volume in a connection. The Cumulative energy dissipated per unit volume of D-region (e_N), was calculated for all the specimens. The variations with respect to drift angle is shown in Fig. 3.34 for specimens with loading type-1, while Fig. 3.35 shows the same for specimens with loading type-2. It can be clearly observed that in both the loading cases and for both kind of specimens (control and rehabilitated), the uppermost curve is for the smallest specimen, while the lowermost curve corresponding to the largest specimen. This proves that during cyclic loading, the energy dissipated per unit volume of the D-region by smaller specimen is more than the larger specimen. This establishes the fact that the energy dissipated per unit volume of the D-region is dependant on specimen size.

3.6.3 Size effect on stress variation with relative deflection

The maximum value of the load of each displacement cycle was used to calculate the bending stresses. The relative deflection for different scaled models were calculated as the ratio of actual deflection to the scale of the model. The evaluated relative deflection and stresses have been plotted for control and the rehabilitated specimens with loading type-1 in Fig. 3.36 while the same with loading type-2 are shown in Fig. 3.37. It is observed from these plot that stresses are highest for the smallest specimen and lowest for the largest specimen corresponding to almost any level of relative deflection level for both control and rehabilitated specimen under both the cases of loading. This is an indication for the existence of size effect.

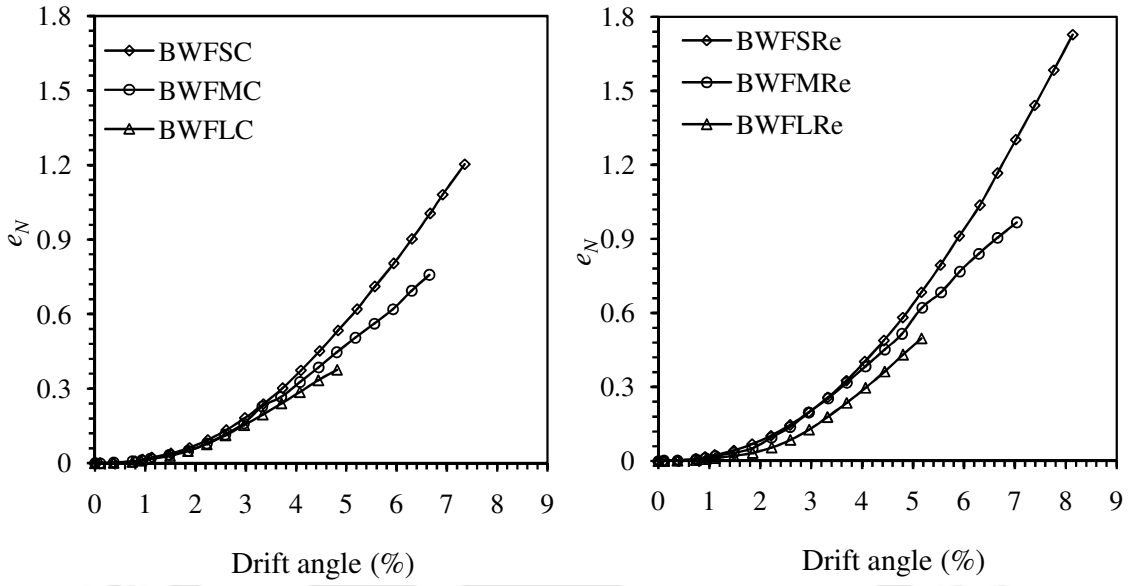

Fig. 3.34 Cumulative energy dissipated per unit volume of D-region for BWFC and BWFRe specimens under loading type-1

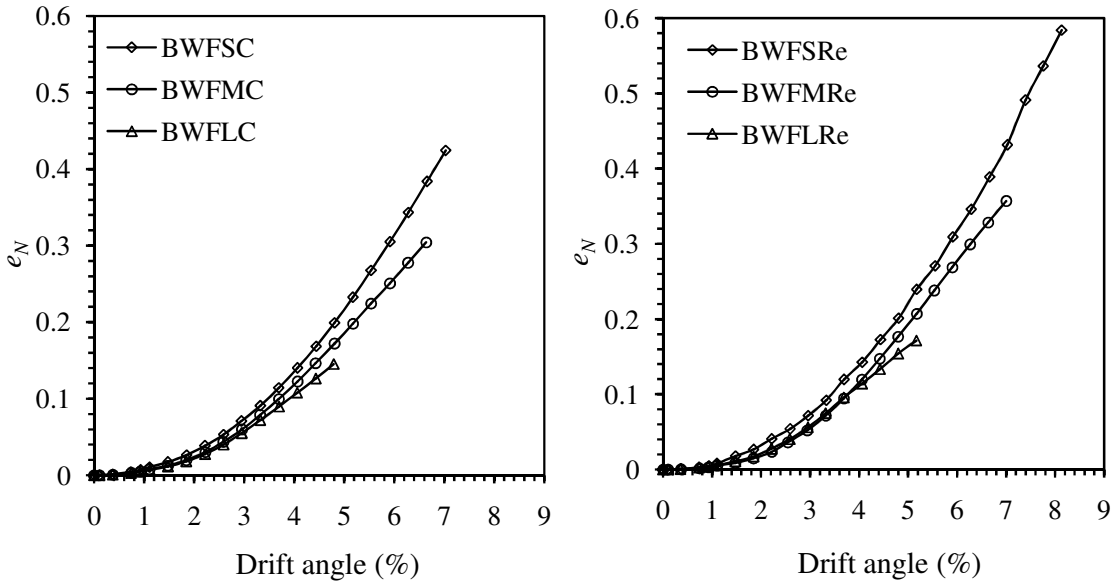

Fig. 3.35 Cumulative energy dissipated per unit volume of D-region for BWFC and BWFRe specimens under loading type-2

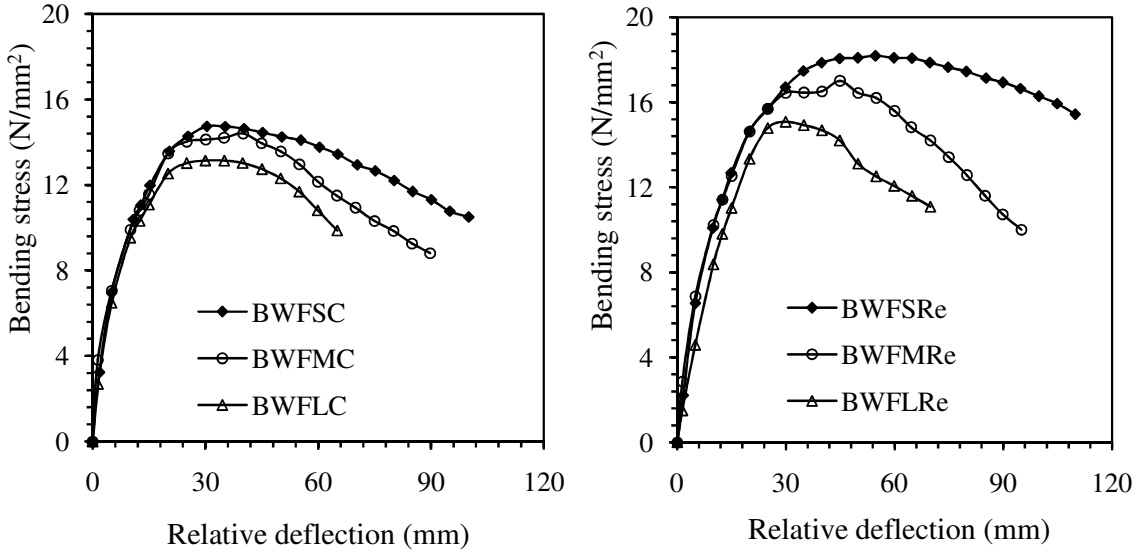

Fig. 3.36 Bending stress versus relative deflection for BWF specimens under loading type-1

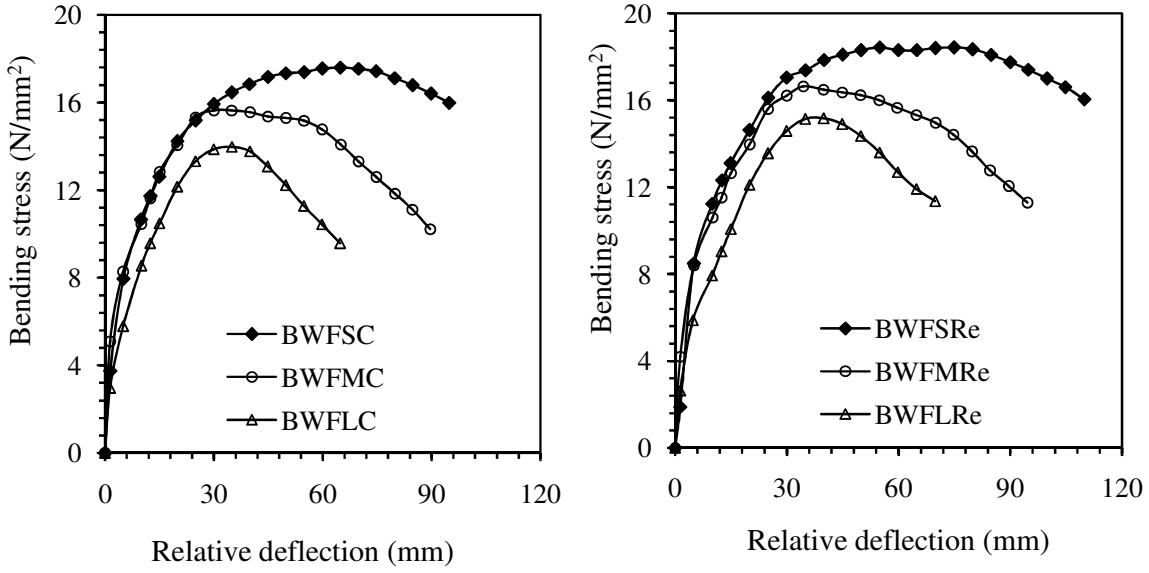

Fig. 3.37 Bending stress versus relative deflection for BWF specimens under loading type-2

3.7 CONCLUDING REMARKS

In this chapter, data of experimental investigation of beam-column connections with beam weak in flexure subjected to different loading characteristics were presented. Parameters related to seismic capacity such as ultimate strength, stiffness degradations, energy dissipation and ductility for both control as well as rehabilitated specimens were analyzed and compared. The analysis of results revealed that the rehabilitated connections exhibited equal or marginally better performance than the corresponding control specimens and hence the adopted rehabilitation strategy could be considered as satisfactory. It is also observed that the characteristic of applied loading does not significantly influence the ultimate load carrying capacity of the specimens, though the extents of damages were observed to be different under different loading types. Further, the results, obtained from test were examined to explore the existence of size effect. Analyzed results were used for drawing bi-logarithmic plot. It was observed that both control and rehabilitated specimens substantiate the size effect law as proposed by Bažant. It was noted that, cumulative energy dissipated per unit volume of the D-region at every drift angle for small specimen was the maximum and it decreased as the specimen size increased. This was an indication for existence of size effect. The variation of flexural stress with respect to relative deflection also agrees with the size effect principle.

CHAPTER 4

STUDY ON REHABILITATED RC BEAM-COLUMN CONNECTIONS WITH BEAM WEAK IN SHEAR

4.1 INTRODUCTION

This chapter describes the findings of experimental investigation and interpretation of those experimental results of beam-column connections with beam weak in shear. Connections with varying sizes namely full, two third and one third size were tested. The control specimens were subjected to either loading type-1 or type-2. Different rehabilitation strategies were employed depending on the degree of damage. Rehabilitated specimens were re-tested with the same loading sequence as that applied on the control specimens. The data recoded during testing were used for post processing to evaluate many important parameters related to seismic capacity of the connections. Performance of rehabilitated specimens were examined and compared with those corresponding to the original deficient control specimens. Further, bi-logarithmic plots were drawn for exploring the possibility of existence of size effect in terms of ultimate strength. Specimen sizes were also correlated with cumulative energy dissipated per unit volume of D-region and stresses.

4.2 TESTING OF LARGE SIZE CONNECTIONS

Loading characteristics and displacement histories (type-1 and type-2) applied to these specimens were similar to those applied to the large size specimens with beam weak in flexure as discussed in the previous chapter. A servo hydraulic dynamic actuator of loading capacity ± 250 kN and having maximum displacement range of ± 125 mm was

used to apply the cyclic displacement. The experiment was stopped for control specimens at a stage when the load came down in the range of 60-70 % of the ultimate load carrying capacity. Similarly, the experiment on rehabilitated specimens was also stopped at about the same magnitude of load. The load carrying capacities of specimens of different sizes subjected to different loading types have been presented in Table 4.1

4.2.1 Behaviour of connections under loading type-1

A close view of the joint region with some cracks develop during testing is shown in Fig. 4.1. The specimen attained their respective peak capacities at that instant. It is seen from these figures that the initiation and propagation of cracks before and after repair followed similar pattern in general. The first visible crack appeared in the beam part at a displacement amplitude of ± 5.0 mm in both control and rehabilitated specimens. More cracks started to develop in the beam and at the joint region as the amplitude of displacement was increased. The specimens at the end of the test are shown in Fig. 4.2.

The hysteretic responses obtained by plotting the test data are presented in Fig. 4.3. It is observed from these loops that BWSLC specimen attained its maximum load carrying capacity of 70.78 kN in the push direction at 22^{nd} cycle at a displacement of 30 mm, while 73.39 kN was attained in the pull direction at 19^{th} cycle at a displacement of 25 mm. Hysteresis loop of BWSLRe specimen show a slightly higher load carrying capacity than that of control specimen both in push and pull directions. BWSLRe specimen attained its maximum load of 76.12 kN in push direction at 22^{nd} cycle at 30 mm displacement and 78.32 kN in pull direction at 25^{th} cycle at 35 mm displacement.

Most of the initial cracks developed in control specimen got widened when the peak load was attained. Spalling of concrete at the joint region was observed at a displacement amplitude of ± 40 mm. No new crack was observed, instead the existing cracks became

sufficiently wider at a displacement of ±50 mm. Wide crack of about 6 mm width was clearly seen at the joint interface of the specimen at a displacement amplitude of ± 55 mm. The ultimate load carrying capacity for BWSLC specimen was found to be 72.085 kN. For rehabilitated specimen, fine hairline cracks at the joint region became wider to about 1 mm width at a displacement of ±35 mm. It was observed that upto peak loading stage most of the cracks were concentrated at the joint region for the rehabilitated specimen. The repairing materials had prevented the early cracking of the joint interface. At a displacement of ±50 mm, the cracks at the joint region became sufficiently wider to about 5 mm, crushing of concrete also started at the joint interface and few cracks from the joint region started propagating towards the column and beam region. The cracks developed at the column region started widening at a displacement of ±55 mm. Rehabilitated specimen also experienced similar damage pattern at the same displacement level as that of the corresponding control specimen. However, the rehabilitated specimen was observed to be still capable of carrying additional load at the displacement level of ± 55 mm, where the test for control specimen was stopped. The experiment for rehabilitated specimen was finally stopped at ± 60 mm for ensuring safety of the set-up. The maximum load for BWFLRe specimen was found out to be 77.220 kN.

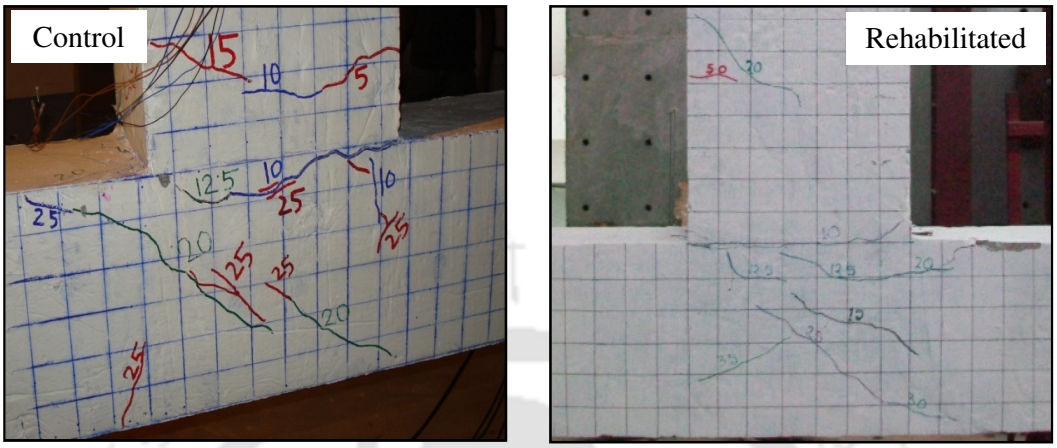

Fig. 4.1 Appearance of cracks for BWSL specimens under loading type-1 corresponding to peak load

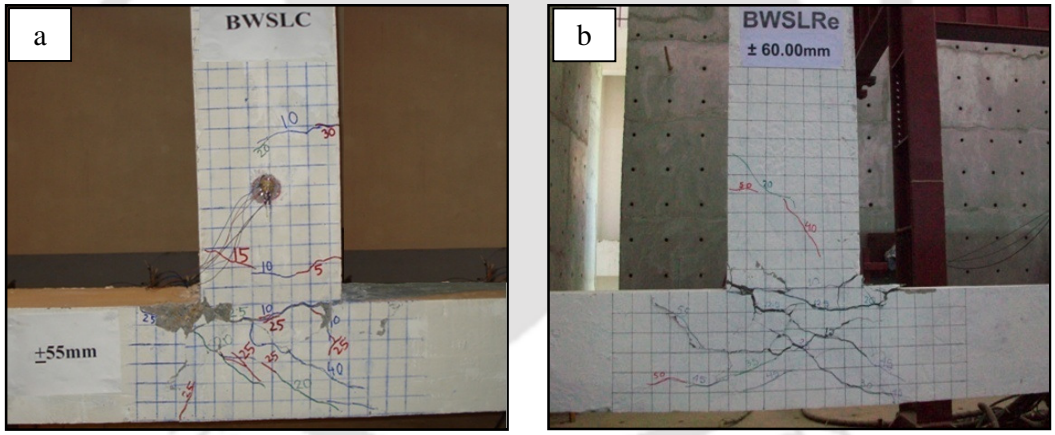

Fig. 4.2 BWSL specimens at the end of test under loading type-1: (a) Control and (b) Rehabilitated

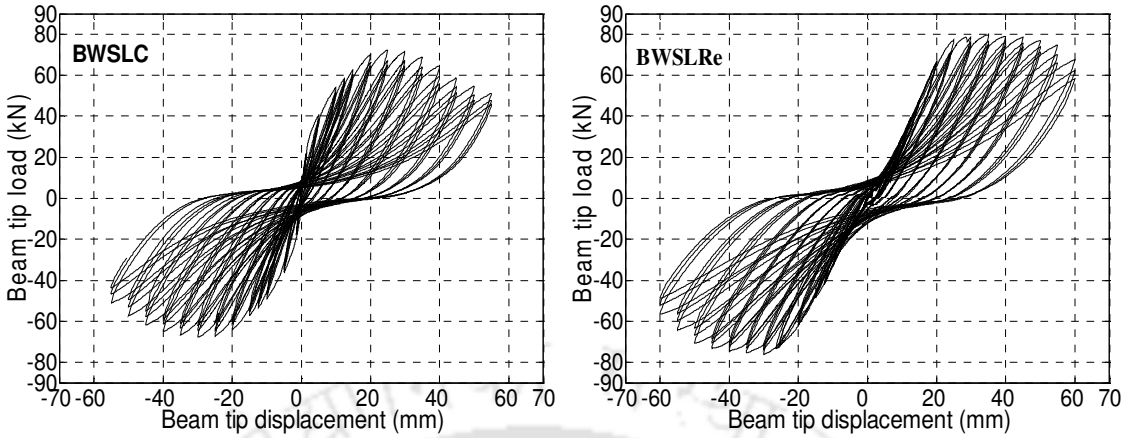

Fig. 4.3 Hysteretic response of BWSL specimens subjected to loading type-1

4.2.2 Behaviour of connections under loading type-2

Appearances of cracks corresponding to the peak loading capacities and the damaged specimen at the end of test are shown in Fig. 4.4 and Fig. 4.5 respectively. Some of the important observations made during testing along with those made during analysis of the hysteresis loops have been discussed in details in this section.

First visible crack appeared in the beam part at a displacement amplitude of ±5.0 mm in both control and the rehabilitated specimens. More cracks started to develop at the joint region and beam part on further increase in displacement amplitude (Fig. 4.4). The initially developed cracks at joint interface for control specimen got widened to a crack width of about 1 mm on reaching a displacement of ±25 mm. At the same displacement of ±25 mm, rehabilitated specimen also suffered similar magnitude of damage.

The plotted hysteresis loops as shown in Fig. 4.6 indicate that control specimen attained its maximum load of 76.63 kN at a displacement of 40 mm in the push direction and 71.49 kN at a displacement of 35 mm in the pull direction. Slightly higher loads were attained by the rehabilitated specimen with a maximum of 86.5 kN in the push and 75.44 kN in the pull directions at the same displacement amplitude of ±45 mm. Existing cracks

at the joint interface became wider upto about 5 mm and alternate closing and opening of cracks became distinct at ±50 mm displacement. Substantiate degradation in load carrying capacity was noticed at this level of excitation and the experiment for control specimen was finally stopped at ±55 mm displacement. The ultimate load carrying capacity for BWSLC specimen was found to be 74.06 kN. Damage patterns in the rehabilitated specimens were quite similar to that developed in the control specimen, where the cracks were mostly concentrated at the joint interface. At a displacement of ± 45 mm, crushing of concrete at the joint interface started. The existing crack width at the joint interface widened to about 3 mm on reaching a displacement of ±50 mm. Although rehabilitated specimen showed more numbers of crack on the joint region as compared to that in corresponding control specimen at the same displacement level, the rehabilitated specimen could be loaded upto the displacement of ±60 mm. The maximum load carrying capacity for BWFLRe specimen was found out to be 80.98 kN. The displacement limits were kept same for both control and rehabilitated specimens when tested under loading type-1 and type-2. This was done for facilitating comparative understanding of their behaviour with respect to numbers of cycles of displacement history. At the end of the test, crack width of about 5 mm was observed at the joint interface in both control and rehabilitated specimens.

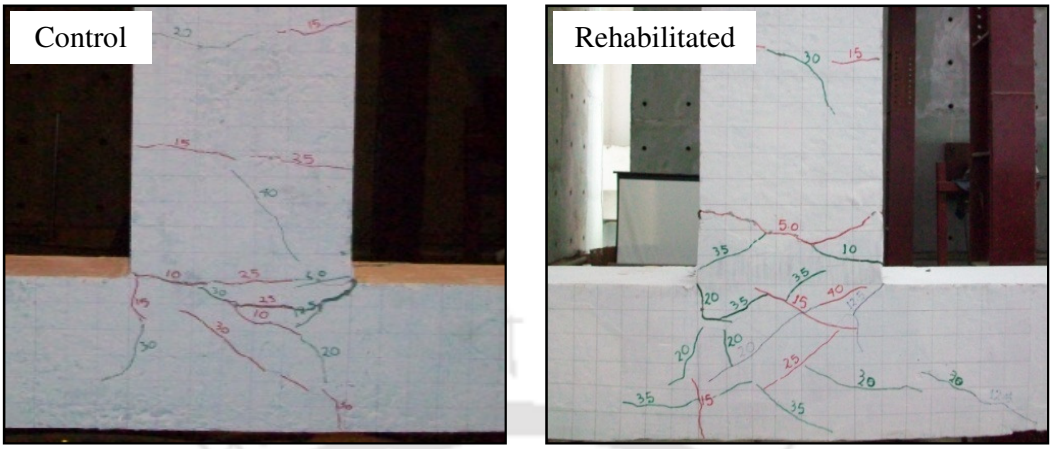

Fig. 4.4 Appearance of cracks for BWSL specimens under loading type-2 corresponding to peak load

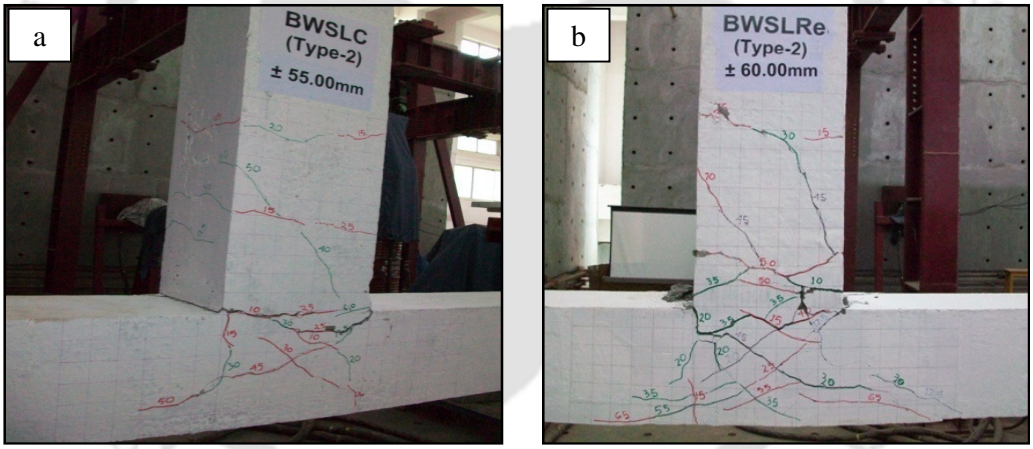

Fig. 4.5 BWSL specimens at the end of test under loading type-2: (a) Control and (b) Rehabilitated

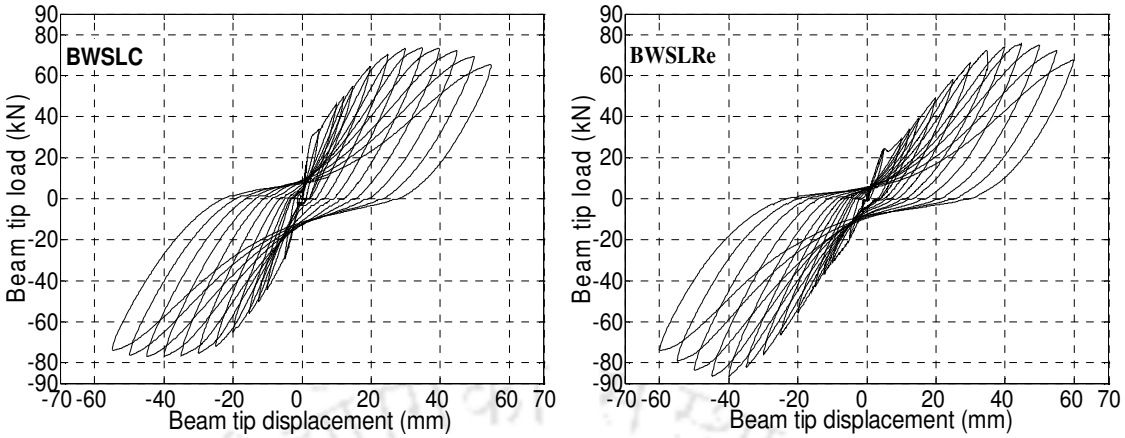

Fig. 4.6 Hysteretic response of BWSL specimens subjected to loading type-2

4.3 TESTING OF MEDIUM SIZE CONNECTIONS

A servo hydraulic dynamic actuator of loading capacity ±250 kN and having maximum displacement range of ±125 mm was used to apply the cyclic displacement. Loading characteristics and displacement histories (type-1 and type-2) applied to these specimens were similar to those applied to the medium size specimens with beam weak in flexure as discussed in the previous chapter. The experiment was stopped when the percentage reduction in load carrying capacity was of similar order as that in the case of BWS large size specimens.

4.3.1 Behaviour of connections under loading type-1

Appearance of cracks corresponding to the peak loading is shown in Fig. 4.7. The first visible crack for control specimen appeared in the beam very near to the junction of beam-column at an amplitude of ±3.33 mm. At the same amplitude of ±3.33 mm, the first crack for rehabilitated specimen shifted away from the junction towards the beam region. A close view of the damaged joint region at the end of the test is shown in Fig. 4.8. The hysteretic responses (control and rehabilitated) obtained by plotting the test data

are shown in Fig. 4.9. Control specimen attained its maximum load of 34.19 kN in the push direction at a displacement of 20 mm and 36.01 kN in the pull direction at 23.33 mm displacement. On further increase in displacement amplitude in control specimen, propagation of crack started gradually along the edges of the joint interface. A crack width of about 2 mm was observed at the joint region at a displacement of ±26.67 mm. Opening and closing of existing cracks were clearly observed and many cracks started widening at an amplitude of ±36.67 mm. At the same displacement of ±36.67 mm, spalling of concrete also started at the joint edges. Cracks at the joint region are immeasurable on crossing a displacement of ±46.67 mm. A wide crack at the joint interface became distinct causing the failure of the specimen at a displacement of ±50 mm. Rehabilitated specimen also exhibited similar cracked pattern. Rehabilitated specimen attained its maximum loads of 39.56 kN and 37.77 kN at the same displacement of ±30 mm. Spalling of concrete started on reaching a displacement of ±33.33 mm. Finally, the experiment was stopped at a displacement of ±53.33 mm. The ultimate load carrying capacity for BWSMC and BWSMRe specimens was found to be 35.10 kN and 38.665 kN respectively.

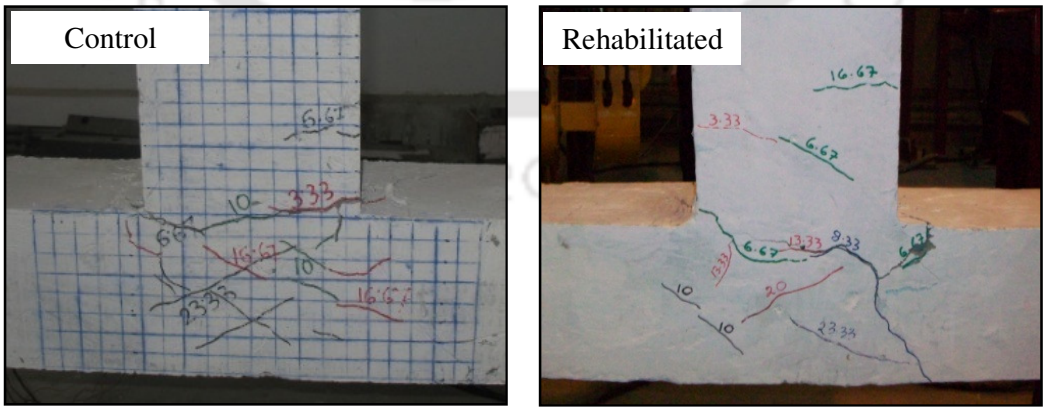

Fig. 4.7 Appearance of cracks for BWSM specimens under loading type-1 corresponding to peak load

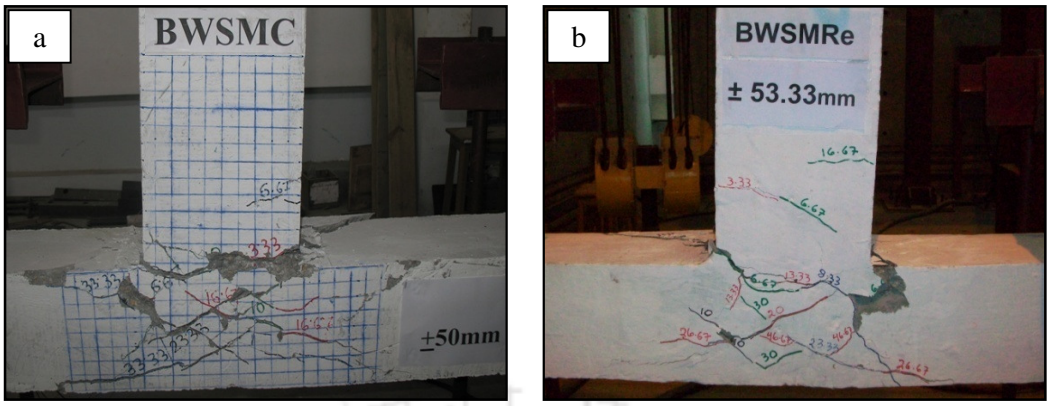

Fig. 4.8 BWSM specimens at the end of test under loading type-1:
(a) Control and (b) Rehabilitated

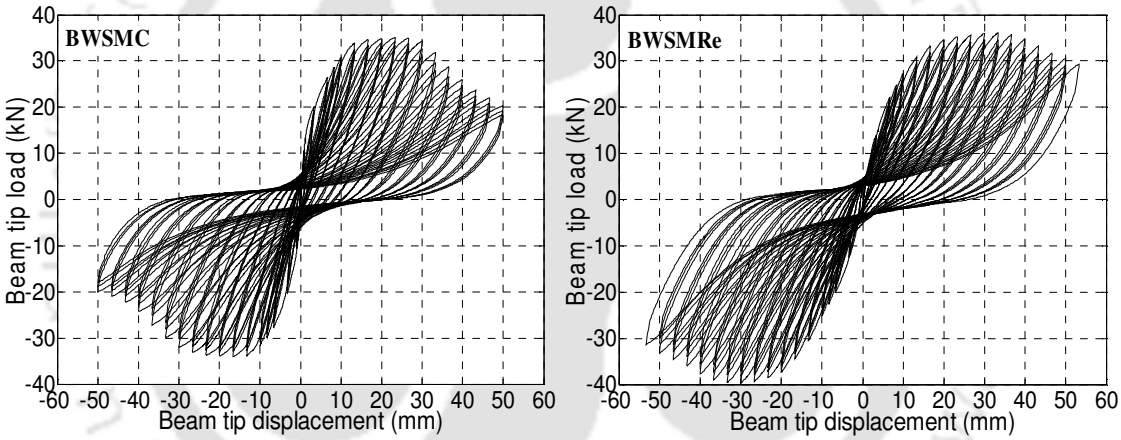

Fig. 4.9 Hysteretic response of BWSM specimens subjected to loading type-1

4.3.2 Behaviour of connections under loading type-2

Appearances of cracks at the initial loading cycles and at the end of testing are shown in Fig. 4.10 and Fig. 4.11 respectively. First visible crack appeared very near the junction of beam-column joint at a displacement amplitude of ±3.33 mm in both control and the rehabilitated specimens. The hysteretic responses obtained by plotting the test data are shown in Fig. 4.12. The maximum push and pull load carrying capacity as observed from these loops are presented in Table 4.1. Behaviour of specimens at a stage when specimens

attained its peak load are shown in Fig.4.10 and the joint region are observed to have suffered minor cracking. Spalling of concrete at the joint interface for control specimen was observed at a displacement of ± 30 mm. The crack width became sufficiently wider to about 5 mm at an amplitude of ±36.67 mm. Closing and opening of crack at joint interface became distinct at a displacement of ± 46.67 mm with more spalling of concrete on both sides of joint edges. Finally at a displacement of ± 50 mm, the experiment for control specimen was stopped. Rehabilitated specimen experienced fine cracks at the joint region, joint interface and at the beam part at the early stages of loading. However, in the subsequent loading cycles, the damage was concentrated in the beam part where a typical shear crack got further widened on increase in displacement amplitude. At a displacement of ± 43.33 mm, a wide crack of about 5 mm extended up to the first lateral tie away from the joint region located in the beam. The specimens became unstable and sudden dropping in load carrying capacity was noticed. The experiment for rehabilitated specimen was stopped at a displacement of ±46.67 mm for ensuring safety of testing equipment.

The joint region and joint interface of the rehabilitated specimen was practically undamaged at the end of the test. This behaviour may be attributed to the excellent performance of epoxy used to fill up the cracks in the damaged joint region. Moreover, the existing shear cracks at the beam part were not repaired as they were apparently very minor surface cracks. Thus, on loading the rehabilitated specimen these cracks widened up as it encountered a strong joint region in its immediate vicinity. Rehabilitated specimen showed slightly higher load carrying capacity as compared to the control specimen. The ultimate load carrying capacity of BWSMC and BWSMRe specimens were found to be 37.08 kN and 41.465 kN respectively.

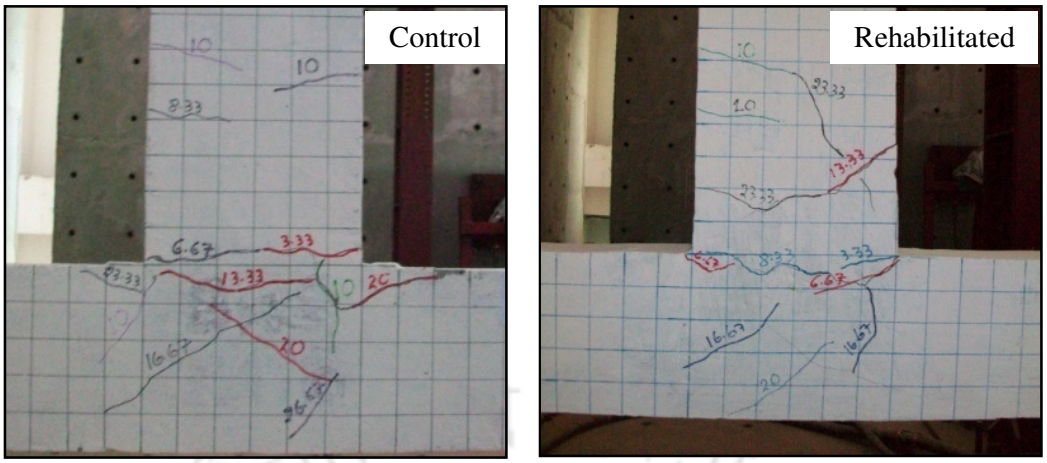

Fig. 4.10 Appearance of cracks for BWSM specimens under loading type-2 corresponding to peak load

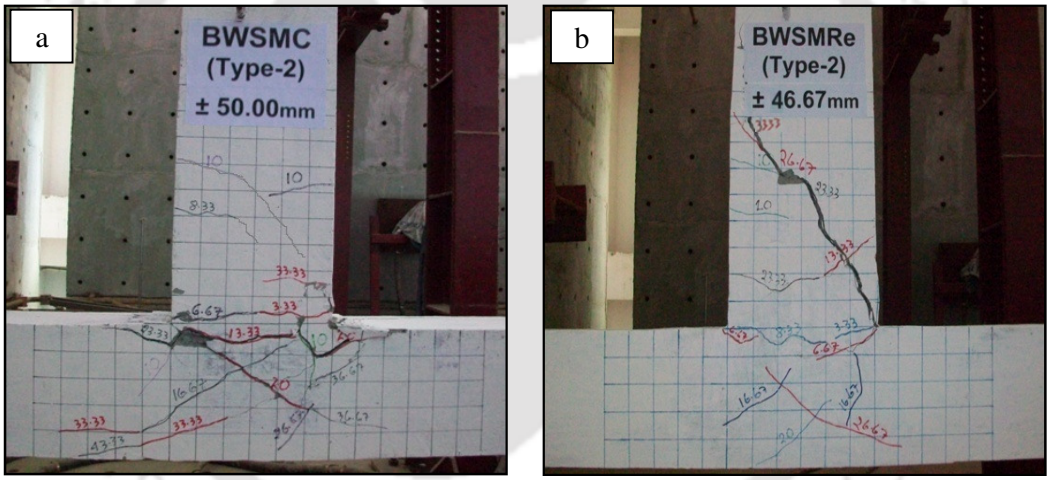

Fig. 4.11 BWSM specimens at the end of test under loading type-2: (a) Control and (b) Rehabilitated

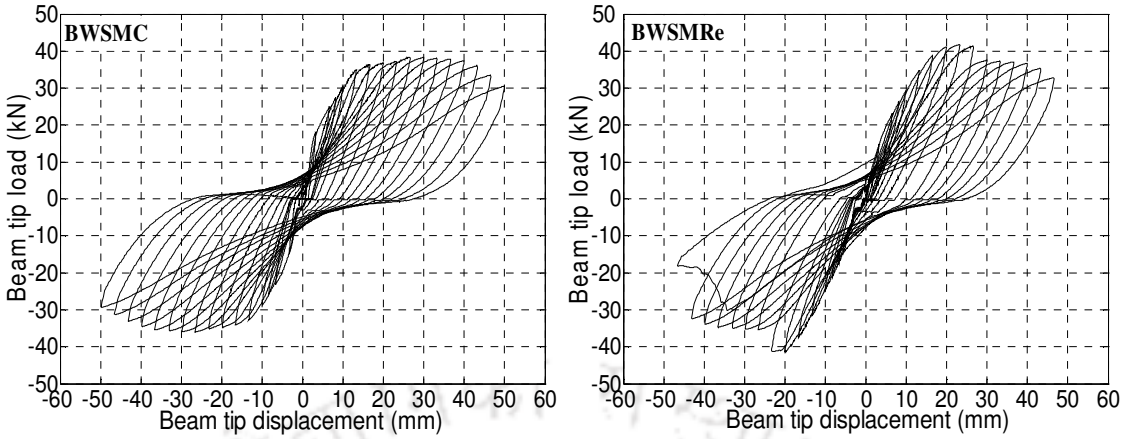

Fig. 4.12 Hysteretic response of BWSM specimens subjected to loading type-2

4.4 TESTING OF SMALL SIZE CONNECTIONS

Loading characteristics and displacement histories (type-1 and type-2) applied to these specimens were similar to those applied to the small size specimens with beam weak in flexure as discussed in the previous chapter. A servo hydraulic dynamic actuator of capacity ± 100 kN and having a maximum displacement range of ± 125 mm was used to apply the cyclic displacement. The experiment was stopped when the percentage reduction in load carrying capacity was of similar order as that in the case of BWS large and medium size specimens.

4.4.1 Behaviour of connections under loading type-1

The testing arrangement of this specimen and the appearances of initial cracks are shown in Fig. 4.13. The condition of the specimens at the end of test is shown in Fig. 4.14. The hysteretic responses obtained by plotting the test data are presented in Fig. 4.15. Some of the important observations made during testing along with those made during analysis of the hysteresis loops have been discussed in details in this section.

The first crack was observed in the beam near the column face at an amplitude of ±3.33 mm in both control and rehabilitated specimens. The control specimen attained its maximum load of 10.54 kN in the push direction at 25th cycle at a displacement of 11.67 mm. The first developed crack became wider at the same amplitude of ±11.67 mm. Similarly, in the pull direction, the specimen attained its maximum load of 9.56 kN at 28th cycle at a displacement of 13.33 mm. Spalling of concrete was noticed at an amplitude of ±18.33 mm. Significant cyclic rotation of the beam was observed near the column face at an amplitude of ±20 mm. Finally, the experiment for control specimen was stopped at a displacement of ±23.33 mm by taking note of percentage degradation in load carrying capacity. The ultimate load carrying capacity of BWSSC specimen was found to be 10.053 kN.

Rehabilitated specimen showed slightly higher load carrying capacity. The specimen attained its maximum load of 10.49 kN at 31st cycles in push direction at a displacement of 16.67 mm. The first crack became wider at a displacement of ±15 mm. A maximum of 12.73 kN was attained in the pull direction at 40th cycles at a displacement of 20 mm. Spalling of concrete also started at the joint interface at the same amplitude of ±20 mm. However, the joint area mostly remained undamaged. At the same stage when the experiment was stopped for control specimen, rehabilitated specimen was observed to achieve the original load carrying capacity. However, the degradation in rehabilitated specimen was not that significant and the experiment was finally stopped at a displacement of ±25 mm. The ultimate load carrying capacity of BWSSRe specimen was found to be 11.61 kN.

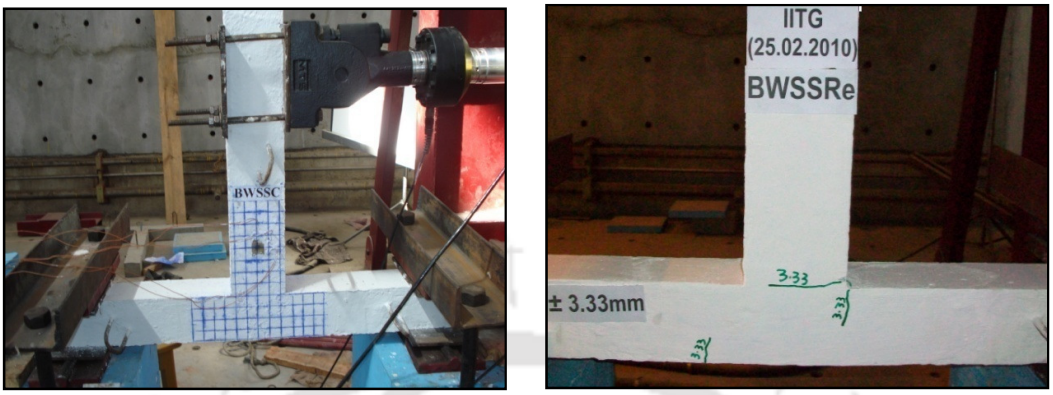

Fig. 4.13 Test set up for BWSS specimens and typical appearance of initial cracks under loading type-1

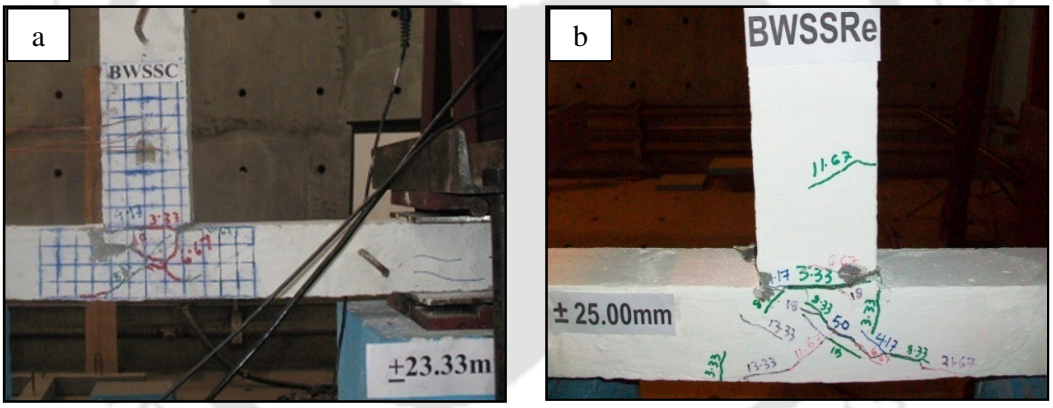

Fig. 4.14 BWSS specimens at the end of test under loading type-1: (a) Control and (b) Rehabilitated

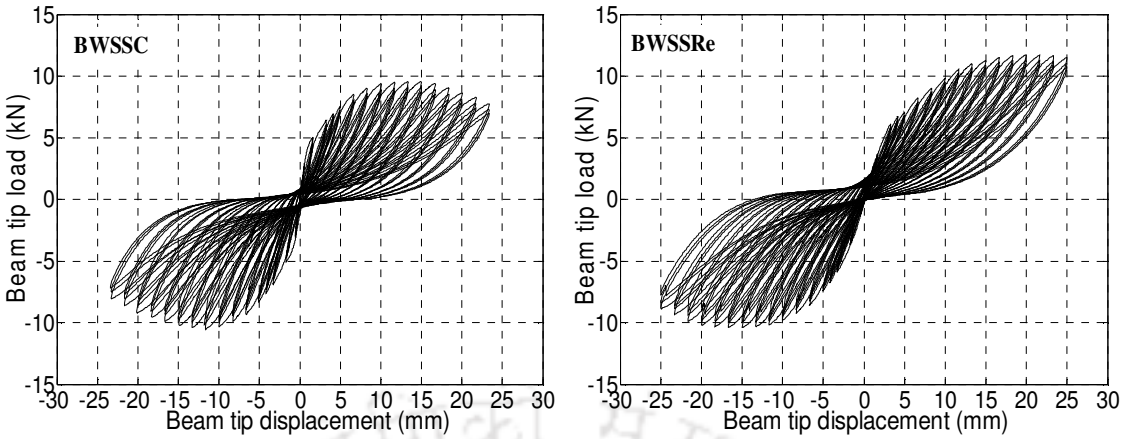

Fig. 4.15 Hysteretic response of BWSS specimens subjected to loading type-1

4.4.2 Behaviour of connections under loading type-2

Appearance of cracks at initial loading cycles and the condition of the specimens at the end of the test are shown in Fig. 4.16 and Fig. 4.17 respectively. It can be seen that the first crack for control specimen appeared in the beam very near to the joint interface. However, the crack shifted away from the joint interface to the beam part for rehabilitated specimen. The visible crack appeared at a displacement of ±3.33 mm for both control and rehabilitated specimens. The initial developed cracks at the joint interface for control specimen got widened on reaching a displacement of ±11.67 mm with more cracks appearing at the joint region. At the same displacement of ±11.67 mm, no crack was however observed at the joint region for the rehabilitated specimen and instead a wide crack was formed at the beam part.

Fig. 4.18 shows the hysterestic responses obtained by plotting the test data. Behaviour of specimens at a stage when peak loads were attained are shown in Fig. 4.16. More cracks started to develop in the joint region of control specimen as the displacement amplitude was further increased. The crack width at the joint interface became sufficiently wider at ±20 mm amplitude. Closing and opening of crack at joint interface became distinct at ±

21.67 mm displacement. The experiment for control specimen was stopped at a displacement of ±23.33 mm. The displacement limits for control specimen was kept same as those for testing under loading type-1. This was done for facilitating comparative understanding of their behaviour. Rehabilitated specimen suffered fine cracks at the joint interface and beam part during the initial loading cycles. However, in subsequent loading cycles the cracking was concentrated at the beam part and the joint region remained practically undamaged. The existing shear crack at the beam further got widened on increase in displacement. At ± 20 mm a shear crack of about 6 mm extended up to the bottom level of the actuator head and spalling of concrete at the beam started. The specimen became unstable and sudden dropping in load carrying capacity was noticed. The experiment was stopped at a displacement of ±23.33 mm for ensuring safety of testing equipment. The ultimate load carrying capacity of BWSSC and BWSSRe specimens were found to be 10.19 kN and 11.82 kN respectively.

The joint region for rehabilitated specimen was practically undamaged and instead severe cracking shifted to the beam part. This beahaviour was similar to that of large and medium rehabilitated specimens under loading type-2. The over strength at the joint region imparted by the high strength epoxy could be the possible reason for this behaviour. Moreover, the initially developed shear cracks at the beam were also not repaired. Thus on further loading, these cracks widened up as the damaged was mostly concentrated on the beam part without transferring to the relatively stronger joint region.

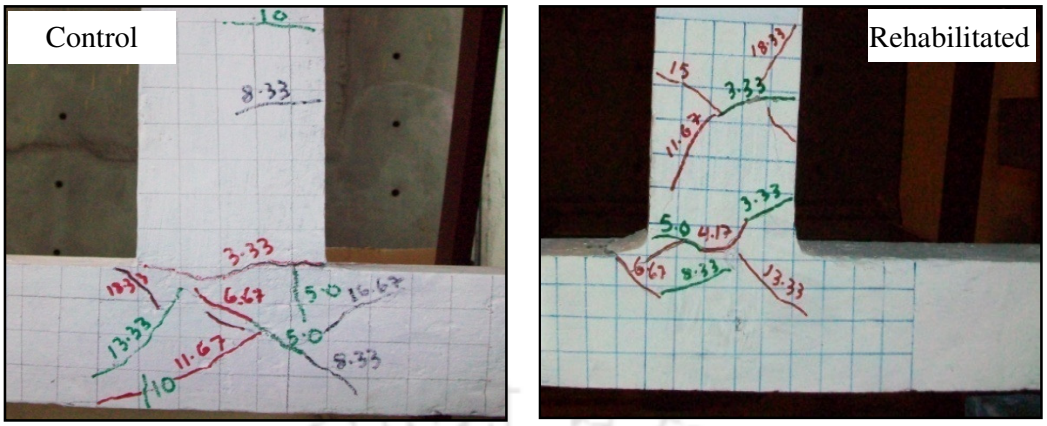

Fig. 4.16 Appearance of cracks for BWSS specimens under loading type-1 corresponding to peak load

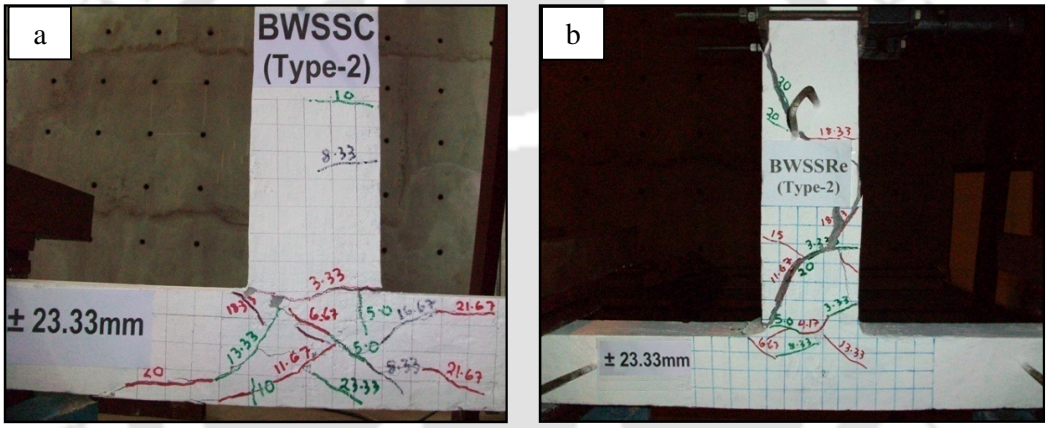

Fig. 4.17 BWSS specimens at the end of test under loading type-2: (a) Control and (b) Rehabilitated

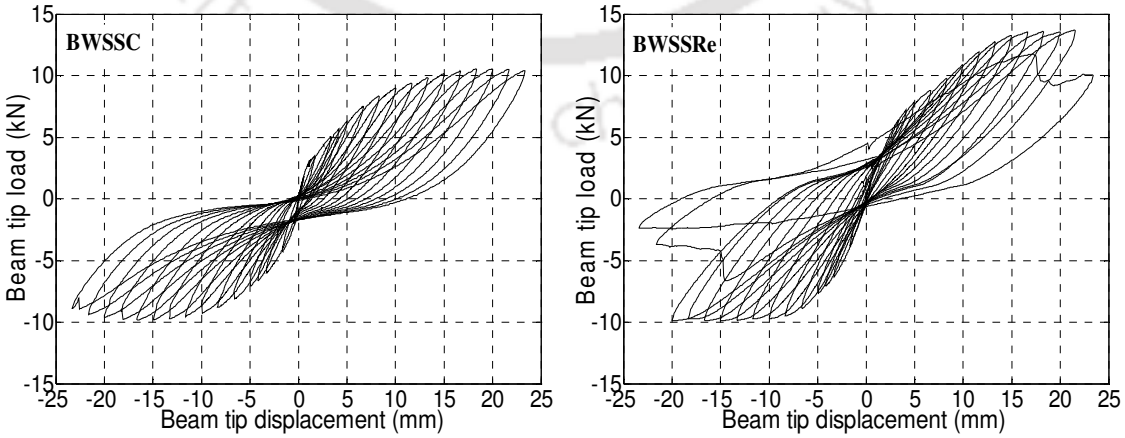

Fig. 4.18 Hysteretic response of BWSS specimens subjected to loading type-2

Table 4.1 Ultimate load carrying capacity for beam weak in shear (BWS) specimens

Specimen size	Control specimens			Rehabilitated specimens		
	+ve load (kN)	- ve load (kN)	Avg. load (kN)	+ve load (kN)	- ve load (kN)	Avg. load (kN)
	Specimens subjected to loading type-1					
Full	73.39 *25, #19	70.78 *30, #22	72.085	78.32 *35, #25	76.12 *30, #22	77.220
Medium	36.01 *23.33, #25	34.19 *20, #22	35.100	37.77 *30, #31	39.56 *30, #31	38.665
Small	9.56 *13.33, #28	10.54 *11.67, #25	10.053	12.73 *20, #40	10.49 *16.67, #31	11.610
	Specimens subjected to loading type-2					
Full	71.49 *35, #9	76.63 *40, #10	74.060	75.44 *45, #11	86.50 *45, #11	80.970
Medium	38.40 *26.67, #10	35.82 *26.67, #10	37.080	41.77 *23.33, #9	41.16 *23.33, #9	41.465
Small	10.54 *18.33, #13	9.840 *16.67, #12	10.190	13.72 *20, #14	9.911 *15, #11	11.820

Note: * and #: displacement and cycle number corresponding to its maximum load
-ve: Push direction and +ve: Pull direction

4.5 COMPARISON OF TEST RESULTS OF CONTROL AND REHABILITATED SPECIMENS

The hysteretic responses of all the connections have been shown in the previous sections. The parameters related to seismic capacity such as ultimate strength, stiffness degradations, energy dissipation and ductility of the specimens were evaluated from these hysteretic responses. Effectiveness of the adopted repair techniques were evaluated by comparing seismic performance of the rehabilitated specimens with that of their corresponding control specimens.

(a) Response cycles and peak loads

The envelope curves of hysteresis loops for control as well as rehabilitated specimens for all loading types are shown in Fig. 4.19-4.24. Comparing these curves at each displacement levels; it can be observed that all the rehabilitated specimens show similar load displacement characteristics with the initial slope being relatively lower with respect to that of the corresponding control specimen. The envelope of hysteresis loops of the rehabilitated specimens however show slightly higher load carrying capacity in both push and pull directions and thus all damaged control specimens could successfully restore the load carrying capacity after rehabilitation. It is also observed that the ultimate load carrying capacity attained by the control specimens under both loading type-1 and type-2 are more or less similar (Table 4.1), though slightly different in peak push and pull load were observed. Thus, it shows that the characteristic of applied loading does not significantly influence the ultimate load carrying capacity of the specimens. On the other hand, comparison on the ultimate load carrying capacity attained by the rehabilitated specimens under loading type-1 and type-2 can not be made because of different applied rehabilitation strategies. Study shows that the appropriately chosen repair strategy could retrieve back the lost capacity even for a severely damaged structural component. Thus, it may be inferred that the applied repair techniques are effective in restoring the load carrying capacity of vital beam-column connections.

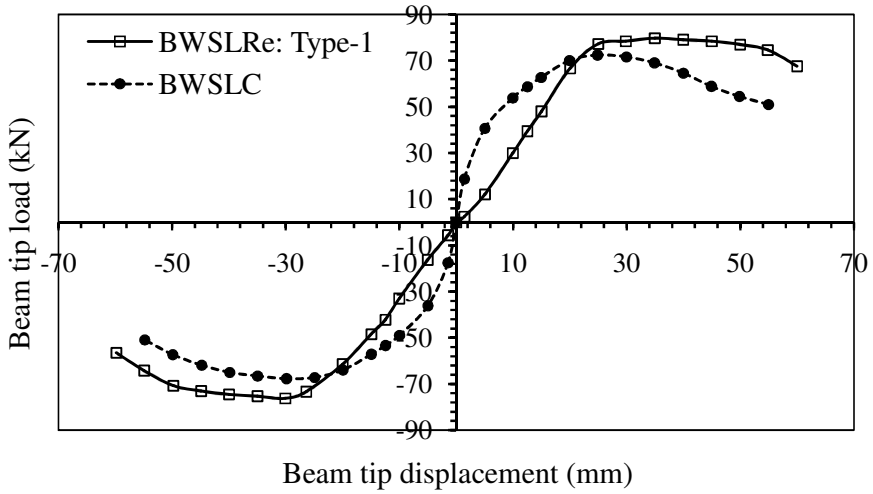

Fig. 4.19 Envelope curves of BWSL specimens under loading type-1

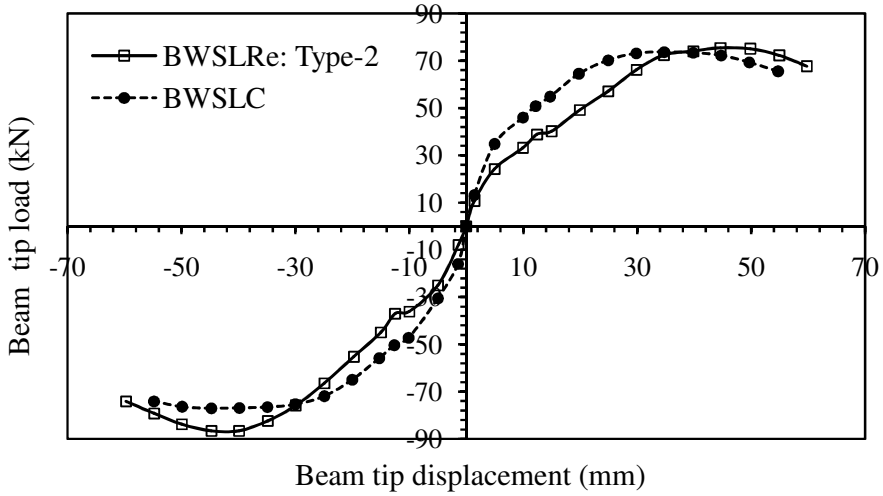

Fig. 4.20 Envelope curves of BWSL specimens under loading type-2

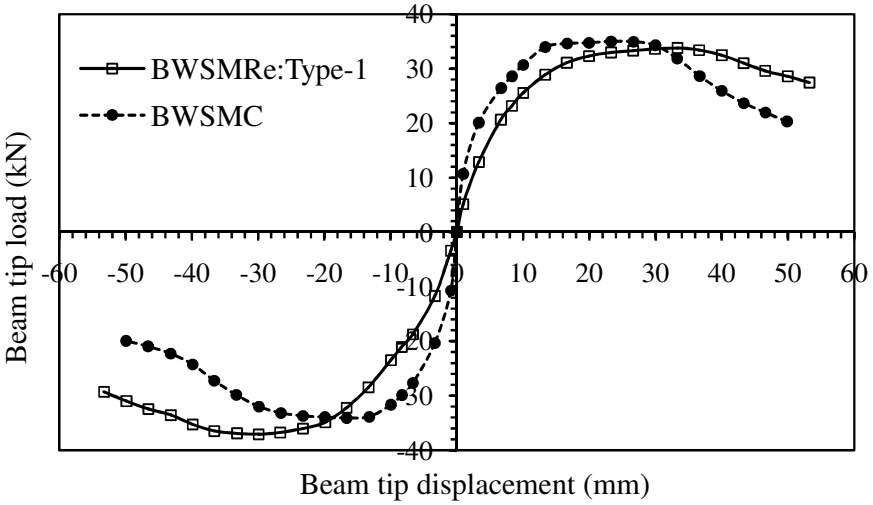

Fig. 4.21 Envelope curves of BWSM specimens under loading type-1

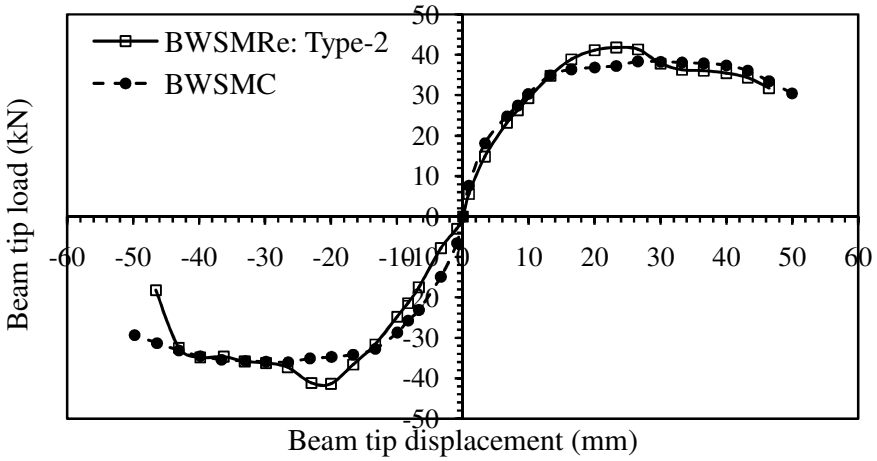

Fig. 4.22 Envelope curves of BWSM specimens under loading type-2

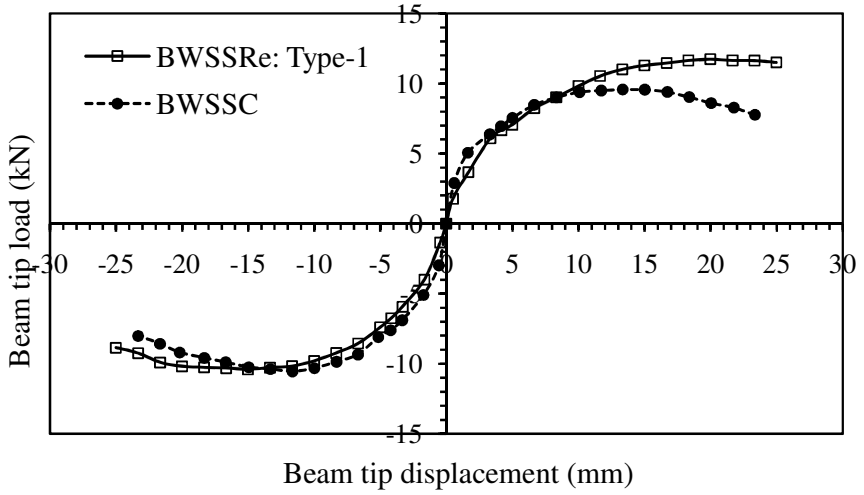

Fig. 4.23 Envelope curves of BWSS specimens under loading type-1

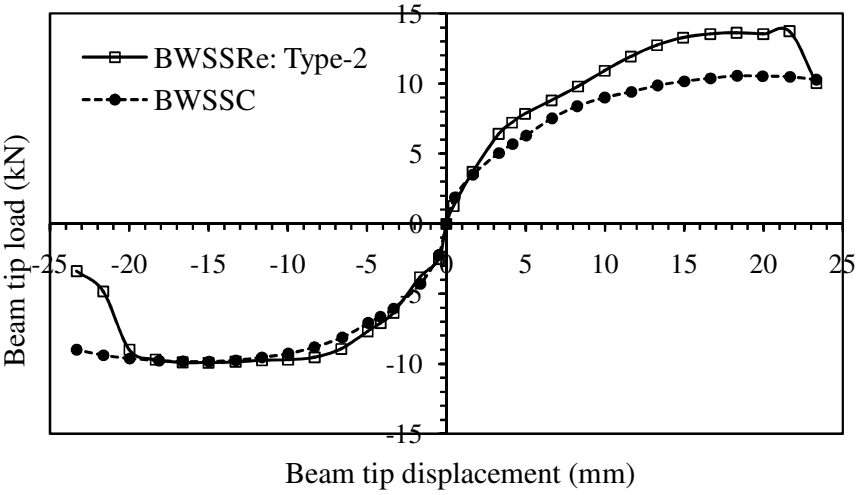

Fig. 4.24 Envelope curves of BWSS specimens under loading type-2

(b) Stiffness degradation

The stiffness for all specimens were evaluated with the same procedure as explained in Sec. 3.5 (b) of Chapter 3. The effectiveness of a rehabilitation techniques in restoring the stiffness of damaged connections were evaluated by comparing stiffness versus drift angle plots for different cases. The stiffness attained by the specimens (control and rehabilitated) corresponding to the drift angle of 0.103 % are presented in Table 4.2. The stiffness attained by the rehabilitated specimens were observed to be relatively lower. The variations of stiffness with respect to drift angle for all specimens are presented in Fig. 4.25-4.30. Comparison of all these curves irrespective of loading types, show a similar degradation trends were observed. The percent reductions in stiffness in both control as well as rehabilitated specimens were evaluated. Comparing drift by drift levels (control and rehabilitated), it has been observed that the stiffness degradation rate of the rehabilitated specimens with increase in lateral movement is little lower as compared to those of the control specimens. This behaviour may be attributed to the ductile properties contributed by the repairing materials. Thus, it can be concluded that all the rehabilitated specimens satisfactorily achieved stiffness level which is very well comparable to those of the control specimens.

Table 4.2 Stiffness (kN/mm) of beam weak in shear (BWS) specimens

Specimens size	Type-1		Type-2	
	Control	Rehabilitated	Control	Rehabilitated
Large	10.82	6.71	10.30	6.66
Medium	8.51	4.62	7.66	4.63
Small	5.05	3.24	4.26	2.74

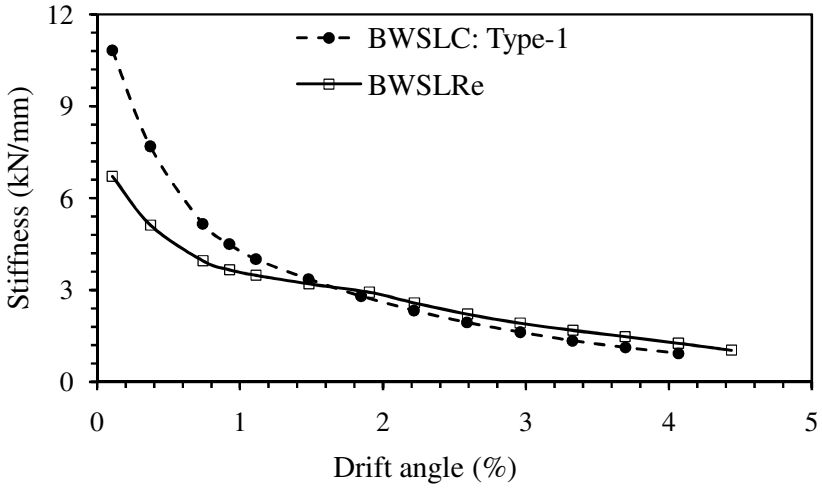

Fig. 4.25 Stiffness versus drift angle for BWSL specimens under loading type-1

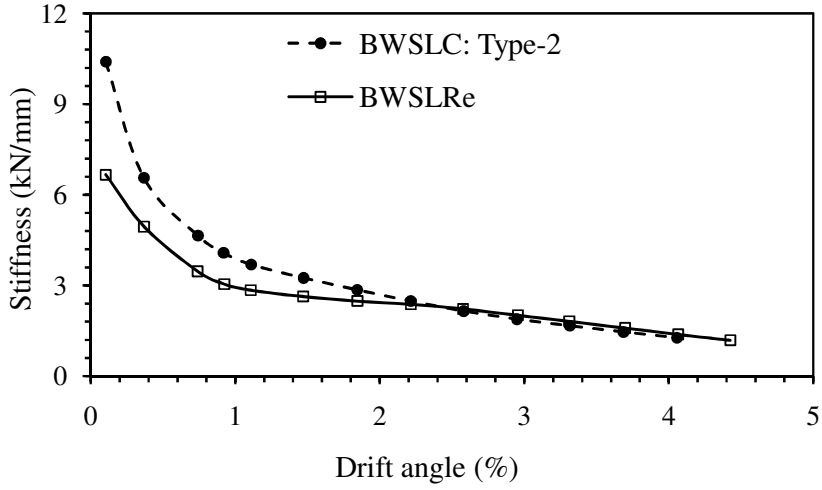

Fig. 4.26 Stiffness versus drift angle for BWSL specimens under loading type-2

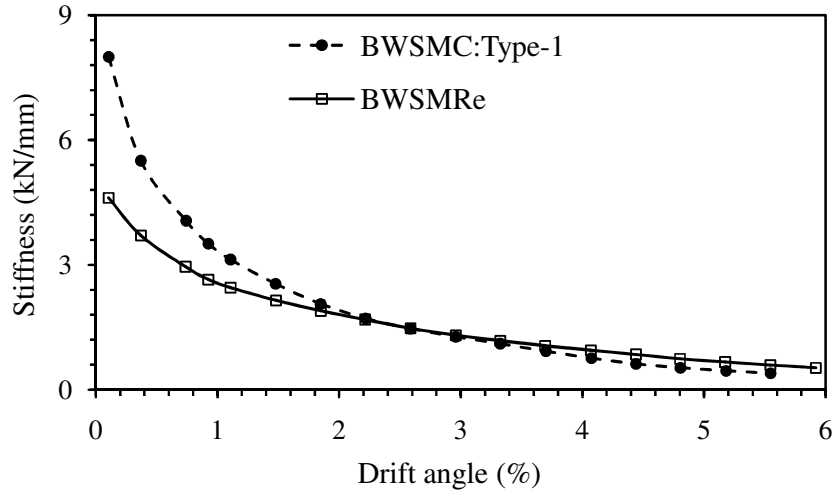

Fig. 4.27 Stiffness versus drift angle for BWSM specimens under loading type-1

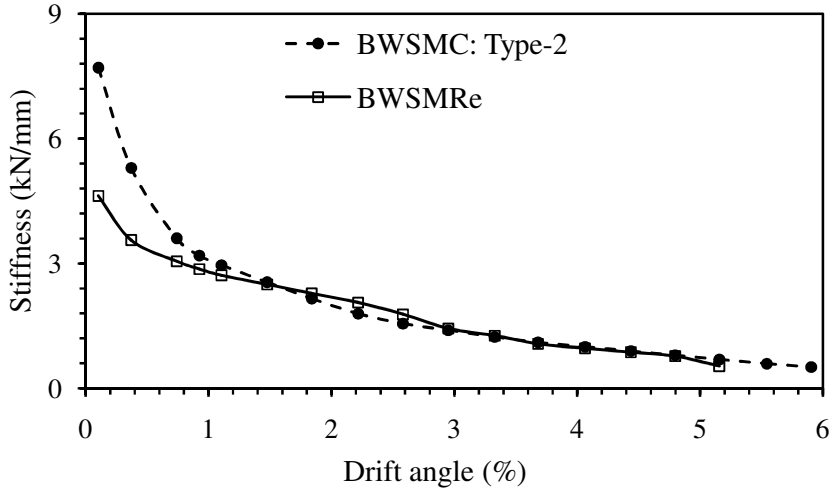

Fig. 4.28 Stiffness versus drift angle for BWSM specimens under loading type-2

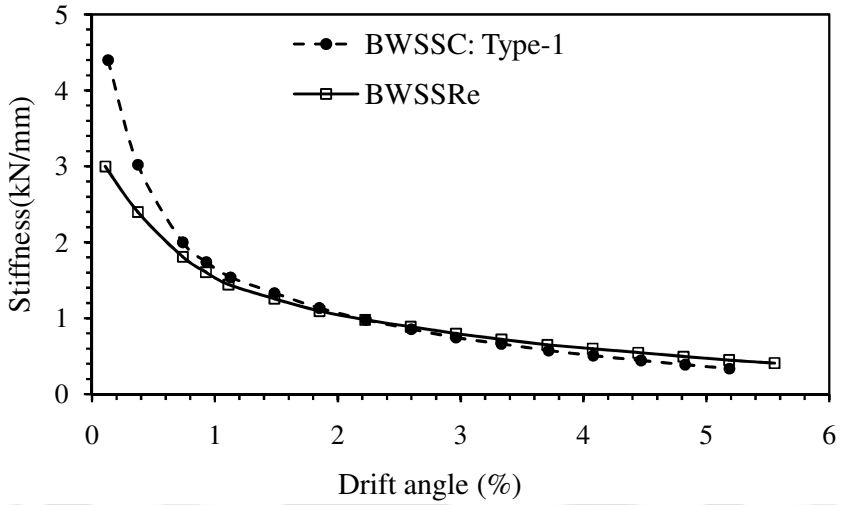

Fig. 4.29 Stiffness versus drift angle for BWSS specimens under loading type-1

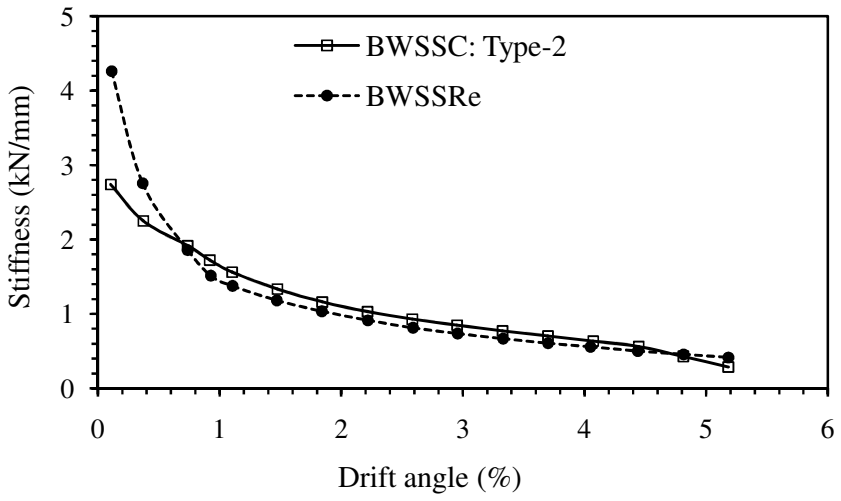

Fig. 4.30 Stiffness versus drift angle for BWSS specimens under loading type-2

(c) Energy dissipation

Variations of energy dissipation versus drift angle for control as well as rehabilitated specimens are shown in Fig. 4.31-4.33. On examination of these plots, it may be seen that the cumulative energy dissipated by the rehabilitated specimens are relatively lower during the initial stages of loading. However, in subsequent loading cycles, the energy dissipated by the rehabilitated specimens was observed to be at par with those of the control specimens. The increase in stiffness at the later loading cycles attracted more load at any drift angle for the rehabilitated specimens in comparison to that of the control specimen. Thus, the total area enclosed by the plot of beam tip load versus beam tip displacement was more for rehabilitated specimens than those of the control specimen. Table 4.3 shows the energy dissipated by the specimens (control and rehabilitated) corresponding to the drift level upto which the control specimens were tested. It is seen from Table 4.3 that the energy dissipated by the rehabilitated specimens are almost equivalent with those of the corresponding control specimens. Thus, it may be observed that by adopting an appropriate rehabilitation methodology, even a severely damaged structure can successfully restore the energy dissipation capacity which is comparable to those of the control specimens.

Table 4.3 Energy dissipation (kN-m) for beam weak in shear (BWS) specimens

Specimen size	Loading type-1		Loading type-2	
	Control	Rehabilitated	Control	Rehabilitated
Large	30.095	29.595	15.183	14.86
Medium	20.564	21.815	10.144	9.738
Small	1.901	1.894	0.889	0.900

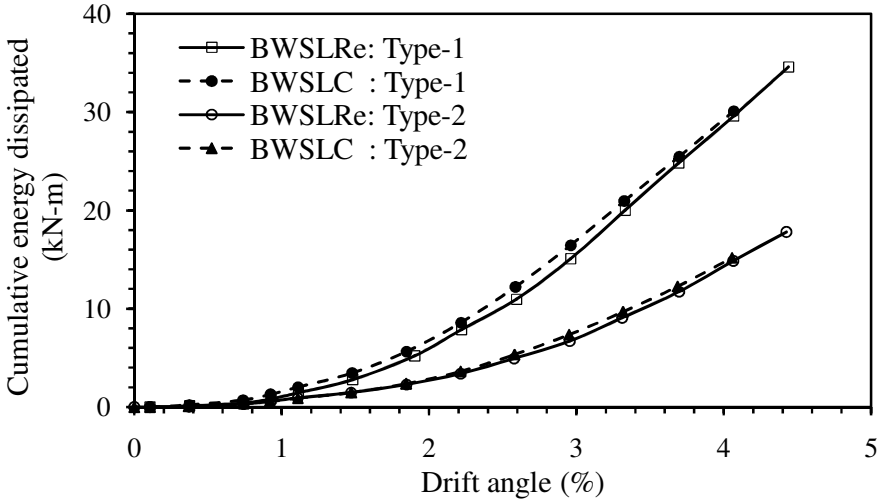

Fig. 4.31 Cumulative energy dissipation for BWSL specimens

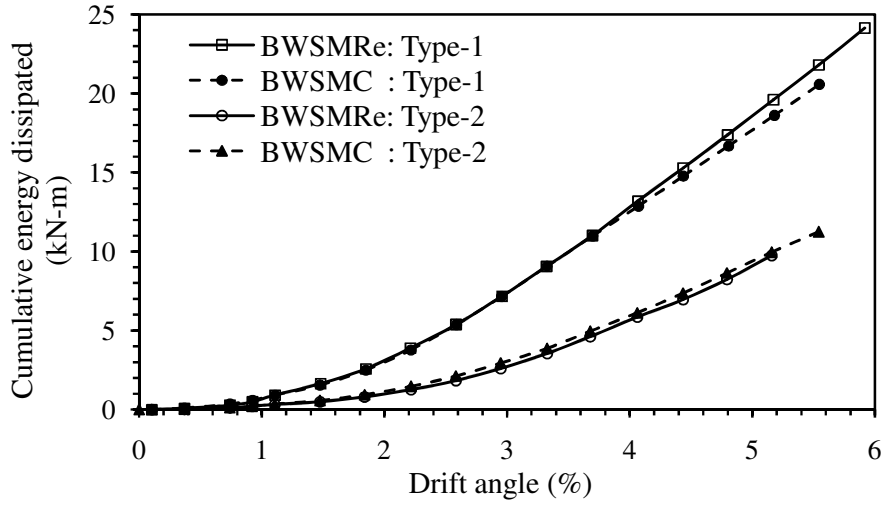

Fig. 4.32 Cumulative energy dissipation for BWSM specimens

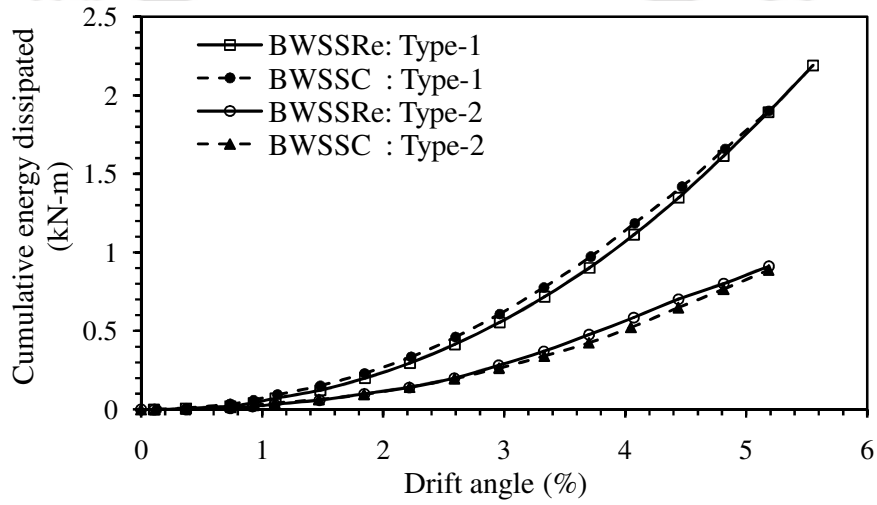

Fig. 4.33 Cumulative energy dissipation for BWSS specimens

(d) Displacement ductility

The displacement ductility for all specimens were evaluated with the same procedure as explained in Sec. 3.5 (d) of Chapter 3. The calculated values are presented in Table 4.4. Control specimens under both loading cases (type-1 and type-2) achieved almost equivalent ductility values. The displacement ductility achieved by the rehabilitated specimens under loading type-1 are found to be marginally higher than those of the control specimens. Rehabilitated specimens (medium and small) under loading type-2 could not however achieve their ductility values as good as their control specimens.

Table 4.4 Displacement ductility of beam weak in shear (BWS) specimens

Loading type	Specimens	Control			Rehabilitated		
		Δ_y	Δ_{20}	Δ_{20}/Δ_y	Δ_y	Δ_{20}	Δ_{20}/Δ_y
Type-1	Large	5.5	45	8.18	5.5	53.5	9.73
	Medium	4.5	38	8.44	4.5	45	10.0
	Small	2.5	22	8.8	2.5	25	10.0
Type-2	Large	7.5	55	7.33	7.5	60	8.00
	Medium	6.0	50	8.33	6.0	46	7.76
	Small	3.5	23	6.57	4.5	22	6.29

Δ_y and Δ_{20} : Displacement at first yield and at 20% drop of peak load (mm)

4.6 INVESTIGATION FOR THE EXISTENCE OF SIZE EFFECT

The results obtained from testing of the specimens were analyzed and bi-logarithmic plot were drawn. Various parameters, which are of practical relevance were also considered and the possible existence of size effects were investigated.

4.6.1 Bi-logarithmic Plot

Ultimate shear stress σ_{N_U} was calculated for these specimens as the failure mode of the specimens was in shear. The stress calculation is furnished in Appendix-B. The stress and calculation of other parameters necessary to carry out regression analysis and to draw bi-logarithmic plot for both control as well as rehabilitated specimens are furnished in Table 4.5. Regression analysis was carried out to determine the constant B and D_0 (Fig. 4.34). The values of these constants for control specimens were determined as 0.598 and 310.44 while the same for rehabilitated specimens were 0.749 and 197.89 respectively. Finally, bi-logarithmic plots for control and rehabilitated specimens were drawn as shown in Fig. 4.35 and Fig.4.36 respectively. It is observed that both the plots show presence of size effect and substantiate Bažant's size effect law.

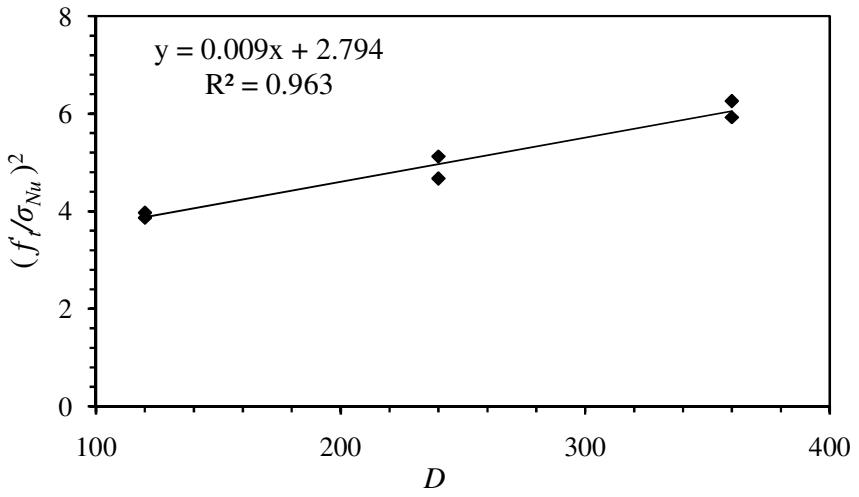

Fig. 4.34 Regression plot for Control BWS specimens

Table 4.5 Parameters of BWS specimens for bi-logarithmic plotting

Specimens	Specimen sizes	Bending stress, σ_{N_U} (N/mm^2)	Depth of specimen, D (mm)	$\left(\frac{f_t'}{\sigma_{N_U}}\right)^2$	Log (D/Do)	$Log\left(\frac{\sigma_{N_U}}{Bf_t'}\right)$
Control	Large	1.0012	360	6.25523	0.06432	-0.17482
		1.0286	360	5.92606	0.06432	-0.16308
	Medium	1.0968	240	5.12139	-0.11176	-0.12250
		1.1587	240	4.66970	-0.11176	-0.11035
	Small	1.2566	120	3.97061	-0.41279	-0.07613
		1.2737	120	3.86456	-0.41279	-0.07025
Rehabilitated	Large	1.0725	360	5.45097	0.25987	-0.24272
		1.1246	360	4.98577	0.25987	-0.22212
	Medium	1.2083	240	4.29469	0.08378	-0.14209
		1.2958	240	3.87343	0.08378	-0.16258
	Small	1.4513	120	2.97703	-0.21724	-0.11137
		1.4775	120	2.87219	-0.21724	-0.10358

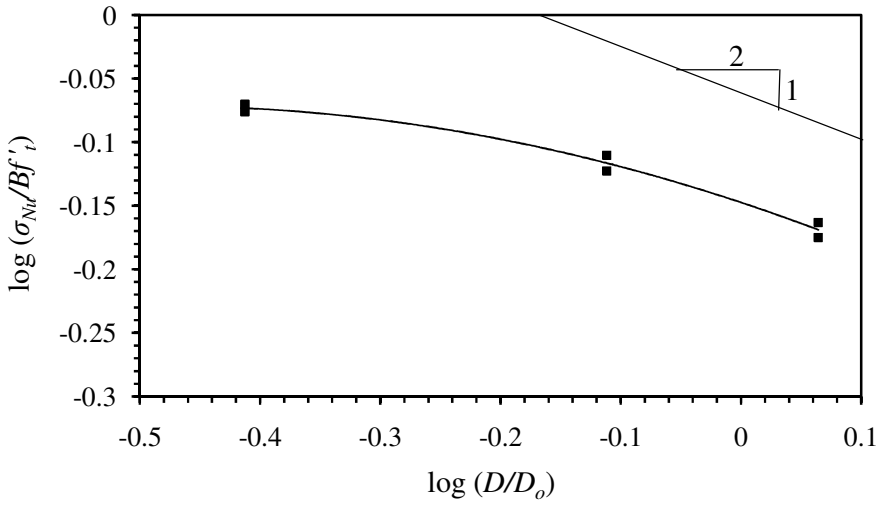

Fig. 4.35 Bi-logarithmic plot for control BWS specimens

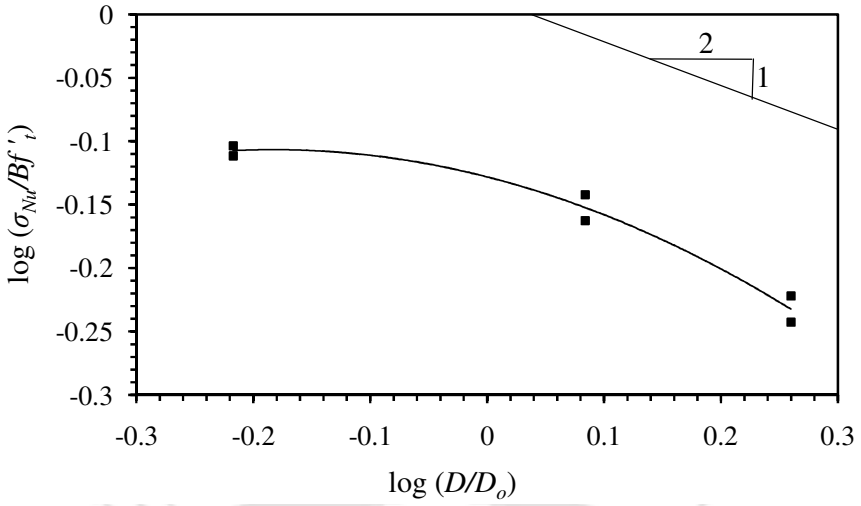

Fig. 4.36 Bi-logarithmic plot for rehabilitated BWS specimens

4.6.2 Size effect on energy dissipated per unit volume of D-region

The Cumulative energy dissipated per unit volume of D-region (e_N), was calculated for all the specimens. The variations with respect to drift angle is shown in Fig. 4.37 for specimens with loading type-1, while Fig. 4.38 shows the same for specimens with loading type-2. The plot clearly showed that in both the loading cases and for both kinds of specimens (control and rehabilitated), the uppermost curve is for the smallest specimen while the lowermost curve corresponding to the largest specimen. Thus, it is observed that during cyclic loading, smaller specimens dissipated higher energy per unit volume of the D-region as compared to the larger specimens, which is an indication for the existence of size effect.

4.6.3 Size effect on stress variation with relative deflection

The relative deflection and stresses in both the loading cases were calculated and the variations of stress with relative deflection have been plotted as shown in Fig. 4.39-4.40 for control and rehabilitated specimens. It is observed that stress are highest for the

smallest specimen and lowest for the largest specimen considered in the present study corresponding to any level of relative deflection in both the loading cases. This also confirms the existence of size effect.

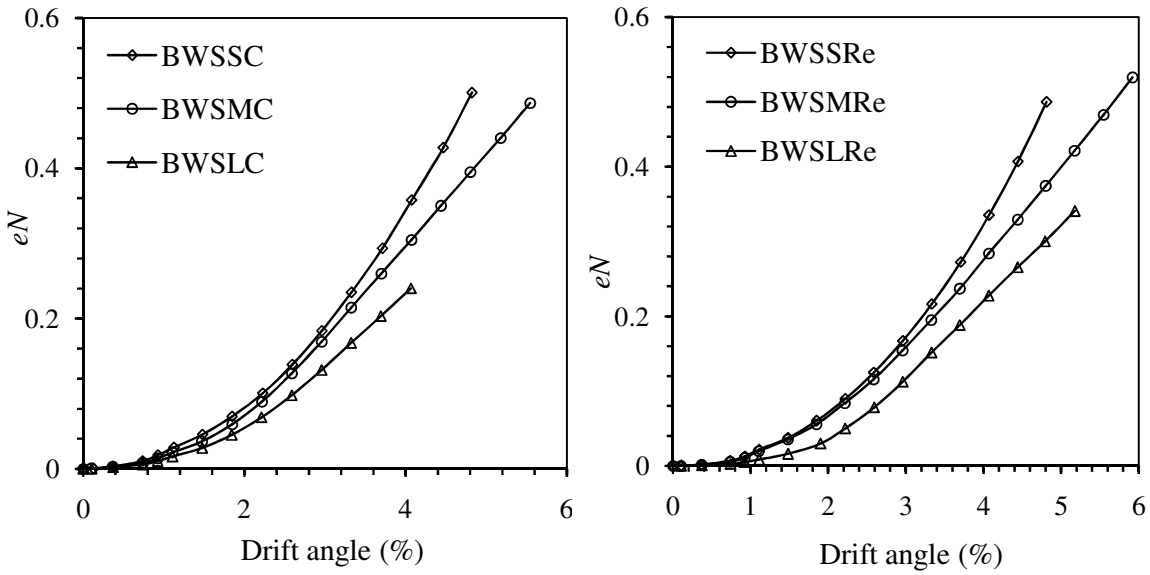

Fig. 4.37 Cumulative energy dissipated per unit volume of D-region for BWSC and BWSRe specimens under loading type-1

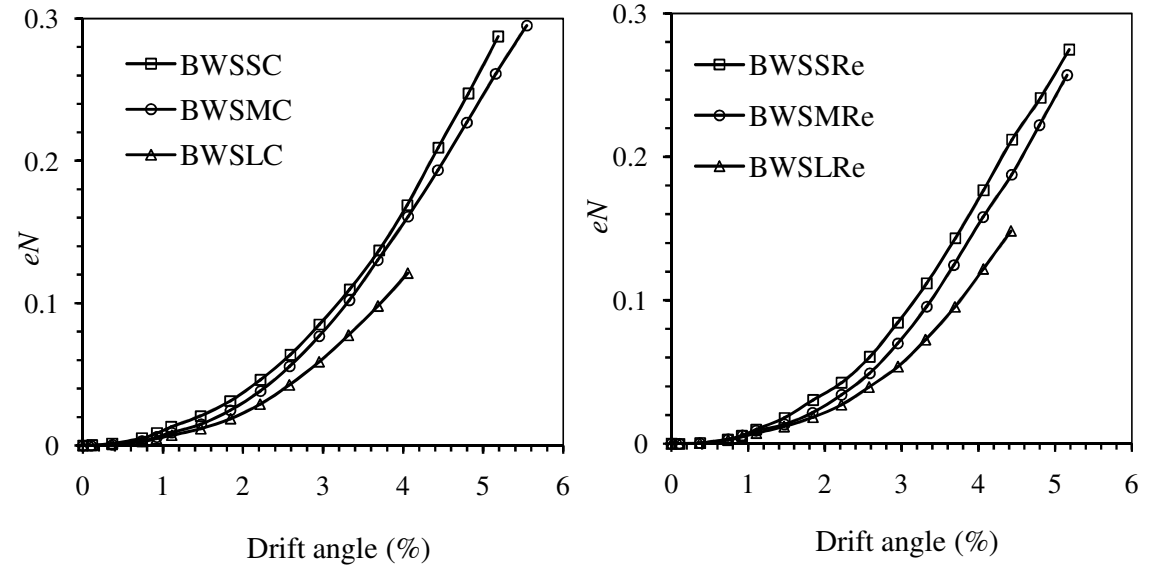

Fig. 4.38 Cumulative energy dissipated per unit volume of D-region for BWSC and BWSRe specimens under loading type-2

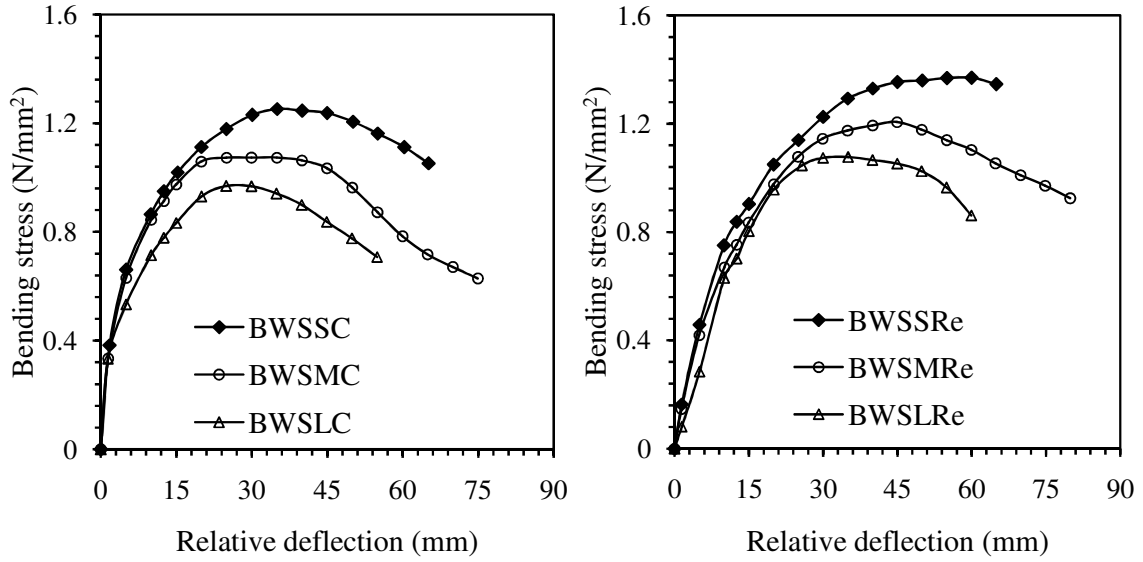

Fig. 4.39 Bending stress versus relative deflection for BWS specimens under loading type-1

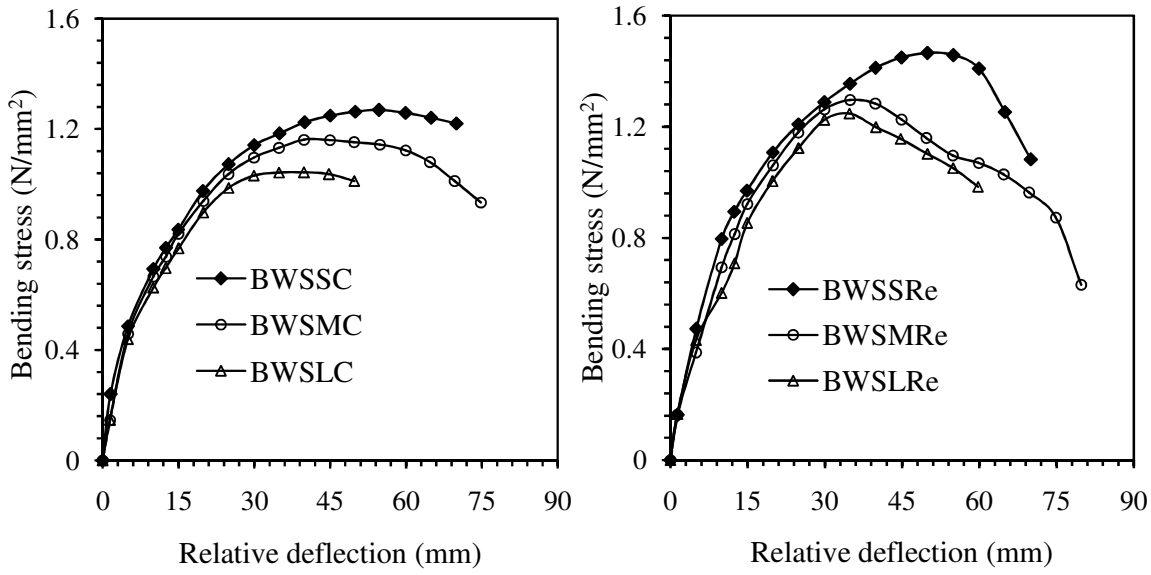

Fig. 4.40 Bending stress versus relative deflection for BWS specimens under loading type-2

4.7 CONCLUDING REMARKS

In this chapter, data of experimental investigation of beam-column connections with beam weak in shear subjected to different loading characteristic were presented. The analysis of results focusing on various parameters related to seismic capacity such as ultimate strength, stiffness degradation, energy dissipation and ductility revealed that the rehabilitated connections exhibited equal or marginally better performance than the corresponding control specimens and hence the adopted rehabilitation strategy could be considered as satisfactory. The failure patterns for each of the connections were also discussed. A distinct shear failure was observed for some rehabilitated specimens under loading type-2. The over strength at the joint region imparted by the injected epoxy perhaps did not allow damage to propagate in the joint region. Further, the results obtained from test were examined to explore the existence of size effect. Bi-logarithmic variation, cumulative energy dissipation per unit volume of D-region and variation of stress with relative deflection were plotted to observe the influence of size effect. It is observed that the bi-logarithmic plot for both control and rehabilitated specimens followed the size effect law as proposed by Bažant [1984].

CHAPTER 5

STUDY ON REHABILITATED RC BEAM-COLUMN CONNECTIONS WITH COLUMN WEAK IN SHEAR

5.1 INTRODUCTION

This chapter describes the findings of experimental investigation on beam–column connections with column weak in shear. Similar to the earlier two chapters, specimens with different sizes namely full, two third and one third size were tested. The control specimens were damaged under loading type-1 or type-2 and were subsequently rehabilitated with either repair method-1 or method-2 depending on the degree of damages for further testing. The data recording from these tests were used for post processing to evaluate many important parameters related to seismic capacity of the connections. Effectiveness of the applied repair technique was assessed based on the comparisons of the seismic performance of rehabilitated specimens with those of the corresponding control specimens. Bi-logarithmic plots were drawn to explore the possibility of existence of size effect in terms of shear strength. Further, specimen sizes were correlated with cumulative energy dissipated per unit volume of D-region as well as stress.

5.2 TESTING OF LARGE SIZE CONNECTIONS

A servo hydraulic dynamic actuator of capacity ±250 kN and having maximum displacement range of ±125 mm was used to apply the cyclic displacement. Loading characteristics and displacement histories (type-1 and type-2) applied to these specimens were similar to those applied to the large size specimens with beam weak in flexure and shear. The experiment was stopped for control specimens at a stage when the load came

down in the range of 60-70 % of the ultimate load carrying capacity. Similarly, the experiment on rehabilitated specimens was also stopped at about the same magnitude of load at which experiment was stopped for control specimens. The load carrying capacities of specimens of different sizes and subjected to different loading types have been presented in Table 5.1

5.2.1 Behaviour of connections under loading type-1

Appearance of initial cracks and the damaged specimens at the end of the test are shown in Fig. 5.1 and Fig. 5.2 respectively. The hysteretic responses obtained by plotting the test data are presented in Fig. 5.3. Some of the important observations made during testing along with those made during analysis of the hysteresis loops have been discussed in details in this section.

The first visible crack appeared at the joint interface at a displacement amplitude of ± 5.0 mm in both control and rehabilitated specimens. More cracks started to develop in the joint and at the column region as the amplitude of displacement was increased (Fig. 5.1). It is observed from the hysteretic response that control specimen attained its maximum load of 56.85 kN and 59.17 kN in the push and pull directions at the same loading cycles of 16^{th} at a displacement amplitude of 20 mm. However, the rehabilitated specimen showed slightly higher load carrying capacity with maximum of 63.08 kN in the push direction at 25 mm displacement and 64.19 kN in the pull direction at a displacement amplitude of 20 mm.

The developed cracks at the joint region in both control as well as rehabilitated specimens gradually propagated into the column on further increase in displacement. The cracks develop in control specimen reached to the weakest shear zone in the column at the displacement amplitude of ± 30 mm. On the other hand, rehabilitated specimen

experienced a slightly higher displacement level of ± 35 mm. The cracks at the joint region in both control and rehabilitated specimens became wider to about 5 mm and spalling of concrete started at a displacement of ± 40 mm. The test was stopped at a displacement of ± 50 mm for both control and rehabilitated specimens at which the load carrying capacity came down to about 60 % of the ultimate capacity. The ultimate load carrying capacity of CWSLC and CWSLRe specimens were found to be 58.01 kN and 64.635 kN respectively. Rehabilitated specimens suffered similar magnitude of damage at the same displacement level. However, damage of the joint area was limited to the spalling of concrete cover and the joint core suffered only fine cracks. The replaced materials at the joint region and the injected epoxy at the column part had prevented the early deterioration of concrete at this region.

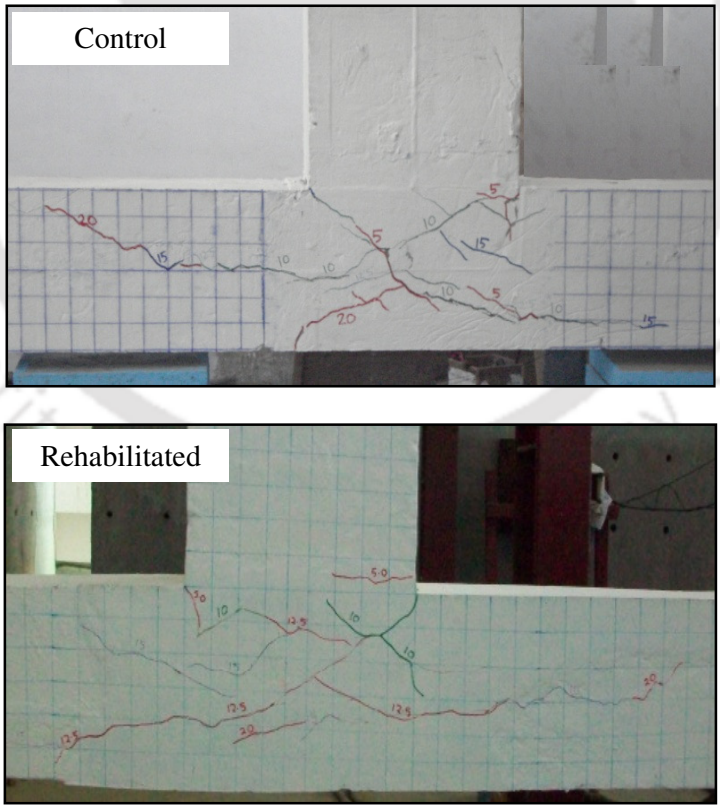

Fig. 5.1 Cracks appearance for CWSL specimens during initial stages of loading under loading type-1

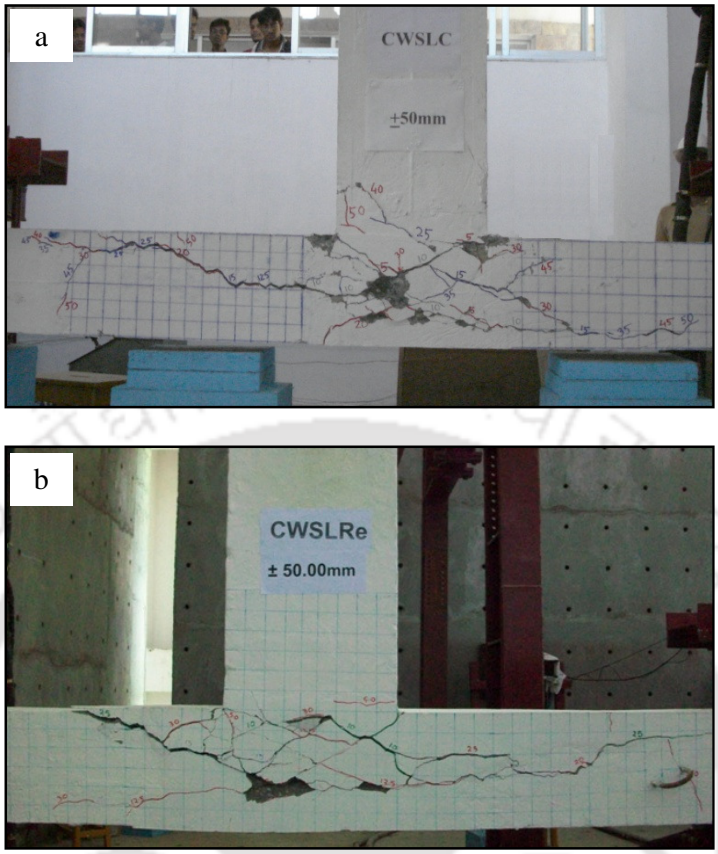

Fig. 5.2 CWSL specimens at the end of test under loading type-1:
(a) Control and (b) Rehabilitated

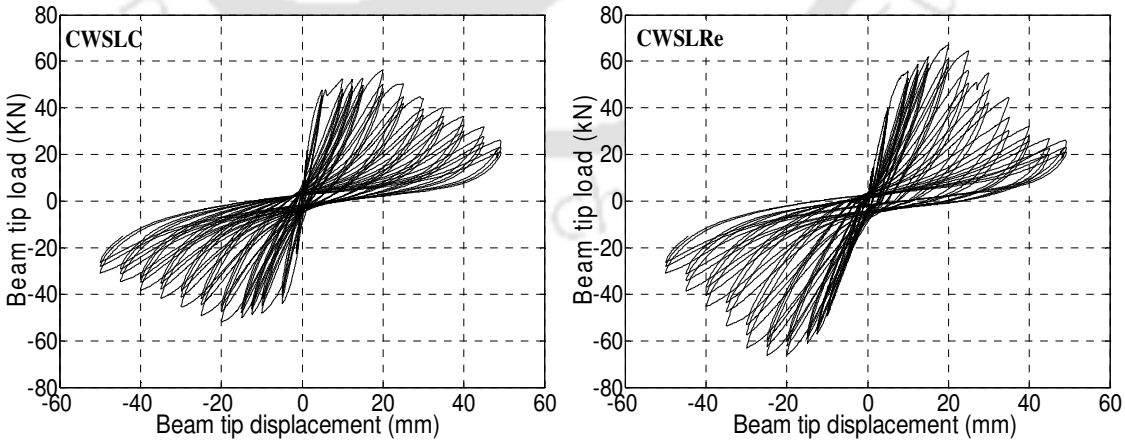

Fig. 5.3 Hysteretic response of CWSL specimens subjected to loading type-1

5.2.2 Behaviour of connections under loading type-2

Appearances of cracks during the initial stages of loading and the damaged specimen at the end of test are shown in Fig. 5.4 and Fig. 5.5 respectively for both control and rehabilitated specimens. It is clear from these figures that the crack patterns on both the specimens were generally similar. Further, comparing the nature of damages with specimens under loading type-1, it was observed that the crack distributions were generally similar in both control as well as the rehabilitated specimens (loading type-1 and type-2). However, the level of damage was relatively lower in this category of testing with specimens experience minor spalling of concrete at the joint region. Further, it was also observed that in all the specimens under loading type-1 and type-2, cracks reached to the weakest shear zone in the column region more or less the same displacement amplitude of loading. Some of the important observations made during testing along with those made during analysis of the hysteresis loops have been discussed in details in this section.

The first visible crack appeared in the beam-column junctions at a displacement amplitude of ± 5.0 mm in both control and rehabilitated specimens. More cracks started to develop in the joint region and gradually propagated toward the column part on further increase in displacement (Fig. 5.4). It is observed from the hysteretic responses as shown in Fig. 5.6, that both the loops are stable. The maximum load carrying capacities as obtained from these loops are presented in Table 5.1. Wider cracks were observed at the joint region in both control and rehabilitated specimens at the stage when specimens attained their peak capacities. The propagated cracks away from the joint region in both the specimens got further widened at a displacement of ± 45 mm. The experiment for both control and rehabilitated specimens were terminated at the same displacement level of ± 50 mm. The displacement limits were kept same for both control and rehabilitated

specimens when tested under loading type-1 as well as type-2. This was done for facilitating comparative understanding of their behaviour. The ultimate load carrying capacity of CWSLC and CWSLRe specimens were found to be 58.930 kN and 61.385 kN respectively

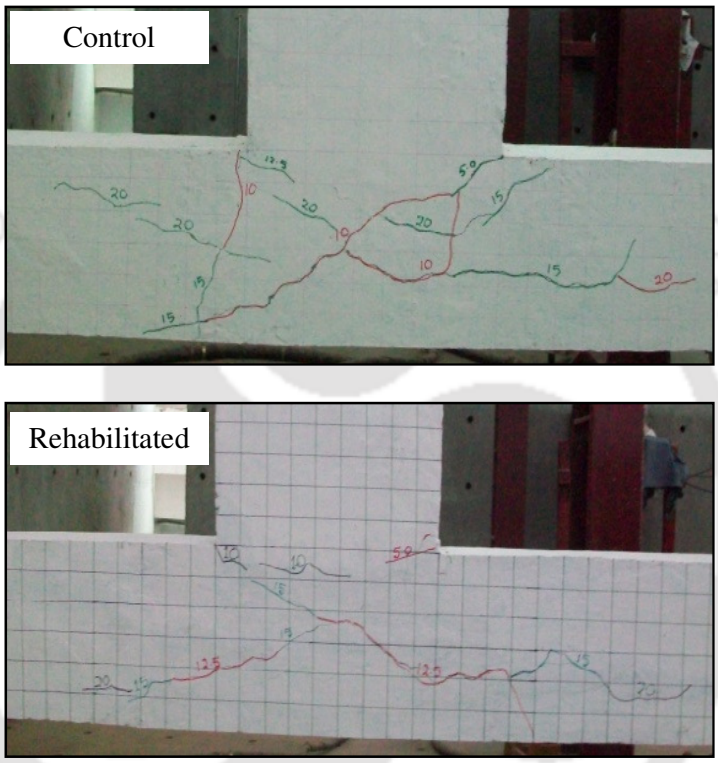

Fig. 5.4 Cracks appearance for CWSL specimens during initial stages of loading under loading type-2

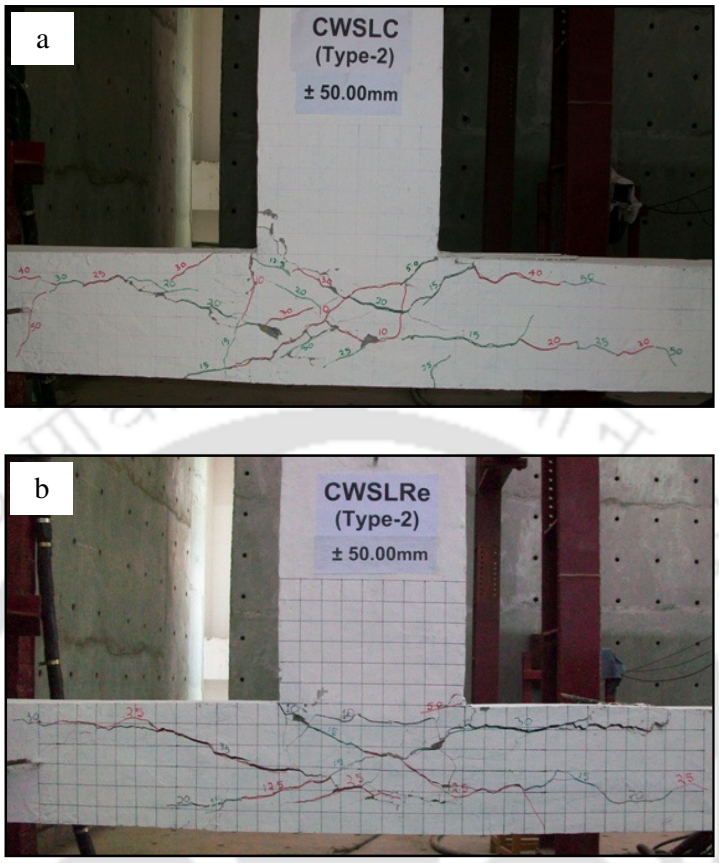

Fig. 5.5 CWSL specimens at the end of test under loading type-2:

(a) Control and (b) Rehabilitated

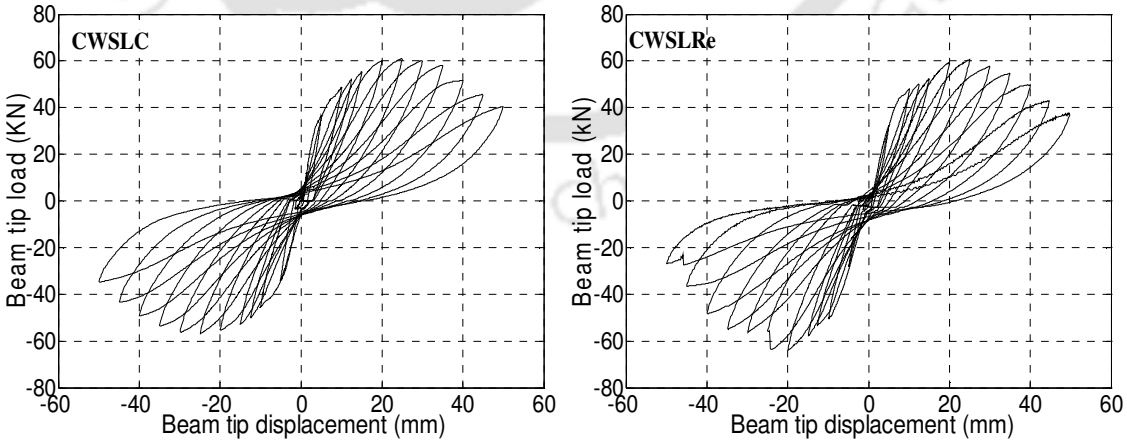

Fig. 5.6 Hysteretic response of CWSL specimens subjected to loading type-2

5.3 TESTING OF MEDIUM SIZE CONNECTIONS

Loading characteristics and displacement histories (type-1 and type-2) applied to these specimens were similar to those applied to the medium size specimens with beam weak in flexure and shear. A servo hydraulic dynamic actuator of loading capacity ±250 kN and having maximum displacement range of ±125 mm was used was used to apply the cyclic displacement. The experiment was stopped when the percentage reduction in load carrying capacity was of similar order as that in the case of CWS large size specimens.

5.3.1 Behaviour of connections under loading type-1

Appearance of cracks during initial stages of loading is shown in Fig. 5.7. The first crack appeared in the junction point of beam and column at a displacement of ± 3.33 mm. More cracks developed at the joint region on further increase in displacement. The developed cracks at the joint region started propagating towards the column region at a displacement of ± 10 mm. The view of the specimens at the end of testing is shown in Fig. 5.8. The figure shows that both control and rehabilitated specimens exhibited similar extent and pattern of damage. The hysteretic responses obtained by plotting the test data are presented in Fig. 5.9. Peak load of 32 kN both in push and pull directions were attained by the control specimen on reaching a displacement of 16.67 mm and 6.67 mm respectively. Slightly higher peak load of 34 kN in push and 37.12 kN in pull directions were attained by the rehabilitated specimen at a displacement of 6.67 mm and 16.67 mm respectively. In both control and the rehabilitated specimens the development of a major crack were noticed at ± 16.67 mm displacement. The crack extended up to the first lateral tie away from the joint region located in the column. Spalling of concrete started at a displacement amplitude of ± 20 mm. Shear reinforcement provided in column started to fail with a loud noise at ± 26.67 mm amplitude. The experiment was stopped at ± 30

mm displacement amplitude for both control and rehabilitated specimens. The ultimate load carrying capacity of CWSMC and CWSMRe specimens were found to be 32.00 kN and 35.56 kN respectively.

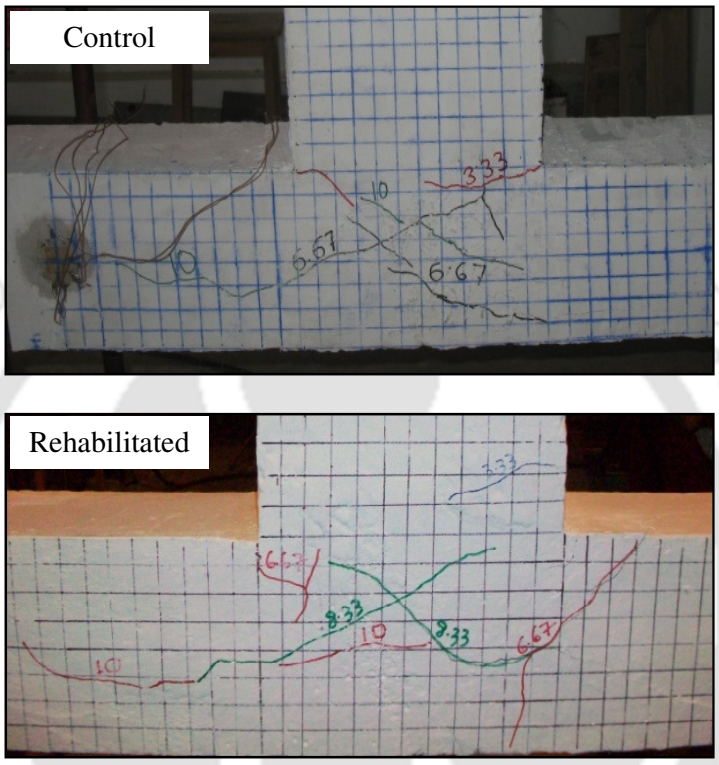

Fig. 5.7 Cracks appearance for CWSM specimens during initial stages of loading under loading type-1

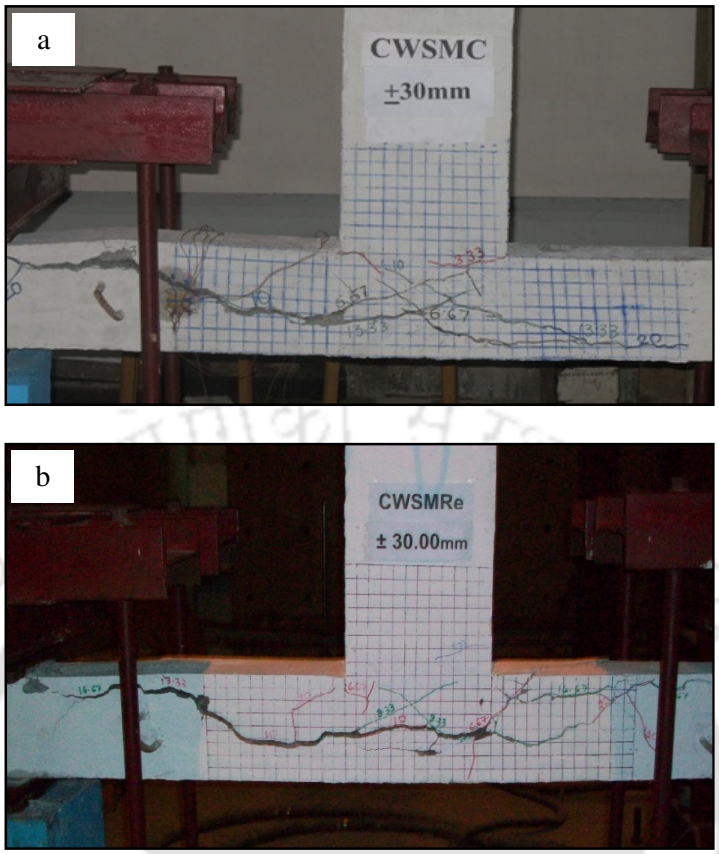

Fig. 5.8 CWSM specimens at the end of test under loading type-1:
(a) Control and (b) Rehabilitated

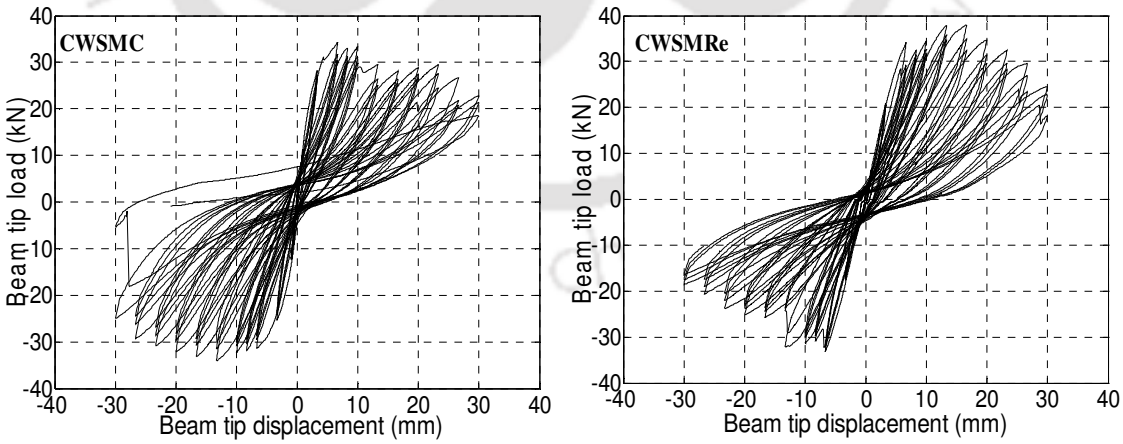

Fig. 5.9 Hysteretic response of CWSM specimens subjected to loading type-1

5.3.2 Behaviour of connections under loading type -2

Initiation and propagation of cracks during the early stages of loading and the damaged specimen at the end of test are shown in Fig. 5.10 and Fig. 5.11 respectively for both control and the rehabilitated specimens. The crack patterns were generally similar in both the specimens. Some of the important observations made during testing along with those made during analysis of the hysteresis loops have been discussed in details in this section. The first visible crack appeared in the beam-column junctions at displacement amplitude of ± 3.33 mm in both the specimens. The hysteretic responses obtained by plotting the test data are shown in Fig. 5.12. The load carrying capacities as observed from these loops are presented in Table 5.1. The developed cracks in both the specimens gradually propagated from the joint area towards the column region on further increase in displacement. The propagated cracks in zones away from the joints region got further widened at a displacement of ± 26.67 mm. No spalling of concrete was however observed either at the joint region or in the column region for the control specimen. While at the same displacement of ± 26.67 mm, spalling of concrete were observed at the weakest shear zone in the column region for the rehabilitated specimen. The experiments in both the control and rehabilitated specimens were stopped at a displacement of ± 30 mm. The displacement limits were kept same as those for testing under loading type-1. The ultimate load carrying capacity of CWSMC and CWSMRe specimens were found to be 31.23 kN and 32.84 kN respectively. At the end of the test no spalling of concrete was observed for a control specimen. A single line crack of about 2 mm width clearly propagated toward the weakest shear zone on both side of column face. The joint region of the rehabilitated specimen suffered a wider crack to about 4 mm with minor spalling of concrete cover both at the joint and at the weakest shear zone in the column region.

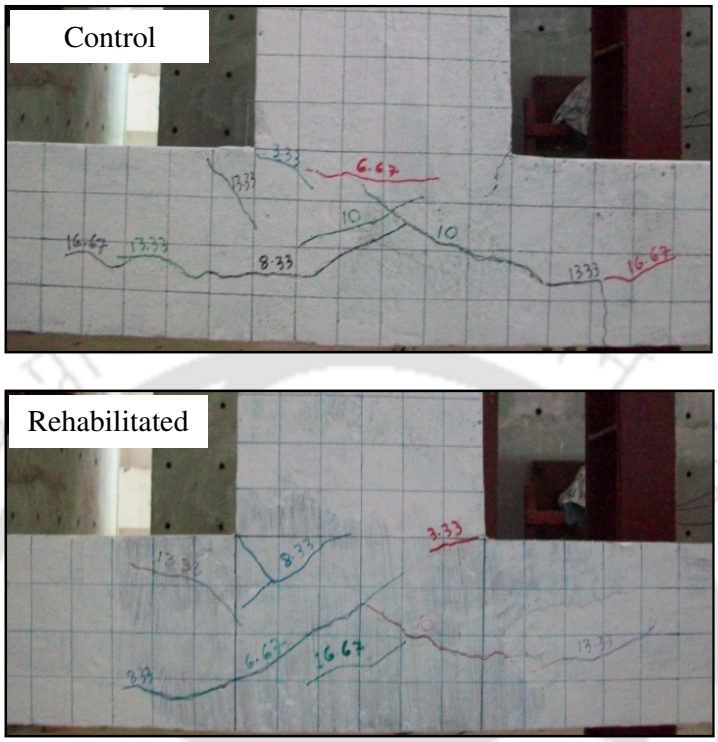

Fig. 5.10 Cracks appearance for CWSM specimens during initial stages of loading under loading type-2

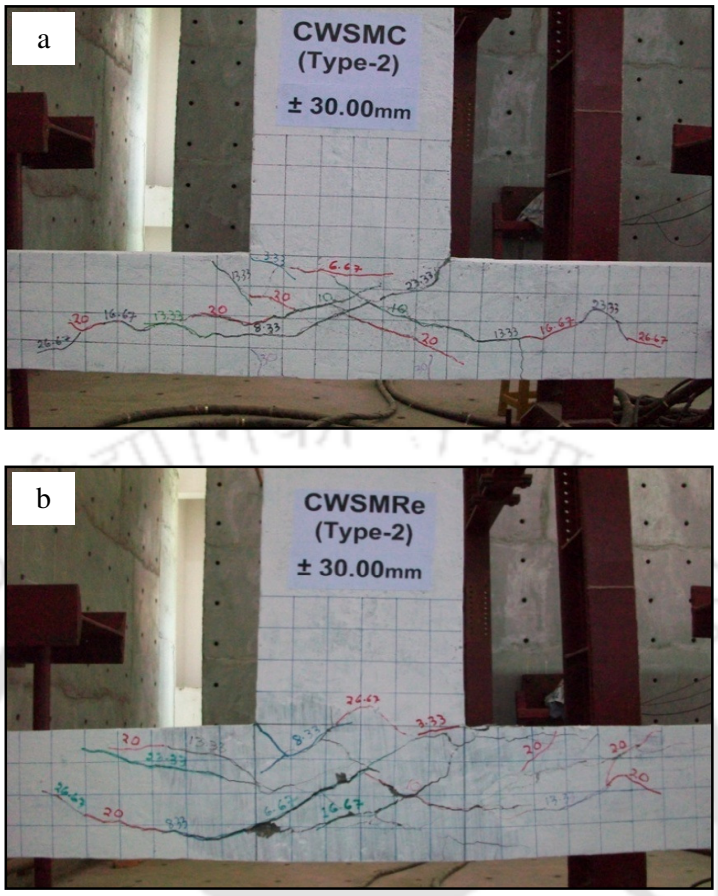

Fig. 5.11 CWSM specimens at the end of test under loading type-2:
(a) Control and (b) Rehabilitated

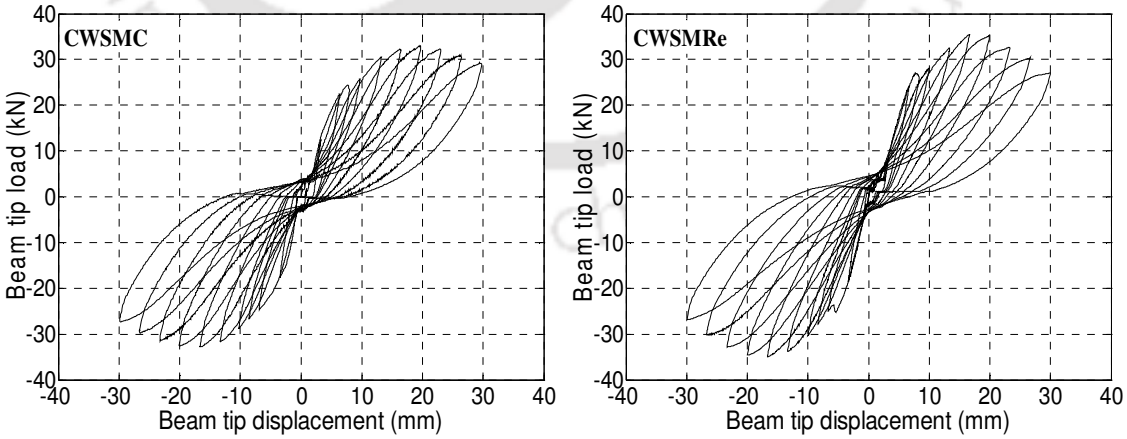

Fig.5.12 Hysteretic response of CWSM specimens subjected to loading type-2

5.4 TESTING OF SMALL SIZE CONNECTIONS

A servo hydraulic dynamic actuator of capacity ±100 kN and having a maximum displacement range of ±125 mm was used to generate the fluctuating displacement. Loading characteristics and displacement histories (type-1 and type-2) applied to these specimens were similar to those applied to the small size specimens with beam weak in flexure and shear. The experiment was stopped when the percentage reduction in load carrying capacity was of similar order as that in the case of CWS large and medium size specimens.

5.4.1 Behaviour of connections under loading type-1

View of control and rehabilitated specimens during initial stages of loading are shown in Fig. 5.13. The first visible crack was observed in the beam-column joint interface for CWSSC specimen and at the joint region for CWSSRe specimen at a displacement amplitude of ± 3.33 mm. In subsequent loading cycle, more cracks started appearing in the joint region in both control and rehabilitated specimens. The behaviour of specimens at the end of testing is shown in Fig. 5.14. The hysteretic responses obtained by plotting the test data are shown in Fig. 5.15. Control specimen attained the maximum load of 8.046 kN in push direction and 9.224 kN in pull direction at 19^{th} cycle at the same displacement of ± 8.33 mm. Slightly higher load of 9.50 kN in push and 10.29 kN in pull direction were attained by the rehabilitated specimen at 16^{th} cycle at the same displacement of ± 6.67 mm. Rehabilitated specimen suffered more damage at the joint region as compared to control specimen. Spalling of concrete at the joint region started at a displacement amplitude of ± 15 mm for control specimen. Developed cracks from the joint region started propagating towards the column region on further increase in amplitude of displacement. The experiment for control specimen was stopped at a

displacement of ± 18.33 mm by taking note of the percentage degradation in load carrying capacity. Early spalling of concrete at the joint region were observed for rehabilitated specimen at a displacement of ± 13.33 mm. Developed cracks from the joint region extended toward the weakest shear zone on both sides of the column region. More spalling of concrete at the joint region was observed at a displacement of ± 15 mm. The shear reinforcement provided in column started to fail causing a wide crack of about 5 mm along the column. This led to the decline in the load carrying capacity to about 64 % and finally the test for rehabilitated specimen was stopped at a displacement of ± 18.33 mm. It was noted that in both control and rehabilitated specimens, no crack were seen in the beam region till the experiment was stopped. The ultimate load carrying capacity of CWSSC and CWSSRe specimens were found to be 8.635 kN and 9.895 kN respectively.

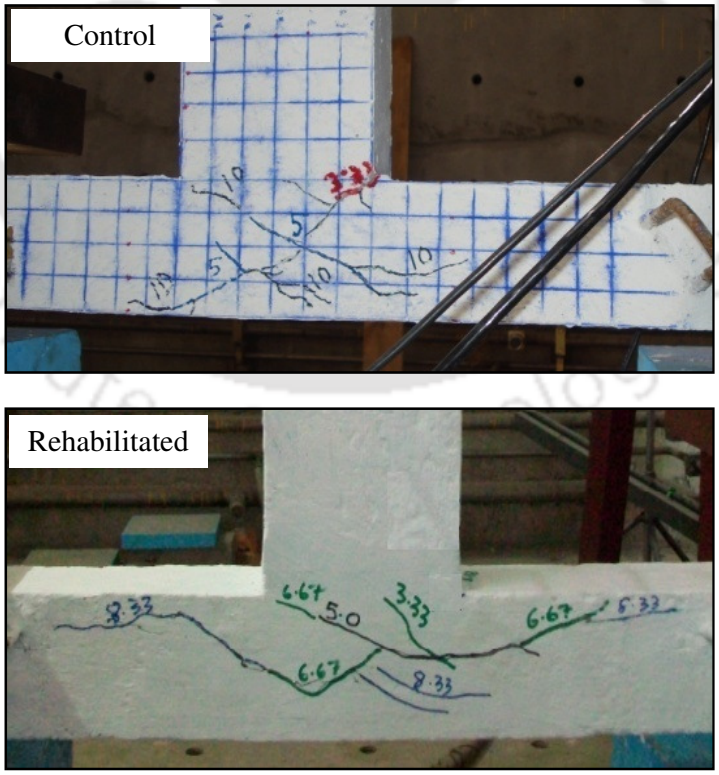

Fig. 5.13 Appearance of cracks for CWSS specimens under loading type-1

corresponding to peak load

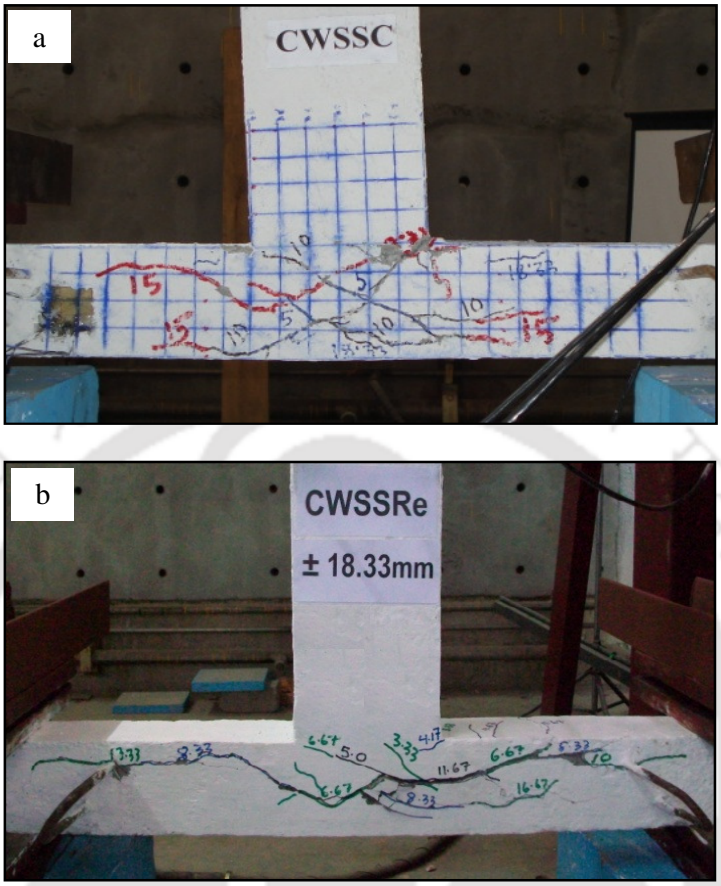

Fig. 5.14 CWSS specimens at the end of test under loading type-1:
(a) Control and (b) Rehabilitated

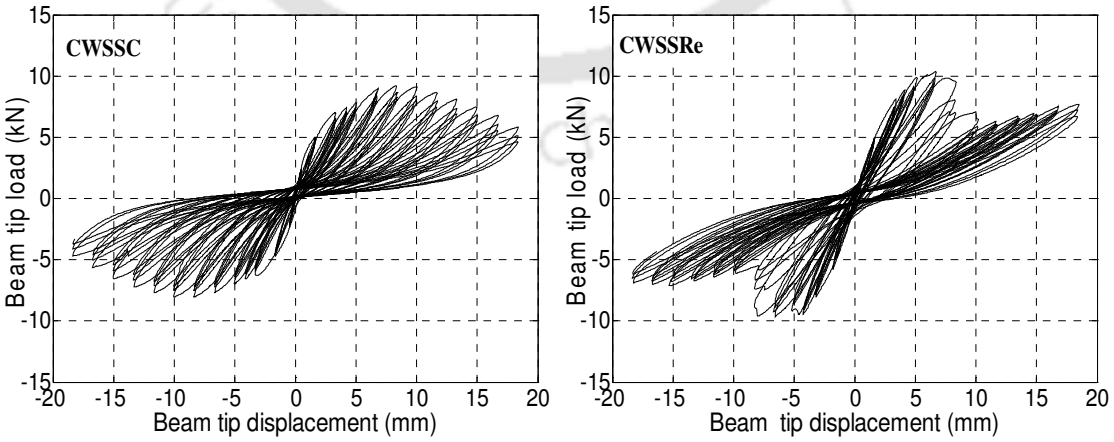

Fig. 5.15 Hysteretic response of CWSS specimens subjected to loading type-1

5.4.2 Behaviour of connections under loading type-2

Appearance of cracks during initial stages of loading and the condition of the specimens at the end of the test are shown in Fig. 5.16 and Fig. 5.17 respectively. The first visible crack appeared in the beam-column junctions at a displacement of $\pm$3.33 mm for control specimen and at $\pm$4.17 mm for rehabilitated specimen. More cracks grew at the joint region and gradually started propagating towards the column region on further increase in displacement (Fig. 5.16). The hysteretic responses obtained by plotting the test data are shown in Fig. 5.18. Control specimen attained the maximum load of 9.89 kN in push direction at 9^{th} cycle at a displacement of 11.67 mm and 7.89 kN in pull direction at 8^{th} cycle at a displacement of 10 mm. Slightly higher load of 10.30 kN in push and 8.53 kN in pull directions were attained by the rehabilitated specimen at the same displacement amplitude as that of control specimen. The behaviour of the specimens at a stage when specimens attained the maximum capacity is shown in Fig. 5.16. At this stage, the crack for a rehabilitated specimen had already propagated towards the weakest shear zone on the column region. However, cracks for control specimen were concentrated at the joint region with only fewer cracks gradually propagating toward column region. A minor spalling of concrete cover at the joint region and joint edge were observed for the control specimen when the peak load carrying capacity degraded by about 60 %. The experiment for control specimen was stopped at a displacement of $\pm$ 18.33 mm. The ultimate load carrying capacity of BWSSC specimen was found to be 8.889 kN. Cracks in the column region for rehabilitated specimen got widened on further increase in displacement. At a displacement of $\pm$ 18.33 mm, crack extended up to the first lateral tie away from the joint region located in the column. The experiment for rehabilitated specimen was stopped at a displacement of $\pm$ 18.33 mm. The ultimate load carrying capacity of BWSSRe specimens was found to be 9.413 kN respectively.

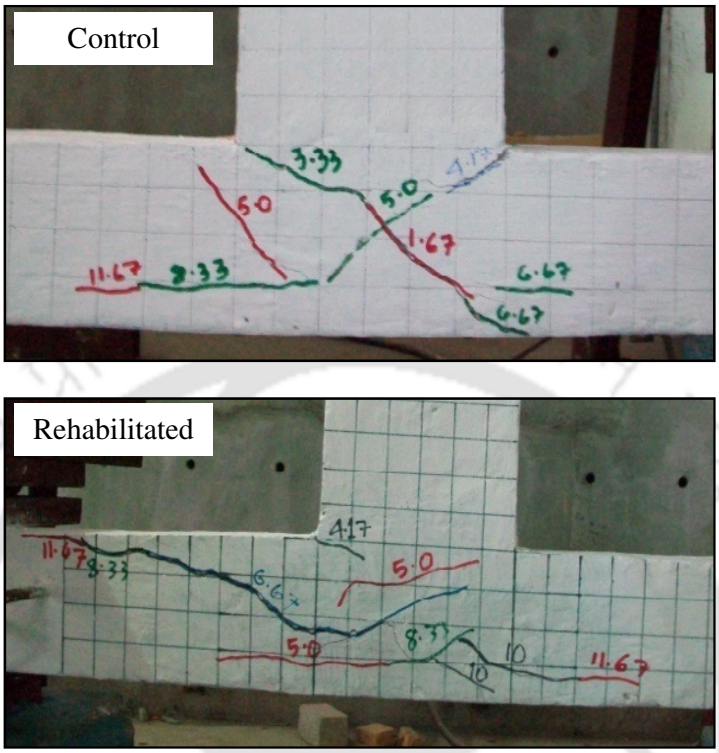

Fig. 5.16 Appearance of cracks for CWSS specimens under loading type-2 corresponding to peak load

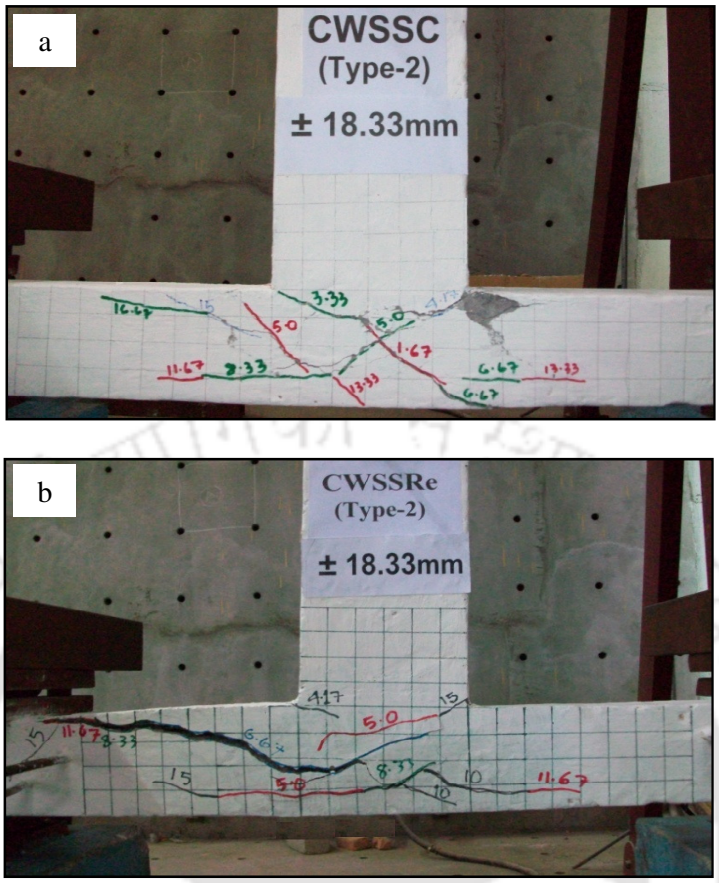

Fig. 5.17 CWSS specimens at the end of test under loading type-2:
(a) Control and (b) Rehabilitated

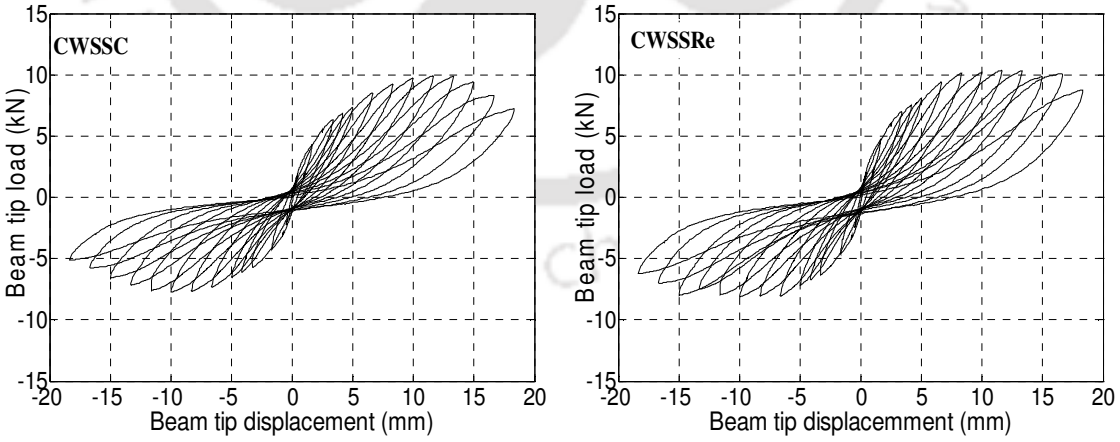

Fig. 5.18 Hysteretic response of CWSS specimens subjected to loading type-2

Table 5.1 Ultimate load carrying capacity of column weak in shear (CWS) specimens

Specimen sizes	Control specimens			Rehabilitated specimens		
	+ve load (kN)	- ve load (kN)	Avg.load (kN)	+ve load (kN)	- ve load (kN)	Avg.load (kN)
	Specimens subjected to loading type-1					
Full	59.17 *20, #16	56.85 *20, #16	58.010	64.19 *20, #16	63.08 *25, #19	64.635
Medium	32.00 *6.67, #7	32.00 *16.67, #19	32.00	37.12 *16.67, #19	34.00 *6.67, #7	35.560
Small	9.23 *8.33, #19	8.046 *8.33, #19	8.635	10.29 *6.77, #16	9.50 *6.67, #16	9.895
	Specimens subjected to loading type-2					
Full	61.09 *25, #7	56.77 *25, #7	58.930	58.83 *25, #7	63.94 *20, #6	61.385
Medium	31.23 *20, #8	31.23 *16.67, #7	31.230	33.38 *16.67, #7	32.30 *16.67, #7	32.840
Small	9.89 *11.67, #9	7.89 *10, #8	8.889	10.30 *11.67, #9	8.53 *10, #8	9.413

Note: * and #: displacement and loading cycle corresponding to its maximum load
-ve: Push direction and +ve: Pull direction

5.5 COMPARISON OF TEST RESULTS OF CONTROL AND REHABILITATED SPECIMENS

The performance of rehabilitation schemes were quantitatively evaluated with reference to their respective control specimen. The hysteretic responses of all the connections have been shown in the previous section. Important parameters related to seismic capacity such as ultimate strength, stiffness degradations, energy dissipation and ductility of the specimens were evaluated from these hysteretic responses.

(a) Response cycles and peak loads

The envelope curves of hysteresis loops for control as well as rehabilitated specimens for all loading types are shown in Fig. 5.19-5.24. These envelopes show slightly higher load carrying capacity in both push and pull directions for rehabilitated specimen. The load carrying capacities summarized in Table 5.1 showed that all damaged specimens could restore their load carrying capacity after rehabilitation. The appropriately chosen repair strategy could retrieve back the lost capacity even for a severely damaged connection. Further, it is also observed that comparable load carrying capacities were attained by the control specimens under loading type-1 and type-2. Thus, it showed that the characteristic of applied loading did not significantly influence the ultimate load carrying capacity of these specimens.

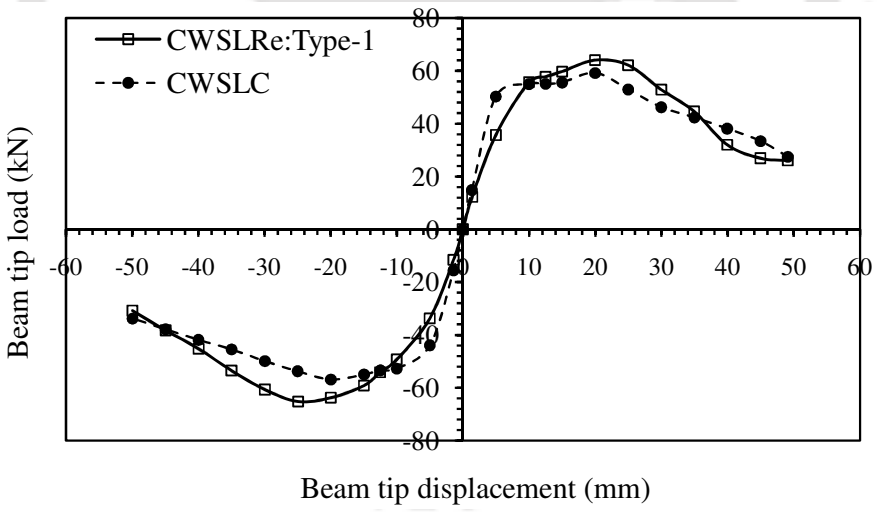

Fig. 5.19 Envelope curves of CWSL specimens under loading type-1

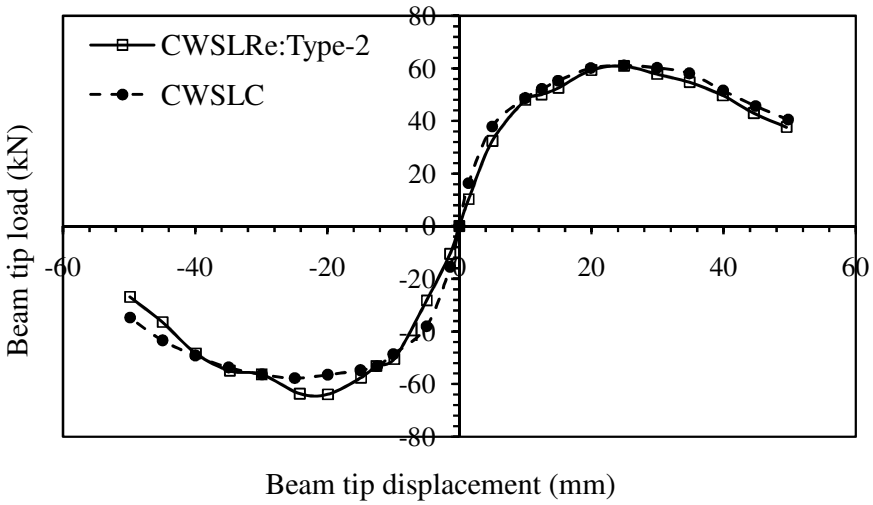

Fig. 5.20 Envelope curves of CWSL specimens under loading type-2

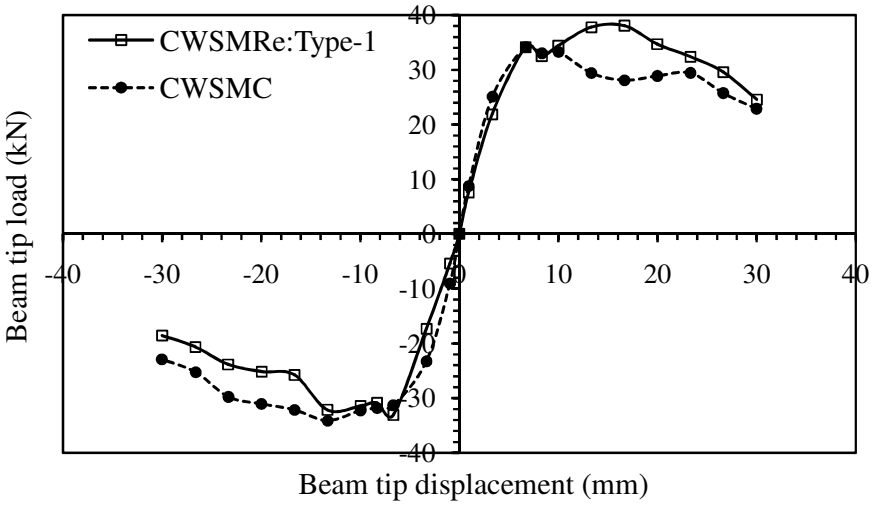

Fig. 5.21 Envelope curves of CWSM specimens under loading type-1

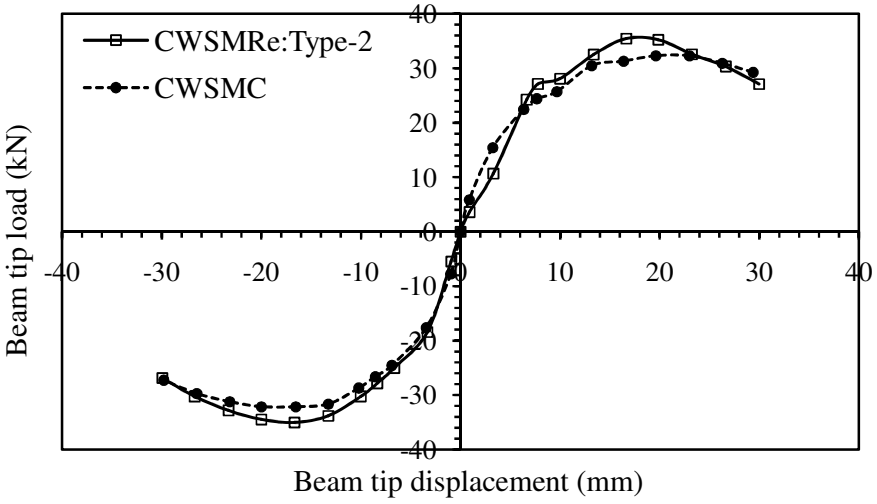

Fig. 5.22 Envelope curves of CWSM specimens under loading type-2

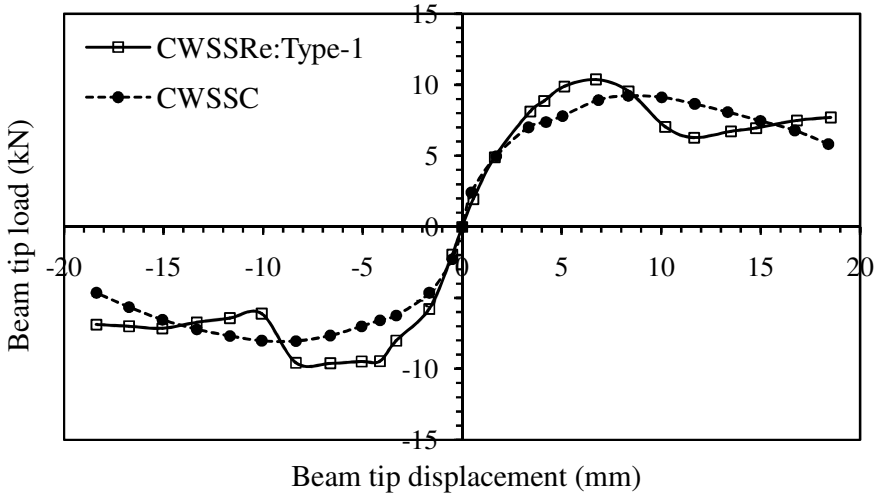

Fig. 5.23 Envelope curves of CWSS specimens under loading type-1

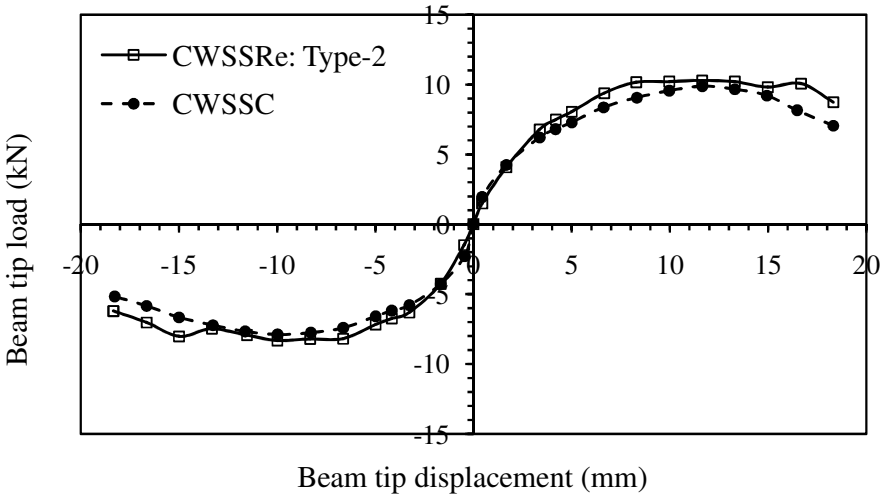

Fig. 5.24 Envelope curves of CWSS specimens under loading type-2

(b) Stiffness degradation

Similar to the earlier cases, the effectiveness of a rehabilitation techniques in restoring the stiffness of damaged connections were evaluated by comparing stiffness versus drift angle plots for different cases. The plots for all the specimens under loading type-1 and type-2 are shown in Fig. 5.25-5.30. Comparing these curves it can be inferred that irrespective of loading types, the trends of stiffness degradation are quite similar in all cases studied. The stiffness attained by the rehabilitated specimen at the beginning of the test was observed

to be relatively lower. However, a comparable stiffness was observed in both control and rehabilitated specimens at the end of the test. The percent reductions in stiffness in both control as well as rehabilitated specimens were evaluated. Comparing at each drift levels, it has been observed that the degradation rate of the rehabilitated specimens with increase in lateral movement is little lower as compared to those of the corresponding control specimens. This behaviour may be attributed to the ductile properties introduced by the repairing materials. Thus, it can be concluded that all the rehabilitated specimens satisfactorily achieved stiffness level which is well comparable to those respective control specimens.

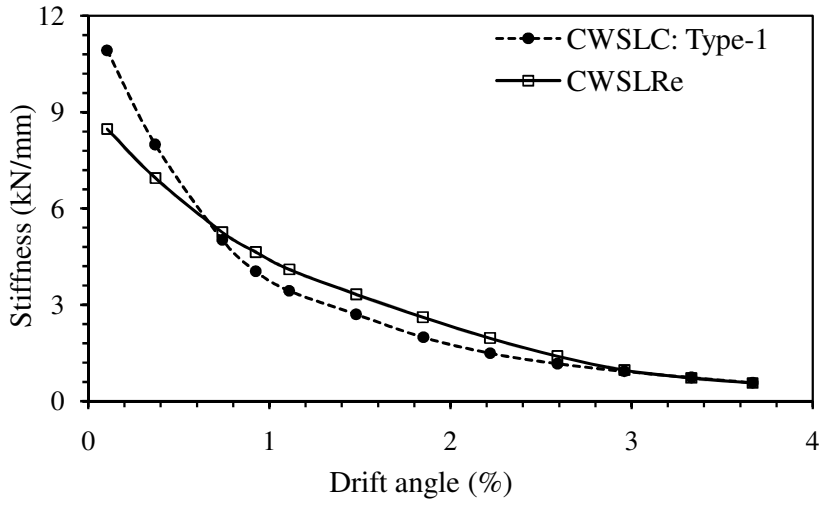

Fig. 5.25 Stiffness versus drift angle of CWSL specimens under loading type-1

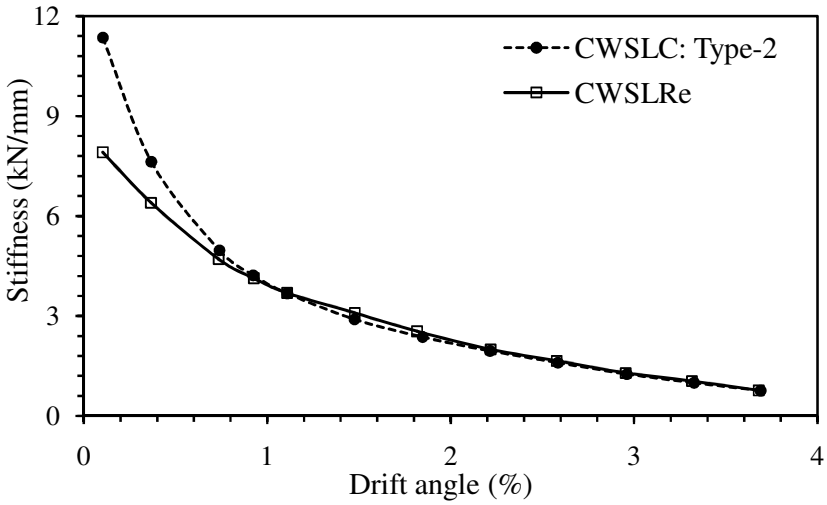

Fig. 5.26 Stiffness versus drift angle of CWSL specimens under loading type-2

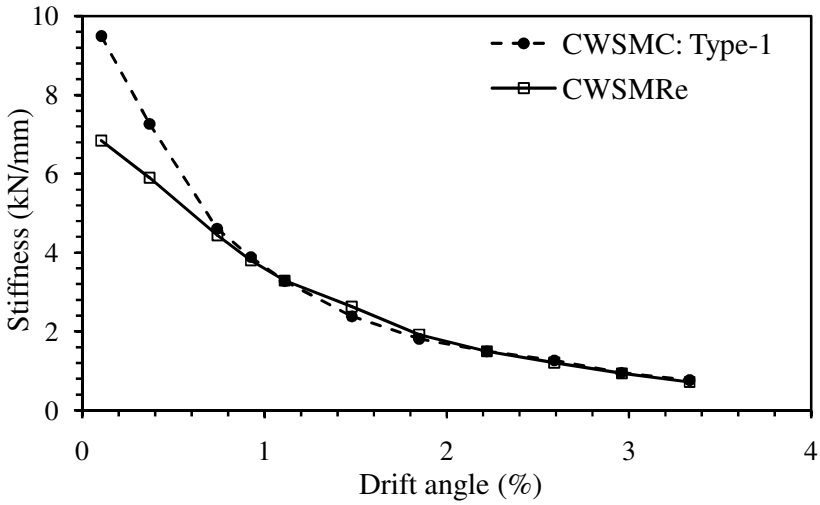

Fig. 5.27 Stiffness versus drift angle of CWSM specimens under loading type-1

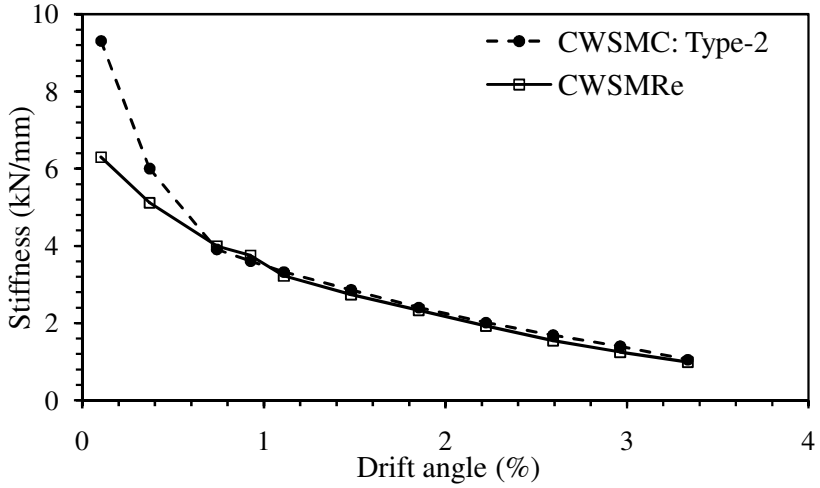

Fig. 5.28 Stiffness versus drift angle of CWSM specimens under loading type-2

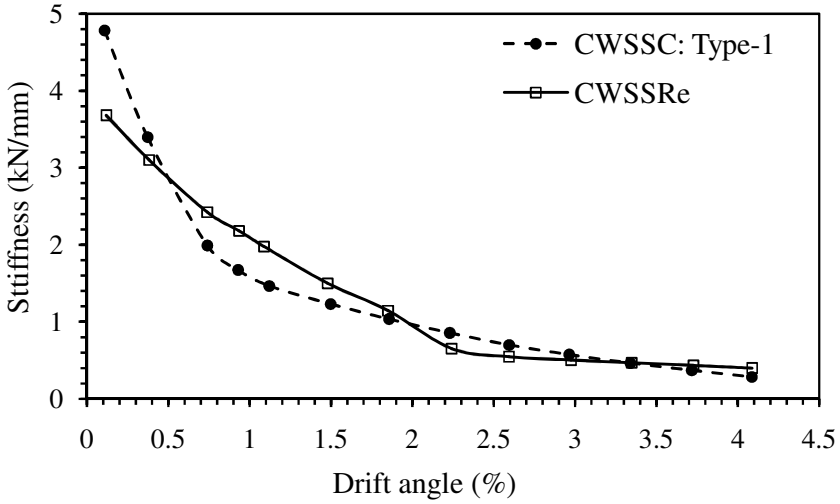

Fig. 5.29 Stiffness versus drift angle of CWSS specimens under loading type-1

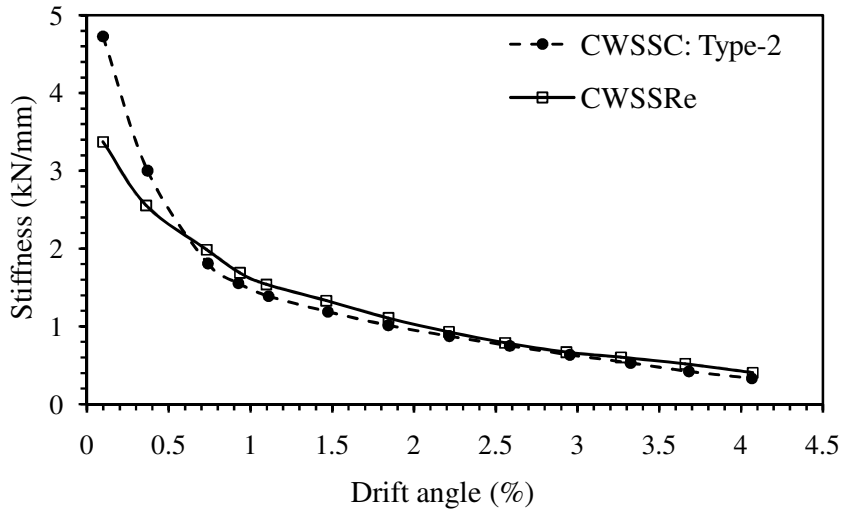

Fig. 5.30 Stiffness versus drift angle of CWSS specimens under loading type-2

(c) Energy dissipation

Fig. 5.31-5.33 show the plots of cumulative energy dissipation with respect to drift angle for control and rehabilitated specimens. It is observed from these plots that cumulative energy dissipated by the rehabilitated specimens are relatively lower during the initial stages of loading. However, in subsequent loading cycles, the energy dissipated by the rehabilitated specimens was observed to be at par with those of the corresponding control

specimens. Corresponding to the drift level upto which the control specimens were tested, the energy dissipated by the rehabilitated specimens in both the loading cases are marginally higher than the corresponding control specimens (Table 5.2). Thus, it may be observed that by adopting an appropriate rehabilitation methodology, even a severely damaged structure would be able to successfully restore the energy dissipation capacity.

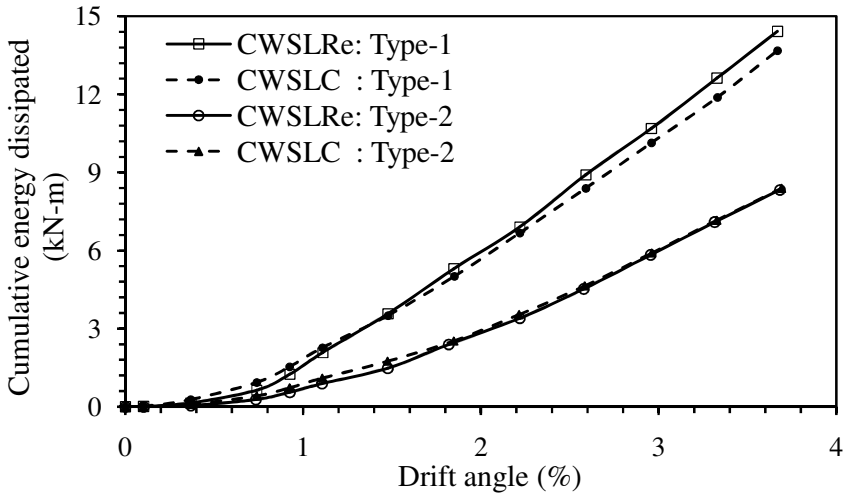

Fig. 5.31 Cumulative energy dissipation for CWSL specimens

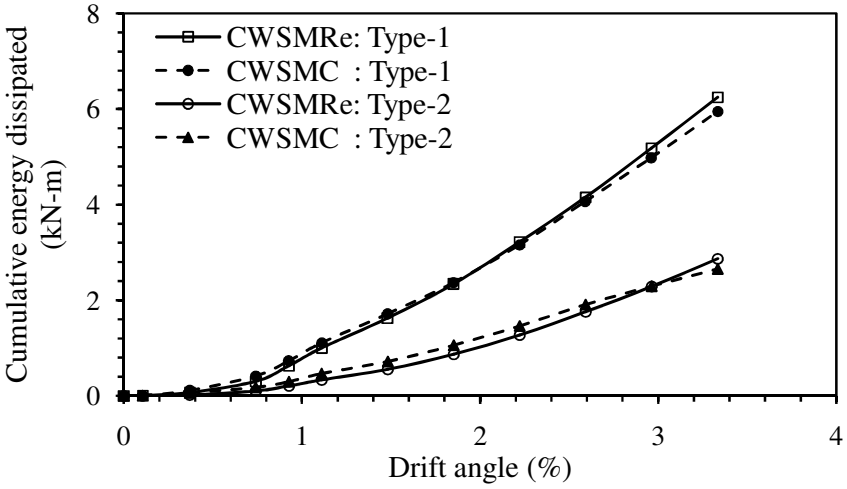

Fig. 5.32 Cumulative energy dissipation for CWSM specimens

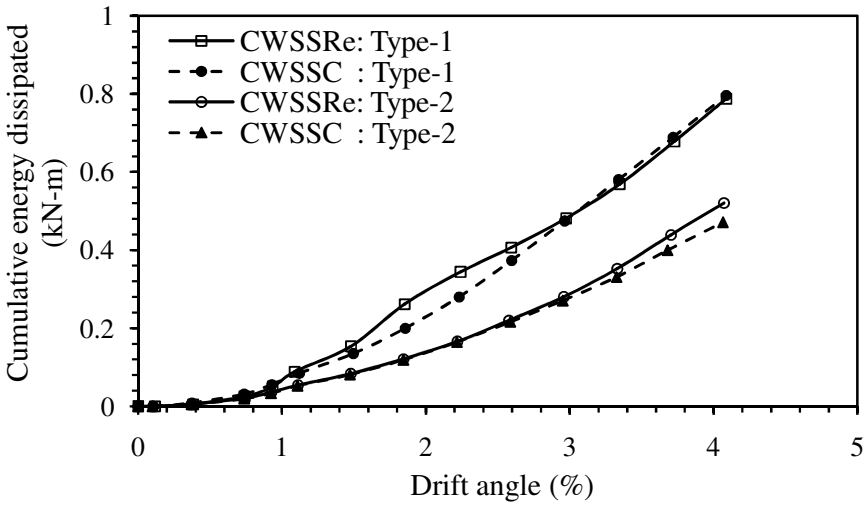

Fig. 5.33 Cumulative energy dissipation for CWSS specimens

Table 5.2 Energy dissipation (kN-m) for column weak in shear (CWS) specimens

Specimens sizes	Loading type-1		Loading type-2	
	Control	Rehabilitated	Control	Rehabilitated
Large	13.683	14.110	8.388	8.495
Medium	5.950	6.265	2.652	2.870
Small	0.645	0.688	0.417	0.465

(d) Displacement ductility

Table 5.3 presents the displacement ductility attained by the specimen corresponding to both loading type-1 and type-2. Control specimens in both loading types achieved almost equivalent ductility values. With the exception of small size rehabilitated specimen under loading type-1, all rehabilitated specimen also attained the ductility values equal or marginally higher than those of the corresponding control specimens. Small size rehabilitated specimen under loading type-1 could not however achieve the ductility

values as good as the control specimens. The early degradation of load carrying capacity could be the reason for this behaviour.

Table 5.3 Displacement ductility of column weak in shear (CWS) specimens

Loading type	Specimens	Control			Rehabilitated		
		Δ_y	Δ_{20}	Δ_{20}/Δ_y	Δ_y	Δ_{20}	Δ_{20}/Δ_y
Type-1	Large	5	31	6.2	5	34	6.8
	Medium	3.75	26	6.93	3.75	27	7.2
	Small	2.25	17	7.56	2.25	10.5	4.67
Type-2	Large	6	41	6.31	6	41	6.31
	Medium	4.5	30	6.67	4.5	30	6.67
	Small	2.5	17	6.8	2.5	18	7.2

Δ_y and Δ_{20} : Displacement at first yield and at 20% drop of peak load (mm)

5.6 INVESTIGATION FOR THE EXISTENCE OF SIZE EFFECT

To explore the existence of size effect, the results obtained from testing of the specimens were analyzed and bi-logarithmic plots were drawn. Various parameters, which are of practical relevance were also considered and the possible existence of size effects were investigated.

5.6.1 Bi-logarithmic Plot

The specimens failed in shear and hence ultimate shear stress was calculated. The calculation of shear stress is shown in Appendix-*B*. The calculated shear stress and other parameters necessary to carry out regression analysis and to draw bi-logarithmic plot for both control as well as rehabilitated specimens are furnished in Table 5.4. Values of the constants B and D_0 for control specimens as determined from the regression analysis were

0.359 and 138.48, while the same for rehabilitated specimens were 0.419 and 107.36 respectively. A typical regression plot for control specimens is shown in Fig. 5.34. Finally, the bi-logarithmic plot for control and rehabilitated specimens were drawn as shown in Fig. 5.35 and Fig. 5.36 respectively. These graphs show the presence of size effect and support Bažant's size effect law similar to earlier cases.

Table 5.4 Parameters of CWS specimens for bi-logarithmic plotting

Specimen	Specimen sizes	Bending stress, σ_{N_U} (N/mm^2)	Depth of specimen , D (mm)	$\left(\frac{f_t'}{\sigma_{N_U}}\right)^2$	Log (D/Do)	$Log\left(\frac{\sigma_{N_U}}{Bf_t'}\right)$
Control	Large	0.4944	300	25.65108	0.33573	-0.25964
		0.5022	300	24.85642	0.33573	-0.25281
	Medium	0.5753	200	18.94540	0.15964	-0.19384
		0.5988	200	17.48245	0.15964	-0.17639
	Small	0.6623	100	14.29228	-0.14138	-0.13264
		0.6818	100	13.48724	-0.14138	-0.12005
Rehabilitated	Large	0.5423	300	21.31667	0.44627	-0.28657
		0.5231	300	22.90948	0.44627	-0.30222
	Medium	0.6435	200	15.13918	0.27018	-0.21226
		0.6297	200	15.81030	0.27018	-0.22168
	Small	0.7589	100	10.88415	-0.03084	-0.14061
		0.7220	100	12.02736	-0.03084	-0.16229

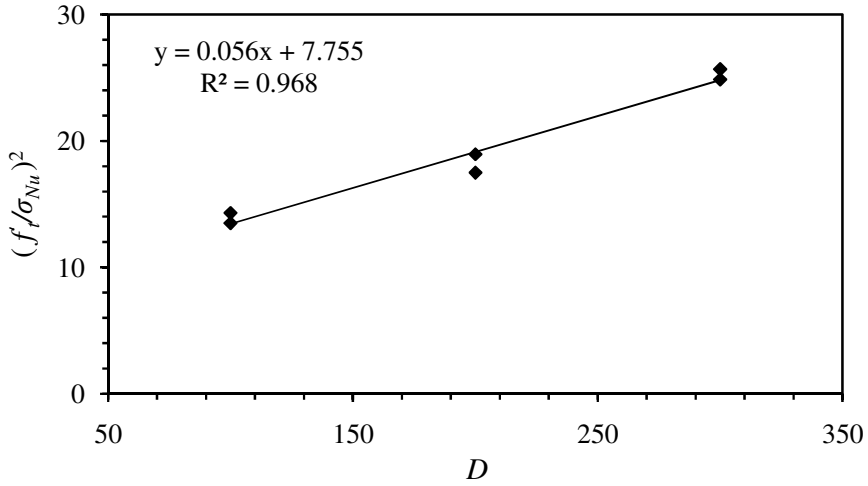

Fig. 5.34 Typical regression plot for Control CWS specimens

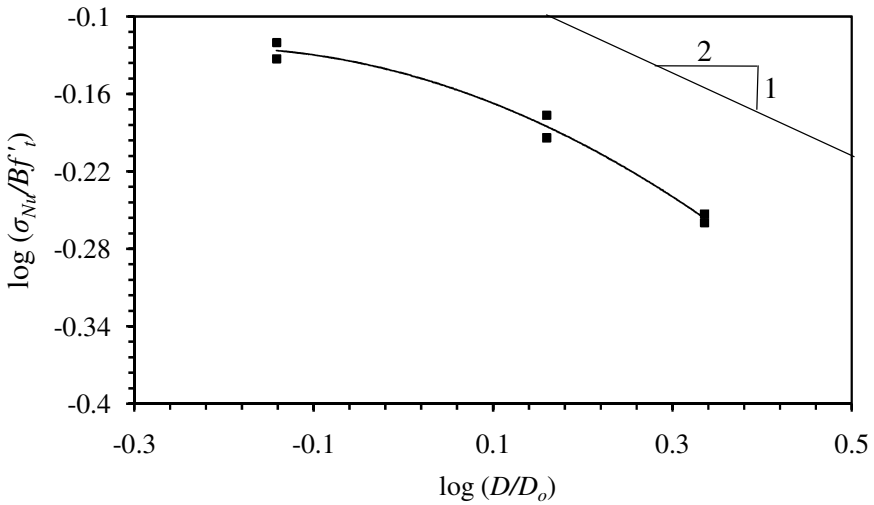

Fig. 5.35 Bi-logarithmic plot for control CWS specimens

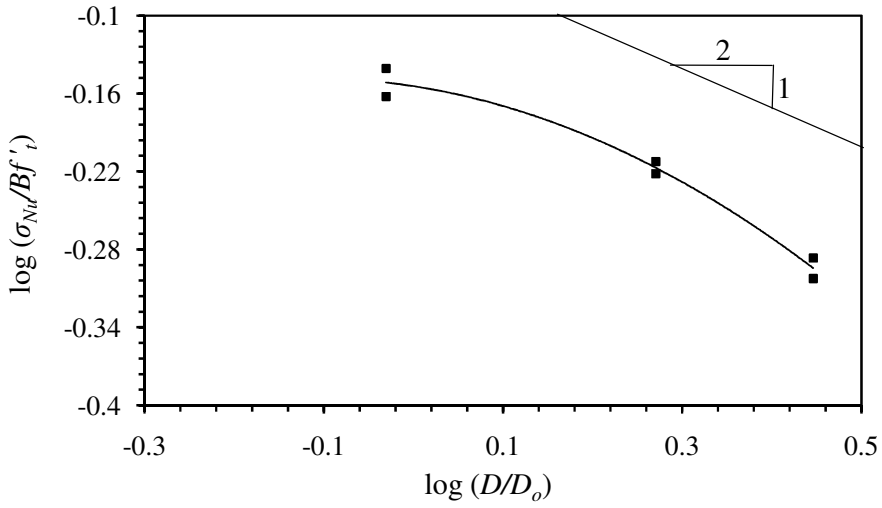

Fig. 5.36 Bi-logarithmic plot for rehabilitated CWS specimens

5.6.2 Size effect on energy dissipated per unit volume of D-region

The cumulative energy dissipated per unit volume of the D-region (e_N) in a connection for all the specimens were plotted with respect to drift angle. Fig. 5.37 show the plot for specimens with loading type-1, while Fig. 5.38 show the same for specimens with loading type-2. It can be clearly observed that in both the loading cases and for both kinds of specimens (control and rehabilitated), the cumulative energy dissipated per unit volume of the D-region is the highest for the smallest specimen and vice versa. Thus, it can be concluded that the cumulative energy dissipated per unit volume increases as the size of the specimen decreases, which is a clear indication of size effect.

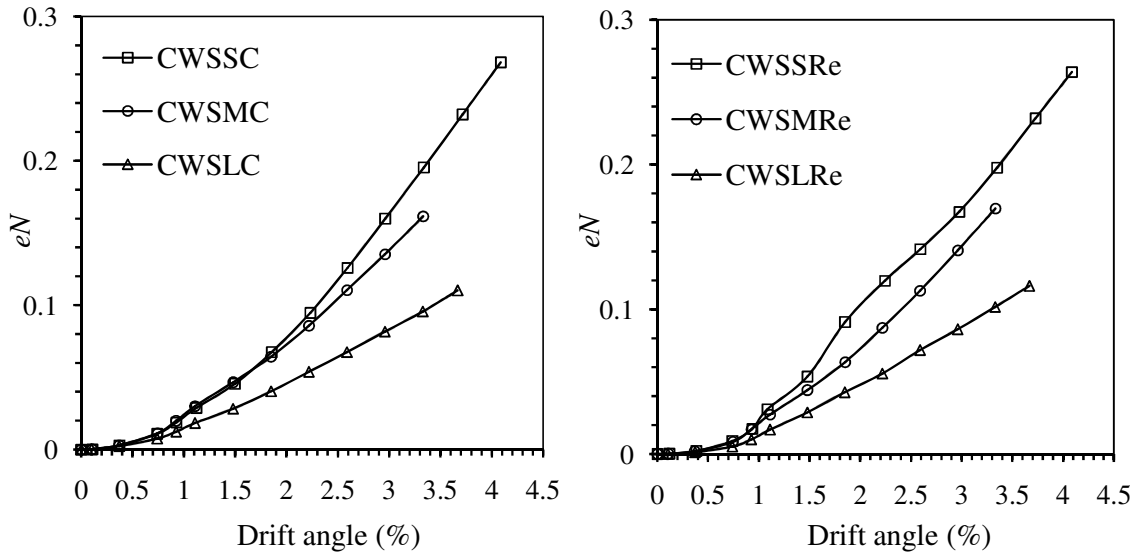

Fig. 5.37 Cumulative energy dissipated per unit volume of D-region for CWSC and CWSRe specimens under loading type-1

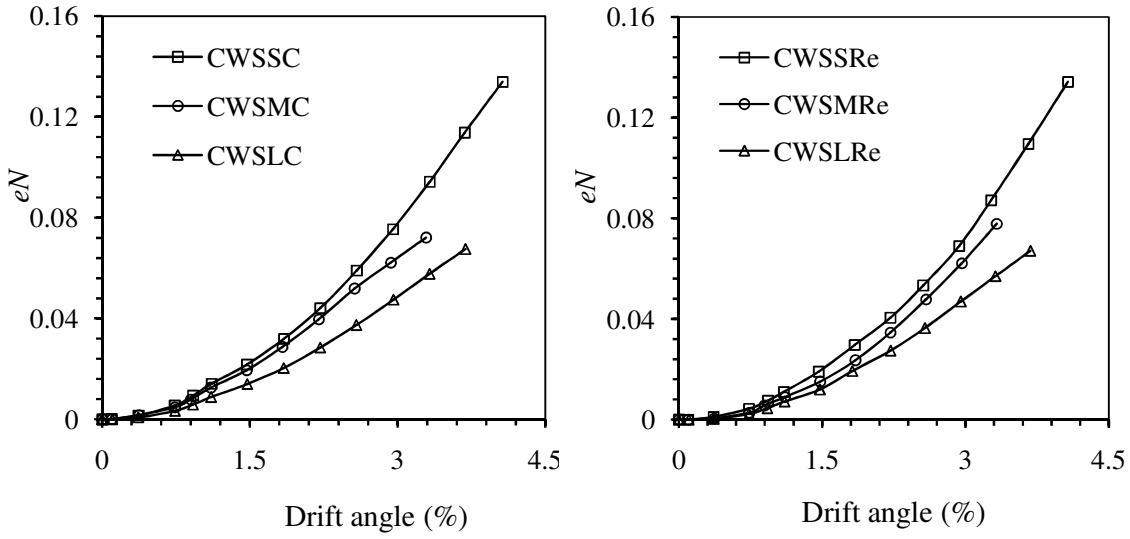

Fig. 5.38 Cumulative energy dissipated per unit volume of D-region for CWSC and CWSRe specimens under loading type-2

5.6.3 Size effect on stress variation with relative deflection

The maximum value of the load corresponding to each displacement cycle was used to calculate the shear stresses. The relative deflection for different scaled models were calculated as the ratio of actual deflection to the scale of the model. The variations of shears stress with relative deflection have been plotted for control and the rehabilitated specimens under loading type-1 in Fig. 5.39 while the same with loading type-2 are shown in Fig. 5.40. The plot for small specimen shows highest stresses at every level of relative deflection while least for large specimen in both the cases. Thus it substantiates the size effect principle.

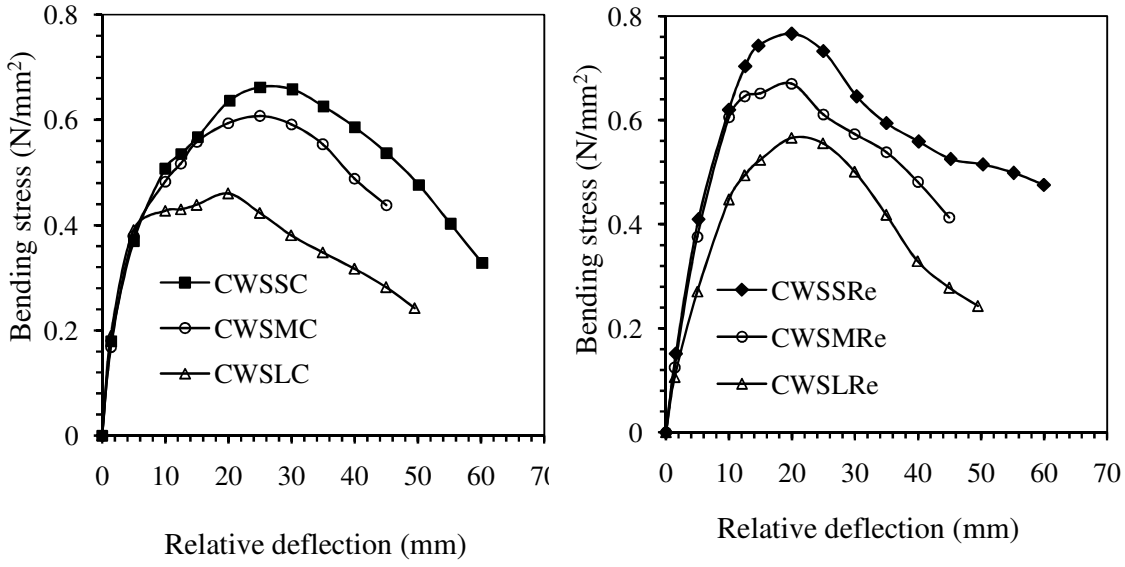

Fig. 5.39 Bending stress versus relative deflection for CWS specimens under loading type-1

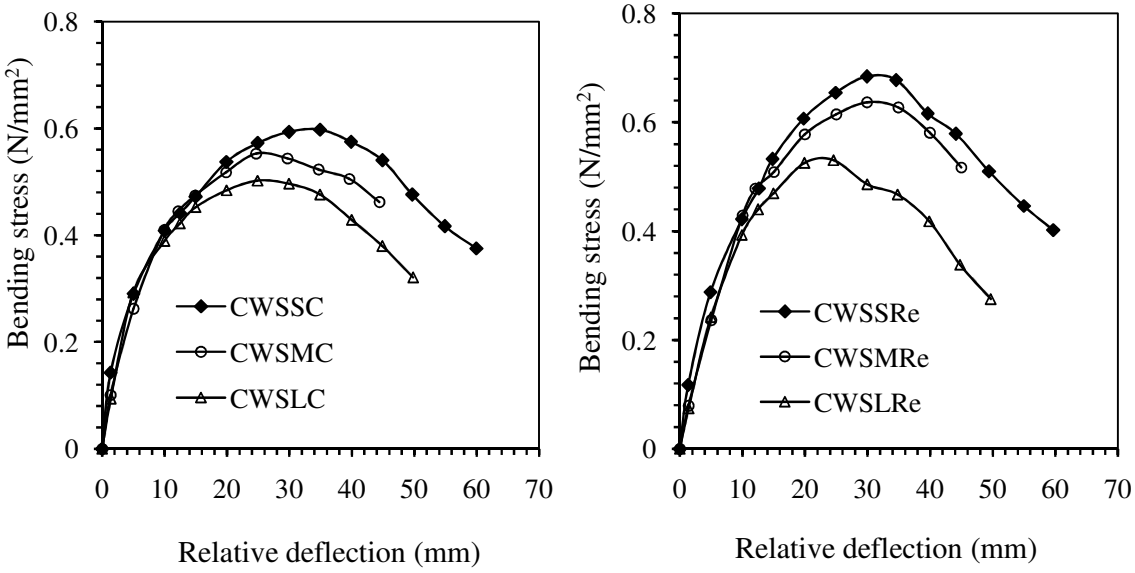

Fig. 5.40 Bending stress versus relative deflection for CWS specimens under loading type-2

5.7 CONCLUDING REMARKS

In this chapter, data for experimental investigation of beam-column connections with column weak in shear subjected to different loading characteristic were presented. Various parameters related to seismic capacity were analyzed and compared. The analysis of results revealed that the rehabilitated connections exhibited equal or marginally better performance as compared to the corresponding control specimens. The appropriately chosen repair strategy could retrieve the lost capacity back even for a badly damaged connections. It is also observed that the characteristic of applied loading does not significantly influence the ultimate load carrying capacity of the specimens, though the extents of damages were observed to be different under different loading types. As before, bi-logarithmic plot for both control and rehabilitated specimens followed the size effect law as proposed by Bažant [1984]. Further, it was also noted that the cumulative energy dissipated per unit volume of the D-region at every drift angle for the smallest specimen was maximum and the value decreased as the specimen size was increased, which is an indication for existence of size effect. The variation of shear stress with respect to relative deflection also supported the size effect principle.

CHAPTER 6

RC BEAM-COLUMN CONNECTIONS UNDER CYCLIC DISPLACEMENT OF HIGHER FREQUENCY

6.1 INTRODUCTION

This chapter describes the finding of experimental investigation and interpretation of experimental results of exterior beam-column connections subjected to cyclic displacement of higher frequency. Two third size specimens of three different deficiencies as described in Sec 2.4 of Chapter 2 were considered for this study. Control damaged specimens were further rehabilitated with either repair method-1or method-2 depending on the degree of damages. Data recorded during testing were used to evaluate many important parameters related to seismic capacity of these connections. Effectiveness of the applied repair techniques were assessed based on the comparison of the seismic performance of rehabilitated specimens with those of the control specimens. Test results of specimens subjected to cyclic displacement of higher frequency (type-3) were compared to those obtained from specimens subjected to cyclic displacement of lower frequency (type-2) in terms of various parameters related to seismic capacity.

6.2 SIGNIFICANCE OF THE STUDY

Most of the test conducted for RC beam-column connections are of quasi-static nature. Obviously, it is advantageous because the quasi-static cyclic testing allows a careful monitoring of the specimen behaviour during the test and the strain-rate effects do not affect the material behaviour. However, these frequencies are substantially lower than those corresponding to the actual seismic excitation. Very few studies on high frequency

testing of RC beam-column connections may be seen in the literature [Agbabian *et al*., (1994) and Dhakal *et al*., (2005)]. Aiming to narrow this gap, the study was targeted to explore the performances of RC exterior beam-column connections subjected to excitations of higher frequency. This study also becomes important for moderate and low seismicity region, where some structures may not have been designed for lateral loads and high frequency excitations such as severe earthquake, explosion and construction induced vibrations may pose more threat than the low-frequency seismic actions.

6.3 TESTING OF RC BEAM-COLUMN CONNECTIONS

The nature and extent of damage in a structure during any event like earthquake depends on the characteristic of loading. Thus, during experimental investigation, number of cycle in the displacement time history, frequency of excitation and the level of displacement amplitude are some of the parameters which were varied. In the experimental studies presented here the frequency of cyclic displacement was kept as 1.0 Hz, which is four times higher than loading type-1 and type-2 considered earlier. The displacement amplitudes were gradually increased with every cycle of displacement with one cycle being maintained for each displacement level. The amplitude of displacement was taken same as that of other loading types (type-1 and type-2) for two third size specimens. The displacement history as shown in Fig. 2.14 (c) of Sec. 2.5.2 were applied to these specimens using a servo hydraulic dynamic actuator of loading capacity ± 250 kN and having a maximum displacement range of ± 125 mm. It may be noted that the crack initiation and propagation could not be observed as the high frequency test was carried out in an uninterrupted manner. The damage inspection was performed at the completion of the testing. The displacement limits till the completion of the experiment for all the specimens were kept same as those for testing under loading type-1and type-2. This was

done for facilitating comparative understanding of the behaviour of these specimens subjected to loading with different loading characteristics. The load carrying capacities attained by different deficient specimens considered in this study have been presented in Table 6.1.

6.3.1 Behaviour of beam weak in flexure connections

A close view of the damaged specimen at the end of testing is shown in Fig. 6.1. Generally, hairline cracks were seen during the initial stages of loading both at the joint region and at the beam-column joint interface. In subsequent loading cycles, major damages were localized at the beam-column joint interface, where crushing of concrete were observed in both control as well as rehabilitated specimens. A wide crack of about 5 mm was observed at the joint interface in both control and rehabilitated specimens. The hysteretic responses obtained by plotting the test data are presented in Fig. 6.2. It is observed from the hysteresis loop that control specimen attained the maximum load of 42.48 kN and 39.03 kN at displacement of 26.67 mm and 20 mm in push and pull directions respectively. Slightly higher loads were attained by the rehabilitated specimens with a maximum of 42.43 kN and 39.86 kN at displacement of 33.33 mm and 30 mm in push and pull directions respectively. The ultimate load carrying capacity for BWFMC and BWFMRe specimens were found to be 40.755 kN and 41.145 kN respectively.

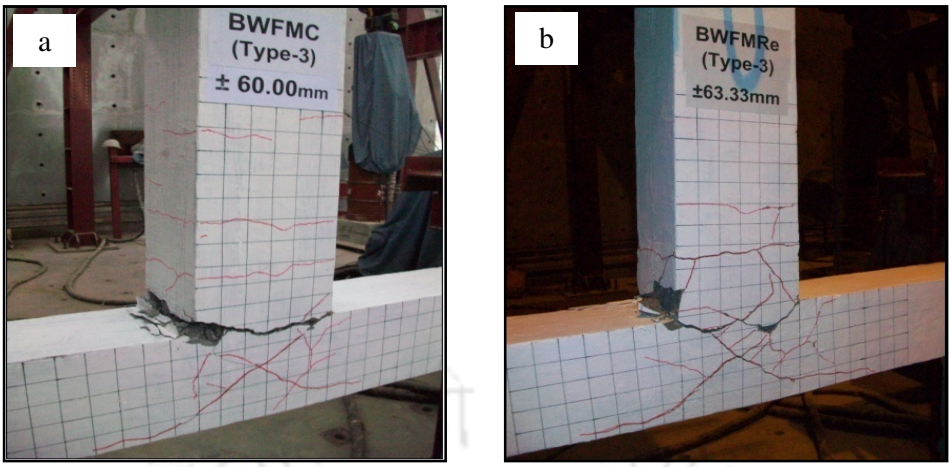

Fig. 6.1 BWF specimens at the end of test under loading type-3:
(a) Control and (b) Rehabilitated

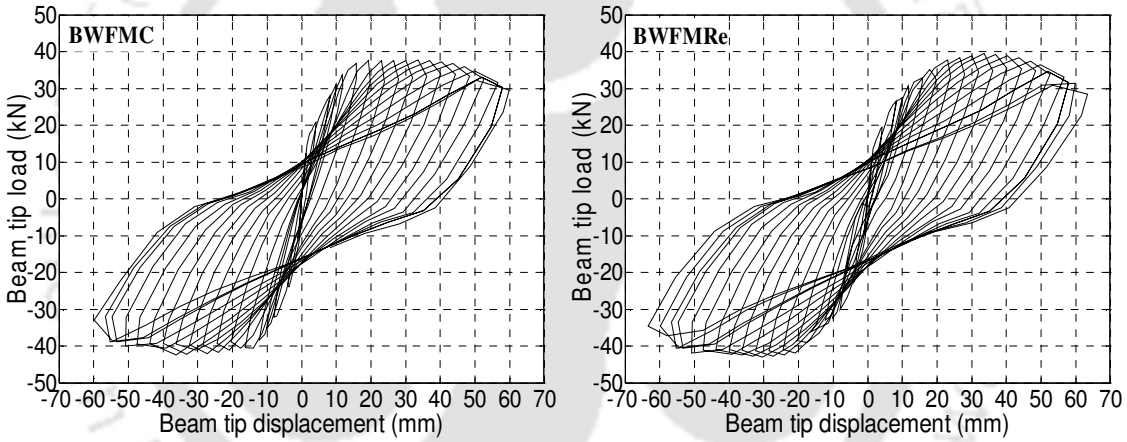

Fig. 6.2 Hysteretic response of BWF specimens subjected to loading type-3

6.3.2 Behaviour of beam weak in shear connections

The conditions of the specimens at the end of testing are shown in Fig. 6.3. At low amplitude, minor cracks were observed near the joint interface and the joint region for both the specimens. However, in subsequent loading cycles, the damages were observed to be concentrated at the beam adjoining the joint interface. Both the control and rehabilitated specimens failed at the weakest shear zone in the beam part without inducing any major damage to the relatively stronger joint region. Severe crushing of concrete and

buckling of main reinforcements were observed. Buckling of main reinforcing beam bars were due to the absence of shear reinforcement. Rehabilitated specimen was more severely damaged as compared to the control specimen. The hysteretic responses obtained by plotting the test data are shown in Fig. 6.4. The maximum load carrying capacities as obtained from these loops are presented in Table 6.1. The loop indicates that rehabilitated specimen showed a rapid degradation after reaching peak load carrying capacity under cyclic displacement of higher frequency. The ultimate load carrying capacity for BWSMC and BWSMRe specimens were found to be 41.07 kN and 41.89 kN respectively.

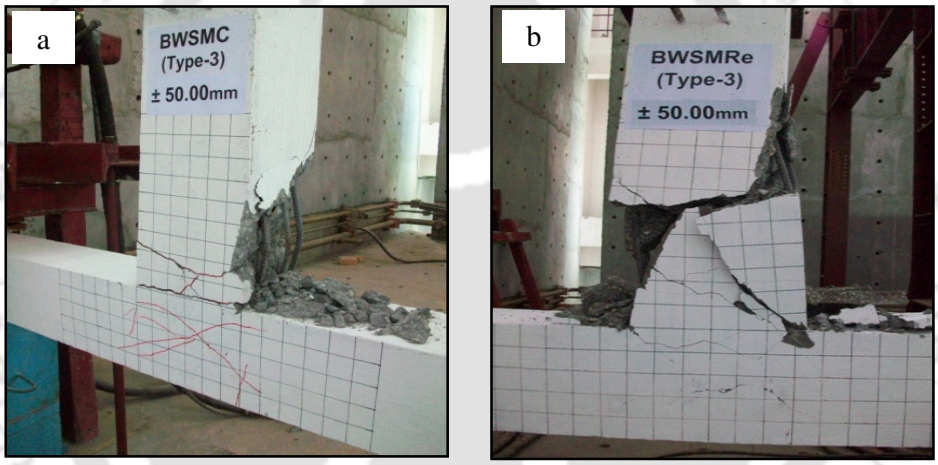

Front view

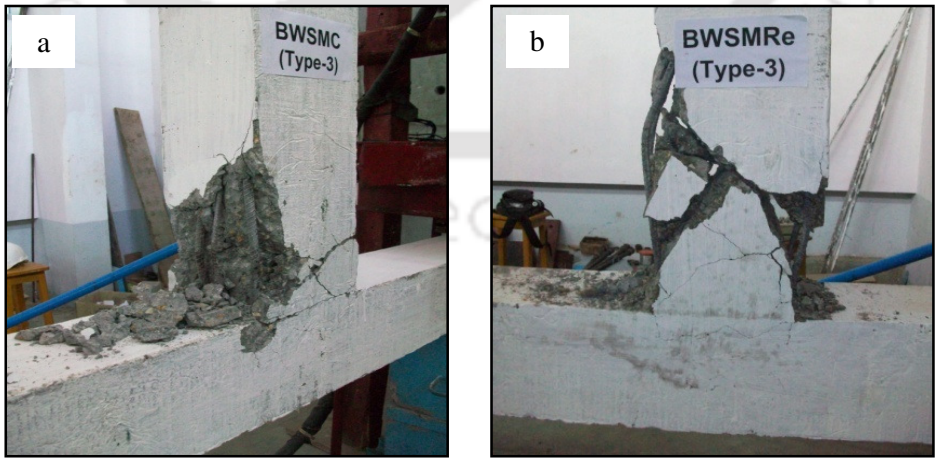

Rear view

Fig. 6.3 BWS specimens at the end of test under loading type-3:
(a) Control and (b) Rehabilitated

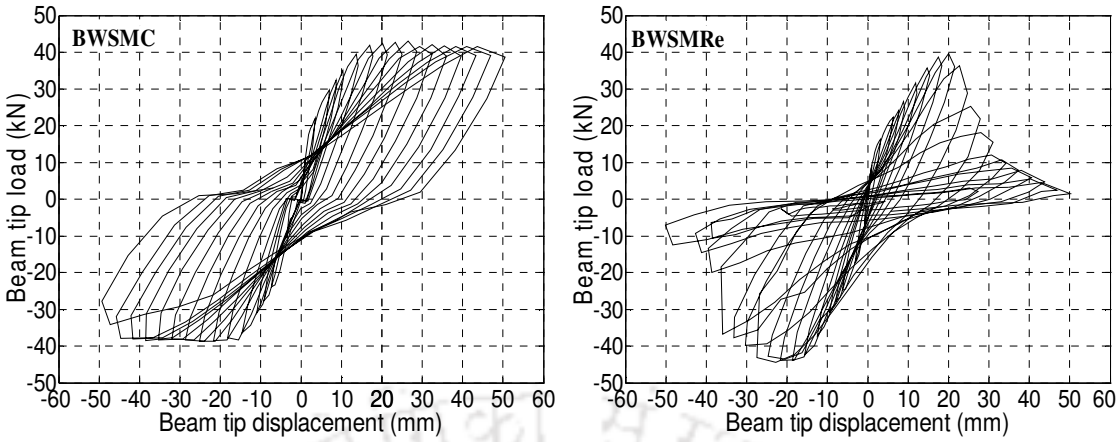

Fig. 6.4 Hysteretic response of BWS specimens subjected to loading type-3

6.3.3 Behaviour of column weak in shear connections

The behaviour of specimens at the end of testing is shown in Fig. 6.5. These figures showed that both control as well as the rehabilitated specimens exhibited a similar failure pattern. Crack initiated from the joint region and then gradually started propagating towards the column region corresponding to a larger displacement amplitude. It was noted in both control and rehabilitated specimens that no crack was observed in the beam region till the experiment was stopped. The hysteretic responses obtained by plotting the test data are shown in Fig. 6.6. The maximum load carrying capacities as obtained from these loops are presented in Table 6.1. A comparable response as that of control specimen was achieved by the rehabilitated specimen. The load carrying capacity as obtained by averaging the push and pull peak load were found to be 35.905 kN and 37.55 kN for control and rehabilitated specimens respectively.

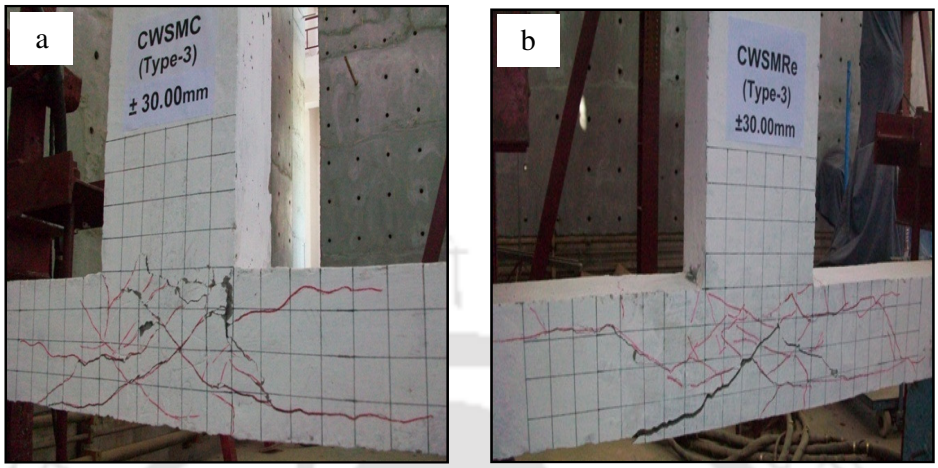

Fig. 6.5 CWS specimens at the end of test under loading type-3:
(a) Control and (b) Rehabilitated

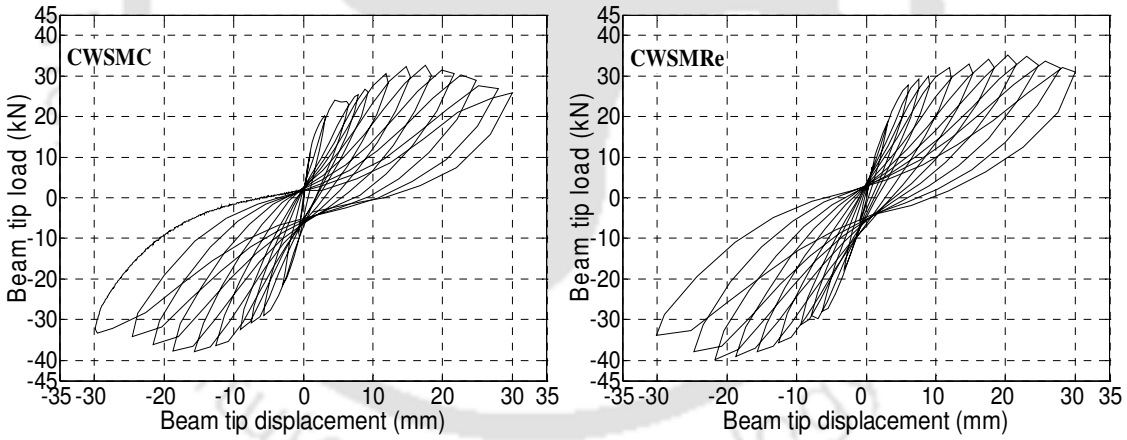

Fig. 6.6 Hysteretic response of CWS specimens subjected to loading type-3

Table 6.1 Ultimate load carrying capacity for connections under loading type-3

Specimens	Control specimens			Rehabilitated specimens		
	+ve load (kN)	- ve load (kN)	Avg.load (kN)	+ve load (kN)	- ve load (kN)	Avg.load (kN)
BWF	39.03 *20, #8	42.48 *26.67,#10	40.759	39.86 *30, #11	42.43 *33.33, #12	41.145
BWS	42.90 *26.67, #10	39.24 *23.33, #9	41.070	39.29 *20, #8	44.49 *23.33, #9	41.890
CWS	33.28 *16.67, #7	38.53 *16.67, #7	35.905	35.20 *20, #8	39.86 *23.33, #9	37.550

Note: * and #: displacement and cycle number corresponding to its maximum load
-ve: Push direction and +ve: Pull direction

6.3.4 Comparison of test results of control and rehabilitated specimens

The hysteretic responses of all the connections have been shown in the previous section. To compare the relative performances of these specimens, parameters related to seismic capacity such as ultimate strength, stiffness degradations, energy dissipation of the specimens were evaluated from these hysteretic responses.

(a) Response cycles and peak loads

The envelope curves of hysteresis loops for control as well as rehabilitated specimens for all the three specimen types are shown in Fig. 6.7-6.9. It may be observed from these curves that rehabilitated specimens showed a similar trend of load recovery with the initial recovery being relatively lower. Envelope curves of BWF and CWS rehabilitated specimens showed slightly higher load carrying capacity in both push and pull directions. In BWS rehabilitated specimens, though the strength under pull type loading was gradually increasing but could not recover the undamaged strength, the strength under push type of loading was fully restored. However, the ultimate load carrying capacities of

all the specimens were found to be marginally higher than those of the control specimens. Thus, the appropriately chosen repair strategy which was base on the extent of damage could retrieve back the lost capacity even for a severely damaged connection.

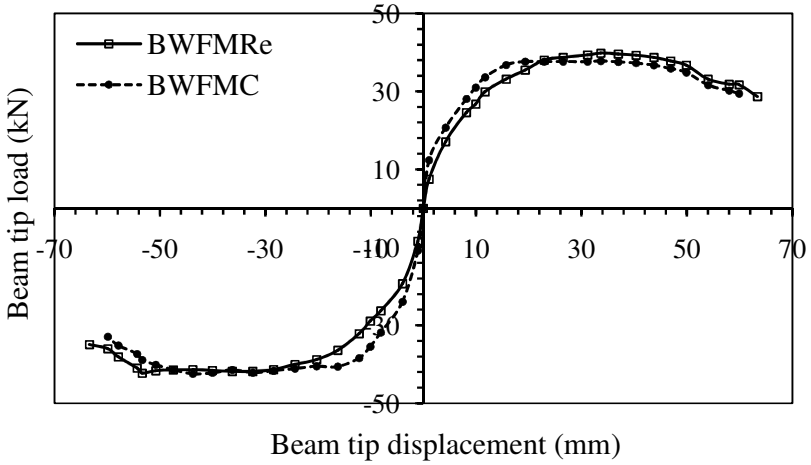

Fig. 6.7 Envelope curves for BWF specimens

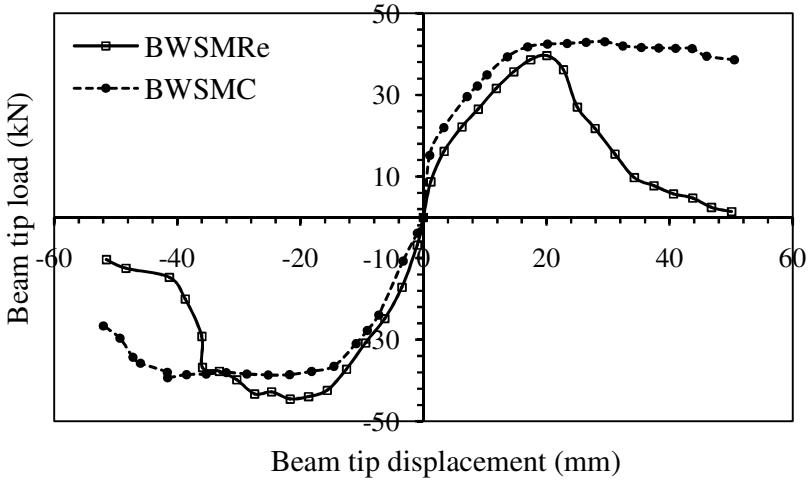

Fig. 6.8 Envelope curves for BWS specimens

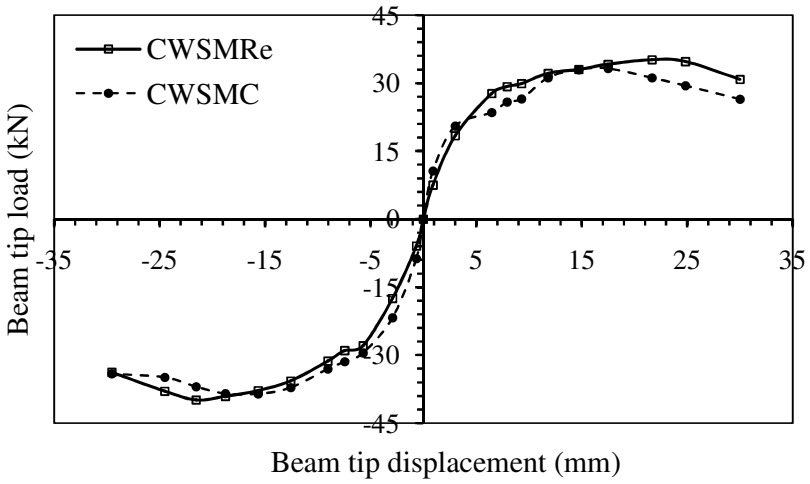

Fig. 6.9 Envelope curves for CWS specimens

(b) Stiffness degradation

The plots of stiffness variation for control as well as rehabilitated specimens for all the three specimen types are shown in Fig. 6.10-6.12. Fig. 6.10 illustrates the plot of BWF control and rehabilitated specimens. The plot showed that the stiffness at different drift angles of both the specimens are well comparable. The initial stiffness of control specimen is 13.79 kN/mm, while that for rehabilitated is 10.66 kN/mm. Thus, after repairing there was a reduction in stiffness of about 22.70 %.

Fig. 6.11 shows the plots of BWSMC and BWSMRe specimens. The initial stiffness of rehabilitated specimen is 7.09 kN/mm, while that for control specimen is 9.37 kN/mm. A reduction in stiffness of about 24.33 % was observed in the rehabilitated specimen. Further, up to a drift angle of 2.59 %, both specimens reflected almost same degradation rate; but subsequently rehabilitated specimen exhibited remarkable degradation till the end of test.

Similarly, from Fig. 6.12, it may be seen that the initial stiffness of CWS control specimens is 10.86 kN/mm, while that of rehabilitated specimen is 7.69 kN/mm. Thus,

after repairing there was a reduction in stiffness of about 29.20 %. Overall, the stiffness at different drift angle of both the specimens are quite comparable.

Thus, it can be concluded that all the rehabilitated specimens could satisfactorily achieve stiffness level which is well comparable to the respective control specimens.

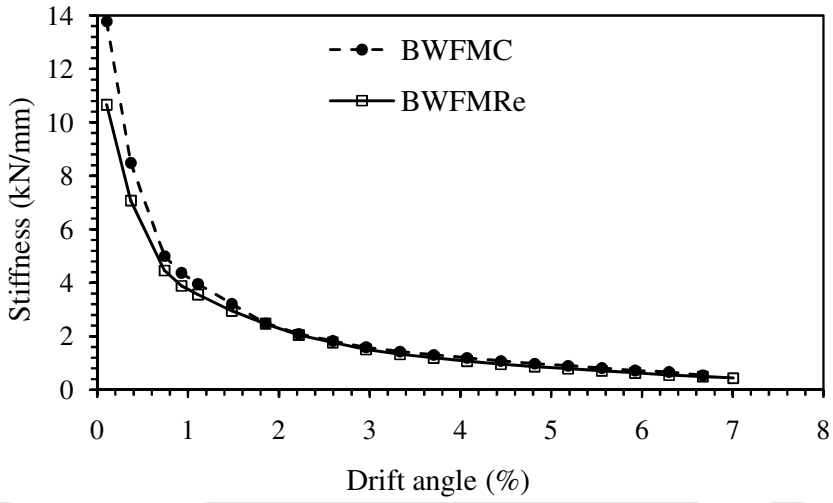

Fig. 6.10 Stiffness versus drift angle for BWF specimens

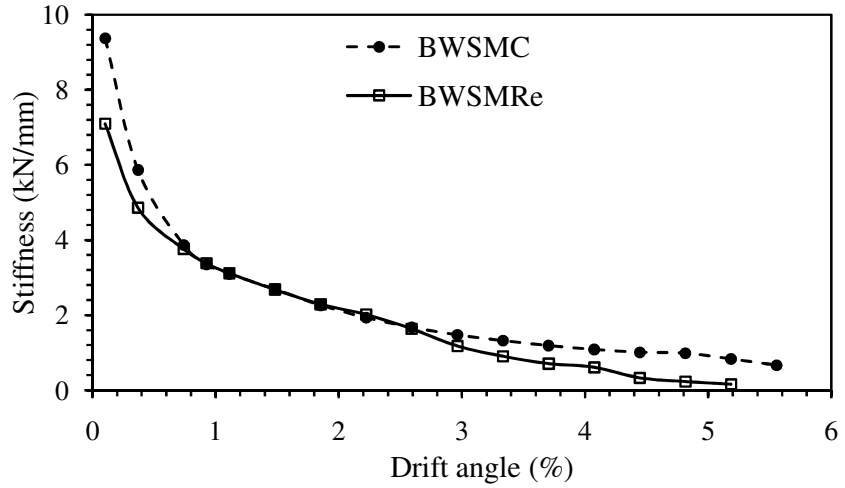

Fig. 6.11 Stiffness versus drift angle for BWS specimens

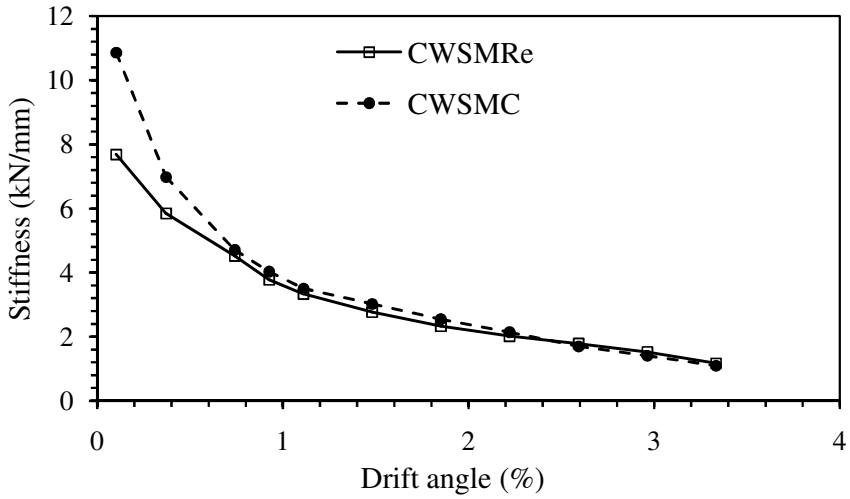

Fig. 6.12 Stiffness versus drift angle for CWS specimens

(c) Energy dissipation

The plots of cumulative energy dissipation versus drift angle for control as well as rehabilitated specimens for all the three specimen types are shown in Fig. 6.13-6.15. Table 6.2 shows the cumulative energy dissipated by the specimens (control and rehabilitated) corresponding to the drift level upto which the control specimens were tested. It is seen from Table 6.2 that the energy dissipated by BWF and CWS rehabilitated specimens are comparable to their respective control specimens. However, poor performance was observed for the rehabilitated BWS specimen, which experienced dropping of energy dissipation at a drift angle of 3.7% till the ultimate drift level.

Table 6.2 Energy dissipation (kN-m) for specimens under loading type-3

Specimens	Control	Rehabilitated
BWF	24.67	25.12
BWS	16.51	10.00
CWS	3.01	2.98

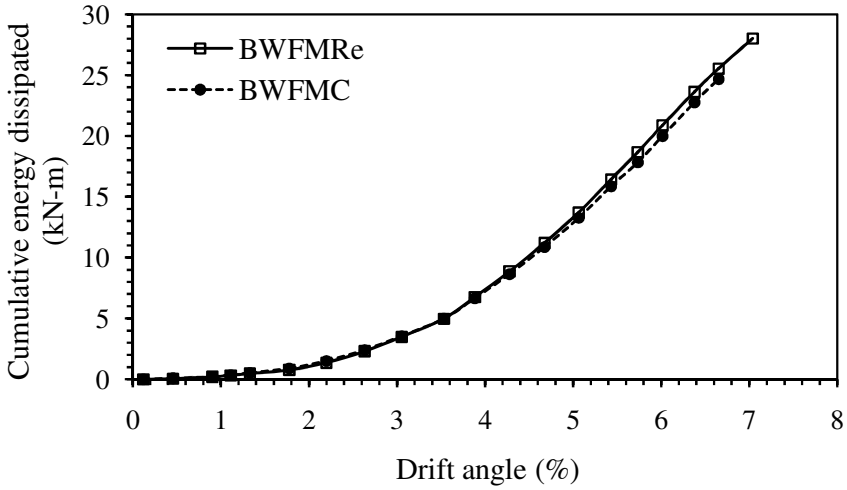

Fig. 6.13 Cumulative energy dissipation for BWF specimens

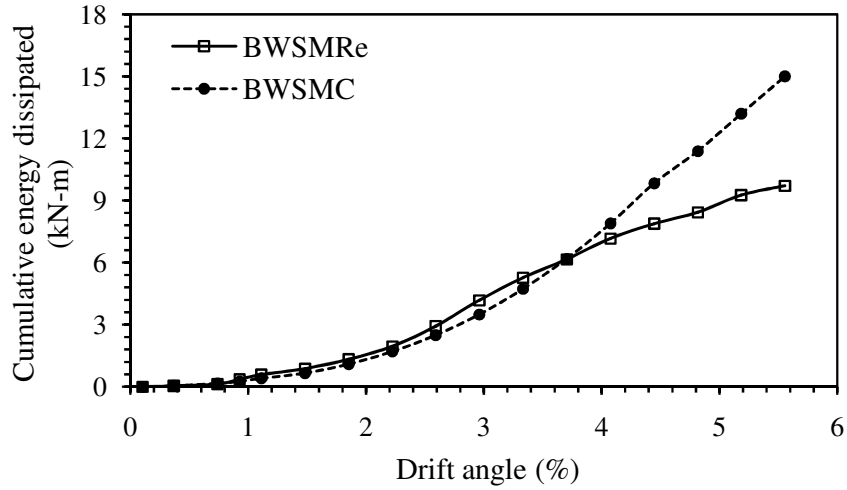

Fig. 6.14 Cumulative energy dissipation for BWS specimens

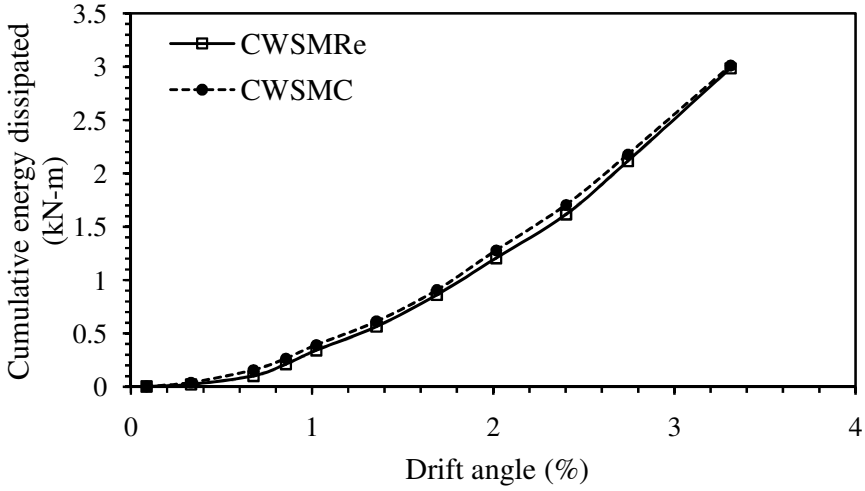

Fig. 6.15 Cumulative energy dissipation for CWS specimens

6.4 COMPARISON OF TEST RESULTS UNDER LOW AND HIGH CYCLIC LOADING FREQUENCY

In order to examine the performances of these connections subjected to excitations of different loading frequencies, test results obtained from the testing of specimens under loading type-3 were compared to those obtained from specimens under loading type-2. However, loading type-1 was not considered for the comparative study as the numbers of cycles per displacement amplitude level are different than those of type-2 and type-3. In this section, hysteretic responses, damage pattern and effects of inertial force were investigated and compared.

6.4.1 Hysteretic response

The hysteretic responses of all the connections under loading type-3 have been shown in section 6.3. Similarly, the hysteretic responses of BWFM, BWSM and CWSM under loading type-2 have been shown in chapters 3, 4 and 5 respectively. The parameters related to seismic capacity such as ultimate strength, stiffness degradations, energy dissipation and ductility of the specimens were evaluated from these hysteretic responses. The envelope curves of hysteresis loops for all control specimens under lower and higher loading frequencies are shown in Fig. 6.16-6.18. It can be observed that similar trend exists for load-displacement curve for all the specimens in both the loading cases. However, the envelopes of hysteresis loops of specimens under loading type-3 show slightly higher load carrying capacity in both push and pull directions. Envelope curves of hysteresis loops of the corresponding rehabilitated specimens are also shown in Fig. 6.19-6.21. These figures also show similar nature as observed for control specimens. The ultimate load carrying capacities of all the specimens are summarized in Table 6.3.

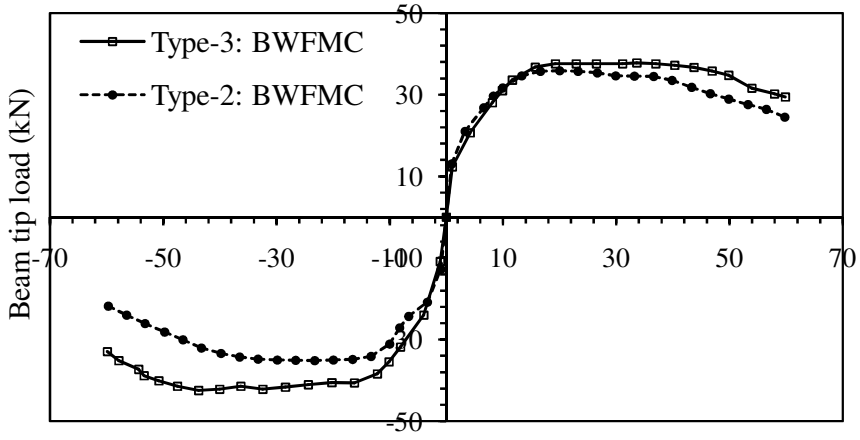

Fig. 6.16 Envelope curves for BWFC specimens under loading type-2 and 3

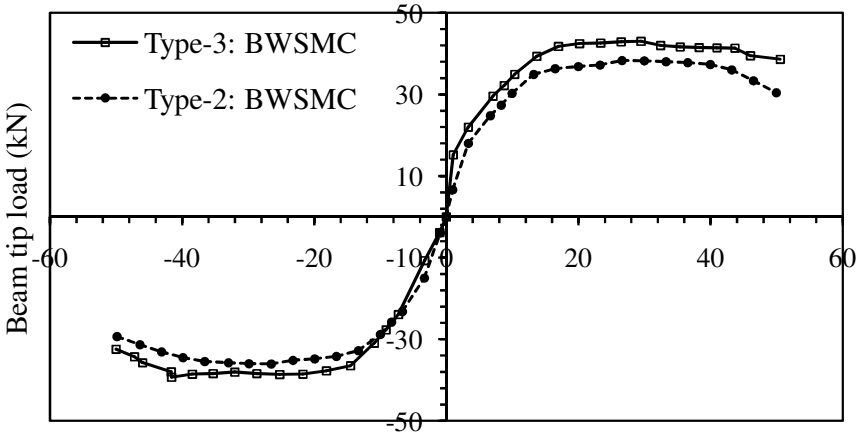

Fig. 6.17 Envelope curves for BWSC specimens under loading type-2 and 3

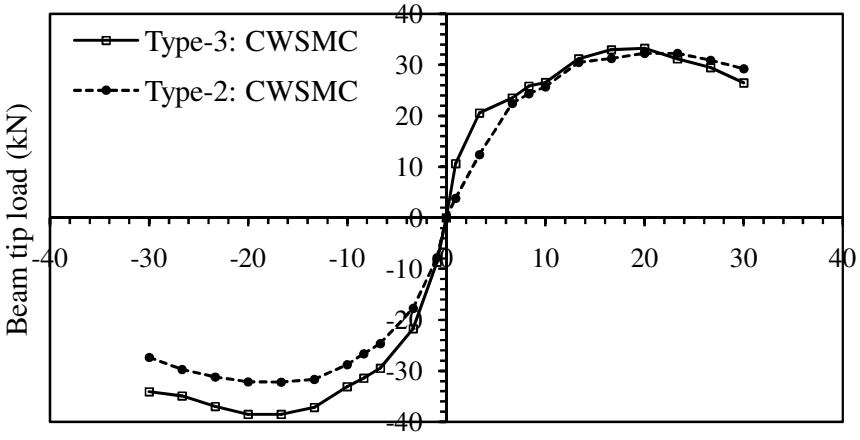

Fig. 6.18 Envelope curves for CWSC specimens under loading type-2 and 3

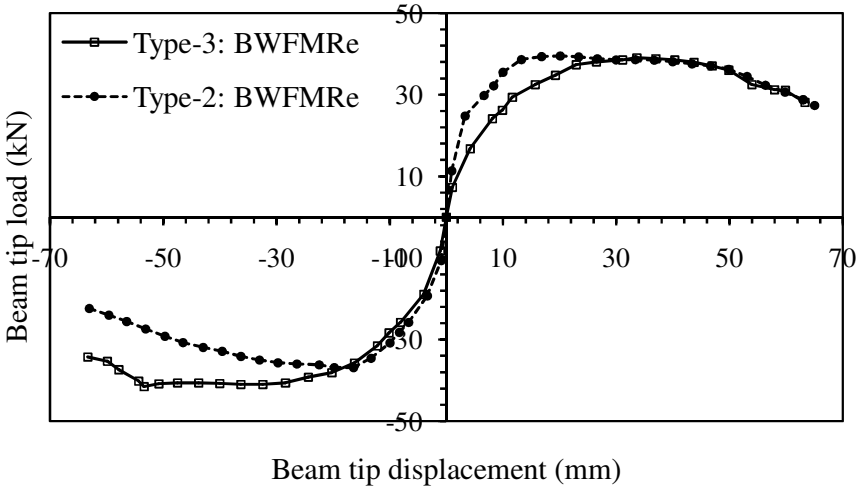

Fig. 6.19 Envelope curves for BWFRe specimens under loading type-2 and 3

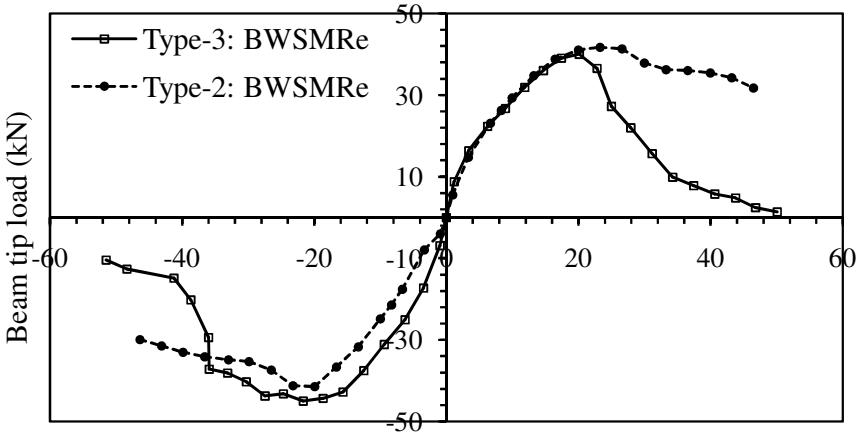

Fig. 6.20 Envelope curves for BWSRe specimens under loading type-2 and 3

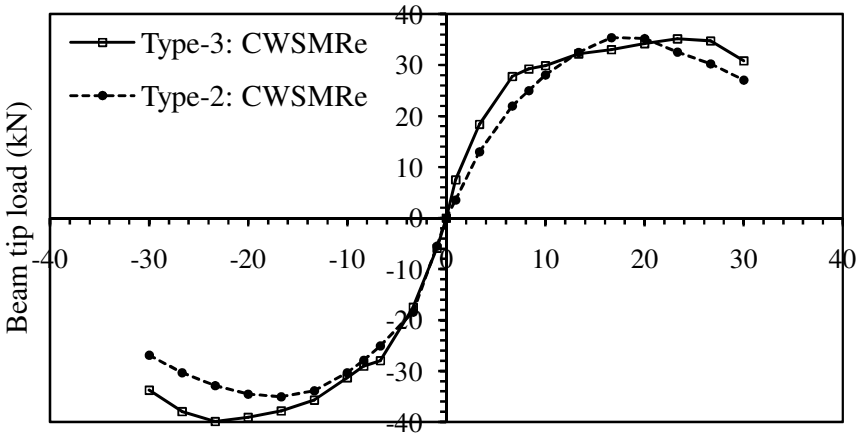

Fig. 6.21 Envelope curves for CWSRe specimens under loading type-2 and 3

Table 6.3 Comparison of performance of specimens under loading type-2 and type-3

Specimens with loading type	Control Specimens			Rehabilitated Specimens		
	Load capacity (kN)	Energy dissipation (kN-m)	Ductility	Load capacity (kN)	Energy dissipation (kN-m)	Ductility
BWF: Type-2	35.995	12.720	9.4	39.250	14.380	10.4
BWF: Type-3	40.755	24.670	9.4	41.145	25.120	10.6
BWS: Type-2	37.080	10.144	8.33	41.465	9.738	7.76
BWS: Type-3	41.070	16.510	7.69	41.890	10.000	4.13
CWS: Type-2	31.230	2.652	6.67	32.840	2.870	6.67
CWS: Type-3	35.905	3.010	7.25	37.550	2.980	7.5

Fig. 6.22-6.24 illustrates the variation of stiffness versus the applied drift angle for control specimens under different loading cases. The trend of degradation was very similar in all the cases studied. At the beginning of the test, specimens under cyclic displacement of higher frequency showed slightly higher stiffness values than those specimens under cyclic displacement of lower frequency. However, all the specimens sustained gradual stiffness degradation till the ultimate drift level.

Stiffness of BWF control specimen with loading type-2 is 11.21 kN/mm, while that for BWF control specimen under loading type-3 is 13.78 kN/mm. Thus, under higher frequency of loading, stiffness of specimen was 18.65 % higher than that of specimen under lower frequency of loading. Stiffness of BWS control specimen under loading type-2 is 7.69 kN/mm, while that for specimen corresponding to the same drift angle under loading type-3 is 10.04 kN/mm. Thus, specimen under cyclic displacement of higher frequency had stiffness, which was about 23.4 % higher than that of specimen under cyclic displacement of lower frequency. Similarly, CWS control specimen with loading type-2 attained a stiffness of 9.31 kN/mm, while that for specimen under loading type-3 is 11.07 kN/mm. Thus, like BWF and BWS specimens the stiffness attained by CWS

specimen under higher loading frequency was also higher (about 15.9 %) than that of specimen under lower loading frequency.

Similarly, variations of stiffness versus drift angle were plotted for rehabilitated specimens (Fig. 6.25-6.27). With the exception of BWS specimen under loading type-3 (Fig. 6.26) where sudden degradation in stiffness was observed at a drift angle of 1.48 %, the degradation in stiffness of BWF and CWS (type-2 and type-3) followed a similar trend as those of respective control specimens.

From these comparisons it can be concluded that specimens subjected to excitation of higher loading frequency exhibited slightly higher stiffness than that of specimens with lower loading frequency. This behaviour may be attributed due to strain rate effect.

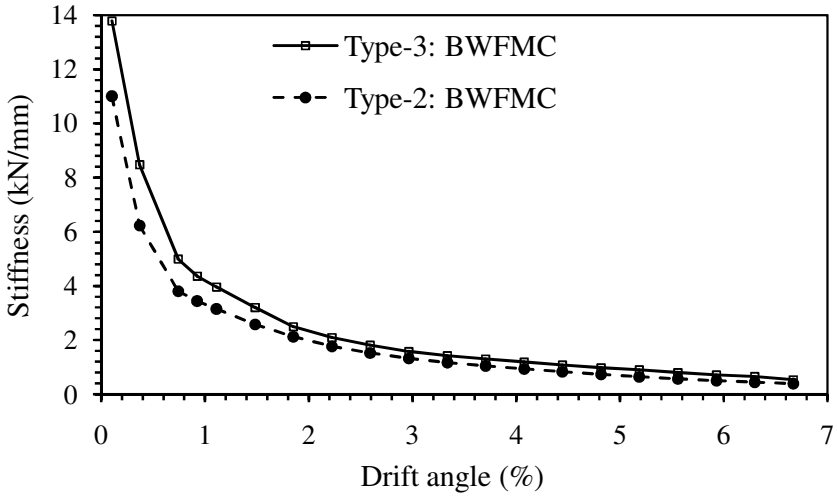

Fig. 6.22 Stiffness variation for BWFC specimens under loading type-2 and 3

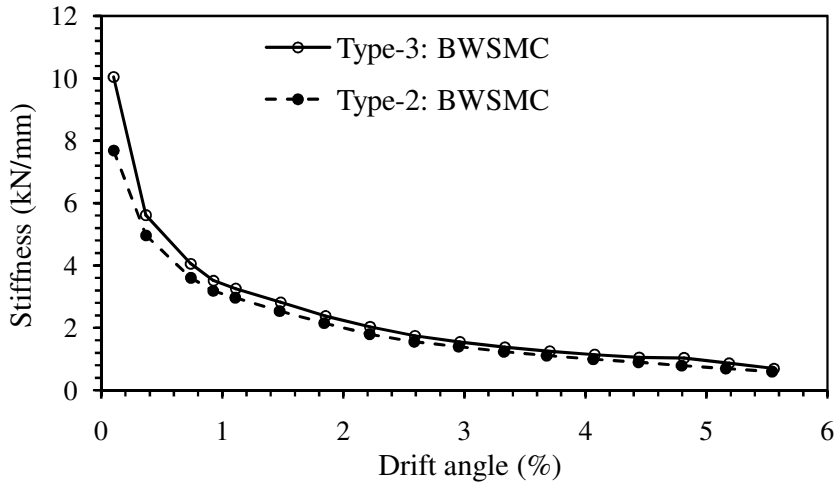

Fig. 6.23 Stiffness variation for BWSC specimens under loading type-2 and 3

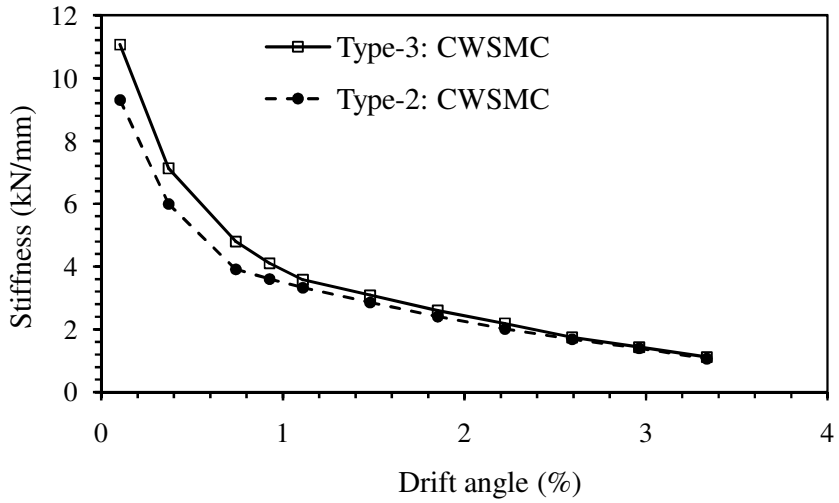

Fig. 6.24 Stiffness variation for CWSC specimens under loading type-2 and 3

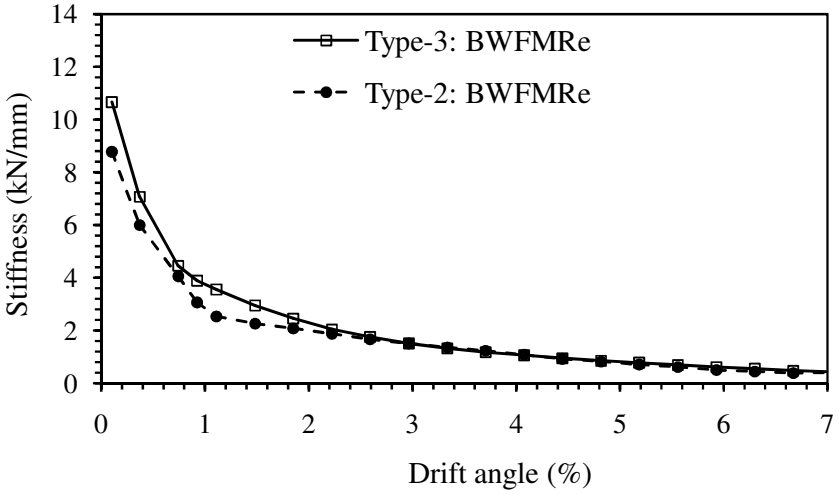

Fig. 6.25 Stiffness variation for BWFRe specimens under loading type-2 and 3

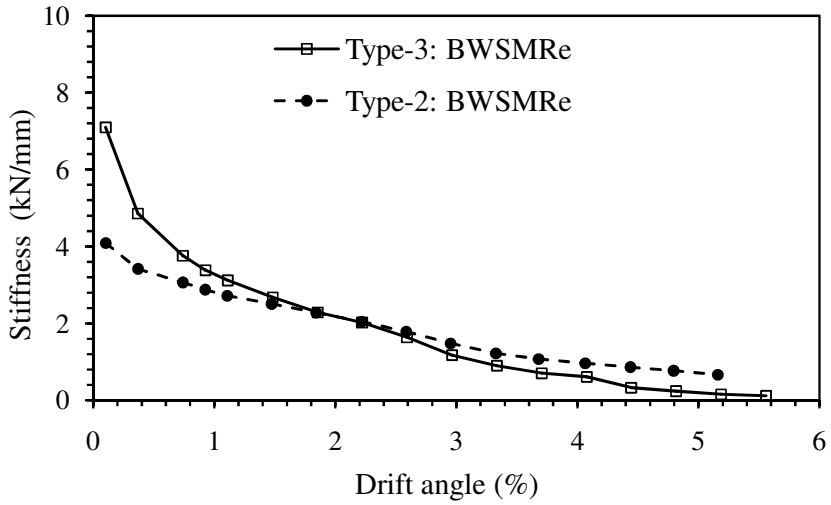

Fig. 6.26 Stiffness variation for BWSRe specimens under loading type-2 and 3

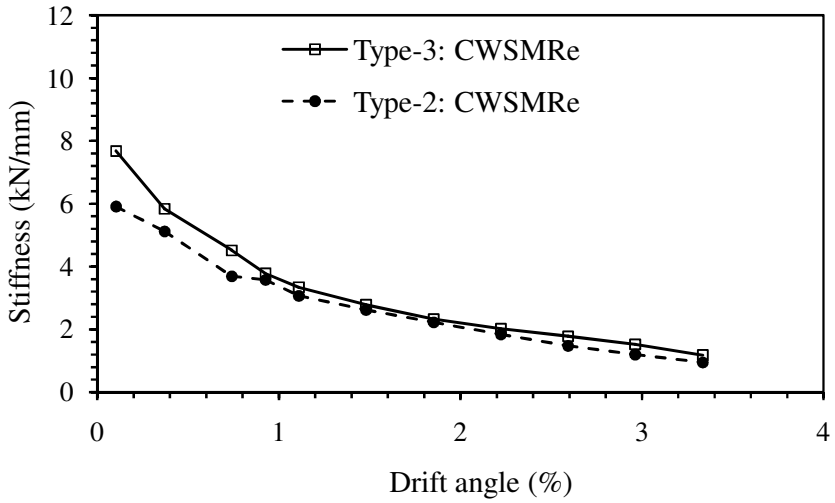

Fig. 6.27 Stiffness variation for CWSRe specimens under loading type-2 and 3

The plots of cumulative energy dissipation versus drift angle for control as well as rehabilitated specimens subjected to loading type-2 and type-3 are shown in Fig. 6.28-6.33. Comparing these plots it can be observed that the higher amounts of energy were dissipated by specimens under cyclic displacement of higher frequency. Similar behaviour was also observed from the study carried out by Shah *et al.* [1987]. The energy dissipated by each specimen corresponding to the drift level upto which the control specimens were tested are presented in Table 6.3. BWF control and rehabilitated

specimens under cyclic displacement of higher frequency dissipated energy, which were about 93.95 % and 74.69 % higher than those of specimens subjected to cyclic displacement of lower frequency. Energy dissipated by BWS control and rehabilitated specimens under loading type-3 were about 62.76 % and 2.69 % higher than those of specimen under loading type-2. Similarly, CWS control and rehabilitated specimens under loading type-3 dissipated energy about 13.50 % and 3.83 % higher than that of specimen under loading type-2.

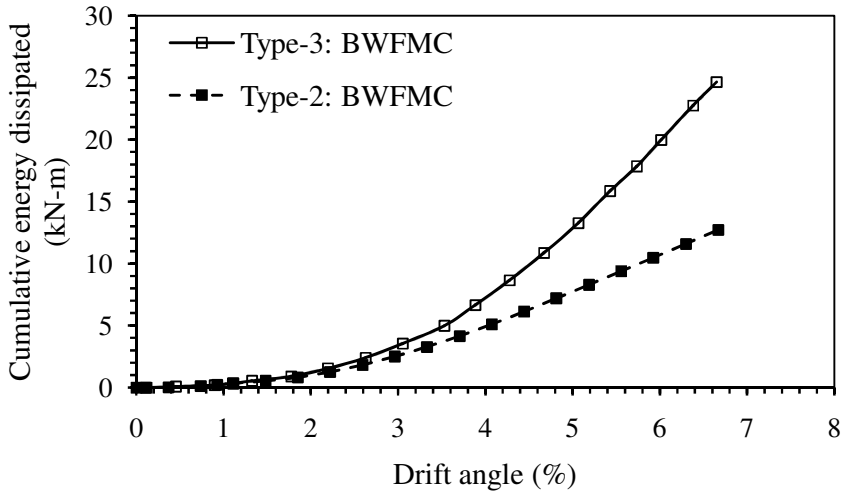

Fig. 6.28 Cumulative energy dissipation for BWFC specimens under loading type-2 and 3

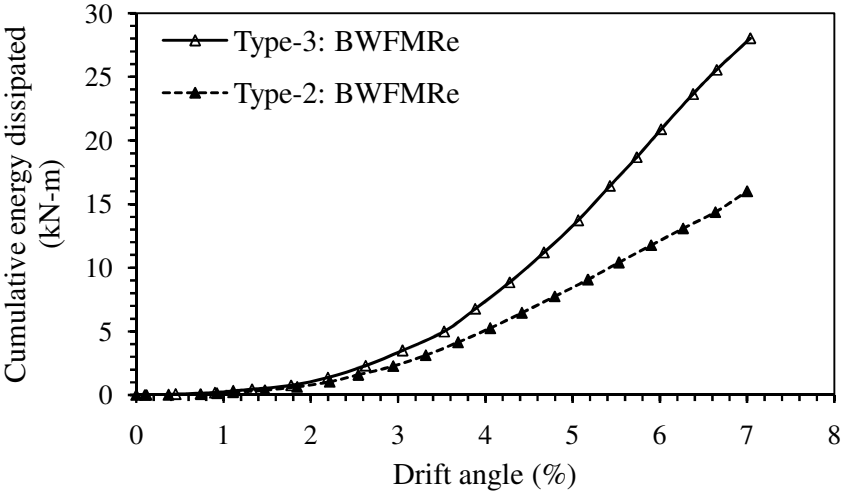

Fig. 6.29 Cumulative energy dissipation for BWFRe specimen under loading type-2 and 3

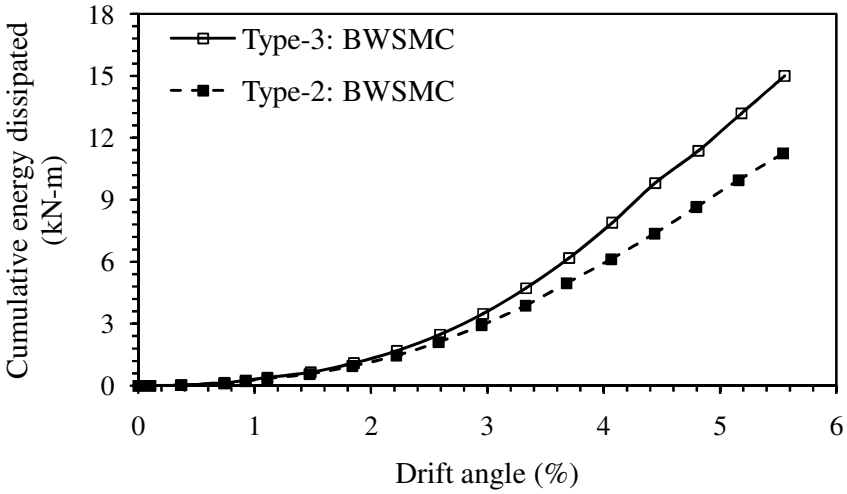

Fig. 6.30 Cumulative energy dissipation for BWSC specimens under loading type-2 and 3

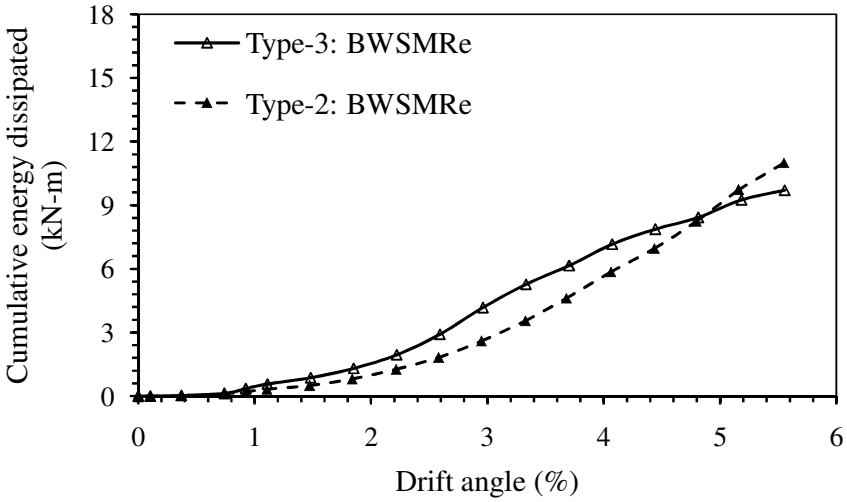

Fig. 6.31 Cumulative energy dissipation for BWSRe specimens under loading type-2 and 3

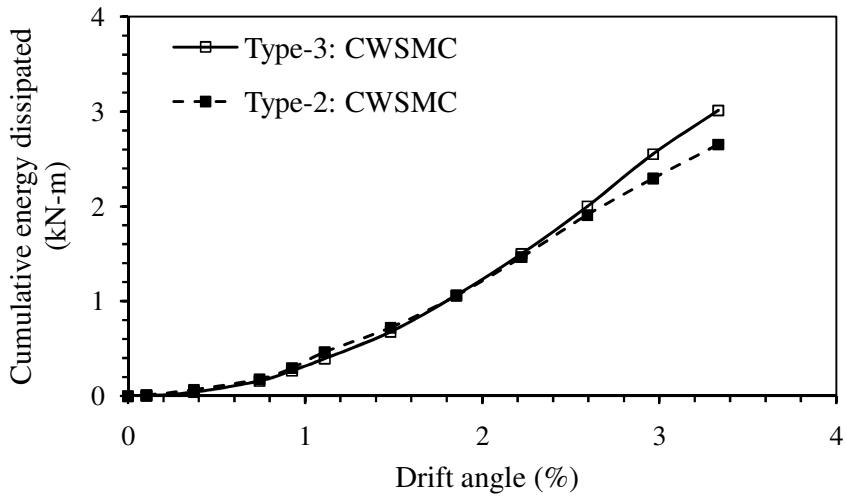

Fig. 6.32 Cumulative energy dissipation for CWSC specimens under loading type-2 and 3

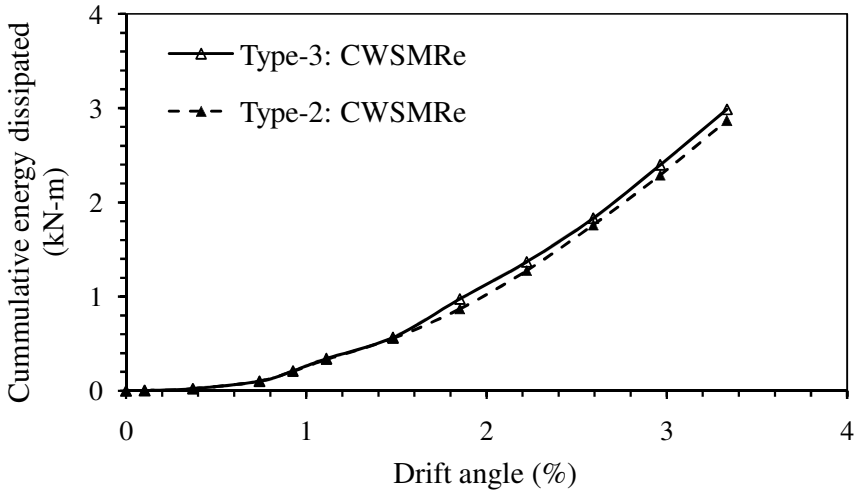

Fig. 6.33 Cumulative energy dissipation for CWSRe specimens under loading type-2 and 3

The displacement ductility for all the specimens under study was evaluated with the same procedure as explained in Sec 3.5.1(d) of chapter 3. The calculated ductility values are listed in the same Table 6.3. Comparable ductility values were achieved by the specimens both under loading type-2 and type-3 (control and rehabilitated). Only BWSMRe under loading type-3 could not attain the ductility values as good as the corresponding control specimen.

6.4.2 Damage pattern and failure mechanism of connections

Crack initiation and propagation were monitored as closely as possible in all the specimens. It was observed that cracks for BWF specimens were widely distributed at the joint region for specimens under cyclic displacement of lower frequency. In contrast, specimens under cyclic displacement of higher frequency, the major damages were localized at the beam-column joint interface. This indicates that the loading frequency is important to appreciate the transfer of load from beam to column. Though, hairline cracks were observed during the initial stages of loading both at the joint region and at the joint interface of specimens in both the loading cases, additional cracks were observed to

develop progressively at the joint region in the specimens under loading of lower frequency (Fig. 6.34). This may be attributed to better load transfer from beam to column under loading type-2.

BWS specimens under cyclic displacement of higher frequency also showed different failure pattern in comparison to those specimens under cyclic displacement of lower frequency (Fig. 6.35). It was observed that cracks were distributed both at joint region and beam part for specimens subjected with displacement of lower frequency. However for specimens under cyclic displacement of higher frequency, the damages were localized at the weakest shear zone of the beam. The damage was mostly concentrated on the beam part without transferring to the relatively stronger joint region. Specimen with loading type-3 was observed as severely damaged as compared to specimen with loading type-2 at the same displacement level.

CWS specimen under both loading types exhibited almost similar extent of damages (Fig. 6.36). However, because of efficient load-transfer occurring at cyclic displacement of lower frequency, the cracks on specimens are well propagated toward the weakest shear zone in the column region.

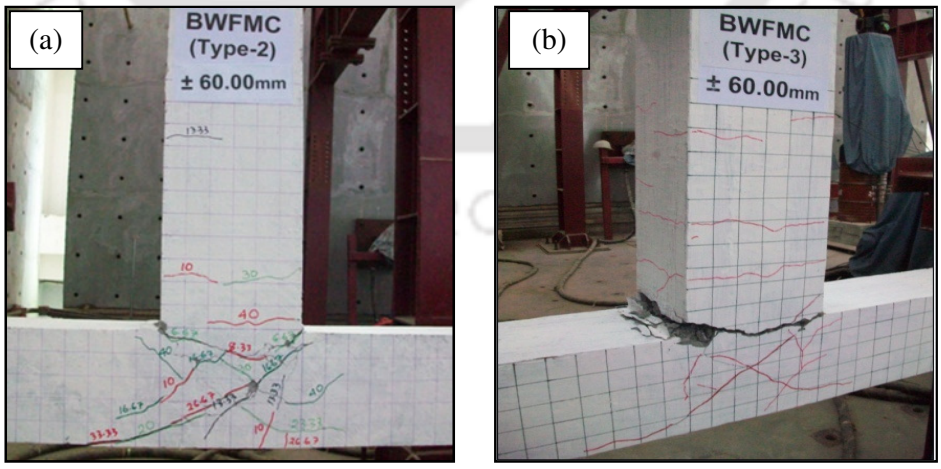

Fig. 6.34 Failure modes of BWF specimens subjected to
(a) Lower frequency and (b) Higher frequency

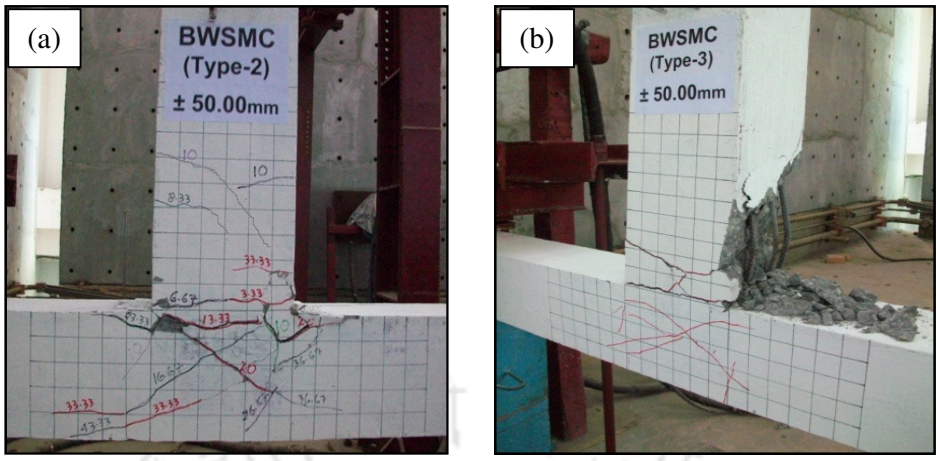

Fig. 6.35 Failure modes of BWS specimens subjected to
(a) Lower frequency and (b) Higher frequency

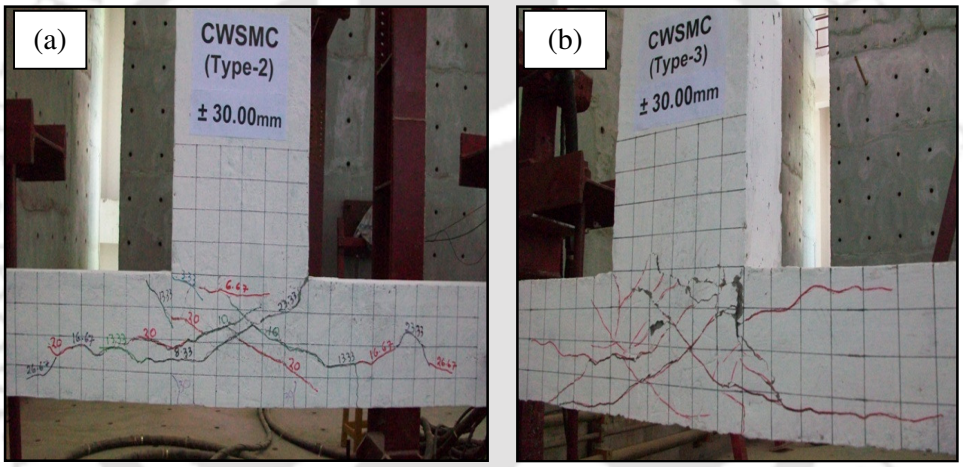

Fig. 6.36 Failure modes of CWS specimens subjected to
(a) Lower frequency and (b) Higher frequency

6.4.3 Effect of inertia forces

In high-speed cyclic loading test, the load cell reading at the loading point would be affected by inertial forces as observed by Dhakal *et al.* [2003]. They further observed that the hysteretic responses of specimens subjected to higher loading frequency are not smooth as those obtained from the lower loading frequency test. There was sudden unloading at the positive and negative peaks of each displacement and the amplitude of each cycle is less than the actual input displacement value. This behaviour may be

attributed to the development of a large acceleration and thus an inertial force in the direction opposite to that of the displacement being applied. This opposite inertia force renders the load cell reading to drop sharply around the peaks of the displacement cycles.

In the current study, the hysteretic responses obtained by plotting the test data for control specimens subjected to cyclic displacement of lower and higher loading frequencies are shown in Fig. 6.37-6.39. The hysteretic responses under a higher loading frequency are not as smooth as compared to those obtained from lower loading frequency. This behaviour may also be attributed to the development of acceleration in the direction opposite to that of the displacement being applied. However, the hysteretic responses under a higher loading frequency as obtained in this study were different from the hysteretic responses shown by Dhakal *et al.* [2005] for gravity designed RC exterior beam-column connections. It may be noted that in this study the frequency of cyclic displacement of 1.0 Hz were applied to the specimens in comparison to 2.0 Hz applied by Dhakal *et al.* [2005]. Therefore the effect of inertia force may not be very prominent for this level of loading frequency as was adopted in the present study. Hysteretic responses as shown in Fig 6.40 were observed from the study carried out by Shah *et al.* [1987] where the loading frequency was used as 1.0 Hz and the inertial force was observed to have insignificant effect.

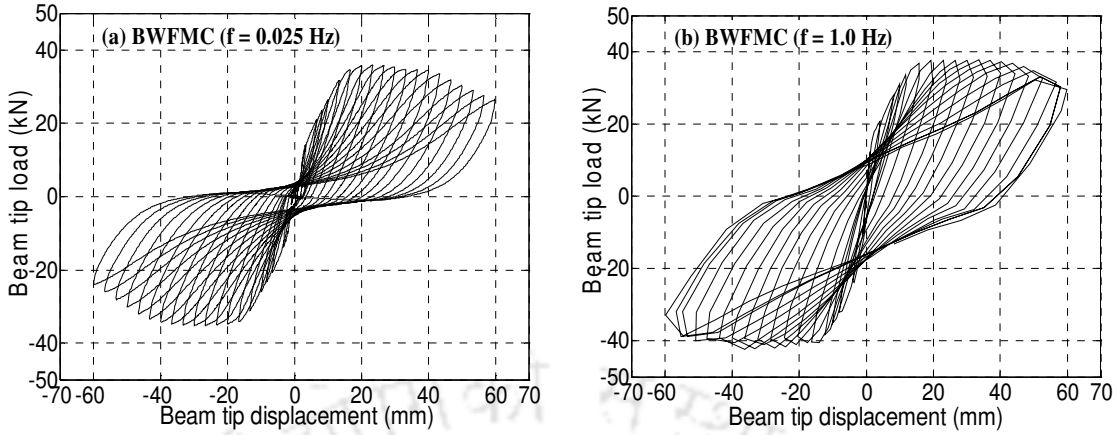

Fig. 6.37 Hysteretic responses of BWFC specimens under different loading frequency

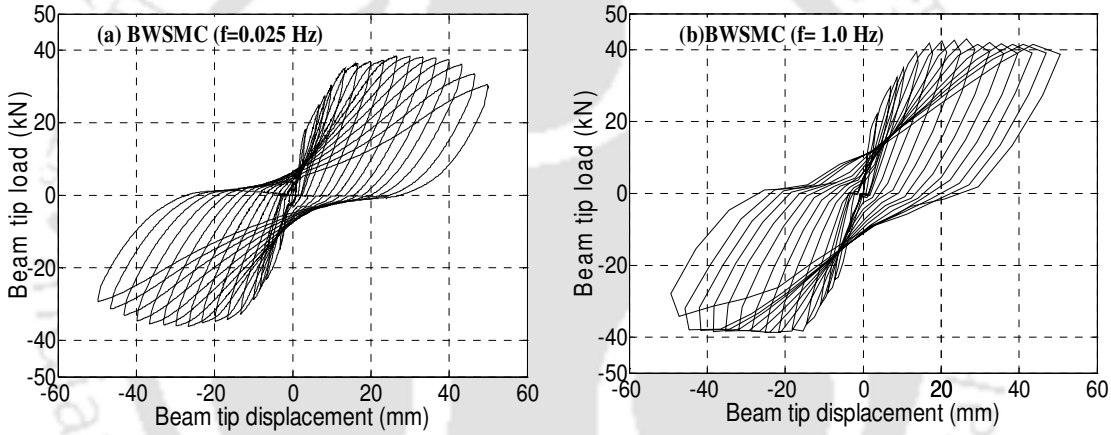

Fig. 6.38 Hysteretic responses of BWSC specimens under different loading frequency

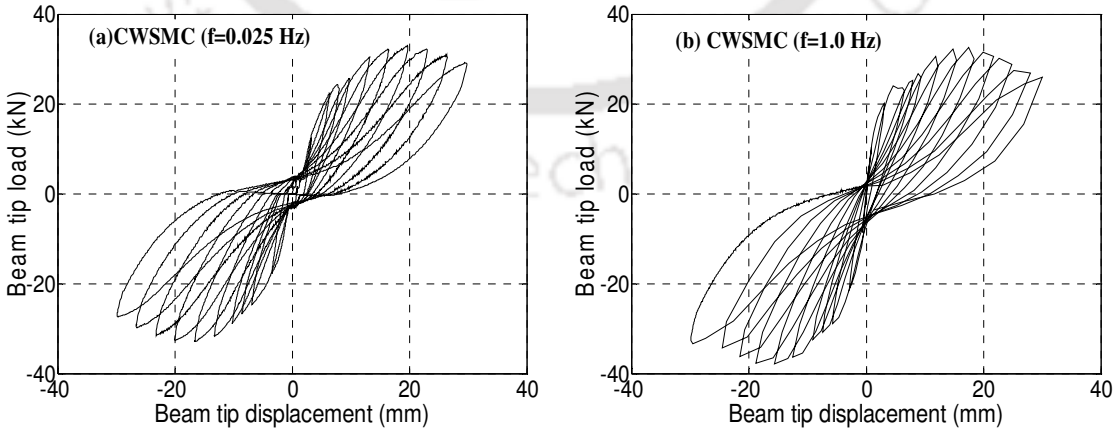

Fig. 6.39 Hysteretic responses of CWSC specimens under different loading frequency

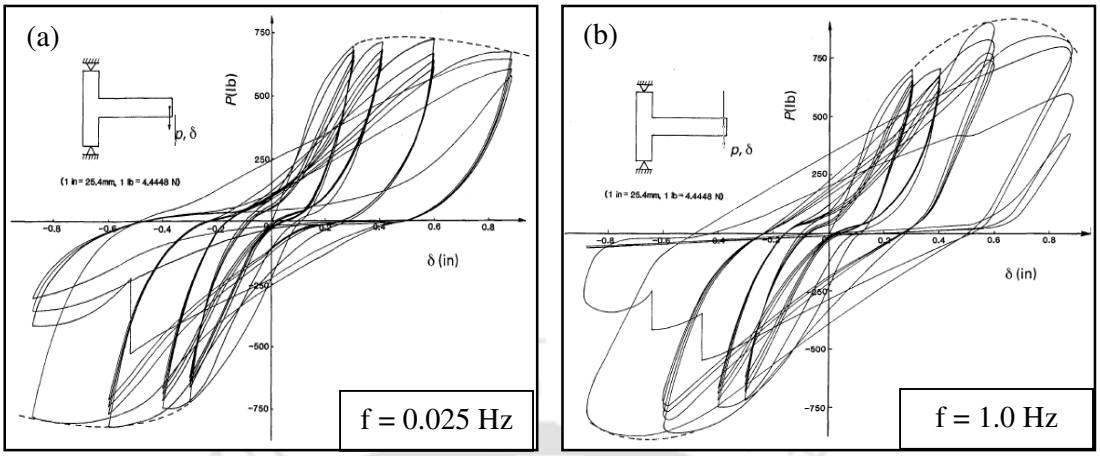

Fig. 6.40 Hysteretic responses of beam-column connections under different loading frequency [Shah *et al.,* 1987]

6.5 CONCLUDING REMARKS

In this chapter, the performances of two-third size exterior RC beam-column connections subjected to cyclic displacement of higher frequency were investigated. The damaged control specimens were rehabilitated and re-tested with the same loading sequences. The analysis of results based on various parameters related to seismic capacity such as ultimate load carrying capacity, energy dissipation, stiffness degradation etc revealed that the proposed rehabilitating techniques satisfactorily restored the damaged connections. Further, the performances of the connections under two different loading frequencies were also compared in term of the above mentioned parameters related to seismic capacity. It was observed that the load carrying capacity, energy dissipation were slightly higher for the specimens tested under higher loading frequency, which is attributed to strain rate effect. Further, the damage patterns and failure of the connections showed that damages were mostly concentrated at a particular zone during higher loading frequency testing as compared to those under lower loading frequency. Among all the deficient

specimens, BWS specimens showed poor performance during high cyclic loading frequency test. Effect of inertia force during high cyclic loading frequency test was also discussed. It was observed that specimen subjected to this level of loading frequency (1.0 Hz) has little affect due to inertial forces.

CHAPTER 7

EVALUATION OF DAMAGE INDICES FOR RC BEAM-COLUMN CONNECTIONS

7.1 INTRODUCTION

A damage index involves consideration of different aspects of structural response with the objective of producing a quantitative measure of structural damage. The index has the potential to play a vital role in retrofit / rehabilitation decision making. In this chapter the evaluation of damage indices for different beam-column connections under different loading types were presented using the Park and Ang [1985] damage index model. Comparison of damage level of control and rehabilitated specimens were made in order to ascertain effectiveness of the adopted rehabilitation technique. Further, assessment of control and rehabilitated specimens before and after rehabilitation using Ultrasonic Pulse Velocity (UPV) test were carried out and UPV were used as indicators of damage status. Finally, a guideline on identification of an appropriate rehabilitation strategy has been proposed for possible use during post disaster period.

7.2 SEISMIC DAMAGE INDEX

Damage indices are intended to be used as numerical indicators of damage of any structural element under any loading type. Parameters such as strain, displacement, strength, energy and intrinsic dynamic properties are used to calculate these damage indices. There are two kinds of indices, namely cumulative and non-cumulative. The first kind indicates damage dependency on both loading amplitude and number of loading cycles. The index is obtained by cumulating the damage inflicted during each loading

cycle. Non-cumulative indices are calculated with maximum mechanical parameters such as displacement, rotation and curvature.

Different approaches were considered for the formulation of damage indices, which have been briefly summarized below:

(a) Measurement of stiffness degradation in order to calculate Modified Flexural Damage Ratio (Roufaiel *et al*, 1987).

(b) Fatigue assessment to evaluate damage to columns based on the maximum displacement amplitude reached during cyclic loading (Banon *et al*, 1982).

(c) Measures based on the energy absorbed in the hysteresis loops (Kratxig *et al*., 1989).

(d) Combined indices comprising the weighted sum of deformation and energy terms as proposed by Park and Ang [1985].

The choice of an appropriate index may vary with the application. Williams and Sexsmith [1995] described the Park and Ang [1985] damage index as the most accurate representation of damage development among all the available cumulative damage index models. This damage index model has been widely used in recent years because of its simplicity and more so due to the fact that it has been calibrated using experimental data from various structures damaged during the past earthquakes.

The model calculates the damage index as a linear combination of damage due to excessive deformation and energy absorption. The Park and Ang [1985] model is written as

$$DI = \frac{\delta_m}{\delta_u} + \frac{\beta_e}{\delta_u Q_y} \int dE \tag{7.1}$$

where δ_m is the maximum deflection attained during seismic loading, δu is the ultimate deflection capacity under monotonic load, Q_y is the yield force, dE is the incremental dissipated hysteretic energy and β_e is the strength degradation parameters.

In the present study, the above-mentioned damage index model was used to evaluate the damage level for both control as well as rehabilitated specimens in order to ascertain effectiveness of the rehabilitation techniques. The values of δ_m, δ_u, Q_y and dE to be used in Eq. 7.1 were obtained from the experiments carried out in this study. The parameter δ_u was approximated by taking the envelope of the cyclic load-deflection loops as no monotonic test data were available (William *et al.*, 1997). The parameter β_e depends on the value of shear and axial forces in the section as well as on the total amount of longitudinal and confining reinforcement. Park [1984] obtained the value of β_e by means of a regression analysis based on 250 experimental results and reported the values of β_e to be ranged between about -0.3 to +1.2. Cosenza *et al.,* [1993] proposed a median value of β_e as 0.15 which has been adopted in the present study.

7.3 RESULTS AND COMPARISON OF DAMAGE INDICES

A typical calculation of damage index is presented in Appendix *C*. The calculated values of damage indices for all specimens based on the Park and Ang [1985] damage model have been presented in Fig. 7.1-7.8. These figures show that the damage indices increase as the damage of specimens grow further with increased drift angles. Further, all the curves of the damage indices are nearly linear, which suggest that the growth of damages in different specimens were stable.

Fig. 7.1-7.3 show the damage indices of BWF control and rehabilitated specimens under different loading types. Under loading type-1 and type-2 all the rehabilitated specimens show lower damage index at every level of drift angle as compared to their respective control specimens. The lower damage index presented by the rehabilitated specimens indicated that the rehabilitated specimens exhibited slightly better performance than that

of control specimens and hence the adopted rehabilitation strategy could be considered as satisfactory. Recalling the physical condition of specimens under loading type-3, both control and rehabilitated specimens exhibited similar extent of damage. Similarly, the damage indices calculated for these specimens also show similar magnitude of damage index at corresponding drift angle. The extent of damages for these specimens type (BWF in both control and rehabilitated) during different stages of testing and at the end of testing have been discussed in Chapter 3 and 6 respectively.

Further, corresponding to the drift level upto which large control specimens were tested, the smallest specimen (control and rehabilitated) presented a lower damage index followed by medium specimens and are highest for the full size specimens. The damage indices calculated for these specimens appear to give accurate representation of the physical damage states of these specimens.

The evaluated damage indices for BWS control and rehabilitated specimens are shown in Fig. 7.4-7.6. It is observed from Fig. 7.4 that control specimens under loading type-1 yield a higher damage index than the corresponding rehabilitated specimens. Thus, under loading type-1, rehabilitated specimen exhibited slightly better performance than those of control specimens. The damage index for specimens under loading type-2 is shown in Fig. 7.5. It can be seen that the largest and smallest control specimens presented a slightly higher damage index than the rehabilitated specimens. However, under the same loading type the rehabilitated medium specimen presented a higher damage index at any drift level than the control specimen. Further, under loading type-3, a higher damage index was calculated for the rehabilitated specimen.The extent of damages in both control and rehabilitated specimens during different stages of testing and at the end of testing for BWS specimens have been discussed in Chapter 4 and 6 respectively. The damage indices

calculated for these specimens are well correlated with the extent of damage experienced by these specimens.

Fig. 7.6-7.8 show the damage indices of CWS control and rehabilitated specimens under different loading types. The plot indicates that rehabilitated specimens presents equal or slightly lesser damage index at corresponding drift level as compared to control specimens. Equal or lower damage index presented by the rehabilitated specimens indicates that these specimens exhibited equal or marginally better performance than the respective control specimens. Further, it was also observed that the damage indices increase as the specimen sizes increased. The calculated damage indices correlated well with the extent of damage experienced by the specimens as discussed in Chapter 5 and 6 respectively for CWS specimens.

The above comparison shows that most of rehabilitated specimens exhibited lower damage indices than the corresponding control specimens, which indicated that the adopted rehabilitation strategy led to effective repair of different damaged specimens. Only two rehabilitated medium size specimens under BWS category under type-2 and type-3 loading displayed slightly higher damage index than the control specimens. Further, the calculated damage indices correlated closely with the extent of damage experienced by both the control and rehabilitated specimens.

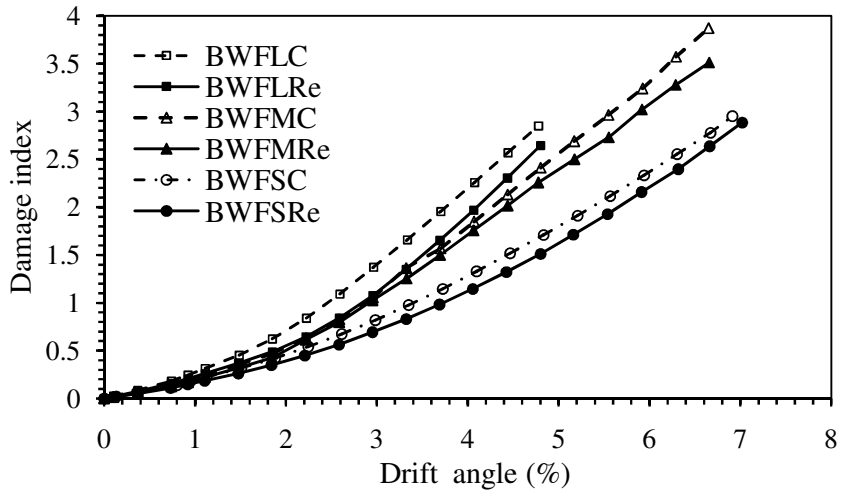

Fig. 7.1 Comparison of damage indices for BWF specimens under loading type-1

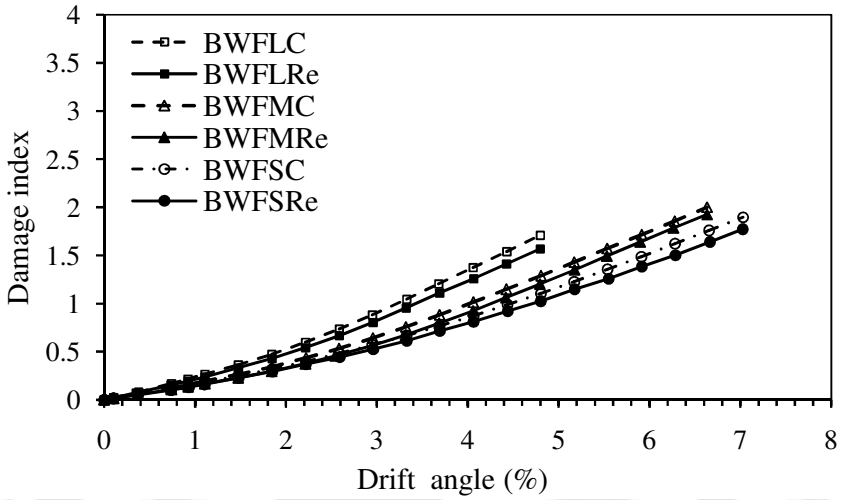

Fig. 7.2 Comparison of damage indices for BWF specimens under loading type-2

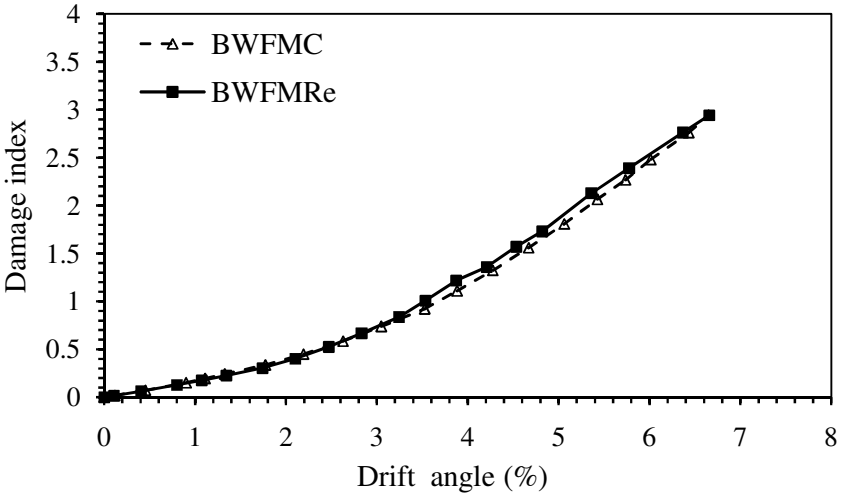

Fig. 7.3 Comparison of damage indices for BWF specimens under loading type-3

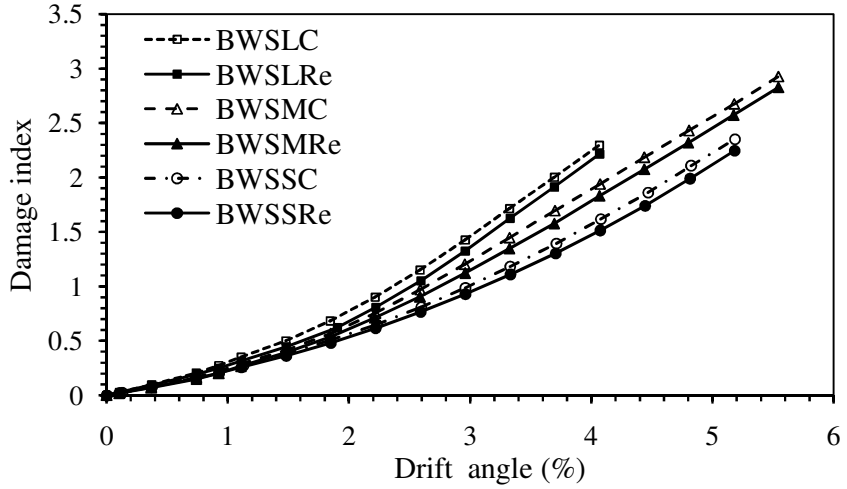

Fig. 7.4 Comparison of damage indices for BWS specimens under loading type-1

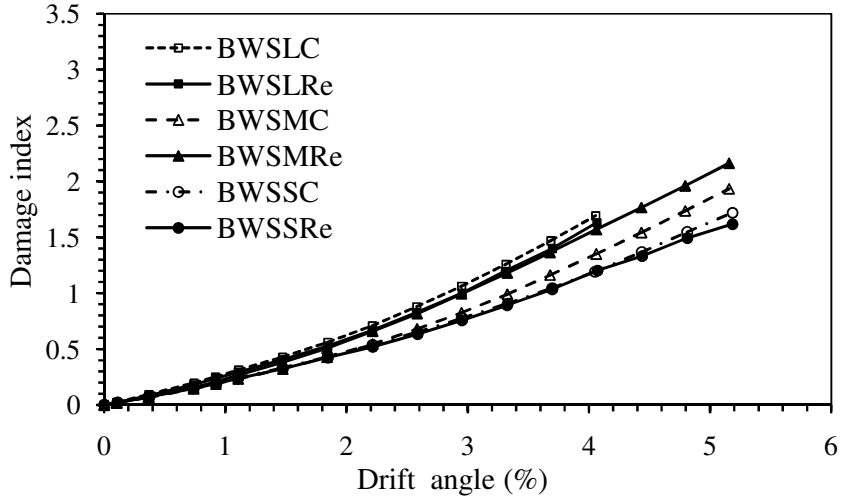

Fig. 7.5 Comparison of damage indices for BWS specimens under loading type-2

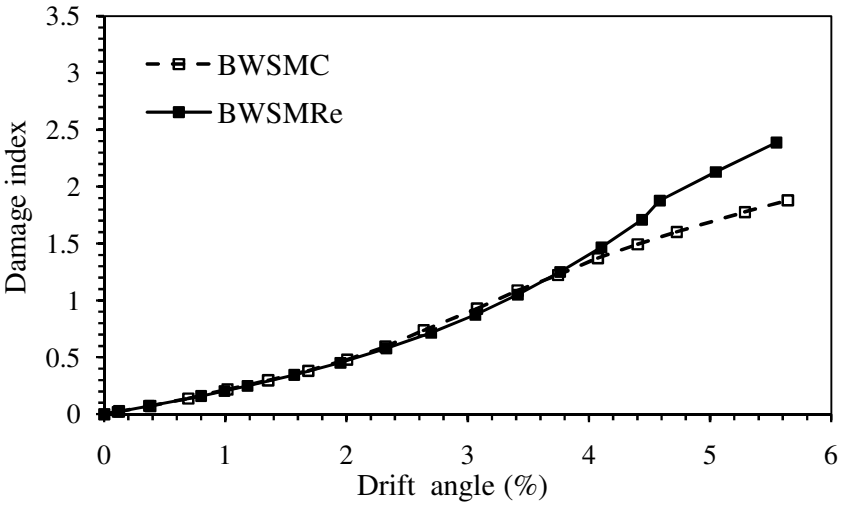

Fig. 7.6 Comparison of damage indices for BWS specimens under loading type-3

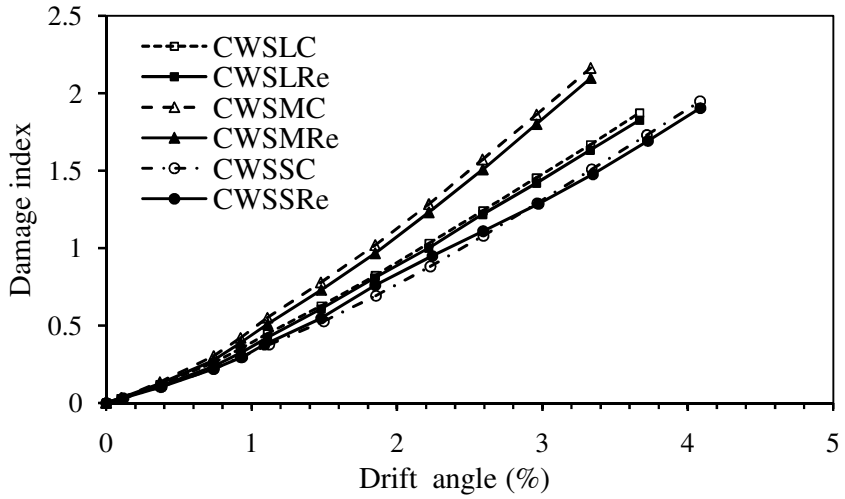

Fig. 7.7 Comparison of damage indices for CWS specimens under loading type-1

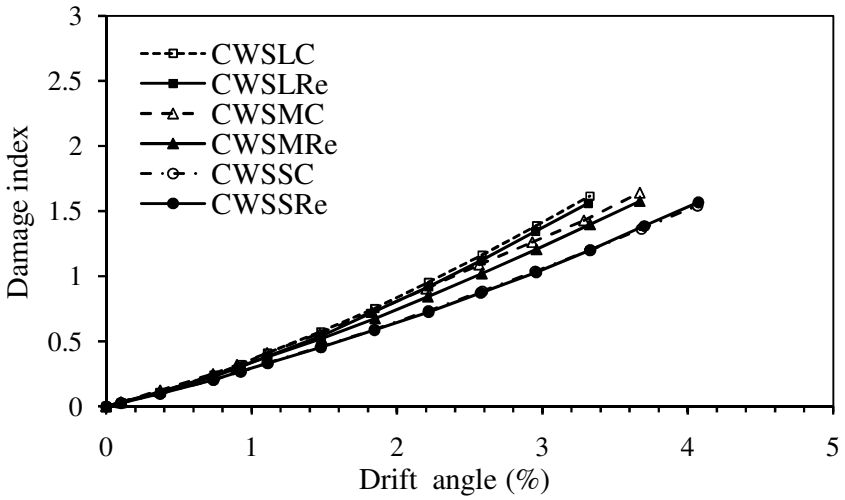

Fig. 7.8 Comparison of damage indices for CWS specimens under loading type-2

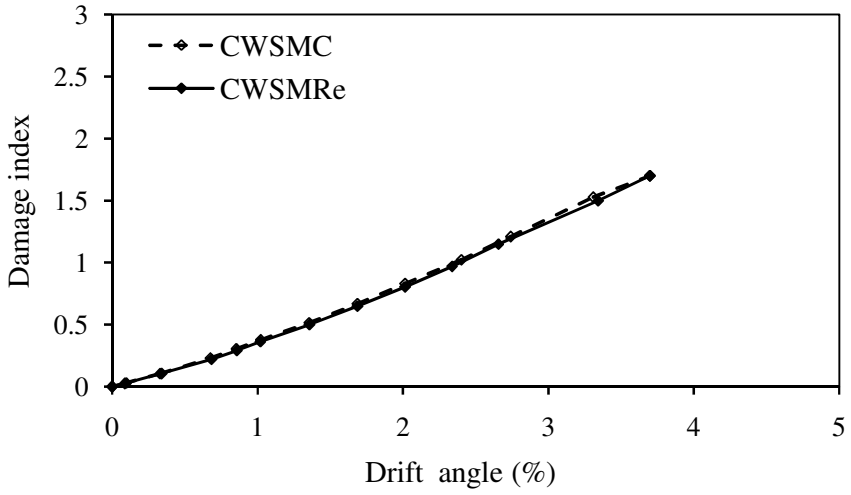

Fig. 7.9 Comparison of damage indices for CWS specimens under loading type-3

7.4 ASSESSMENT OF SPECIMENS BEFORE AND AFTER REHABILITATION USING ULTRASONIC PULSE VELOCITY TESTING

Ultrasonic scanning is a recognized non-destructive test (NDT) method to assess the homogeneity and integrity of concrete structure. The procedures of assessment have been discussed in Sec 2.7 of Chapter 2. Typical results of UPV test for damaged control and corresponding rehabilitated specimens under different loading types are presented in Table 7.1-7.3. Table 7.1-7.2 presented typical results of larger specimen under loading type-1 and type-2. Typical locations of transducers on the specimens are shown in Fig. 7.10. It may be seen that the UPV values were collected from both damaged as well as zones away from the effected region. It was observed that in most of the locations, the UPV values from the damaged control specimen were below 3.0 km/sec. The UPV values below 3.0 km/sec indicate that the quality of the concrete at these zone are doubtful as per guidelines given by IS: 13311 (Part-I)-1992. However, after rehabilitations it has been observed that the UPV values improved considerably in the same location. Thus, it may be inferred that the cracks could be filled up by the injected epoxy. The UPV values after rehabilitation were above 3.5 km/sec for zone injected with epoxy resin and more than 4.5 km/sec for zone completely replaced with micro concrete. Thus, it indicated that the quality of concrete fall in the good to excellent scale as per quality assessment guidelines. UPV tests were also done on the undamaged zone of each specimen. The UPV values in these zones were found out to be more than 4.5 km/sec indicating excellent quality of concrete. Thus, this knowledge about the UPV values on the undamaged and damaged zones of control as well as rehabilitated specimen provided a very important platform for comparative analysis regarding the effectiveness of rehabilitation and also to reliably assess the condition of damaged concrete before rehabilitation.

Table 7.1 Results of UPV test of control and rehabilitated specimens under loading type-1 along with crack pattern

Specimen	UPV values (km/sec)	
	Damaged control	Rehabilitated
BWFL (Loading type-1)	Varies from 2.1 to 2.8 in the damaged zone and with 5.5 in the undamaged zone	Varies from 5.0 to 6.3 in zone replaced with micro concrete and 4.5 to 5.0 in zone injected with epoxy
BWSL (Loading type-1)	Varies from 2.3 to 3.0 in the damaged zone and 5.5 in the undamaged zone.	Varies from 5.9 to 6.2 in zone replaced with micro concrete and 5.0 to 5.3 in zone injected with epoxy.
CWSL (Loading type-1)	Varies from 1.9 to 2.7 in the damaged zone and 5.0 in the undamaged zone.	Varies from 5.5 to 6.4 in zone replaced with micro concrete and 4.2 to 4.5 in zone injected with epoxy.

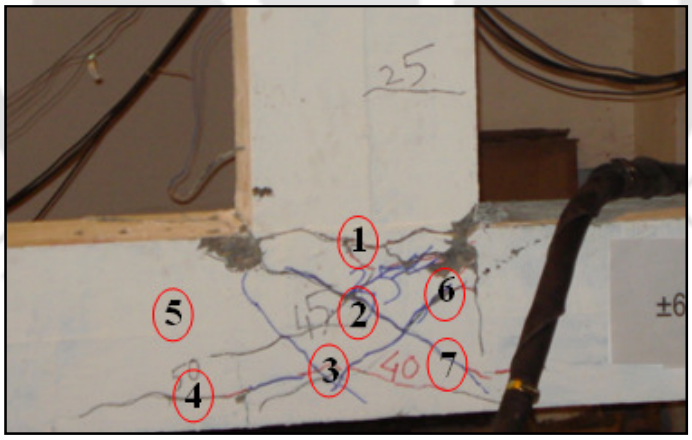

Fig. 7.10 Typical location of transducers on the specimen

Table 7.2 Results of UPV test of control and rehabilitated specimens under loading type-2 along with crack pattern

Specimen	UPV values (km/sec)	
	Damaged control	**Rehabilitated**
BWFL (Loading type-2)	Varies from 2.3 to 3.1 in the damaged zone and 5.4 in the undamaged zone	Varies from 3.8 to 4.5 in the repaired zone
BWSL (Loading type-2)	Varies from 2.7 to 3.2 in the damaged zone and 5.5 in the undamaged zone.	Varies from 3.9 to 4.6 in the repaired zone.
CWSL (Loading type-2)	Varies from 2.5 to 3.0 in the damaged zone and 5.2 in the undamaged zone.	Varies from 3.9 to 4.2 in the repaired zone.

Table 7.3 Results of UPV test of control and rehabilitated specimens under loading type-3 along with crack pattern

Specimen	UPV values (km/sec)	
	Damaged control	**Rehabilitated**
BWFM (Loading type-3)	Varies from 2.1 to 3.3 in the damaged zone and 5.5 in the undamaged zone.	Varies from 3.9 to 5.0 in the repaired zonee
BWSM (Loading type-3)	Varies from 2.3 to 3.2 in the damaged zone and 5.5 in the undamaged zone.	Varies from 5.7 to 6.3 in zone replaced with micro concrete and 4.5 to 5.0 in zone injected with epoxy.
CWSM (Loading type-3)	Varies from 2.5 to 3.1 in the damaged zone and 5.0 in the undamaged zone.	Varies from 4.6 to 5.0 in the repaired zone

7.5 GUIDELINES REGARDING REHABILITATION FOR FIELD APPLICATION

In order to effectively carry out repairing of distressed or damaged structures, guidelines are required so that appropriate rehabilitation techniques can be employed for post-earthquake usage. The studies on beam-column connections provided reasonable amount of knowledge about the behaviour of different deficiencies and rehabilitated specimens which were damaged to different levels under different loading types. Based on these studies, step-by-step guidelines have been prepared and presented in Table 7.4. These guidelines will be useful to the field engineers while taking decision on adopting an appropriate rehabilitation strategy during post disaster period. Effort have been made to correlate the state of physical damage of specimens like crack width, crack type with the repair methods for restoring the damaged specimens to their respective original states. UPV test were carried out on undamaged, damaged and corresponding repaired zone for all the specimens. Comparative study has been carried out in order to have understanding of the recorded UPV values for assessing effectiveness of rehabilitation techniques. Quality of concrete in the repaired zone based on Ultrasonic Pulse Velocity (UPV) test was also utilized for correlating with the repair methods.

In the experimental investigation, testing of specimens were stopped when load came down in the range of 60-70 % of ultimate load carrying capacity. It was observed that specimens under loading type-1 experienced higher degree of damages as compared to specimens under loading type-2. Crushing of concrete at the joint area extended up to joint core for specimens subjected to loading type-1. However, minor crushing of concrete at the joint area, which was limited to concrete covering the reinforcing bars were observed for specimens under loading type-2. Observing extent of the physical damage in specimens, complete removal of crushed concrete at the damaged zone and

epoxy injection for cracks away from the joint region were considered necessary for specimens subjected to loading type-1. Crushed concrete parts were replaced with fresh concrete possessing a compatible strength with the existing concrete. However, partial removal of loose concrete and epoxy injections for cracks were necessary for rehabilitation of such specimens as minor crushing of concrete at the joint region for specimens subjected to loading type-2 were limited to concrete cover only,

Further, trial tests were done in order to ascertain the effectiveness of the adopted repair techniques (RM1 or RM2) to restore the damaged connections to their original capacity. In this regard two deficient specimens of medium sizes (BWF and BWS) which were damaged under loading type-1 were rehabilitated with RM1 technique. From the test carried out, it was observed that BWF rehabilitated specimen could restore about 78 % and 80 % of strength and energy dissipation capacities respectively of those of control specimens. Similarly, BWS rehabilitated specimen could restore about 70 % and 74 % of strength and energy dissipation respectively of those of control specimens. Thus, based on the observation of these parameters related to seismic capacity, it may be inferred that the specimens damaged under loading type-1 and rehabilitated with RM1 were not able to restore the lost capacity of the connections to the original state. Therefore, further trial tests were carried out in which the specimens damaged under loading type-1 were rehabilitated by RM2 technique. The analysis of results revealed that both the rehabilitated connections exhibited strength and energy dissipation capacities equal or marginally higher than the corresponding control specimens. Therefore, from these two trial tests, rehabilitation strategies were reaffirmed. Specimens, where major fragmentation of concrete is observed, need to completely replace the crushed concrete at the damaged zone with concrete of compatible strength followed by epoxy injection under high pressure for sealing of cracks away from crushed zone. However, minor crushing of

concrete in an area can be addressed by partial replacement of damaged concrete followed by epoxy injection in order to seal any cracks around the damaged zone.

The extents of damage in this study were characterized by physical indicators like maximum crack width, extent of concrete spalling and crushing, buckling of main reinforcing bars. In this study, high pressure epoxy injections were used at the joint region for a crack width beyond 0.02 in. (0.5 mm) and upto a maximum of 5.0 mm. When structures experienced cyclic loading, cracks from the joint region may extend either towards beam or column region. The bond between the reinforcing bars and surrounding concrete can be effectively restored by epoxy injection. Studies conducted by various researchers confirmed that epoxy injection can effectively restore the bond of reinforcing bars with surrounding concrete.

Table 7.4 Rehabilitation guidelines correlating damage states and repair methods

Damage states	Repair method (RM)
• Partial fragmentation of concrete extended upto covers to the reinforcing bars. • Core of the specimens unaffected. • Maximum crack width in the specimen is within 5.0 mm. • NDT values in effected zone is around 3.0 km/sec.	RM1: Partial removal of damaged concrete, patching with micro concrete and epoxy injection in cracked zone
• Major fragmentation of concrete. • Cracks extending inside the core of the specimen. • Crack width beyond crushed zone upto 5.0 mm. • Buckling of reinforcement. • NDT values in crushed zone is much lower than 3.0 km/sec.	RM2: Complete removal of damaged concrete, replacement with micro concrete and epoxy injection in cracked zone

7.6 CONCLUDING REMARKS

In this chapter, Park and Ang damage model have been employed for evaluating the damage index of connections in both control and rehabilitated specimens. The calculated damage index revealed that the adopted rehabilitation strategy could be considered as satisfactory, since most cases of rehabilitated specimens presented a lower damage index as compared to the index of the corresponding control specimens. The calculated indices also correlated well with the extent of damage experienced by the specimens. Further, guidelines regarding rehabilitation strategies have been prepared for field application. The guideline correlates the physical damage of specimens and the associated repair methods for restoring the damaged specimen to original state. Further, quality of concrete in the repaired zone was also correlated to the repair method based on Ultrasonic Pulse Velocity (UPV) test.

CHAPTER 8

DEVELOPMENT OF FRAGILITY FUNCTIONS FOR EXTERIOR RC BEAM-COLUMN CONNECTIONS

8.1 INTRODUCTION

Fragility functions are developed to identify the appropriate repair method required to restore the beam-column connections damaged due to earthquake loading. There are many way to obtain fragility functions. Developing fragility functions from experimental studies considered to be the most reliable one among the different methods. However, in spite of minimizing the various uncertainties, development of fragility functions from experimental studies is not well reported because realistic experiments have time and economic constraints along with other difficulties. This chapter presents the development of fragility functions from the current experimental results obtained from the extensive testing carried out in the laboratory. Drift angle was used as the demand parameters which generally refer to as engineering demand parameter (*EDP*). Damage states identify from the progression of damage during testing are linked with the repair methods. Four probability distributions were fit to the data and suitability of each distribution were evaluated using standard statistical methods. Fragility functions have been developed both for control and rehabilitated specimens. The results of this effort are families of fragility functions that indicate the required repair method for a damaged connection.

8.2 FRAGILITY FUNCTIONS

Fragility functions are probability distributions that are used to indicate the probability that a components, elements or system will be damaged to a given or more severe damage state as a function of a single predictive demand parameter such as story drift or floor

acceleration. The damage state probability proposed by Porter *et al.* [2007b] using lognormal distribution is defined as:

$$F_{dm}(edp) = P\left[DM \geq dm | EDP = edp\right] \tag{8.2}$$

$$F_{dm}(edp) = \Phi\left[\frac{\ln(edp/\theta)}{\beta}\right] \tag{8.3}$$

where F_{dm} (edp) denotes the fragility function for damage state *dm,* defined as the probability that the component reaches or exceed damage state *dm,* corresponding to a particular engineering demand parameter (*EDP*). The function Φ denotes the standard normal (Gaussian) cumulative distribution function. The parameter θ and β denotes the median value and logarithmic standard deviation. These parameters can be evaluated using the following expression (Ang and Tang, 1975).

$$\theta = \exp\left(\frac{1}{M}\sum_{i=1}^{m} \ln ri\right) \tag{8.4}$$

$$\beta = \sqrt{\frac{1}{M-1}\sum_{i=1}^{M}\left[\ln\left(\frac{r_i}{\theta}\right)\right]^2} \tag{8.5}$$

where M = number of sample

i = index of specimens and

r_i = *EDP* at which damage was observed to occur in specimen i.

In the present study, the fragility functions depict the probability of a suitable repair method that a earthquake damaged structural elements will require to restore to its original condition given a specific level of earthquake demand. An *EDP* is the measure of earthquake demand on a structural component. Probability models link the *EDP* to the damage measure and in turn to the method of repair. Therefore, the probability of

exceeding the damage requiring a specific repair method is modeled in the form of fragility functions.

8.2.1 Engineering demand parameter (*EDP*)

An *EDP* is a scalar or functional quantity that defines the earthquake demand on a component at any point in the load history. In developing fragility functions, it is important to identify an *EDP* that most accurately and precisely to relates damage. Importantly, use of drift as the demand parameter by many researchers to develop a fragility functions have been reported in literature (Gulec *et al.,* 2010). For the current study a drift angle as defined in Sec. 3.5.1 (b) of Chapter 3 which is the best single valued demand parameter for many structural elements was used.

8.2.2 Identification of damage states (*DS*)

Damage measures provide a description of the extent of damage sustained by a component during an earthquake. The extent of damage is characterized by damage states. Damage states (*DS*) are linked to specific repair method and models are developed for defining the probability of a connection exceeding a specific damage level for a given earthquake demand. Thus, identification of the appropriate damage states is the most important step for developing fragility functions. Damage states describing connections damage are observable either by visual inspection or by measurement through appropriate instrumentation. In this study the damage states are characterized by direct indicators of damage such as maximum concrete crack width, extent of concrete spalling, crushing and the initiation of buckling and fracture of reinforcing bars which can result in failure of the component.

The damage states identified by Pagni and Lowes [2006] from the results of previous experimental research were used as the basis to identify the level of damage states in the current study. These damaged states are then linked with the repair method. The specimens were damaged under cyclic loading with different characteristics. The same specimens were rehabilitated and then retested. Thus, the defined damage states are based on the actual observed damage from the current experimental study. The damage states and their associated repair methods were listed in Table 8.1. These damage states were assembled from the analysis of the progression of damage observed from 42 numbers of specimens tested in the structural engineering laboratory at IIT Guwahati. These damage states are characterized by visual observation on the damaged specimens which is presented in the following paragraphs:

(a) Concrete cracking

The first indication of damage in RC components is typically the initiation, propagation and opening of concrete cracks. Two critical damage states arise in defining damage states associated with concrete cracking. The crack width at which surface finishes, such as paint or plaster, have to be repaired and the crack width at which epoxy injection of cracks is required to restore the component to its pre-earthquake strength and stiffness. Damage states (*DS*) 1.0 refers to cracking in the interface of the beam and the joint region. These cracks are appeared first when the loading starts at a low demand. The cracks may initiate from the joint corners and progress horizontally along the joint interface. Damage states (*DS*) 1.1 corresponds to initial cracking within the joint panel. Widths of these cracks are immeasurable. Damage states (*DS*) 1.2, 1.3 and 1.4 are subsequent stages after formation of initial cracks as shown in Fig. 8.1. Pagni and Lowes [2006] recommended that the development of visible, hairline cracking may be used as an

indicator of the need to replace surface finishes and repair were not required for the cracks smaller than 0.02 in. (0.5 mm). However, a crack width beyond 0.02 in., epoxy injection is necessary to restore the bond between the materials. Gulec *et al.* [2010] similarly suggested that epoxy-resin injection is required for a maximum measured crack width larger than 0.02 in. (0.5 mm) but less than 0.12 in. (3 mm). In the current study, a maximum crack width of 2.0 mm for which an epoxy injection was performed at beam and column part of the connections (*DS* 2.0 and *DS* 2.1 in Fig. 8.2). For specimens with lesser degree of damage the repair of the joint region includes patching of spalled concrete and then followed by epoxy injection into a cracked zone (*DS* 2.0 in Fig. 8.2). A maximum crack width of about 5.0 mm at joint region was chosen to repair with epoxy resin injection. Damage state (*DS*) 2.3 in Fig. 8.2 relates with the progression of damage when initial cracks at the joint interface further widened. *DS* 3.0 in Fig. 8.3 describes the damage initiating within the joint region and then cracks propagating towards the column region. For this damage state associated with repair method-2 (*RM2*), the loose concrete at the joint region was completely removed and then the created voids were filled with high strength polymer modified concrete (micro concrete). Wide cracks which were left on the surface of the column region away from the joint region were injected with epoxy resin.

(b) Concrete spalling and crushing

Spalling of cover concrete and crushing of joint core concrete represents the next phase of damage. Crushing of core concrete refer to fragmentation of concrete within the region encircled by rebars. Repair methods for extensive spalling require replacement of fragmented aggregates rather than just patching with concrete. For joints, Pagni and

Lowes [2006] recommended that replacement is required if 80 % or more the joint surface area spalls.

Damage states (*DS*) 2.2 and 2.4 shown in Fig. 8.2 indicate the transition from cracking to spalling. Crushing of concrete at the edges of beam-column joint interface and cracking at the joint region is no longer measurable. Damage states (*DS*) 3.1 as shown in Fig. 8.3 indicates crushing of the concrete extending into the joint core. Spalling of more than the cover concrete is considered crushing. Breaking and falling away of concrete thicker than the cover leads to exposure of the interior aggregate and large portion of the rebar. Damage of this extent requires a different repair strategy where completely removal of loose concrete on the damaged area is necessary. The voids created were then filled with a high strength concrete.

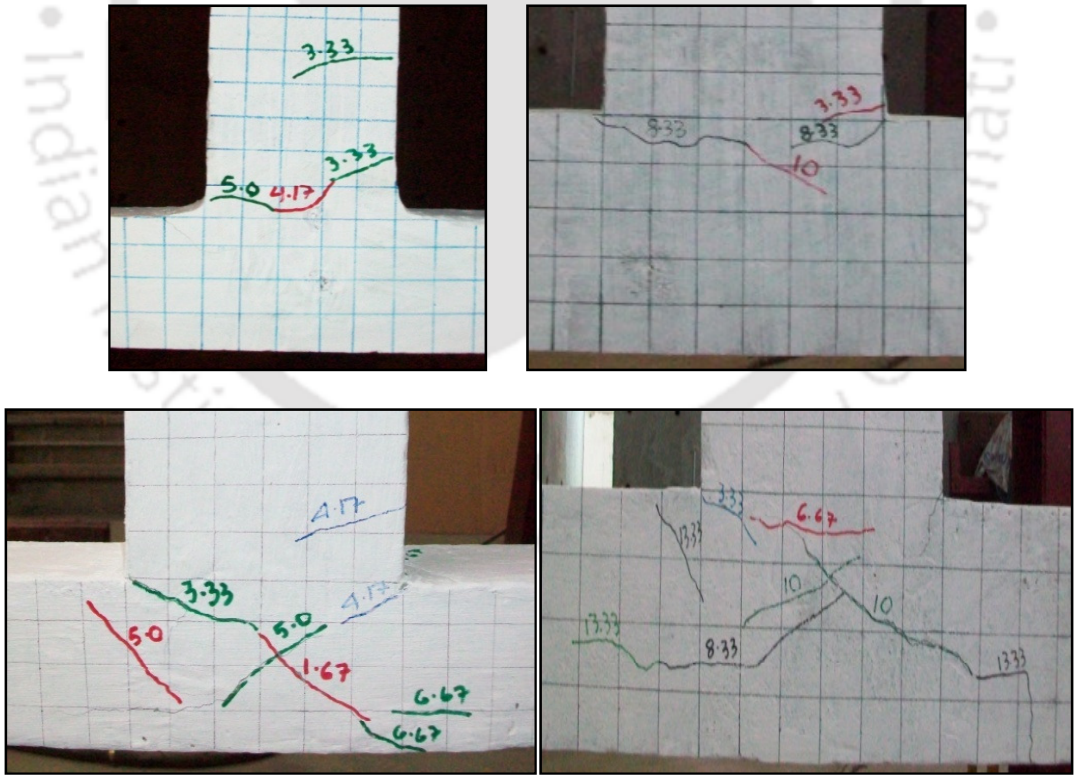

Fig. 8.1 Damage states in RM0 for a typical specimens

Table 8.1 Damage states and associated repair methods

ID	Damage states (*DS*)	Repair method (*RM*)
1.0 1.1 1.2 1.3 1.4	Initial hair line cracking at the beam- column interface. Initial hair line cracking within the joint area. Initial hair line cracking in the beam / column. Max crack width within the joint area is measurable but less than 0.5 mm. Max crack width in the beam / column is measurable but less than 0.5 mm.	*RM0* (Cosmetic repair): Replace and restore surface finish
2.0 2.1 2.2 2.3 2.4	Maximum crack width within the joint area is measurable but less than 5.0 mm Crack width in the beam / column is measurable but less than 2.0 mm. Crushing of concrete at beam-column interface edges. Hinge formation of beam-column interface Large crack of concrete surface within the joint area.	*RM1*: Epoxy resin injections in beam / column and patching of spalled concrete at joint area and epoxy injection.
3.0 3.1 3.2	Cracks extend into beam / column with width greater than 2.0 mm. Crushing of concrete extends to joint core. Failure of connections: (a) Ductile and brittle failure (60-70 % drop of peak load). (b) Buckling of column reinforcement in zone with low shear reinforcement. (c) Buckling of beam reinforcement in zone with low shear reinforcement.	*RM2*: Removal of damaged concrete, replacement with micro concrete and epoxy injection in cracked zone.

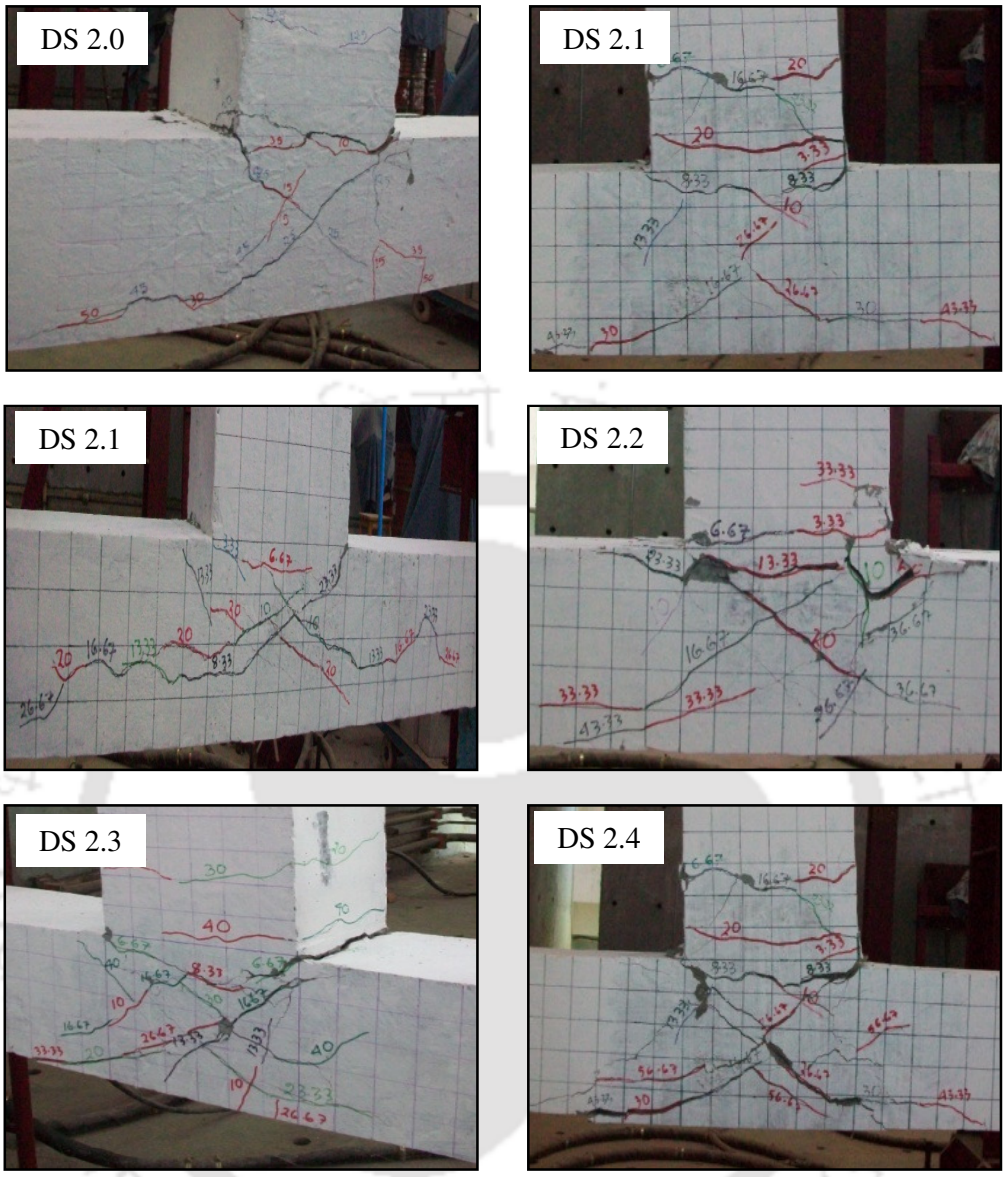

Fig. 8.2 Damage states in RM1 for a typical specimens

(c) Joint failure

Joint failure may be characterized by a loss in lateral or gravity load carrying capacity. Typically, RC components fail as a result of buckling and/or fracture of reinforcing bars. Pagni and Lowes [2006] reviewed experimental data for older joints and identified three potential mechanisms for significant strength loss: loss of gravity load-carrying capacity due to buckling of column longitudinal reinforcement, complete anchorage failure for

beam longitudinal reinforcement passing through the joint which result in loss of beam moment capacity and pull-out of discontinuous beam reinforcement resulting in loss of beam moment capacity. The present study included three typical deficiencies where different failure modes were observed in each deficiency type. Buckling of column reinforcement (*DS* 3.2b) and buckling of beam reinforcement (*DS* 3.2c) in zone with low shear reinforcement are shown in Fig. 8.3.

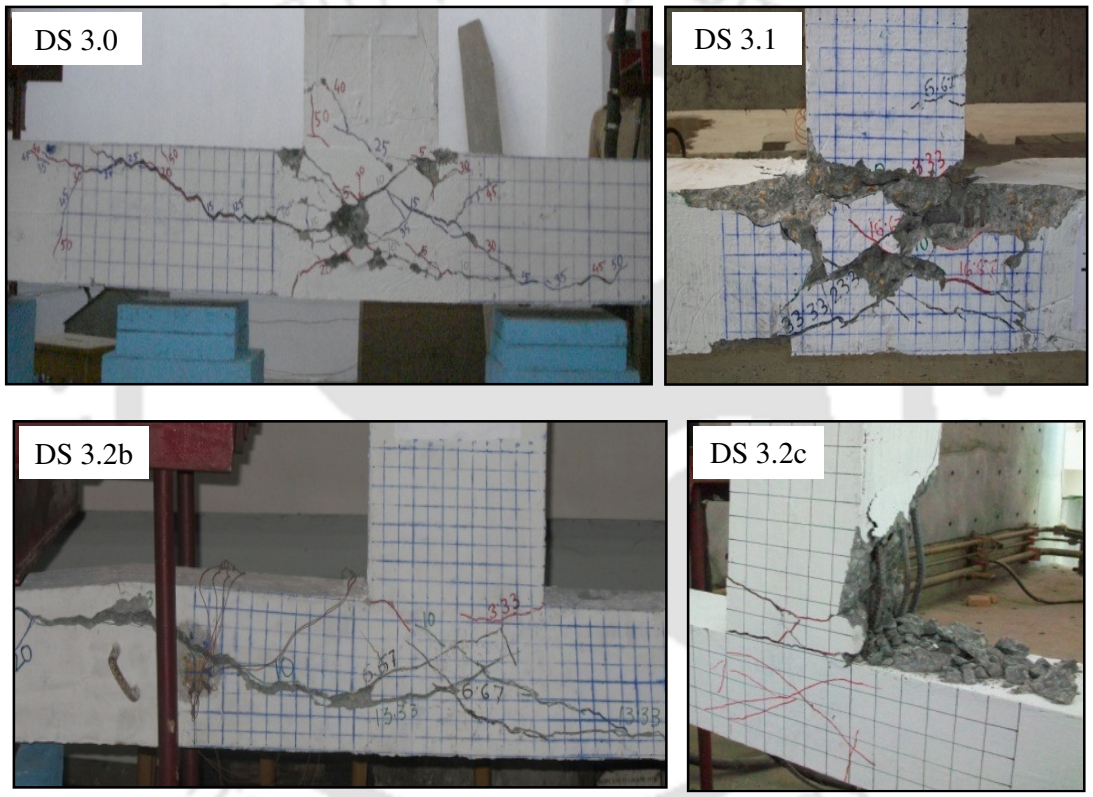

Fig. 8.3 Damage states in RM2 for a typical specimens

8.2.3 Repair methods (*RM*)

Two repair methods (*RM1* and *RM2*) were employed to restore the damaged connections subjected to different loading types to its original capacity. Another repair method included in development of fragility functions is the cosmetic repair (*RM0*). Cosmetic repairs are made when the residual cracks widths are narrow and structural repair is not

necessary. The scope of this repair method is limited to the repair of surface finishes to restore the aesthetic appearances.

8.3 Statistical analysis of damage data

Similar analytical process was used to develop fragility functions for both control and rehabilitated connections. The functions depict the probability of a suitable repair method that a earthquake damaged structural elements will require to restore to its original condition given a specific level of earthquake demand. The collected data were utilized to link *EDPs* with *RMs* using standard probability distributions. The maximum likelihood method was used to fit these distributions to the data. Then, standard goodness-of-fit test was performed to evaluate the distributions. Finally, most suitable distribution was identified for development of fragility function.

8.3.1 Standard probability distributions

Four standard probability distributions were considered to model the data. The distributions considered are lognormal, Weibull, beta (Haldar and Mahadevan, 2000) and gamma (Hayter, 2002). Each of these probability distributions are defined by two parameters that were determined using the method of maximum likelihood. The lognormal distribution was commonly used in most fragility curve analysis [Shinozuka *et al.* (2000), Aslani (2005), Pagni and Lowes (2006), Porter *et al.* (2007a)]. The lognormal distribution includes only positively valued data.

8.3.2 Evaluation of fragility functions

The hypothesis testing to evaluate the fragility functions was first introduced by Shinozuka [2000]. Thus, once the standard probability functions have been fit to the data,

standard goodness-of-fit tests were used to evaluate how well the probability functions model the data. Three standard goodness-of-fit tests were considered the Kolmogorov-Smirov (*K-S*), the Chi- Square (χ^2) and the Lilliefors tests.

(a) Kolmogorov-Smirov (*K- S*) test

The *K-S* goodness-of-fit test is a nonparametric test based on the cumulative distribution function (*CDF*) rather than the probability distribution function (*PDF*) of a continuous variable. The *K-S* test provides a numerical confirmation of the visual analysis for the best fit of the curve when comparing selected distribution function. The *K-S* test requires the computation of D_n , the maximum difference between two *CDFs* defined as:

$$D_n = \max \left| F_X(x_i) - S_n(x_i) \right| \tag{8.6}$$

where D_n, is the *K-S* parameter that depends on the sample size *n.*

$F_x(x_i)$ is the theoretical *CDF* of the assumed distributions at the i^{th} observations of the order of sample x_i

$S_n(x_i)$ is the corresponding stepwise *CDF* of the observed ordered samples.

Goodness-of-fit is determined from the comparison of the K-S parameter (D_n) to the critical value (D_n^{α}) for a selected significance level (α). The critical value is determined from a standard mathematical table where the number of data points and the significance level must be known. The significance level (α) is related to the probability of the K-S test parameter (D_n) as

$$P(D_n \le D_n^{\alpha}) = 1 - \alpha \tag{8.7}$$

According to the *K-S* test, if D_n is less than or equal to the tabulated value of D_n^{α}, the assumed distribution is acceptable at the significance level α. The highest probability determines the best fit distribution. A commonly used confidence level is 95 %, in which

the corresponding significance level is 5 %. Typical *K-S* goodness-of-fit test for one-sample is shown in Fig. 8.4.

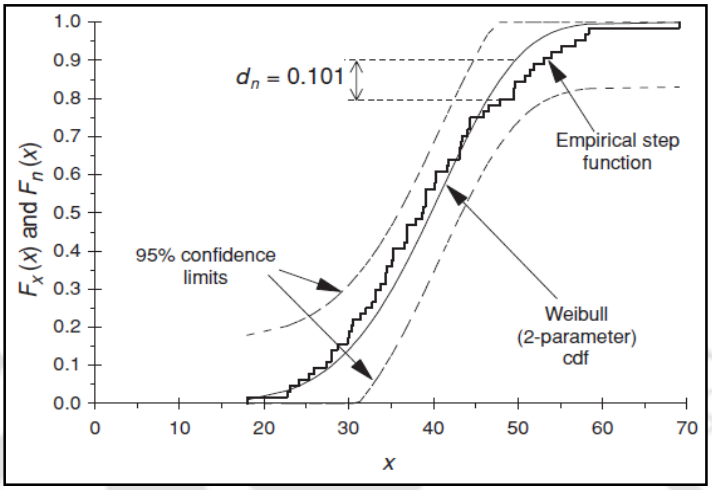

Fig. 8.4 *K-S* for one-sample goodness-of-fit test (Kottegoda and Rossa, 1997)

(b) Chi- Square (χ^2) test

The Chi-square test compares the observed and theoretical frequencies. The observed data are sub-divided into m intervals and the number of observations in each interval n_i is compared with the theoretical number of observations e_i. The theoretical distribution is acceptable at the significance level α if

$$\sum_{i=1}^{m} \frac{(n_i - e_i)^2}{e_i} < c_{1-\alpha,f} \tag{8.8}$$

$$f = m - k - 1 \tag{8.9}$$

where $c_{1-\alpha,f}$ is the value of the χ^2 distribution

f is the degree of freedom

k is the number of parameters in the distribution which is two for all distributions.

In applying the χ^2 test, it is desirable that the numbers of interval (m) and the number of observation (e_i) should be at least 5 for satisfactory results (Haldar and Mahadevan, 2000) and the total number of data points should exceed 50 (Kottegoda and Rosso, 1997).

K-S test has the advantage over the χ^2 test as it is not necessary to divide collected data into number of interval (m). Thus, the error of judgment associated with the number or size of the distribution could be avoided.

(c) Lilliefors test

The Lilliefors test examines the goodness-of-fit of the normal distribution for a given data set (Lilliefors, 1967). This test is appropriate for the small sample size and is exact. For the current study it was used with the log of the data to evaluate the acceptability of the distributions.

8.4 Fragility functions of RC beam-column connections

The experimental data, *EDP*, damage states and repair methods (*RMs*) provides the basis for developing repair-specific fragility functions. These functions define the probability that structures would undergo a particular level of damage which corresponds to a specific repair method to restore the damaged connections to its original condition for a specific level of earthquake demand. Cumulative frequency distribution function was obtained by plotting demand parameter in ascending order for a given damage states which was experimentally observed against $\left(\frac{i-0.5}{n}\right)$, where i is the position of the drift level within the sorted data and n is the samples number. This empirically derived cumulative frequency distribution function provides the portion of the data set which does not exceed a particular value of demand. For a level of damage state, four different probabilities were fitted to the empirical cumulative probability distributions in order to

investigate which probability distribution provides a better fit to the data. Each of these probability distributions were defined by two parameters.

8.4.1 Fragility functions of control specimens

Fig. 8.5 shows the theoretical and empirical fragility functions fitted with different distributions function. These functions predict the probability that a repair method will be suitable for a given earthquake demand. The figure typically compares the empirical cumulative distribution corresponding to the damage states which grouped according to the first repair method (*RM0*) using the four probability distributions. It can be seen that the selected distribution fits the data well and provides comparable good fit to the data. Fig. 8.5 also shows the graphical representations of the *K-S* goodness-of-fit test for 5% significance levels. It can be seen from these figures that all the distributions are valid for this category of damage states under cosmetic repair (*RM0*).

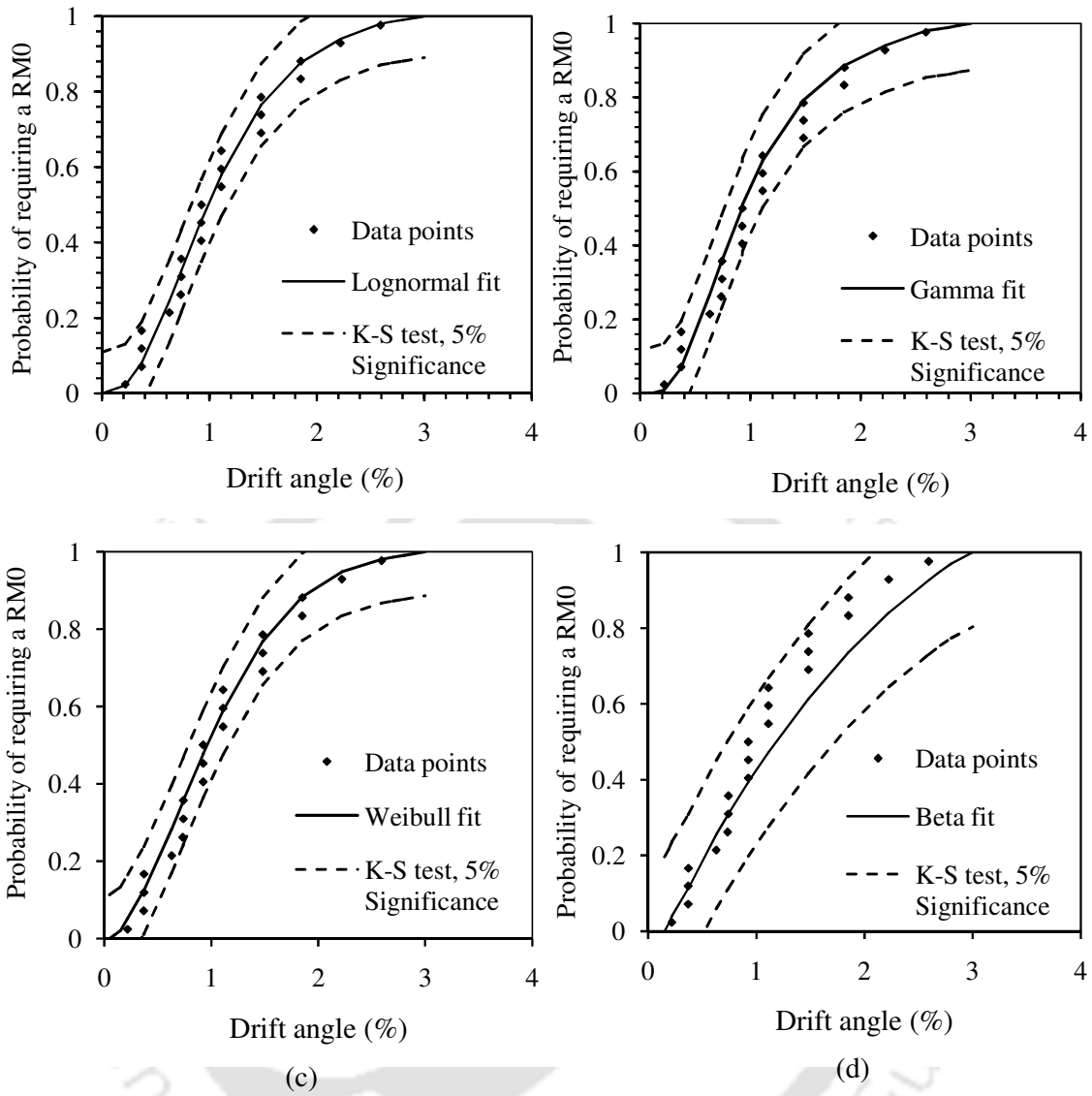

Fig. 8.5 Fragility functions for control specimens under cosmetic repair (*RM0*) defined by four probability distributions: (a) lognormal (b) gamma (c) Weibull and (d) beta.

The fragility functions for all other damage states, which have been grouped according to the repair method using all the four distribution, have been developed. The best distribution is determined using the *K-S* test. The alternative to this test would be the Chi-square test. The *K-S* parameter (D_n) as defined in Eq. 8.6 may be called the error. The error is compared to a critical value (D_n^{α}) for the selected significance level. A commonly

used significance level is 5 %. The values of the defined significance level were obtained from tables VI furnished in Hayter [2002]. The distribution providing the highest probability is considered as the best fit distribution, in which the error will be less than the critical value. The complete results of *K-S* test for each of the selected distributions considered for development of fragility function for control specimens are furnished in Table 8.2. The error values may be compared to the critical values for each of the three repair methods. Comparing the data furnished in Table 8.2, it may be concluded that each of the distribution provided comparable good fit to the data. However, the lognormal distribution provided the best fit among the different distributions followed by the gamma distribution when the critical values for each of the repair method were compared.

The results of Chi-square test for all selected distributions are furnished in Table 8.3. The number of intervals (m) was chosen as 5, significance level (α) was chosen to be 5% and the degree of freedom (f) for all distribution was calculated as 2. The critical values of the Chi-Square distribution were obtained from tables II furnished in Hayter [2002], in which the result of $c_{1-\alpha,f}$ was found to be 5.991 in all cases. The values furnished in Table 8.3 indicate that the Chi-Square value (error) is smaller than the Chi-Square critical value for degree of freedom 2 in all cases. But, the lognormal distributions provided best results among all distributions. However, the applications of Chi-Square are somewhat questionable since it is not satisfied for all cases because of the small size of the data sets.

Table 8.2 *K-S* test results for selected distributions for control specimens

Repair Method		RM0	RM1	RM2
Sample size	n	21	28	19
Critical Value	$\alpha = 0.05$	0.287	0.250	0.301
Lognormal distribution	Median (θ)	0.925	3.923	4.592
	Std. deviation (β)	0.617	0.328	0.298
	K-S parameter (D_n)	0.109	0.062	0.091
	$P(D_n \leq D_n^{\alpha})$	0.938	0.999	0.994
Gamma distribution	Parameter (k)	3.013	9.706	11.74
	Parameter (λ)	0.367	0.425	0.408
	K-S parameter (D_n)	0.113	0.072	0.092
	$P(D_n \leq D_n^{\alpha})$	0.922	0.997	0.993
Weibull distribution	Parameter (k)	1.73	3.601	3.761
	Parameter (w)	1.19	4.444	4.134
	K-S parameter (D_n)	0.125	0.082	0.095
	$P(D_n \leq D_n^{\alpha})$	0.893	0.984	0.989
Beta distribution	Parameter (q)	0.842	2.192	0.885
	Parameter (r)	1.407	4.467	1.055
	Lower bound (a)	0.218	1.587	2.593
	Upper bound (b)	3.11	9.303	7.585
	K-S parameter (D_n)	0.196	0.077	0.140
	$P(D_n \leq D_n^{\alpha})$	0.420	0.992	0.801

Table 8.3 Results of χ^2 test for selected distributions for control specimens

Distributions	Eq. 8.8	RM0		RM1		RM2		Degree of freedom
		Error	*P*	Error	*P*	Error	*P*	
lognormal	$\sum_{i=1}^{m} \frac{(n_i - e_i)^2}{e_i}$	1.329	0.5145	2.659	0.448	0.055	0.814	2
Gamma		1.410	0.4942	2.755	0.431	0.024	0.877	2
Weibull		1.727	0.422	2.664	0.446	1.049	0.592	2
Beta		1.859	0.3948	0.696	0.874	0.971	0.615	2
Critical value	$c_{1-\alpha,f}$							5.991

Note: $P\ (D_n \leq D_n^{\alpha}) = P$

To quantify the quality of lognormal distribution, Lilliefors goodness-of-fit test were performed. This test is a variant of the *K-S* test and is used when the distribution parameters are unknown (Lilliefors, 1967). The test parameters (D_n) of the Lilliefors test corresponds to the maximum differences between the empirical cumulative distribution functions and the CDF proposed for the observed samples. The null hypothesis (*Ho*) for the Lilliefors test is that the population *X* comes from the hypothesized probability distribution. At a specified significance level (α), if D_n is less than or equal to D_{crit}, the null hypothesis is accepted. The D_{crit} associated with selected values of sample sizes were obtained from tables I furnished in Lilliefors [1967]. The parameters of the lognormal distribution were estimated using the method of maximum likelihood and evaluated using Lilliefors goodness-of-fit test are furnished in Table 8.4. The table showed lognormal distribution is acceptable in all cases.

Table 8.4 Lognormal distribution parameters of control specimens and the corresponding Lilliefors test results

Repair Group	Lognormal		Lilliefors test results			
	θ	β	D_{crit}	D_n		*Ho*
RM0	0.925	0.617	0.188	0.109		Accept
RM1	3.923	0.328	0.169	0.062	$D_n < D_{\text{crit}}$	Accept
RM2	4.592	0.298	0.195	0.091		Accept

As mentioned earlier, many researchers [Shinozuka *et al.* (2000), Aslani (2005), Pagni and Lowes (2006), Porter *et al*. (2007a)] developed fragility functions based on experimental results using different probability distributions. It was reported that lognormal distribution is the best fit for variety of structural component failure. In this study, it was observed on the basis of different applied goodness of fit test that each of the distribution provides comparable good fit to the data. However, the lognormal distribution provided the best fit among all the distributions. Therefore, in this study the fragility functions fitted by lognormal distribution are only presented in Fig. 8.6. The lognormal distribution was chosen as the preferred distribution because (i) the lognormal distribution is commonly used for definition of fragility function and (ii) goodness-of-fit test results indicates that lognormal distribution provided the best fit among all the distributions.

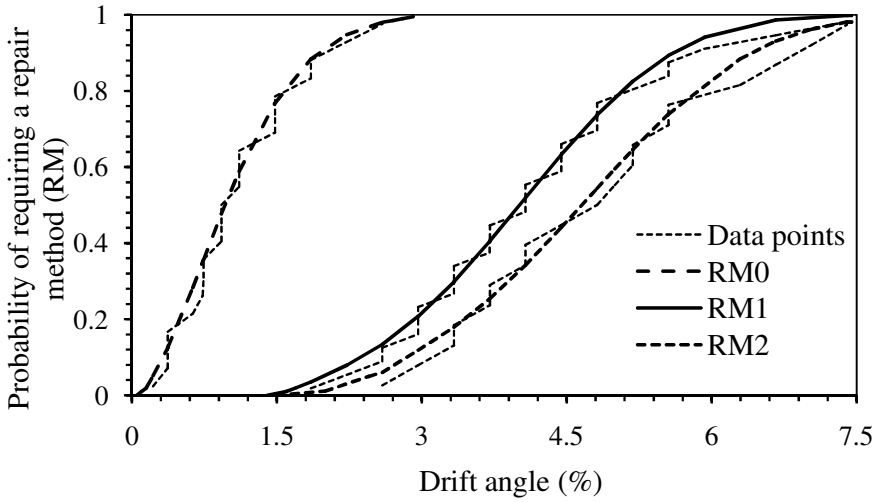

Fig. 8.6 Fragility function of control specimens evaluated using the lognormal distribution

8.4.2 Fragility functions of rehabilitated specimens

Probabilistic fragility curves were also developed for the rehabilitated connections. The control specimens which were damaged under different types of loading were rehabilitated with different repairing strategies and retested under similar loading sequence. The progression of damaged in each specimens were also monitored at various stages of loading. The fragility functions for rehabilitated connections were developed using similar procedure as that for control connections considering the same level of damage states.

Fig. 8.7 shows the functions considering different distributions function. This figure typically compares the empirical cumulative distribution corresponding to the damage states which grouped according to the first repair method (*RM0*) using the four probability distributions. The figures indicate that all selected distribution comparable fit to the data well. The test indicates that all the assumed distribution functions valid for this category of damage states. Similarly, goodness-of-fit test were also performed and

observed that all the distributions were also valid for the other two levels of damage states as well.

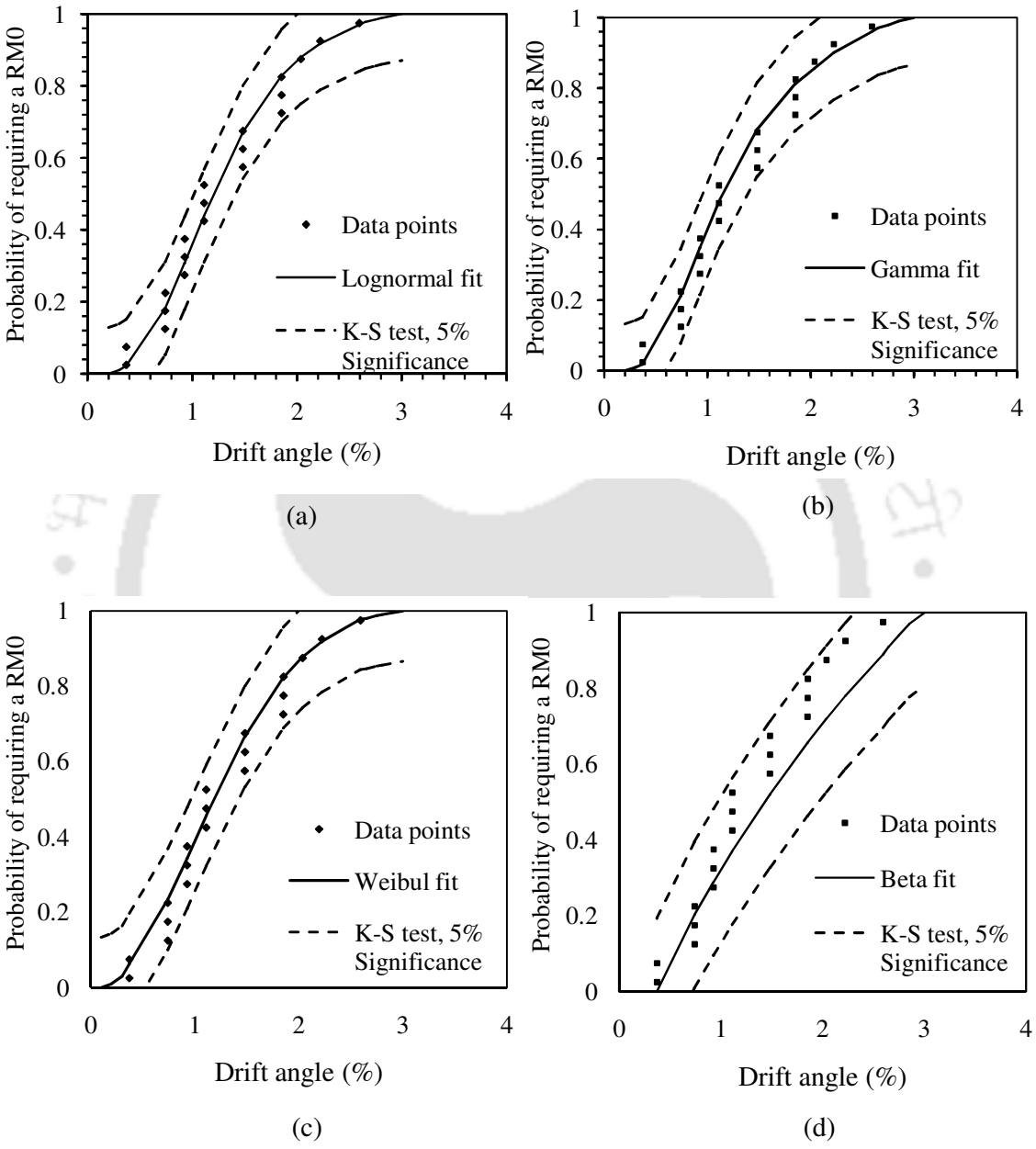

Fig. 8.7 Fragility functions for rehabilitated specimens under cosmetic repair (*RM0*) defined by four probability distributions: (a) lognormal (b) gamma (c) Weibul and (d) beta.

Similar to the control connections, fragility functions with damage states using all four probability distributions were developed. The standard goodness of fit test was performed. The complete results of the test for each of the selected distribution are furnished in Table 8.5 and 8.6. The test results revealed that each of the distribution provided comparable good fit to the data. However, on comparing the critical values for each repair method, it is observed that the lognormal distribution provided the best fit among all the distributions. Further, the Lilliefors test as shown in Table 8.7 indicates that the lognormal distribution is correct for all cases. Fig. 8.8 illustrates the fragility functions of the rehabilitated connections (represent with thick lines). For comparison purpose, the fragility curves of the specimens before rehabilitation are also presented as dotted lines. It can be observed from this figure that both the curves (before and after rehabilitation) for each repair method show a similar shape. Therefore, the probability of suitability a repair method was also nearly the same.

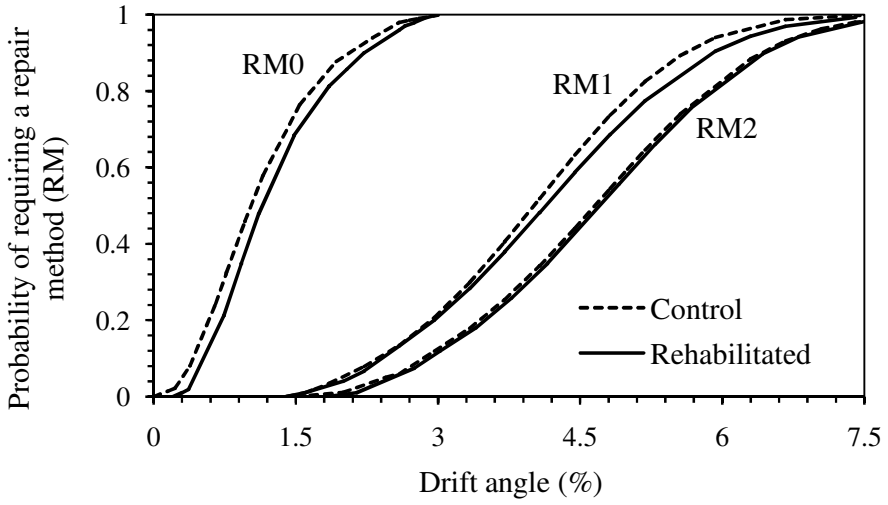

Fig. 8.8 Fragility functions for rehabilitated specimens evaluated using lognormal distribution

Table 8.5 *K-S* test results for selected distributions for rehabilitated specimens

Repair Method		RM0	RM1	RM2
Sample size	n	20	24	16
Critical Value	α=0.05	0.294	0.269	0.327
Lognormal distribution	Median (θ)	1.144	4.05	4.555
	Std. deviation (β)	0.542	0.338	0.287
	K-S parameter (D_n)	0.129	0.078	0.169
	$P(D_n \leq D_n^{\alpha})$	0.855	0.991	0.691
Gamma distribution	Parameter (k)	4.39	8.807	12.45
	Parameter (λ)	0.295	0.485	0.383
	K-S parameter (D_n)	0.131	0.094	0.153
	$P(D_n \leq D_n^{\alpha})$	0.819	0.969	0.796
Weibull distribution	Parameter (k)	2.039	3.388	3.827
	Parameter (w)	1.415	4.61	5.082
	K-S parameter (D_n)	0.133	0.112	0.160
	$P(D_n \leq D_n^{\alpha})$	0.796	0.891	0.748
Beta distribution	Parameter (q)	0.891	0.831	0.653
	Parameter (r)	1.248	1.268	0.955
	Lower bound (a)	0.37	2.222	2.963
	Upper bound (b)	3.112	8.889	7.407
	K-S parameter (D_n)	0.194	0.202	0.124
	$P(D_n \leq D_n^{\alpha})$	0.392	0.247	0.940

Table 8.6 Results of χ^2 test for selected distributions for rehabilitated specimens

Distributions	Eq. 8.8	RM0		RM1		RM2		Degree of freedom
		Error	*P*	Error	*P*	Error	*P*	
lognormal	$\sum_{i=1}^{m} \frac{(n_i - e_i)^2}{e_i}$	1.542	0.463	2.959	0.398	0.330	0.566	2
Gamma		1.698	0.428	0.418	0.936	0.484	0.487	2
Weibull		1.726	0.422	0.288	0.962	0.031	0.860	2
Beta		2.982	0.225	0.237	0.983	0.0938	0.760	2
Critical value	$c_{1-\alpha,f}$							5.991

Note: $P(D_n \leq D_n^{\alpha}) = P$

Table 8.7 Lognormal distribution parameters for rehabilitated specimens and the corresponding Lilliefors test results

Repair Group	Lognormal		Lilliefors test results			
	θ	β	D_{crit}	D_n		*Ho*
RM0	1.144	0.542	0.190	0.129		Accept
RM1	4.050	0.338	0.182	0.078	$D_n < D_{crit}$	Accept
RM2	4.550	0.287	0.180	0.213		Accept

8.5 CONCLUDING REMARKS

In this chapter, fragility functions for both control and rehabilitated exterior RC beam-column connections were developed considering the results of current experimental studies. The results of this effort were families of fragility functions that indicate the required repair method for a damaged connection. Four standard probability distributions were used to model data. Goodness-of-fit tests were employed to decide the best fit distributions. The results of the goodness-of-fit test showed that each of the distributions

provided comparable fit to the data. However, in general the lognormal distributions provided the most acceptable probabilities when compared to the critical values for each of the repair method were compared. Finally, the developed fragility functions for control specimens and corresponding rehabilitated specimens were observed to be of similar shape and therefore, the probability of requiring a repair method was also nearly the same.

CHAPTER 9

SUMMARY AND CONCLUSIONS

9.1 SUMMARY

In the present study, the performances of RC exterior beam-column connections under cyclic loading were evaluated and documented in terms of various parameters related to seismic capacity such as load carrying capacity, stiffness degradation, energy dissipation, displacement ductility etc. Three common types of deficiencies in RC beam-column connections were considered namely (a) beam-column connections with beam weak in flexure (BWF), (b) beam-column connections with beam weak in shear (BWS) and (c) beam-column connections with column weak in shear (CWS). In each type, three geometrically similar specimens: full, two-third and one-sthird scaled sizes were considered. These specimens were treated as control (undamaged) specimens. In order to explore the effect of loading type, three different loading types were considered in the test program. The different loading types considered in the test program were characterized by a number of cycles for a particular displacement (type-1 and type-2) and frequency of excitations (type-3). Depending on the extent of damages, the damaged control specimens were rehabilitated by adopting two rehabilitation strategies. Forty two specimens were tested (eighteen specimens each under loading type-1 and type-2 and six specimens under loading type-3) consisting of control and rehabilitated types of three different sizes. The design of control specimens with beam weak in flexure were done following provisions of the relevant design codes, while all the provisions of code were not followed for the specimens of other two types in order to attain a predefined deficiency. A typical full scale residential building with floor to floor height as 3.3 meters and the beam of 3.0

meters effective span were considered. Two-third and one-third sized specimens were proportionately scaled down in all the three dimensions. The diameter of the reinforcing bars, development length, length of special confinement zone, cover of reinforcement, coarse aggregate etc. were also scaled down appropriately.

Displacement controlled loading was applied to all the specimens using a servo hydraulic dynamic actuators (MTS make). The amplitudes of the displacement histories as reported by Choudhury [2010] have been adopted in this study. Amplitude of the displacement histories were scaled down for two-third and one-third models respectively. The experiment for control specimens were stopped at a stage when the load came down in the range of 60-70 % of the ultimate load carrying capacity. Similarly, the experiments on rehabilitated specimens were also stopped at about similar range. The ultimate load carrying capacity of all the forty two specimens as obtained by experimental investigation have been furnished in the respective chapters.

The rehabilitation strategy was aimed to retrieve back the lost capacity of the damaged connections to the original seismic capacity in term of the previous mentioned important seismic capacity related parameters. Two rehabilitation strategies were employed depending on the extent of damages. These were (a) partial removal of loose concrete on the damaged area and the voids created were replaced with micro concrete followed by epoxy injection into crack zone and (b) complete removal of crushed concrete on the damaged area and the voids created were replaced with micro concrete followed by epoxy injection into crack zone.

The analysis of results revealed that the rehabilitated RC beam-column connections under loading type-1 and type-2 exhibited equal or marginally better performance than the corresponding control specimens and hence the adopted rehabilitation strategy could be considered as satisfactory. It was also observed that the number of cycles for a particular

amplitude did not significantly influence the ultimate load carrying capacity of the specimens. Further, the analysis of results based on various parameters related to seismic capacity such as ultimate load carrying capacity, energy dissipation, stiffness degradation etc revealed that the adopted rehabilitation strategy for specimens subjected to cyclic displacement of higher frequency also satisfactorily restored the damaged connections. Comparison of the performances of the connections under two different loading frequencies, it was observed that the load carrying capacity and energy dissipations were slightly higher for the specimens tested under higher loading frequency, which could be attributed to strain rate effect. The damage patterns and failure of the connections showed that damages were mostly concentrated at a particular zone during higher loading frequency testing as compared to those under lower loading frequency. Further, BWS specimens showed poor performance among all the deficient specimens during high cyclic loading frequency test.

The results obtained from test were examined to explore the existence of size effect. Analyzed results were used for drawing bi-logarithmic plot. For the purpose of statistical regression of data, the size effect law proposed by Bažant [1984] was used. Different plots were drawn for control and rehabilitated specimens in each of the cases. In all the cases, it was found that these graphs followed the well established size effect law as proposed by Bažant [1984]. It was also noted that, cumulative energy dissipated per unit volume of the D-region at every drift angle for small specimen was the maximum and it decreased as the specimen size increased. This is an indication for existence of size effect. The variation of stress with respect to relative deflection also agrees with the size effect principle in all cases. Further, size effect was observed to be more and more prominent as the specimens behave in more and more brittle manner.

A well known damage model i.e the Park and Ang [1985] damage index model were employed for evaluating the damage indices of the connections in both controls as well as rehabilitated specimens. Most of the rehabilitated specimens presented lower damage indices, indicating that the adopted rehabilitation strategy was effective. Further, the calculated indices also correlated well with the extent of actual observed damage during experimentation.

Based on the above study, guidelines for rehabilitation of beam-column connections were prepared. The guideline correlated the physical damage of specimens and the repair methods for restoring the damaged specimens to original state. Quality of concrete in the repaired zone was also correlated to the repair method based on Ultrasonic Pulse Velocity (UPV) test. These guidelines would thus be useful to the field engineers while taking decision on identification of an appropriate rehabilitation strategy during post disaster period.

Fragility functions for exterior RC beam-column connections were developed considering the results of current experimental studies. The results of this effort were families of fragility functions that identify the required repair method for a damaged connection. Four standard probability distributions were used to model data both control and rehabilitated specimens. Goodness-of-fit tests were employed to decide the best fit distributions. The results of the goodness-of-fit test showed that each of the distributions provided comparable fit to the data. However, in general the lognormal distributions provided the most acceptable probabilities when compared to the critical values for each of the repair method. Finally, the developed fragility functions for control specimens and corresponding rehabilitated specimens were observed to be of similar shape. Therefore, the probability of suitability a repair method was also nearly the same.

9.2 MAJOR CONCLUSIONS

Based on experimental studies carried out on RC beam-column connections under different loading types, the following conclusions have been drawn:

1. Comparison of important parameters related to seismic capacity showed that the adopted rehabilitation strategy was satisfactory as the damaged connections after rehabilitation exhibited equal or marginally better performance.
2. Numbers of cycles for a particular displacement amplitude did not greatly influence the ultimate load carrying capacity of the specimens.
3. It was observed that the bi-logarithmic plots for both control and rehabilitated specimens followed closely the size effect law as proposed by Bažant in all the cases studied.
4. The cumulative energy dissipated per unit volume at every drift angle indicated the existence of size effect. This established that the energy dissipation per unit volume increased as the specimen size decreased**.**
5. The variation of stresses with respect to relative deflection showed the existence of size effect for all the cases studied.
6. Comparison of the performance of the connections under two different loading frequencies (type-2 and type-3) showed that the load carrying capacity and energy dissipation were slightly higher for the specimens tested under higher loading frequency.
7. Most of the rehabilitated specimens presented lower damage indices as compared to that for corresponding control specimen. This indicates that the adopted rehabilitation strategy was effective.

8. The developed fragility functions for control specimens and corresponding rehabilitated specimens were of similar shape and therefore, probability of suitability a repair method was also nearly the same.

9.3 SCOPE FOR FUTURE WORK

Additional work may be undertaken in the following areas:

1. Three typical deficiencies of RC beam-column connections were considered in the present study. The prohibitive cost of material and manpower primarily limited the number of such deficiency types. However, other possible deficiency types may be considered for further investigation.
2. The present study was considered two rehabilitation techniques. However, other techniques such as vacuum impregnation may also be adopted to rehabilitate different similar types of damaged deficient specimens.
3. Three different sizes of specimens were considered for size effect investigation in the present study. However, specimens with more numbers of sizes may be attempted for better acceptability of results.
4. Most of the tests conducted for RC beam-column connections considered quasi-static loading to investigate the change in structural behaviour. Seismic loading is truly random and fast, it does have a considerable impact on the structural response. Thus, a higher and varying loading frequency can be considered for further studies.
5. Additional experimental data are required to develop more accurate fragility functions. This requires additional testing of RC beam-column connections.

REFERENCES

Abdel-Fattah, B., and Wight, J. K. (1987). "Study of moving beam plastic hinging zones for earthquake-resistant design of reinforced concrete buildings." *ACI, Structural Journal*, 31-39.

ACI-224r (1994a). "Control of cracking in concrete structures." ACI, Manual of Concrete Practice, Detroit, Michigan.

ACI Com. 546 (1996). "Concrete Repair Guide." Farmington Hills: ACI. Applied Technology Council (1998). FEMA 308: Repair of Earthquake Damaged Concrete and Masonry Wall Buildings. Washington D.: FEMA.

ACI 352R-02 (2002). "Recommendations for design of beam-column-joints in monolithic reinforced concrete structures." *American Concrete Institute*, ACI-ASCE, Committee 352, Detroit.

ACI 318 (2005). "Building code requirements for structural concrete."

ACI 318-08 (2008). "Building code requirements for structural concrete and commentary."

Agbabian, M.S., Higazy, E. M., Abdel-gaffar, A. M., and Elnashai, A. S. (1994). "Experimental observations on the seismic shear performance of RC beam-column connections subjected to varying axial column force." *Earthquake Engineering and Structural Dynamics, 23*, 859-876.

Alcocer, M., and Jirsa, J. O. (1993). "Strength of reinforced concrete frame connections rehabilitated by jacketing." *ACI, Structural Journal*, 249-261.

Al-Salloum, A. Y., and Almusallam, T. H. (2007). "Seismic response of interior RC beam-column joints upgraded with FRP sheets I: Experimental study." *Journals of Composite for Constructions*, ASCE, 11(6), 575-589.

Alsayed, S. H., Al-Salloum, Y. A., Almusallam, T. H., and Siddiqui, N. A. (2010). "Seismic response of FRP-upgraded exterior RC beam-column joints." *Journal of Composites for Construction, ASCE*, 14(2), 195-208.

Ang, A. H. S., and Tang, W. H. (1975). "*Probability Concepts in Engineering Planning and Design. "Vol. 1—Basic Principles*, John Wiley & Sons, New York.

Ang, A.H-S., Kim, W. J., and Kim, S. B. (1993). "Damage estimation of existing bridge structures." *Structural Engineering in Natural Hazards Mitigation*, ASCE Structures Congress, Irvine, CA, Proceedings, 2, 1137-1142.

Applied Technology Council, ATC-13 (1985). "Earthquake damage evaluation data for California." Applied Technology Council, Redwood City, California.

Aslani, H. (2005). "Probabilistic Earthquake Loss Estimation and Loss Disaggregation in Buildings." *Doctoral Thesis*, Stanford University, Stanford, CA.

Bažant, Z. P. (1984). "Size effect in blunt fracture: Concrete, rock, metal." *Journals Engineering Mechanics*, ASCE, 110(4): 518–535.

Bažant, Z. P., and Pfeiffer, P.A. (1986). "Shear fracture tests of concrete." *Materials and Structure*, 19,111-121.

Bažant, Z. P., and Pfeiffer P., A. (1987). "Determination of fracture energy from size effect and brittleness number." *ACI Materials Journals*, 84(6), 463-480.

Bažant, Z. P., and Planas, J. (1998). "Fracture and size effect in concrete and other quasibrittle materials." CRC Press, Boca Raton: Fla.

Banon, H., Biggs., and Irvine, H. M. (1981). "Seismic damage in reinforced concrete frames." *Journals of Structural Engineering*, ASCE, 114(7), 1588-1605.

Belgin, C. M., and Sener, S. (2008). "Size effect on failure of overreinforced concrete beams." *Engineering Fracture Mechanics*, Elsevier, 75(8), 2308-2319.

Beres, A., EI-Borgi., White, R. N., and Gergely, P. (1992). "Experimental results of repaired and retrofitted beam-column joint tests in lightly reinforced concrete frame buildings." Technical report NCEER-92-0025, SUNNY/Buffalo.

Bindiganavile, V., and Banthia, N. (2006). "Size effects and the dynamic response of plain concrete." *Journal of Materials in Civil Engineering*, ASCE, 18(4), 485-491.

Bligh, R. A., Fischer, S., and Ghosh, S. K. (2005). "Structural retrofit of special moment-resisting frames of concrete." *Concrete International*, 27(6), 47-53.

Bracci, J. M., Reinhorn, A. M., Mander, J. B., and Kunnath, S.K. (1989). "Deterministic model for seismic damage evaluation of RC structures." Technical Report NCEER-89-0033, National Center for Earthquake Engineering Research, State University of New York, Buffalo, NY.

Chutarat, N., and Aboutaha, R. S. (2003). "Cyclic response of exterior reinforced concrete beam-column joints reinforced with headed bars-experimental investigation." *ACI, Structural Journal*, 100(2), 259-264.

Chung, Y. S., Meyer, C., and Shinozuka, M. (1990). "Automatic seismic design of reinforced concrete building frames." *ACI, Structural Journal*, 87(3), 326-340.

Choudhury, A., M. (2010). "Study on size effect of RC beam-column connections with and without retrofitting under cyclic loading." *Doctoral Thesis*, Department of Civil Engineering, Indian Institute of Technology, Guwahati, India.

Corazao, M., Durrani, A. J., and Taylor, H. (1988). "Repair and strengthening of concrete structures damaged by earthquakes." *Ninth World Conference on Earthquake Engineering*, Tokyo-Kyoto, Japan, VII-389,VII-394.

Corazao, M., and Durrani, A. J. (1989). "Repair and strengthening of beam-to-column connections subjected to earthquake loading." Technical report NCEER-89-0013, National Center for Earthquake Engineering Research, State University of New York at Buffalo, N.Y.

Corazao, M., Duranni, A.J., and Taylor, H. (1988). "Repair and strengthening of concrete structures damaged by earthquake." Proceeding of Ninth World Conference on Earthquake Engineering, Vol. III, Tokyo-Kyoto, Japan, 389-395.

Cosenza, E., Manfredi, G., Ramasco, R. (1993). "The use of damage functionals in earthquake engineering: a comparison between different methods." *Earthquake Engineering and Structural Dynamics*; 22:855–868.

Dhakal, R. P., and Pan, T. C. (2003). "Characteristic of high-speed cyclic test of beam-column joint." *ACI, Structural journals,* 100 (2), 188-196.

Dhakal, R. P., Pan, T. C., Irawan, P., Tsai, K. C., Lin, K. C., and Chen, C. H. (2005). "Experimental study on the dynamic response of gravity-designed reinforced concrete connections." *Engineering Structures,* Elsevier *27*, 75-87.

Durrani, A. J., and Wight, J. K. (1985). "Behaviour of interior beam-to-column connections under earthquake-type loading." *ACI Journal Proceedings*, 82(3), 343-349.

Ehsani, M. R., and Alameddine, F. (1991). "Design recommendations for type 2 high-strength reinforced concrete connections." *ACI, Structural Journal*, 277-291.

El-Amoury, T., and Ghobarah, A. (2002). "Seismic rehabilitation of beam-column joints using GFRP sheets." *Engineering Structures*, 24, 1397-1407.

Elfahal, M. M., Krauthammer, T., Ohno, T., Beppu, M., and Mindess, S. (2005). "Size effect of normal strength concrete cylinder subjected to axial impact." *International Journal of Impact Engineering*, Elsevier, 31,461-481.

Federal Emergency Management Agency (FEMA). "Repair of Earthquake Damaged Concrete andMasonry Wall Buildings." FEMA 308 (1998): 24-42.

Filiatrault, A., and Isabelle Lebrun. (1996). "Seismic rehabilitation of reinforced concrete joints by epoxy pressure injection technique." *ACI,* SP 160-3.

FIB Bulletin 24 (2003)."Seismic assessment and retrofit of reinforced concrete buildings." State-of-art report prepared by Task Group, 7.1, 306.

French, C.W., Thorp, G.T., Tsai, W. (1990). "Epoxy repair techniques for moderate earthquake damage." *ACI, Structural Journal*, 87(4), 416,424.

Ghobarah, A., and Said, A. (2002). "Shear strengthening of beam-column joints." *Engineering Structures*, 24 (7), 881-888.

Gosain, N.K., Brown, R.H., and Jirsa, J. O. (1977). "Shear requirement for load reversals on RC members." *Journal of Structural Engineering*, ASCE, 103 (7), 1461-1476.

Gulec, C. K., Whittaker, A. S., and Hooper, J. D. (2010). "Fragility functions for low aspect ratio reinforced concrete walls." *Engineering Structures*, Elsevier, 32(9), 2894-2901.

Hadi, M. N. S. (2010). "Rehabilitating destructed reinforced concrete T- connections by steel strap." *Journal of Construction and Building materials*, Elsevier, 25(2), 851-858.

Hanson, N.W., and Connor, H.W. (1967). "Seismic resistance of reinforced concrete beam-column Joints." *Journal of Structural Division*, 93, 533-560.

Hakuto, S., Park, R., and Tanaka, H. (2000). "Seismic load tests on interior and exterior beam-column joints with substandard reinforcing details." *ACI, Structural Journal*, 97(1), 11-25.

Haldar, Achintya and Sankaran Mahadevan. (2000). "Probability, Reliability, and Statistical Methods for Engineering Design." John Wiley & Sons, Inc.

Hayter, A. J. (2002). "Probability and statistic for engineers and scientists." Duxbury, Thompson Learning, USA.

IS 456 (2000). "Plain and reinforced concrete - Code of Practice." Bureau of Indian Standard, New Delhi.

IS 1608 (1995). "Mechanical testing of metals - tensile testing." Bureau of Indian Standard, New Delhi.

IS 1893 (I) (2002). "Criteria for earthquake resistant design of structures - Part 1 : General provisions and buildings." Bureau of Indian Standard, New Delhi.

IS 2386: Part 1 (1963). "Methods of test for aggregates for concrete - Part 1: Particle size and shape." Bureau of Indian Standard, New Delhi.

IS 2386: Part 3 (1963). "Methods of Test for aggregates for concrete - Part 3: Specific gravity, Density, Voids, Absorption and Bulking." Bureau of Indian Standard, New Delhi.

IS 432 : Part 1 (1982). "Specification for mild steel and medium tensile steel bars and hard-drawn steel wire for concrete reinforcement: Part I Mild steel and medium tensile steel bars.: Bureau of Indian Standard, New Delhi.

IS 4031: Part 4 (1988). "Methods of physical tests for hydraulic cement: Part 4 Determination of consistency of standard cement paste." Bureau of Indian Standard, New Delhi.

IS 4031: Part 5 (1988). "Methods of physical tests for hydraulic cement: Part 5 Determination of initial and final setting time." Bureau of Indian Standard, New Delhi.

IS 4031: Part 6 (1988). "Methods of physical tests for hydraulic cement: Part 6 Determination of compressive strength of hydraulic cement (other than masonry cement)." Bureau of Indian Standard, New Delhi.

IS 4031: Part 11 (1988). "Methods of physical tests for hydraulic cement: Part 11 Determination of Density." Bureau of Indian Standard, New Delhi.

IS 12269 (1987). "Specification for 53 grade ordinary Portland cement." Bureau of Indian Standard, New Delhi.

IS 13311: Part 1(1992). "Non-destructive testing of concrete: Part 1 Ultrasonic pulse velocity." Bureau of Indian Standard, New Delhi.

IS 13920 (1993). "Ductile detailing of reinforced concrete structures subjected to seismic forces- Code of Practice." Bureau of Indian Standard, New Delhi.

Issa, C. A., and Debs, P. (2007). "Experimental study of epoxy repairing of cracks in concrete." *Construction and Building Materials*, Elsevier, 21, 157-163.

Jain, S.K., and Murty, C.V.R. (2006). "Proposed draft provision and commentary on ductile detailing of RC structures subjected to seismic forces." Document No. :: IITK-GSDMA-EQ11-V-3.0 :: IITK-GSDMA-EQ16-V2.0.

Jeng ,Y. S., and Shah, S. P. (1985). "A fracture toughness criteria for concrete." *Engineering Fracture mechanics*, 21(50), 1055-1069.

Jeong, S. H., Elnashai, A. S. (2004). "Parametrized vulnerability functions for as–built and retrofitted structures." PEER Report 2004/05, Proceedings of International Workshop on performance–based seismic design concepts and implementation, Bled Slovenia, 185–196.

Jeong, G.D., and Iwan, W.D. (1988). "Effect of earthquake duration on the damage of structure." *Earthquake Engineering and Structural Dynamics,* 16(8), 1201-1211

Joshi, M. K., Murty, C.V.R., and Jaisingh, M.P. (2005). "Cyclic behaviour of precast RC connections." *The Indian Concrete Journal*, 79(11), 43-50.

Karayannis, C. G., Chalioris, C. E., and Sideris, K.K. (1998). "Effectiveness of RC beam-column connection repair using epoxy resin injections." *Journal of Earthquake Engineering*, 2(2), 217-240.

Karayannis, C. G., Chalioris, C. E., and Sirkelis, G. M. (2008a). "Local retrofit of exterior beam-column joints using thin RC jackets-An experimental study." *Journals of Earthquake Engineering and Structural Dynamics*, 37, 727-746.

Karayannis, C. G., and Sirkelis, G.M. (2008b). "Strengthening and rehabilitation of RC beam-column joints using C-FRP jacketing and epoxy resin injection." *Journals of Earthquake Engineering and Structural Dynamics*, 37, 769-790.

Krauthammer, T., Elfahal, M. M., Ohno, T., Beppu, M., and Mindess, S. (2003). "Size effect of high strength concrete cylinder subjected to axial impact." *International Journals of Impact Engineering*, Elsevier, 28, 1001-1016.

Koc, V., and Sener, S. (2009). "Size effect in normal- and high-strength concrete with different notches under the axial load." *Journal of Materials in Civil Engineering*, ASCE, 21(9), 433-445.

Kottegoda, N. T., and Rosso, R. (1997). "Applied statistics for civil and environmental engineers." The McGraw-Hill Companies, Inc.

Kunnath, S. K., Reinhorn, A. M., and Lobo, R. F. (1992). "IDARC version 3.0: A program for inelastic damage analysis of RC structures." Technical Report NCEER-92-0022, National Center for Earthquake Engineering Research, State University of New York, Buffalo, NY.

Kratiz, W. B., Meyer, I.F., and Meskouris, K. (1989). "Damage evolution in reinforced concrete members under cyclic loading." *Proceedings 5th International Conference on Structural Safety and Reliability (ICOSSAR 89),* San Francisco, CA, Vol. II, 795-802

Leung, C. K. Y., Chen, Z., Lee, S. Ng, M., Xu, M., and Tang , J. (2007). "Effect of size on the failure of geometrically similar concrete beams strengthened in shear with FRP strips." *Journal of Composites for Construction*, ASCE, 11(5), 487-496.

Lignos, D. G., Kolios, D., and Miranda, E. (2010). "Fragility assessment of reduced beam section moment connections." *Journal of Structural Engineering*, ASCE, 136(9), 1140-1150.

Li B., and Kulkarni, S. A. (2010). "Seismic behavior of reinforced concrete exterior wide beam-column joints." *Journals of Structural Engineering*, ASCE, 136(1), 36-36.

Lilliefors, H., W. (1967). "On the K-S Test for Normality with Mean and Variance Unknown." *Journal of the American Statistical Association*,62: 399-402.

Megget, L. M., and Park, R. (1971). "Reinforced concrete exterior beam-column joints under seismic loading." *New Zealand Engineering*, 26(11), 341-353.

Moshe, A. A., Yankelevsky, D. Z., and Farhey, D. N. (1993). "Cyclic behavior of epoxy-repaired reinforced concrete beam-column joints." *ACI, Structural Journals*, 90(2), 170-179.

Mosallam, A. S. (2000). "Strength and ductility of reinforced concrete moment frame connections strengthened with quasi-Isotropic laminates." *Composites Part B-Engineering,* 31(6-7), 481-497.

Mork, K. J. (1992). "Stochastic analysis of reinforced concrete frames under seismic excitation." *Soil Dynamics and Earthquake Engineering*, 1(3), 145-161.

Mukherjee, A., Joshi, M. (2005). "FRPC reinforced concrete beam-column joints under cyclic excitation." *Composite Structures*, 70:185-199.

Murty, C. V. R., Rai, D. C., Bajpai, K. K., and Jain, S. K. (2003). "Effectiveness of reinforcement details in exterior reinforced concrete beam-column joints for earthquake resistance." *ACI, Structural Journal*, 100 (2), 149-156.

Mirza, M. S., Labonte, L. R. S, McCutcheon, J. O. (1972). "Size effect in model concrete mixes." Paper presented in ASCE National Convention, Cleveland, April.

Naeim F, Kelly, J., M. (1999). "Design of seismic isolated structures from theory to practice." John willey & sons, inc.

Nie, J., Bai, Y., and Cai, C.S. (2008). "New connection system for confined concrete columns and beams. I: experimental study." *Journals of Structural Engineering*, ASCE, 134(12), 1787-1799.

Park, Y.J. (1984). "Seismic damage analysis and damage-limiting design of R/C structures." PhD Thesis, Department of Civil Engineering, University of Illinois, Urbana, IL.

Park, Y.J., and Ang, A.H.S. (1985). "Mechanistic seismic damage model for reinforced concrete." ASCE, 111(4), 722-739.

Park, R. (1986). "Ductile design approach for reinforced concrete frames." *Earthquake Spectra,* 2(3), 565-619.

Park, Y. J., Ang, A. H. S., and Weng, Y. K. (1987). "Damage limiting a design of buildings." *Earthquake Spectra*, 3(1), 1-26.

Paulay, T. (1989). "Equilibrium criteria for reinforced-concrete beam-column joints." *ACI, Structural Journal*, 86(6), 635-643.

Paulay, T., and Priestley, M. J. N. (1992). "Seismic design of reinforced concrete and masonry buildings." John Wiley & Sons, INC.

Pagni, C. A., and Lowes, L. N. (2006). "Fragility functions for older reinforced concrete beam-column joints." *Earthquake Spectra*, 22 (1), 215–238.

Popov, E., and Bertero, V.V. (1975). "Repaired R/C members under cyclic loading." *Engineering and Structural Dynamics*, 4, 129-144.

Porter, K., Hamburger, R., and Kennedy, R. (2007a). "Practical development and application of fragility functions." *Structural Engineering Research Frontiers*, ASCE, 249, 23.

Porter, K., Kennedy, R., and Bachman, R. (2007b). "Creating fragility functions for performance-based earthquake engineering." *Earthquake Spectra*, 23 (2), 471-489.

Roufaiel, M. S. L., and Meyer, C. (1987a). "Analytical modeling of hysteresis behavior of RC frames." *Journals of Structural Engineering*, ASCE, 113(3), 445-457.

Rossetto, T., Elnashai, A.S. (2003). "Derivation of vulnerability functions for European type RC structures based on observational data." *Engineering Structures*, 25 (10), 1241-1263.

Sabnis, G., M, Mirza, M., S (1979). "Size effects in model concretes?" *Journal of Structural Division*, ASCE, 105(ST6), 1007-1020.

Saleh, H. A., Al-Salloum, A. Y., Almusallam, T. H., and Nadeem, A. S. (2010). "Seismic response of FRP-upgraded exterior beam-column joints." *Journals of Composite for Constructions*, ASCE, 14(2), 195-208.

Sasmal, S., Ramanjaneyulu, K., Balthasar Novak, Srinivas, V., Kumar, K. S., Korkowski, C., Roehm, C., Lakshmanan, N., and Iyer, N.R. (2010). "Seismic retrofitting of non ductile beam-column sub-assemblage using FRP wrapping and steel plate jacketing." *Journals of Construction and Building Materials*, Elsevier, 25(1), 175-182.

Scribner, C. F., and Wight, J. K. (1980). "Strength decay in reinforced concrete beams under load reversals."*Journal of Structural Division*, Proceedings of the American Society of Civil Engineers, 106(ST4), 861-876.

Sezen, H., Elwood, K. J., Whittaker, A. S., Mosalam, K. M., Wallace, J. W., and Stanton, J. F. (2000). "Structural Engineering Reconnaissance of the August 17, 1999 Earthquake.": Kocaeli (Izmit), Turkey, PEER 2000/09, University of California, Berkeley, USA.

Sener, S., Bažant, Z. P., and Becq-Giraudon, E. (1999). "Size effect on failure of bond splices of steel bars in concrete beams." *Journals of Structural Engineering,* ASCE, 125(6), 653-660.

Sener, S., Begimgil, M., and Belgin, C. (2002). "Size effect on failure of concrete beam with and without fibre." *Journal of Materials in Engineering*, ASCE, 14(5), 436-440.

Sener, S., Barr BIG, and Abusiaf, H. F. (2004). "Size effect in axially loaded reinforced column." *Journal Structural Engineering*, ASCE, 130(4):662-670.

Shome. N., and Cornell. C., A. (1999). " Probabilistic seismic demand analysis of nonlinear structures." *Report No. RMS-35, Dept. of Civil and Environmental Engineering*, Stanford Univ., California.

Shah, S. S., Wang, M. L., and Chung, L. (1987). "Model concrete beam-column joints subjected to cyclic loading rates." *Material and Structures*, 20, 85-95.

Shash, A. A. (2005). "Repair of concrete beams- a case study." *Construction and Building Materials*, Elsevier, 19, 75-79.

Sordo, E., Teran, A., Guerrero, J. J., Juarez, H., and Iglesias, J. (1989). "Ductility and resistance requirement imposed on a concrete building." *Earthquake Spectra*, 5(1), 41-50.

Stephens, J. E., and Yao, J. T. P. (1987). "Damage assessment using response measurement." *Journals of Structural Engineering*, ASCE, 113(3), 787-801.

Stone, W. C., and Taylor, A. W. (1993). "Seismic performance of circular bridge columns designed accordance with AASHTO/CALTRANS standards." NIST Building Science Series 170,. National Institute of Standards and Technology, Gaithersburg. MD, 1993.

Stoppenhagen, D. R., Jirsa, J. O. and Wyllie, L. A. (1995). "Seismic repair and strengthening of a severely damaged concrete frame." *ACI, Structural Journals*, 92(2), 177-187.

Shannag, M. J., and Alhassan, M. A. (2005). "Seismic upgrade of interior beam-column sub-assemblages with high performance fiber reinforced concrete jackets." *ACI, Structural Journals*, 102(1), 131-138.

Shinozuka, M. , Fend, M. Q., Lee, L., and Naganuma, T. (2000). "Statistical Analysis of Fragility Curves." *Journal of Engineering Mechanics*, 126 (12), 1224- 1231.

Shinozuka, M., and Sang-Hoon, K. (2002). "Fragility curves of concrete bridges retrofitted by column jacketing." *Earthquake Engineering and Engineering Vibrations*, 2, 195-205.

Tsai, A. (1992). "Effective Repair with Resin for Bond Failure of RC Members." Proceedings of the 10th World Conference of Earthquake Engineering: 5211-5216.

Tsonos, A. G. (2001). "Seismic rehabilitation of reinforced concrete joints by removal and replacement technique." *European Earthquake Engineering*, 3, 29-43.

Tsonos, A.G. (2002). "Seismic retrofit of exterior R/C beam-to-column joints using two-sided and three-sided jackets." *Structural Engineering Mechanics*, 13 (1), 17-34.

Tsonos, A., Tegos, I., and Penelis, G. (1994). "Influence of axial force variations on the seismic behavior of exterior beam-column Joints." *European Earthquake Engineering,* 9 (3): 51-63.

Wang, M. L., and Shah, S.P. (1987). "Reinforced concrete hysteresis model based in the damage concept." *Earthquake Engineering and Structural Dynamics*, 15(8), 993-1003.

Wang, M. L. (1994). "Response of various non-linear reinforced concrete models." 12 International Modal Analysis Conference, Honolulu, Proceedings, II, 1512-1519

Walsh, P. F. (1972). "Fracture of plain concrete." *Indian Concrete Journal,* 46(11), 469-470 and 476.

Whitman, R. V., Reed, J. W., and Hong, S.T. (1974). "Earthquake damage probability matrices." Proceedings of the 5th World Conference on Earthquake Engineering, Rome, 2531–2540.

William, M. S., and Sexsmith, R. G. (1995). "Seismic damage indices for concrete structures: a state-of-the-art review." *Earthquake Spectra*, 11(2), 319-349.

William, M. S., Villemure, I., and Sexsmith, R. G. (1997). "Evaluation of seismic damage indices for concrete elements loaded in combined shear and flexure." *ACI, Structural journal*, 94 (3), 315-322.

APPENDIX-A

ANALYSIS AND DESIGN OF THE SPECIMENS

A1. RC BEAM-COLUMN CONNECTIONS WITH BEAM WEAK IN FLEXURE

A1.1 Full scaled (BWFLC) specimens

(a) Analysis of beam

The analysis of beam was done after removing material factor of safety of concrete and steel.

Calculation of neutral axis depth

Equilibrium equation for a doubly reinforced RC beam is given by

$$C_{uc} + C_{us} = T_u$$

Where,

C_{uc} = Resultant compressive force in concrete,

C_{us} = Resultant compressive force in the compressive steel,

T_u =Resultant tensile force in tension steel,

x =Neutral axis depth.

$$C_{uc} = 0.36 \times 1.5 \times f_{ck} \times b \times x$$

$$= 0.54 \times 30 \times 300 \times x$$

$$= 4860 \times x \text{ N}$$

and $C_{us} = \in_{s1} \times E_s$

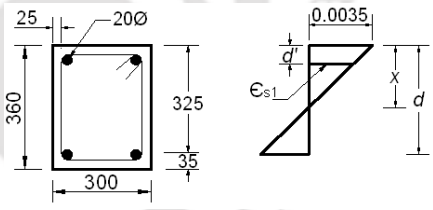

A_{st}=A_{sc}= 628.32mm^2

Fig. A1 Strain diagram of beam

Where, $\in_{s1}$ is the strain in compressive steel and E_s is modulus of elasticity of steel.

From Figure A1.

$$\in_{s1} = 0.0035\left(\frac{x - d'}{x}\right)$$

$$C_{us} = 2 \times 10^5 \times 0.0035 \times \left(\frac{x - 35}{x}\right) \times 628.32$$

$$= 439824 \times \left(\frac{x - 35}{x}\right) \text{ N}$$

$T_u = f_y \times A_{st}$

$=500\times628.32 \qquad (f_y = 500N/mm^2)$

$=314160$ N

Substituting these values in Equilibrium equation

$$4860\times x+439824\times\left(\frac{x\text{-}35}{x}\right)=314160$$

Solving the equation, the depth of neutral axis is

x=44.8 mm

Corresponding stress developed in compressive steel is

$$f_{S1} = 0.0035\left(\frac{x-d'}{x}\right)\times E_s$$

$$=0.0035\left(\frac{44.8-35}{44.8}\right)\times2\times10^5$$

$=153.125$ N/mm^2

Moment carrying capacity of beam is given by

$M_u = C_{uc}\times x \times(\text{d-}0.42\times x)+C_{us}\times(d - d'),\ (d' = \text{effective cover})$

$= 4860\times44.8\times(325\text{-}0.42\times44.8) +153.125\times628.32\times(325\text{-}35)$

$= 94.565$ KN-m.

As the beam-column connections is a strong column-weak beam (*proved in subsequent section)*. Hence, assuming the beam as fixed like a cantilever (Fig. A2)

Ultimate load carrying capacity of beam,

$P_u = M_u / L$

$= 94.565/1.35$

$= 70.048$ KN

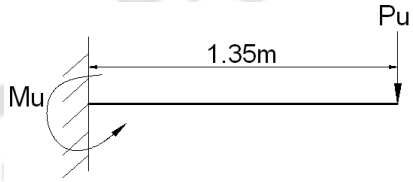

Fig. A2 Force and moment diagram

Design of shear reinforcement in beam

Percentage of tensile reinforcement provided, p_t =0.58% (Ref. Table 2.11)

From IS: 456-2000, Table 19: Corresponding shear stress can be obtained on interpolate the values for M30 and p_t =0.58%.

% of steel	Design shear strength of concrete
0.5	0.5
0.75	0.59

$\therefore \tau_c = 0.529 \text{N/mm}^2$

Shear resisted by Concrete

$V_c = \tau_c bd$

$=0.529\times300\times325$

$=51.57 \text{ KN} < 70.048 \text{ KN}$

Hence shear design is required

Shear to be resisted by steel

$V_{us} = V_u - V_c$

$= 70.048 - 51.57$

$= 18.48 \text{ KN}$

Use 2-legged 6mm dia. Stirrups Mild steel bars

$A_{sv}=2\times28.27=56.54 \text{ mm}^2$

$$V_{us} = \frac{f_y \times A_{sv} \times d}{S_v}$$

$$18480 = \frac{250\times56.54\times325}{S_v}$$

$\therefore S_v = 249 \text{ mm}$

The spacing should not exceed d/2 (i.e 325/2=162.5mm) in any part of beam (as per Clause 6.3.5 of IS: 13920-1993)

As per Clause 26.5.1.6 of IS: 456-2000 the minimum shear reinforcement is given by

$$S_v = \frac{A_{sv} \times f_y}{0.4b}$$

$$= \frac{56.54\times250}{0.4\times300}$$

$= 120 \text{ mm}$

As per Clause 6.3.5 of IS: 13920-1993, Confine hoops spacing over a length 2*d* at end of beam should be least of:

1. d/4 = 325/4 = 81.25mm
2. 8 times of smallest dia. Bar = 8x20=160mm
3. It need not be less than 100 mm

Therefore, provide 2-legged 8mm dia. stirrups@ 75mm c/c upto 2d (i.e 650mm) and then 2-legged 6mm dia. stirrups @120mm c/c for remaining length of beam.

(b) Design of Column

$T_u = f_y \times A_{st}$

$= 500 \times 628.32$

$= 314160\text{N}$

$$C_{us} = 2\times10^5 \times 0.0035 \times \left(\frac{x-35}{x}\right) \times 628.32$$

$$= 439824 \times \left(\frac{x-35}{x}\right) \quad \text{N}$$

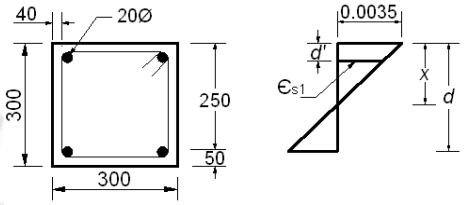

$A_{sc} = 628.32\text{mm}^2$

Fig. A3 Strain diagram of column

Axial load applied on Column

$P_u = 0.1 \times f'_{ck} \times A_g$

$= 0.1 \times 0.8 \times 30 \times 300 \times 300$ ($f'_{ck} = 0.8 f_{ck}$, Where f'_{ck} is Cube Strength

$= 216$ kN

The equilibrium equation for evaluation of neutral axis depth is given as

$C_{uc} + C_{us} - T_u = P_u$

Substituting the above values (taking, C_{uc} as calculated earlier)

$$4860x + 439824 \times \left(\frac{x-50}{x}\right) - 314160 = 216000$$

On solving the above equation

$x = 77.2\text{mm}.$

Corresponding stress developed in steel is

$$f_{S1} = 0.0035\left(\frac{77.2-50}{77.2}\right) \times 2\times10^5$$

$= 246.63\ \text{N/mm}^2$

Moment carrying capacity of column is given by

M.R = $C_{uc} \times x \times (d - 0.42 \times x) + C_{us} \times (d - d')$

$= 4860 \times 77.2 \times (250 - 0.42 \times 77.2) + 628.32 \times 246.63 \times (250 - 50)$

$= 112.62$ KN-m.

Design of shear reinforcement in column

$P_t = 0.698\%$ (Ref. table 2.11)

Similar to earlier case, on interpolating the values, the permissible shear stress = 0.57 N/mm^2

As per Clause 40.2.2 of IS: 456-2000

$$\delta = 1 + \left(\frac{3P_u}{A_g f_{ck}} \right) \quad \text{but not exceeding 1.5}$$

$$\delta = 1 + \left(\frac{3 \times 216 \times 10^3}{300 \times 300 \times 20} \right)$$

$$= 1.24 < 1.5$$

$$\therefore \tau_c = 1.24 \times 0.57 = 0.7068 \text{ N/mm}^2$$

Effective depth of column=300-40-(20/2) = 250 mm

Shear resisted by concrete

$$V_c = \tau_c bd$$

$$= 0.7068 \times 300 \times 250$$

$$= 53.01 \text{ kN}$$

Shear force due to possible plastic hinge formation in the longitudinal beam

$$V_u = M_u{}^{br} / h_{st}$$

$$= 94.565/3.3$$

$$= 28.65 \text{ KN} < V_c$$

This indicates concrete of column alone is capable of resisting the shear force. However, nominal shear design is provided as per the following clauses.

Design of lateral ties

As per Clause 7.4.1 of IS: 13920-1993, special confinement length (l_0) should not be less than

(a) least lateral dimension (i.e.300mm)

(b) 1/6 th of clear span (i.e. (3300-360)/6 =490mm)

(c) 450mm

Hence, adopt 495 mm from joint on either side of column.

For special confinement zone, try 12 mm diameter bars,

Clause 7.4.8 of IS: 13920-1993 gives the equation of area of cross section 'A_{sh}' of the bar forming rectangular hoop.

$$A_{sh}=0.18\times S\times h\times\frac{f_{ck}}{f_y}\times\left(\frac{A_g}{A_k}-1\right)$$

h= 300 – (2 ×40) + (2×12) =244

$A_g = 9 \times 10^4$ mm^2

$A_k = (300-2\times40+2\times12)^2 = 59536$ mm^2

$$\therefore \quad A_{sh}= 0.18\times S\times h\times\frac{f_{ck}}{f_y}\times\left(\frac{A_g}{A_k}-1\right)$$

$$113.09 = 0.18\times S\times 244\times\frac{30}{500}\times\left(\frac{9\times10^4}{59536}-1\right)$$

S = 83.87 mm

Provide 2-legged 12 mm dia. lateral ties @ 75mm c/c up to 495mm from the joint and beyond that provide 2-legged 6 mm diameter @ 150mm c/c (i.e.300/2) (Clause 7.3.3 of IS: 13920-1993).

(c) Design of Joint

Check for strong column-weak beam condition

$$\sum M_C / \sum M_B = \frac{112.62+112.62}{94.565}$$

= 2.38 > 1.1 (As per IS: 13920-1993)

> 1.2 (As per ACI 318)

Hence, the connections satisfy the criteria of strong column-weak beam condition.

$V_{col} = V_u$ = 28.65 kN

Force developed at top bars of beam

$T_1 = 1.25\times A_{st}\times fy$

= 1.25×628.32×500

= 329.70 KN

$V_{joint} = T_1 - V_{col}$

= 329.70 – 28.65

= 364.05 KN

Check for joint shear strength

$$b_c \le (b_b + b_c)/2$$

$$b_j \le b_b + h$$

$$b_c = 300\ ; b_b = 300\ ; h = 300$$

$$b_j \le \frac{300+300}{2} \le 300$$

$$b_j \le 300 + 300 \le 600$$

Hence $b_j = 300$

Effective area of joint resisting shear

$$A_c = b_j \times h$$

$$= 300 \times 300 = 90000\ \text{mm}^2$$

Shear strength of joint as per Clause 8.2.1 of IITK-GSDMA-EQ11-V4.0 AND EQ16-V3.0

$$= 1.0\sqrt{f_{ck} \times A_c}$$

$$= 402.49\ \text{KN} > 364.05\ \text{KN}.$$

Hence O.K

A1.2 Two-third (BWSMC) and one-third (BWFSC) scaled specimens

The design calculations followed similar steps as that of full scaled specimen.

A2. RC BEAM-COLUMN CONNECTIONS WITH BEAM WEAK IN SHEAR

A2.1 Full scaled specimen (BWSLC)

Under this category the cross section and longitudinal reinforcement of beam was maintained same as that of earlier case. However, the shear reinforcement was reduced to make the beam weak in shear.

$V_c = 51.57$ KN (As calculated earlier)

To make the beam weak in shear, spacing of shear reinforcement was increased increase. Provide 2 –legged 6mm dia. stirrups @ 600mm c/c.

Shear resisted by steel,

$$V_{us} = \frac{\left(f_y \times A_{sv} \times d\right)}{S_v}$$

$$= \frac{\left(250 \times 2 \times 28.26 \times 325\right)}{600}$$

$$= 7.65 \text{ KN}$$

Total shear resisted by the section of beam,

$$V_u = V_{us} + V_c$$

$$= 51.57 + 7.65$$

$$= 59.22 \text{ KN} < 70.048 \text{ KN}$$

Hence, the beam is weak in shear.

However, to keep a predefined failure location and to ensure that the failure does not occur near tip of the beam, only the first stirrup near the joint is maintained at a spacing of 600 mm c/c and for the rest part spacing is decreased to 240mm c/c.

A2.2 Two-third (BWSMC) and one-third (BWSSC) scaled specimens

The design calculations are similar for these type as that of full scaled specimen.

A3. RC BEAM-COLUMN CONNECTIONS WITH COLUMN WEAK IN SHEAR

A3.1 Full scaled specimens (CWSLC)

The cross section of the column was adopted 300 mm×240 mm and cross section of beam was adopted 450 mm×300 mm.

(a) Analysis of Beam

As in the earlier cases the analysis has been done after removing factor of safety for concrete and steel.

The equilibrium equation is given by

$$C_{uc} + C_{us} = T_u$$

Where

C_{uc} = Resultant compressive force in concrete,

C_{us} = Resultant compressive force in the compressive steel,

T_u =Resultant tensile force in tension steel,

x =Neutral axis depth.

C_{uc}=0.36×1.5×f_{ck} ×b×x

=0.54×25×240×x

=3240×x N

$$C_{us} = 2\times10^5\times0.0035\times\left(\frac{x-35}{x}\right)\times972.48$$

$$= 659736\times\left(\frac{x-35}{x}\right) \text{ N}$$

T_u=f_y×A_{st}

=500×942.48 ($f_y = 500N/mm^2$)

=471.24 N

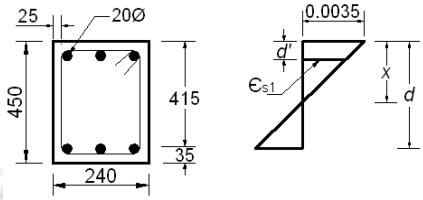

A_{st}=A_{sc}= 942.48mm^2

Fig. A4 Strain diagram of beam

Substituting values in Equilibrium equation and solving for x

$\therefore$ x= 60.20 mm

Moment carrying capacity of beam is given by

$$M_u = C_{uc}\times x \times(d\text{-}0.42\times x)+C_{us}\times(d - d')$$

$$= 3240\times60.2\times(415\text{-}0.42\times60.2) +659736\times\left(\frac{60.2-35}{60.2}\right)\times(415\text{-}35)$$

= 180.94 N-mm

Ultimate load carrying capacity of beam is

$P_u = M_u / L$

$=180.94/1.35$

$=134.029$ KN.

Design of Shear Reinforcement in Beam

Percentage of tensile reinforcement provided, p_t =0.873% (Ref. Table 2.11)

From IS: 456-2000, Table 19: Corresponding shear stress can be obtained on interpolate the values for M25 and p_t =0.873%.

% of steel	Design shear strength of concrete
0.75	0.54
1.00	0.60

Therefore, $\tau_c = 0.569$ N/mm^2

Shear resisted by Concrete

$$V_c = \tau_c b d$$

$$=0.529\times240\times415$$

$$=56.67\ \text{KN} < 134.029\ \text{KN}$$

Hence shear design is required

Shear resisted by steel

$$V_s = V_u - V_c$$

$$= 134.029\text{-}56.67$$

$$= 78.27\ \text{KN}$$

Using 2-legged 8mm dia. stirrups

$$A_{sv}=2\times50.26=100.54\text{mm}^2$$

$$V_s = \frac{f_y \times A_{sv} \times d}{S_v}$$

$$78270=\frac{500\times100.54\times415}{S_v}$$

Therefore, S_v =265mm

As per Clause 3.6.5 of IS: 13920-1993, near the beam- column joint spacing should not exceed than d/4 (i.e 415/3=103.75mm).

Therefore, provide 2-legged stirrups 8mm dia.@75mm c/c through out the beam.

(b) Analysis of Column

$$T_u = f_y \times A_{st}$$

$$=500\times628.32$$

$$=314160\ \text{N}$$

$$C_{uc} = 0.54\times f_{ck} \times b \times x$$

$$=0.54\times25\times240\times x$$

$$=3240\times x\ \text{N}$$

$$C_{us} = 2\times10^5 \times0.0035\times\left(\frac{x-50}{x}\right)\times628.32$$

$$= 439824\times\left(\frac{x-50}{x}\right)\ \text{N}$$

Axial load applied on Column

$$P_u = 0.1 \times A_g \times f'_{ck}$$

$$= 0.1 \times 0.8 \times 25 \times 240 \times 300 \qquad (f'_{ck} = 0.8 f_{ck}, \text{ Where } f'_{ck} \text{ is Cube Strength}$$

$$= 144 \text{ KN}$$

The depth of neutral axis x is calculated from the following equilibrium Equation

$$C_{uc} + C_{us} - T_u = P_u$$

On substituting the values, the neutral axis depth calculated as

x=80.78 mm.

Corresponding stress developed in steel is

$$f_{S1} = 0.0035\left(\frac{80.78 - 50}{80.78}\right) \times 2 \times 10^5$$

$$= 226.72 \text{ N/mm}^2$$

Moment carrying capacity of column is given by

$$\text{M.R} = C_{uc} \times x \times (d - 0.42 \times x) + C_{us} \times (d - d')$$

$$= 3240 \times 80.78 \times (250 - 0.42 \times 80.78) + 628.32 \times 226.72 \times (250 - 50)$$

$$= 90.067 \text{ KN-m.}$$

Check for strong column-weak beam condition of the sub-assemblage

$$\sum \text{M}_\text{C} / \sum \text{M}_\text{B} = \frac{90.067 + 90.067}{180.94}$$

$$= 0.99 < 1.1$$

The sub-assemblage is a weak column-strong beam condition as per IS: 13920-1993 and ACI-318. The conditions for assuming the beam as a cantilever beam like that of beam weak in flexure case is no more valid, since the sub-assemblage is a weak column-strong beam condition. Thus, the calculation of the ultimate load carrying capacity of the specimen has not been done. Moreover, lesser shear reinforcement was provided in column in order to make the specimen shear deficient in column. For large specimens a 2-legged 6 mm dia. mild steel bar with a spacing of 900 mm c/c has been provided as lateral ties.

A3.2 Two-third (CWSMC) and one-third (CWSSC) scaled specimens

The design calculations of these types followed similar steps as that of full scaled specimen.

APPENDIX-B

CALCULATION OF ULTIMATE STRESSES

B.1 Beam weak in flexure (BWF) specimens

The failure modes of the specimens for control and rehabilitated specimens were in flexure and hence bending stress was calculated. The analysis is based on the approach proposed by Bažant and Planas [1998] in which the nominal stress at maximum load is given by the expression:

$$\sigma_{N_U} = C_N \frac{P}{(bD)} \tag{B.1}$$

where, C_N = Coefficient introduced for convenience, P = Applied load (obtained experimentally) and (bD) = Area of the cross section of beam with b is the width and D is the depth. It may be noted that the area contributed by reinforcement is not considered in area calculation (Belgin and Sener, 2008).

For a cantilever beam, C_N was calculated as:

$$C_N = \frac{6\,l}{D} \tag{B.2}$$

where, l = Span of the beam

For large specimen; using Eq. (B.2), Value of coefficient is:

$$C_N = 6 \times \frac{1350}{360}$$
$$= 22.5$$

A=10,8000mm^2 and P = 73.285 kN (obtained from test for control specimen with loading type-1)

Using Eq. (B.1), the ultimate nominal bending stress is:

$$\sigma_{N_U} = 22.5 \times \left(\frac{73.285 \times 10^3}{108000} \right) = 15.2677 \ N/mm^2$$

Similarly, σ_{N_U} for all specimen sizes, control and rehabilitated were calculated and listed in Table B1.

Table B1 Calculation of bending stress of beam weak in flexure (BWF) specimens

Specimens	*b* *(mm)*	*D* *(mm)*	*l* *(mm)*	*A*= x*D* *(mm^2)*	C_N	P_{-1} *(N)*	P_{-2} *(N)*	σN_{u-1} *(N/mm^2)*	σN_{u-2} *(N/mm^2)*
BWFLC	300	360	1350	108000	22.5	73285	73605	**15.2677**	15.3344
BWFMC	200	240	900	48000	22.5	34845	35995	16.3336	16.8726
BWFSC	100	120	450	12000	22.5	9885	10200	18.5344	19.1250
BWFLRe	300	360	1350	108000	22.5	84085	78065	17.5177	16.2635
BWFMRe	200	240	900	48000	22.5	40995	39250	19.2168	18.3984
BWFSRe	100	120	450	12000	22.5	11890	11360	22.2937	21.3000

Note: σN_{u-1}: Bending stress corresponding to ultimate load (P_{-1}) under loading type-1.

σN_{u-2}: Bending stress corresponding to ultimate load (P_{-2}) under loading type-2.

B.2 Beam weak in shear (BWS) specimens

The failure modes of these specimens were in shear and hence shear stress was calculated for this type of specimens. Bažant and Planas [1998] proposed the expression for maximum shear stress similar to Eqn. B.1 as follows:

$$\sigma_{N_U} = C_N \frac{P}{(bD)} \tag{B.3}$$

where, P is the load, (bD) is the area of cross section of the beam and C_N is the coefficient.

For a cantilever beam, C_N was calculated as equal to 1.5.

For large size specimen; A=108000mm^2 and P = 72.085 kN (obtained from test for control specimen with loading type-1)

Using Eqn. (B.3), the ultimate shear stress is

$$\sigma_{N_U} = 1.5 \times \left(\frac{72.085 \times 10^3}{108000} \right) = 1.0012\, N/mm^2$$

Similarly, σ_{N_U} for all the specimen sizes and for control as well as rehabilitated were calculated and listed in Table B2.

Table B2 Calculation of shear stress of beam weak in shear (BWS) specimens

Specimens	*b* *(mm)*	*D* *(mm)*	*l* *(mm)*	*A= bxD* *(mm^2)*	C_N	P_{-1} *(N)*	P_{-2} *(N)*	σN_{u-1} *(N/mm^2)*	σN_{u-2} *(N/mm^2)*
BWSLC	300	360	1350	108000	1.5	72085	74060	**1.0012**	1.0286
BWSMC	200	240	900	48000	1.5	35100	37080	1.0968	1.1587
BWSSC	100	120	450	12000	1.5	10053	10190	1.2566	1.2737
BWSLRe	300	360	1350	108000	1.5	77220	80970	1.0725	1.1246
BWSMRe	200	240	900	48000	1.5	38665	41465	1.2083	1.2958
BWSSRe	100	120	450	12000	1.5	11610	11820	1.4513	1.4775

Note: σN_{u-1}: Shear stress corresponding to ultimate load (P_{-1}) under loading type-1.

σN_{u-2}: Shear stress corresponding to ultimate load (P_{-2}) under loading type-2.

B.3 Column weak in shear (CWS) specimens

The failure mode of these specimens was in shear, and hence shear stress was calculated for this type of specimens.

Ref. to Fig. B1, the equilibrium equation for the forces may be written as

$$S \times h = P \times l \tag{B.4}$$

where, S = Shear forces transmitted on column corresponding to the applied load P on the beam tip.

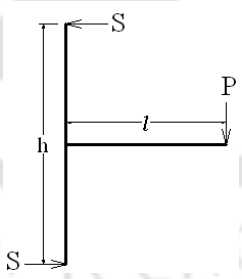

Fig. B1 Free body diagram of forces

For large control (CWSLC) specimen

P = 58.010 kN (obtained from test for control specimen under loading type-1)

l, Span of the beam = 1350 mm

h, Height of column = 3300 mm

A, Area of column section ($b \times D$) = 240x300 = 72000mm^2

Substituting the value of ultimate load carrying capacity P as found experimentally in Eq. (B.4), we get

$$S \times 3.3 = 58.01 \times 1.35$$

$$S = 23.731 \text{ kN.}$$

Maximum shear stress is given by

$$\sigma_{N_U} = C_N \frac{S}{A} \tag{B.5}$$

For a cantilever beam, C_N was calculated as equal to 1.5

Substituting all the value in Eq. (B.5), we get

$$\sigma_{N_U} = 1.5 \times \left(\frac{23.73 \times 10^3}{240 \times 300} \right) = 0.4944 \ N/mm^2$$

Similarly, σ_{N_U} for all the specimen sizes and for control as well as rehabilitated specimens were calculated and listed in Table B3.

Table B3 Calculation of shear stress of column weak in shear (CWS) specimens

Specimens	b (mm)	D (mm)	l (mm)	h (mm)	C_N	P_{-1} (N)	P_{-2} (N)	S_{-1} (N)	S_{-2} (N)	σN_{u-1} (N/mm^2)	σN_{u-2} (N/mm^2)
CWSLC	240	300	1350	3300	1.5	58010	58930	23731	24108	**0.4944**	0.5022
CWSMC	160	200	900	2200	1.5	30000	31230	12273	12776	0.5753	0.5988
CWSSC	80	100	450	1100	1.5	8635	8889	3533	3636	0.6623	0.6818
CWSLRe	240	300	1350	3300	1.5	64635	61383	26033	25111	0.5423	0.5231
CWSMRe	160	200	900	2200	1.5	35560	32840	14547	13435	0.6435	0.6297
CWSSRe	80	100	450	1100	1.5	9895	9413	4048	3851	0.7589	0.7220

Note: σN_{u-1}: Shear stress corresponding to ultimate load (P_{-1}) under loading type-1.

σN_{u-2}: Shear stress corresponding to ultimate load (P_{-2}) under loading type-2.

S_{-1} and S_{-2}: Shear forces on column under loading type-1 and type-2

APPENDIX C

EVALUATION OF DAMAGE INDICES

The Park and Ang [1985] damage index comprises a deformation term and cumulative energy term. The model formulation is as follow

$$DI = \frac{\delta_m}{\delta_u} + \frac{\beta_e}{\delta_u Q_y}\int dE \qquad \text{(C.1)}$$

where, δ_m = the maximum deflection attained during seismic loading (mm)

δu = the ultimate deflection capacity under monotonic load (mm)

β_e = strength degradation parameter

Q_y = the yield force (kN) [see Fig. 3.30 of Sec. 3.5(d)]

dE = the incremental dissipated hysteretic energy (kN-mm)

The values of δ_m , δ_u , Q_y and dE of this model were yielded from the test results. Further, the parameter δ_u may be approximated by taking the envelope of the cyclic load-deflection loops in case of no monotonic test data are available (William *et al.*, 1997). For the quantitative estimation of strength degradation parameter (β_e), extensive experimental results reported a range between about -0.3 and 0.12 with a median of about 0.15 (Cosenza *et al.,* 1993).

For sub-assemblage with beam weak in flexure large control specimen under loading type-1 we have, δ_u =65.00mm, β_e =0.15, Q_y= 58.63 kN

Using Eqn. (C.1), the damage index for first drift level is:

$$\begin{aligned} DI_{0.104} &= \frac{\delta_m}{\delta_u} + \frac{\beta_e}{\delta_u Q_y}\int dE \\ &= \frac{1.40}{65.0} + \frac{0.15}{65.0\times 58.63}\times 18.40 \\ &= 0.022 + 0.00072 \\ &= 0.022 \end{aligned}$$

Repeating with similar step all the indices in subsequent drift level were calculated as listed in Table C1

Table C1 Typical calculation of damage index

Drift angle (%)	Maximum deformation (δ_m)	Cumulative energy ($\int dE$)	Deformation term (δ_m/δ_u)	Energy term $\left(\frac{\beta_e}{\delta u Q y}\int dE\right)$	Damage index (DI)
0.104	**1.4**	**18.4**	**0.022**	**0.000**	**0.022**
0.370	5.0	182.4	0.077	0.007	0.084
0.741	10	691.59	0.155	0.027	0.181
0.926	12.5	1300	0.193	0.051	0.243
1.111	15.0	2104.7	0.232	0.083	0.314
1.481	20.0	3632.3	0.311	0.143	0.451
1.852	25.0	6079.7	0.387	0.239	0.623
2.222	30.0	9587.6	0.465	0.377	0.839
2.593	35.0	14077	0.543	0.554	1.093
2.963	40.0	19171	0.620	0.755	1.370
3.333	45.0	24567	0.698	0.967	1.660
3.704	50.0	30133	0.775	1.186	1.955
4.074	55.0	35846	0.852	1.411	2.257
4.444	60.0	41843	0.930	1.647	2.570
4.815	65.0	47176	1.000	1.857	2.850

Similarly, indices for all the connections (both control and rehabilitated) under different loading conditions were evaluated.

LIST OF PUBLICATIONS FROM THIS THESIS

Conference Proceedings:

1. Marthong, C. M., Deb, S. K., and Dutta, A. (2011). "Performance of rehabilitated RC beam-column sub-assemblage under cyclic loading", *Proceedings of* 36th Conference on Our World in Concrete and Structures, Singapore, August 14-16.

2. Marthong, C. M., Dutta, A., and Deb, S. K. (2011). "Effect of loading frequency on performance of RC beam-column connections." *National Conference on Recent Advances in Civil Engineering,* IT-BHU**,** India, October 14-16,

Journals:

1. Marthong, C. M., Dutta, A., and Deb, S. K. (2011). "Seismic rehabilitation of deficient exterior RC beam-column connections." *Journals of Construction and Building Materials,* Elsevier (to be communicated).

2. Marthong, C. M., Deb, S. K., and Dutta, A. (2011). "Behaviour of RC beam-column connections under cyclic loading of higher frequency." *Journals of Construction and Building Materials,* Elsevier (to be communicated).

3. Marthong, C. M., Dutta, A., and Deb, S. K. (2011). "Study on size effect of rehabilitated RC beam-column connections under cyclic loading." *Journal of Structural Engineering, ASCE* (to be communicated).

4. Marthong, C. M., Deb, S. K., and Dutta, A. (2011). "Fragility functions for exterior RC beam-column connections." *Engineering Structures,* Elsevier (to be communicated).